N° d'Ordre : D.U. 2746

UNIVERSITE BLAISE PASCAL
U.F.R. Sciences et Technologies

ECOLE DOCTORALE DES SCIENCES FONDAMENTALES N° 885

THESE
Presentée pour obtenir le grade de
DOCTEUR D'UNIVERSITE
Specialité : Chimie Physique

Par **Angelica BIANCO**

Formation photoinduite du radical hydroxyle dans la phase aqueuse du nuage : impact sur les acides carboxyliques et les acides aminés.

Hydroxyl radical photogeneration in cloud aqueous phase : impact on carboxylic acids and amino acids.

Soutenue publiquement le 4 novembre 2016

President :

Dr. LAJ Paolo (Physicien, Université Joseph Fourier, Grenoble)

Rapporteurs :

Pr. VILLENAVE Eric (Professeur, Université de Bordeaux, Bordeaux)

Pr. WORTHAM Henri (Professeur, Aix-Marseille Université, Marseille)

Examinateurs :

Dr. DEGUILLAUME Laurent (Physicien Adjoint, Université Blaise Pascal, Clermont Ferrand)

Dr. GEORGE Christian (DR, CNRS-Université Claude Bernard, Lyon)

Directeurs de thèse :

Dr. BRIGANTE Marcello (Maître de Conférences HDR, Université Blaise Pascal, Clermont Ferrand)

Dr. MAILHOT Gilles (DR, CNRS-Université Blaise Pascal, Clermont Ferrand)

Clouds come floating into my life,

No longer to carry rain or usher storm

But to add color to my sunset sky.

Rabindranath Tagore, Stray Birds

A mamma, papà, Elia e Alice,

solide fondamenta dei miei castelli di carte.

Mots clés: Photochimie, Chimie atmospherique, Chimie radicalaire, Acides carboxyliques, Acides aminés

Keyword : Photochemistry, Atmospheric chemistry, Radical Chemistry, Carboxylic acids, Amino acids

Table of contents

Motivation

The water cycle is all about storing water and moving water on, in, and above the Earth. Although the atmosphere may not be a great storehouse of water, it is the superhighway used to move water around the globe. Chemical and photochemical processes in surface water has aroused the interest of the scientific community for the reason that water is one of the most primordial needs for humankind and many lifeforms on Earth. Nevertheless, this is only the lowest level of the cycle: for this reason it is necessary to study the atmospheric aqueous phase composition and reactivity and, in particular, cloud water.

Atmospheric water is in equilibrium with gas and particulate phase and atmosphere in general is linked with global warming, health, oceans, land use, climate patterns and many other vital topics.

These chapters try to set the scene for the work carried out during this thesis by introducing important concepts and by situating them on the global puzzle of the Earth's system.

Introduction

Clouds have always fascinated people, from children to old wise men. Children are fascinated by their fluffy white shapes and they see faces, fantastic landscapes and all sorts of wonderful images. In ancient times, the seers went a stage further: they believed that the pictures seen in clouds have a meaning about the things that were to come. Also in contemporary imagination, white clouds symbolize serenity and positive thinking while dark clouds conjure up depressing or pessimistic thoughts. In comics, clouds are used to give voice to the character's thoughts.

Different names based on their shape and their height in the sky are given to the clouds. Some clouds are near the ground, others are almost as high as jet planes fly, some are puffy like cotton and others are grey and uniform.

Clouds seem so simple from our perspective, just large masses of airborne water that take random shapes in the sky, occasionally dropping some of their water in various forms of precipitation on our heads. In reality, these beautiful feather pillows floating above us cover 70% of the earth are majestically complicated, and their very specific shapes are determined by different physical processes in the atmosphere. There is actually a huge amount that we still don't understand about clouds and how they operate, but significant progress has been made during the last century that has allowed us to uncover a lot of their inner workings. Whether they are hurling baseball-sized hailstones to the ground or frying radio towers with lightning strikes, clouds are always performing amazing feats of physics at both the microscopic and macroscopic levels.

Even if clouds seem so immense and deep, the aqueous phase of clouds and fog constitutes a small volume of the atmosphere ($\sim 10^{-7}$ vol vol^{-1}) [1] and only 0.03% (12000 km^3) of fresh water on Earth but clouds are of fundamental importance for the terrestrial climate in general. In fact, they are a physical obstacle to incoming and outgoing irradiation and they are also chemical reactors for the different atmospheric constituents. A cloud is a complex ecosystem (composed of solid, liquid and gas phases) where physical, microphysical, chemical, photochemical and microbiological transformations take place and it is impossible to study a single compartment without taking into account the others.

Figure 1 shows the classification of clouds on the basis of altitude and shapes.

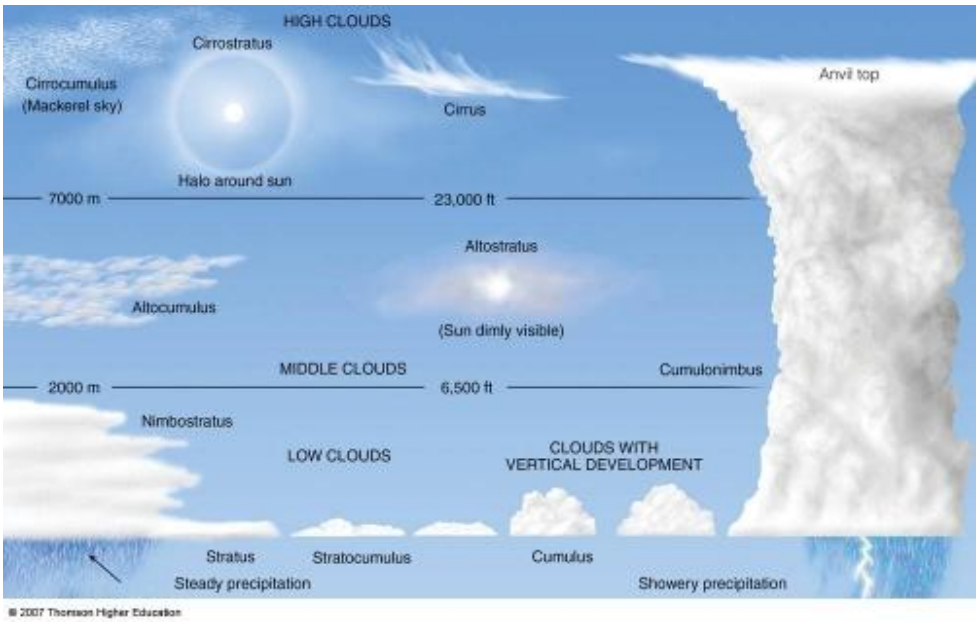

Figure 1:Cartoon showing different cloud types and levels [2].

The first scientific question was "how clouds are formed?". The first hypothesis was one of homogeneous nucleation but Bergeron, in 1922, discovered that clouds are normally formed in the presence of cloud condensation nuclei (CCN) or ice nuclei (IN). This theory is now confirmed and is the basis of our knowledge of cloud water, as discussed in Chapter 1.

After answering this first "microphysical" question, scientists' interest moved to the characterization of the composition of cloud aqueous phase. The first paper reporting the concentration of inorganic compounds in cloud aqueous phase appeared in 1982 [3], rapidly followed by a growing interest in the subject.

The chemical composition of the cloud aqueous phase, which is highly variable in time and space and in terms of droplet size, is correlated to the uptake of gases, the dissolution of CCN constituents and chemical reactions. Inorganic composition and physico-chemicals parameters were studied for many locations and are well described, they are useful to understand the origin of the air mass and can impact on the transformation pathways of dissolved compounds. For this reason, the main parameters are reported in Chapter 1.

Isaac Newton in 1679 said "If I have seen further, it is by standing on the shoulders of giants". The research works described in Chapter 1 represent the giants, the basis for any further research on cloud water aqueous phase.

Another interesting point, that has been deeply analysed in this manuscript, is the capacity of cloud water to transform the dissolved organic and inorganic compounds through photochemical reactions. Heikes et al.[4], in 1982, measured hydrogen peroxide for the first time, while Jacob et al. [5], in 1986, described the behavior of the hydroxyl radical in cloud

water. The main pathways of production and consumption of oxidants such as hydrogen peroxide and free radicals are described in Chapter 2. This bibliographic study is the starting point of this thesis and it is useful to understand the impact of hydroxyl radical photogeneration and its correlation with the concentration of inorganic sources, presented in Chapter 5.

Following the hystory of the first studies on cloud water, the next question was "what is the nature of the organic matter dissolved in cloud water?". The first paper on this topic was published in 1987 [6] and showed that cloud particles contain "complex proteins and cellulose". Additionally, the authors found "some degraded material (likely protein) and an unidentified orange−brown material". Until now, even if the dissolved organic matter remains still unknown, scientists measured the concentration of carboxylic acids and some other compounds for different sites. The presence of oxidized organic matter gives rise to another crucial question: "oxidized organic matter comes from the dissolution of the CCN, from the gas phase, or is it produced in cloud aqueous phase through the transformations of precursors?". Chamaides and Davis [7], in 1983, investigate the sources of formic acid in cloud water and report that the "hydroxyl radical can both produce and destroy formic acid". This is a milestone of the study of cloud aqueous phase reactivity.

Nowadays, it is well recognized that cloud chemical processes can lead to the formation of new low volatile compounds like carboxylic acids, as described in Chapter 3, as well as aldehydes that modify aerosol particles in terms of their (micro)physical and chemical properties (particle size, chemical composition, and morphology). If water evaporates from cloud droplets, secondary organic aerosols (SOAs) may be formed and they could act as CCN. These SOAs affect the effective radiative forcing from aerosol–radiation interactions (ERFari) and from aerosol–cloud interactions (ERFari). So clouds could change Earth's *albedo* and consequently affect the climate system.

The oxidative pathway is not the only possibility: the reaction of organic matter with free radicals could lead to the functionalization or formation or dimers/high weight molecular compounds as the result of the recombination of organic radicals. To understand the reactivity of carboxylic acids, it is helpful to choose a proxy, like tartronic acid, and to study its reactivity at low concentration under direct and indirect photolysis. Experimental results will be implemented in a model to predict the behavior of short chain carboxylic acids in cloud water. The results are reported in Chapter 6.

Twenty years ago scientists discovered the presence of microbiological activity in clouds. The logical consequence is the presence of dissolved organic matter related to living and dead

cells, like amino acids. These compounds were never detected in cloud water, but were studied related to other atmospheric aqueous media, as reported in Chapter 3. In this work, a method for the detection of amino acids was adapted and clouds samples were analyzed, as reported in Chapter 7. Moreover, tryptophan, an essential amino acid that could be considered a marker of microbiological activity, was quantified in cloud water samples and its reactivity with the hydroxyl radical was investigated, as reported in Chapter 8.

Chapter 9 reports an invited divulgatif review concerning the comparison between chemical, photochemical and microbiological processes, as a perspective of a future collaboration to understand the impact of microorganisms on cloud water chemistry.

Chapter 1

Cloud microphysics

Historically, cloud physics was the first studied section. Cloud physics is the study of the physical processes that lead to the formation, growth and precipitation of atmospheric clouds. Clouds consist of microscopic droplets of liquid water (warm clouds), tiny crystals of ice (cold clouds), or both (mixed phase clouds).

Homogeneous nucleation

Cloud formation requires a vertical movement of an air mass. When water evaporates from an area of the Earth's surface, the air over this area becomes moist. Moist air is lighter than the surrounding dry air, and tends to lift, creating an unstable situation. When enough moist air is accumulated, it rises as a single parcel, without mixing with the surrounding air. The process happens several times and the result is a series of discrete parcels of moist air rising to form clouds. This process occurs when one of three possible lifting agents, cyclonic/frontal, convective, or orographic movement, causes air containing invisible water vapor to rise and cool to its dew point, the temperature at which the air becomes saturated. During this ascent, the volume of air undergoes adiabatic cooling and the relative humidity grows. When the air mass reaches the Lifting Condensation Level (LCL), the air mass achieves the saturation needed to form cloud water droplets. The value of Liquid Water Content (LWC) reached is from 0.02 to 0.94 g m^{-3}.

Cloud droplet formation is determined by Clausius Clapeyron's equation (Equation 1)

$$e_s(T) = e_{s_0} \exp\left(\frac{l_v}{R_v T_0}\right) \exp\left(-\frac{l_v}{R_v T}\right)$$

Equation 1: Clausius Clapeyron equation.

where $e_s(T)$ is the saturation vapor pressure above a water surface in function of the temperature T, T_0 is the reference temperature for which $e_s(T_0) = e_{s_0}$, l_v is the vaporization heat and R_v is the gas constant for water steam [8]. It is necessary to form an aggregate of molecules, called "proto-droplet" to form a droplet from moist air. If we are in the condition of oversaturation (the value of "e" is higher than "e_s"), the proto-droplet grows. But e_s depends on the diameter of the droplet and the smaller it is, the higher the value of e_s required to reach equilibrium which is also a function of the surface tension. Droplets are spherical and the effect of curvature favors evaporation and hinders its growth (Kelvin effect). The process of homogeneous nucleation is plausible only if water molecules have very weak kinetic

energy, for temperatures lower than −40°C: this process is possible only in the high troposphere.

Heterogeneous nucleation

Cloud condensation nuclei or CCNs (also known as cloud seeds) are small particles on which water vapor condenses. A typical raindrop is about 2 mm in diameter, a typical cloud droplet is on the order of 0.02 mm, and a typical cloud condensation nucleus (aerosol) is in the order of 0.1 µm – 1 µm in diameter, as shown in Figure 2. CCN diameter may range from a few microns to a few tenths of micron. There are much smaller nuclei in the atmosphere, called Aitken nuclei, but they usually play no role in cloud formation. Nuclei that have diameters of several microns and are composed of a hygroscopic, or moisture-attracting, substance (*e.g.*, sea salt) are called giant condensation nuclei. The number of cloud condensation nuclei in the air can be measured and it ranges between 100 to 1000 CCN cm^{-3}. The total mass of CCNs injected into the atmosphere has been estimated to be about $2x10^{12}$ kg over a year.

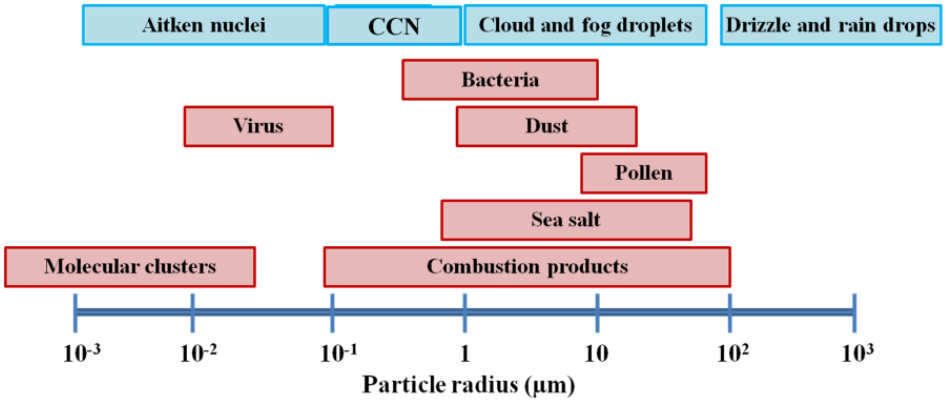

Figure 2: Comparison of dimensions of particles and aerosols in atmosphere (adapted from "Formation of haze, fog and clouds: Condensation nuclei").

There are many different types of atmospheric particles that can act as CCN. The particles may be composed of dust or clay, soot or black carbon from grassland or forest fires, sea salt from ocean wave spray, soot from factory smokestacks or from internal combustion engines, sulfate from volcanic activity, phytoplankton or the oxidation of sulfur dioxide and secondary organic matter formed by the oxidation of volatile organic compounds (Secondary Organic Aerosol, SOA). The ability of these different types of particles to form cloud droplets varies according to their size and also their exact composition, as the hygroscopic properties of these constituents are very different. Sulfate and sea salt, for example, readily absorb water whereas soot, organic carbon and mineral particles do not. This is made even more complicated by the fact that many of the chemical species may be mixed within the particles (in particular the

sulfate and organic carbon). Additionally, while some particles (such as soot and minerals) do not make very good CCN, they act as very good ice nuclei in colder parts of the atmosphere.

The number and type of CCNs can affect the lifetimes and radiative properties of clouds as well as the amount of clouds and hence have an influence on climate change; the details are not well understood but they are the subject of research. There is also speculation that solar variation may affect cloud properties via CCNs, and thus affect climate.

Because of the Kelvin effect, cloud condensation nuclei are necessary for cloud droplets formation. As explained before, without CCN the effect of curvature on a spherical droplet favors evaporation and hinders its growth. Cloud droplets are initially formed by the condensation of water vapor onto condensation nuclei when the oversaturation of air exceeds a critical value according to Köhler's theory (Equation 2).

$$ln\left(\frac{p_w D_P}{p^0}\right) = \frac{4M_w\sigma_w}{RT\rho_w D_P} - \frac{6n_s M_w}{\pi\rho_w D_P^3}$$

Equation 2: Köhler's equation.

where p_w is the droplet water vapor pressure, p^0 is the corresponding saturation vapor pressure over a flat surface, σ_w is the droplet surface tension, ρ_w is the density of pure water, n_s is the moles of solute, M_w is the molecular weight of water, and D_P is the cloud drop diameter [9]. At small radii, the level of oversaturation needed for condensation to occur is so high that it does not happen naturally. Raoult's Law describes how the vapor pressure is dependent on the amount of solute in a solution. At high concentrations, when the cloud droplets are small, the oversaturation required is smaller than without the presence of a nucleus. The precise processes of how a cloud forms and grows is not completely understood, but scientists have developed theories explaining the structure of clouds by studying the microphysics of individual droplets.

The main mechanism behind this process is adiabatic cooling. Water vapor in saturated air is normally attracted to condensation nuclei such as dust and salt particles that are small enough to be held aloft by normal circulation of the air. The water droplets in a cloud have a average radius of about 0.02 mm. The droplets may collide to form larger droplets which remain suspended as long as the drag force of the air is greater than the gravitational force.

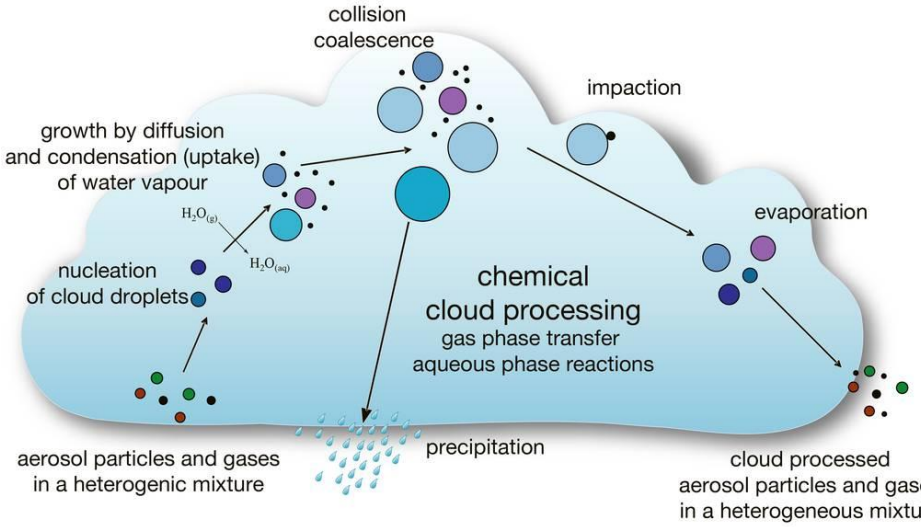

Figure 3: Cloud droplets nucleation (with kind permission of Deguillaume).

As said before, the initial growth of cloud condensation nuclei and their subsequent activation to form droplets is generally calculated with the assumption that cloud droplet activation occurs as an equilibrium process described by Köhler's theory, as shown in Figure 3. Chuang et al [10] show that this assumption is not valid under certain conditions present in nature. They demonstrate that there is a poor empirical correlation between cloud droplets and CCN concentrations and organic compounds can alter a particle's Köhler curve. Many authors such as Gill et all. [11], Blanchard [12] and Husar and Shu [13] demonstrate the existence of a organic film on atmospheric aerosol particles made of non-volatile organic compounds which can have different effects on cloud water droplet formation. The effect of such organic matter can affect droplet formation in three ways: changes in droplet surface tension, gradual dissolution of solute due to limited solubility and changes in the mass accommodation coefficient. All these effects lead to the inhibition of droplets growth. The general idea is that some amphiphilic organic compounds can form compressed films on the surface of the droplets. This coating may inhibit droplet growth for long enough so that some fraction of droplets grow in conditions of relatively high oversaturation. For this reason they achieve larger sizes than they would have if the entire population of drops had grown simultaneously [14].

For this reason it is very important to understand the organic composition of particles and cloud water.

When the protodroplet is formed, thermodynamic processes of condensation and evaporation take place: if the relative humidity continues to increase, the condensation of water on the surface of the aerosol particle grows as does the volume of the droplet. If the relative humidity

decreases, the water evaporates. Other microphysical phenomena of collision and coalescence can increase the size of droplets.

To summarize, when moist air ascends adiabatically, temperature decreases and relative humidity increases. Haze droplets grow following Köhler's curve and, if they reach the critical ray, they increase in size spontaneously, becoming activated droplet. If the air mass reaches the LCL, larger droplets are activated before smaller droplets. Their growth implicates a decrease of air humidity and oversaturation stops increasing. Equilibrium between oversaturation and droplet activation is reached and a cloud with droplets of different dimensions is formed. Droplets size is correlated to aerosol concentration and dimension and to the lifting rate of air mass. Collision and coalescence lead to the formation of rain drops which are heavy enough to fall to the ground.

The equilibrium between cloud water droplets, gas and particulate phase, leads to the absorption/desorption of chemical compounds and to their chemical, photochemical, microbiological or microphysical transformation. Moreover, clouds can transport chemical compounds for long distances.

Cloud chemistry

The term "cloud chemistry" comprises both cloud composition as well as the reactions that take place in clouds. Cloud water chemical composition is variable and the reactivity is influenced by many physico-chemical parameters such as pH, temperature and solar irradiation. Chemical compounds in cloud water droplets can come from the dissolution of aerosols and for some species, like iron, this is the only source in cloud aqueous phase [15]. Moreover water condensed-phase (liquid or solid) can dissolve gases and it allows the occurrence of reactions that would not otherwise happen or would be much slower. In this sense "clouds may be considered to serve as catalysts of atmospheric reactions" [16] (Figure 4). The uptake and reactivity of organic and inorganic matter in clouds, especially sulfur and nitrogen oxides and acids, has received particular attention in the context of gaining improved understanding of the processes responsible for acid deposition and climate change [17], because it is important to fully understand these processes.

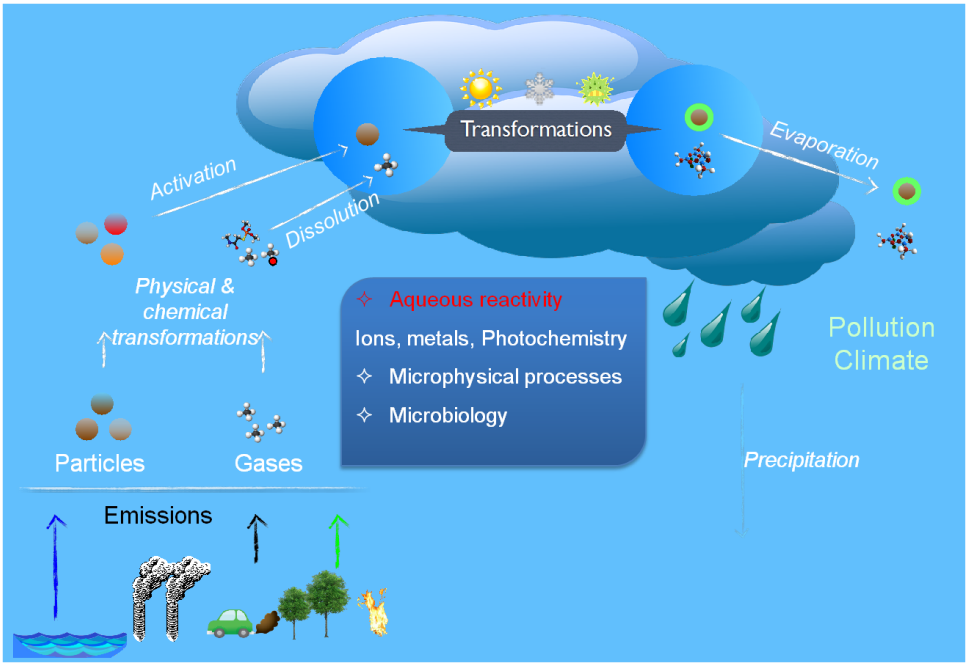

Figure 4: Transformations in clouds (with kind permission of Deguillaume).

Dissolution of aerosols

Cloud water composition is directly related to its air mass origin, and it largely depends on the availability of soluble ionic species. Main ionic species present in cloud water include chloride, from seawater, sulfate and nitrate anions, and ammonium and sodium ions as cations. In regions influenced by industrial emissions of sulfur and nitrogen oxides, cloud water concentrations of H_3O^+ are commonly 10^{-1} mol L^{-1} [18]. The fact that cloud droplets are formed on aerosols and CCN has immediate implications for cloud water composition. Let's consider an ammonium sulfate aerosol particle with a dry diameter of 0.1 µm that serves as a nucleus for a cloud droplet of 10 µm diameter. The amount of ammonium sulfate contained in the particle is 10^{-17} mol which correspond to 10^{-5} mol L^{-1} [16]. This concentration is at the low end of the range of concentrations of sulfate in cloud water in regions influenced by industrial emissions. In general the fractional uptake of soluble aerosol species into cloud water is fairly high. A recent study shows that, contrary to earlier studies [19,20], the main factor controlling bulk solute concentration is the concentration of incoming air masses rather than cloud liquid water content (LWC) [21]. A conceptual model developed by Ogren et al. [22] qualitatively describes the variation of non-volatile solute concentrations with cloud drop size in three regions with different drop size: in Region I drop diameter is lower than approximately 5 µm and contains freshly activated (or non-activated) droplets close to their equilibrium size at the prevailing oversaturation. In this so-called "equilibrium growth" region, solute concentrations sharply decrease with increasing drop size, because at their critical diameter, larger droplets

are more dilute than smaller ones as a result of the interactions between the Kelvin and the Raoult effect. Region II, ranging from approximately 5 to 50 μm, represents droplets which have freely grown by water condensation beyond their critical size. In this "condensation growth" region, solute concentrations increase with increasing drop size, because small drops grow faster than large drops (inverse correlation between growth and radius, as shown by Köhler's theory), i.e. large drops experience less dilution as compared to smaller ones. In Region III, with drops above approximately 50 μm in diameter, coalescence of drops becomes important. As larger drops collide more efficiently with smaller ones, solute concentrations decrease with increasing drop size in this "coalescence growth" region.

Dissolved gases

The situation is different in the case of gases: in general, a gaseous substance does not dissolve entirely in cloud water in view of the rather limited solubility of most atmospheric gases in water. The equilibrium concentration of a gas physically dissolved in a liquid is given by Henry's law and depends strictly on the solubility coefficient of the gas [16] (Equation 3)

$$[S_{aq}] = H_s p_s = H_s x_s p_{atm}$$

Equation 3: Henry's law.

Where $[S_{aq}]$ is the concentration of solute in water, H_s is the Henry's law solubility coefficient, p_s is the mixing ratio pressure, x_s is the molar mixing ratio in air and p_{atm} is the atmospheric pressure.

Several studies investigated the behavior of gases such as O_3, HClO, NO_x and H_2O_2 in the presence of clouds, showing a general decrease in gaseous concentrations resulting from the diffusion to the liquid phase. Similarly, the budget of radical species can be affected as well. In particular, it is recognized that aqueous phase photochemistry has an important effect on hydroxyl radical ($HO^{\bullet}$) concentration. The perturbation of the $HO^{\bullet}$ concentrations in the presence of clouds is partially linked to the alteration of hydrogen peroxide (H_2O_2) behavior. Hydrogen peroxide, hydroxyl radical and peroxyl radical ($HO_2^{\bullet}$) are soluble and can reach very high concentrations in a relatively small volume of water controlling liquid phase oxidation processes [23]. Otherwise O_3 does not diffuse in cloud water: O_3 molecules react on the internal surface of the droplet, before being able to enter the bulk droplet. Furthermore, because O_3 molecules are not formed in the aqueous phase, their chemical destruction rate per surface unit is equal to the net transfer flux of ozone from the gas-phase. As a result, the

washout of ozone is irreversible [24]. Diffusion of oxidant species such as H_2O_2, $HO^{\bullet}$ and $HO_2^{\bullet}$ and O_3 reactivity leads to a faster reactivity in the aqueous phase than in the gas phase.

Many campaigns of measurements on different sites were organized and inorganic composition of cloud water was largely studied [25-29]. Nevertheless, the development of numeric models is needed to have a better description and prediction of the complex interactions between microphysical and chemical processes. Many models, based on campaign measurements, were developed by Herrmann et al [30], Ervens et al [31], Leriche et al [32], and Deguillaume et al [33].

The study of the chemical composition of cloud water droplets assumes fundamental importance in understanding its variability in function of environmental conditions. The chemical compounds reactivity is then studied in the laboratory and these data are useful for the development of atmospheric cloud water models for the prediction of the behavior of chemicals in such a complex medium.

Cloud water droplets composition

Physico−chemical parameters

Liquid Water Content

The liquid water content (LWC) is the measure of the mass of water in a cloud in a specified amount of dry air. It is typically measured per volume of air (g m^{-3}) or mass of air (g kg^{-1}). The classification of the cloud is highly related to the liquid water content as well as its origin. Clouds that have low densities, such as cirrus clouds, contain very little water, thus resulting in relatively low liquid water content values of around 0.03 g m^{-3}. Clouds that have high densities, like cumulonimbus, have much higher liquid water content values that are around 1-3 g m^{-3}, so more liquid is present in the same amount of space. Measurements of cloud liquid water are central to many aspects of cloud microphysics research. The observed liquid water content is often compared with the adiabatic value to infer the effects of precipitation and entrainment on cloud structure [34]. The liquid water content (LWC) of clouds is one of the main controls of chemical concentrations in cloud water. According to theoretical formulation by Junge [35], the concentration of a cloud water solute is proportional to its concentration in the air and inversely proportional to LWC. However, the cloud environment is very complex and other factors tend to distort this relationship. It is commonly observed that solute concentration decreases with increasing LWC, however the functional form of this relationship remains open to question.

Redox potential

In aqueous solutions, redox potential is a measure of the tendency of the solution to either gain or lose electrons when it is subject to change by introducing a new species. Redox potential is defined as pε as reported in Equation 4, where a_{e^-} is the activity coefficient of the electron donor species. A solution with a higher (more positive) reduction potential species will have a tendency to gain electrons from the new species (i.e. to be reduced by oxidizing the new species) and a solution with a lower (more negative) reduction potential will have a tendency to lose electrons to the new species (i.e. to be oxidized by reducing the new species). In the field of environmental chemistry, the reduction potential is used to determine if oxidizing or reducing conditions are prevalent in water or soil, and to predict the oxidation states of different chemical species in the water, such as dissolved metals.

$$p\epsilon = -Log_{10}a_{e^-}$$

Equation 4: Definition of pε.

$p\epsilon$ values in water range from −12 to 25; the levels where the water itself becomes reduced or oxidized, respectively.

The redox potential of cloud water was measured only by Sinner et al.: they report a value of 2.5 – 2.6 V [36].

Conductivity

The conductivity of an electrolyte solution is a measure of its ability to conduct electricity. The IS unit of conductivity is Siemens per meter (S m^{-1}). Ionic species in cloud water are responsible for the conductivity of this medium because there is a linear correlation between ion concentration and its conductivity via molar conductivity. The total conductivity of the solution is expressed as the sum of the partial conductivity of each ion. This kind of measurement permits us to estimate the ionic concentration of cloud water and to compare it with other atmospheric media: the range values measured by Cini et al. [37] is 47-485 µS cm^{-1} while Kawamura et al. [38] measured 6-190 µS cm^{-1}. Ionic species that mainly influence conductivity are H_3O^+, HO^- and then SO_4^{2-}, Ca^{2+} and other inorganic ions. Cloud water has a similar conductivity to source fresh water [39].

pH

pH values in cloud water droplets are influenced by the solubilization of gaseous carbon dioxide which gives at equilibrium a pH value of 5.6. Other species coming from gaseous (SO_2, HNO_3, NH_3, carboxylic acids) or particulate phase (H_2SO_3, $CaCO_3$) can change this

value after solubilization. The simultaneous presence of many acid and basic compounds, such as nitrates, sulfate, ammonium, carbonates, and many organic acids, such as acetate and formate, leads to a buffer effect. Generally, the pH value is lower for air masses influenced by anthropic emissions caused by the solubilization of SO_2, HNO_3 and carboxylic acids from the gas or the particulate phase [40,41]. Measured pH values are between 2.2 and 7.3 [42].

Inorganic ions

The role of clouds in the atmospheric cycle of inorganic substances has been discussed in many publications in the past [43,44] focusing on the oxidation/transformation of sulfur and nitrogen compounds [45,46]. Several in situ investigations of cloud chemistry have already been reported, and most of them are based on specific single campaigns. These studies showed a high variability in the cloud chemical composition, which is driven by both source proximity and local microphysics. The main inorganic anions in cloud water aqueous phase are chlorides, nitrates, sulfates, sodium, ammonium, magnesium, potassium and calcium. Integrated studies considering different cloud experiments can be difficult, especially because cloud sampling methodologies are not standardized and not easily comparable. Table 1 shows the concentration in µmol L^{-1} of the main ions in cloud water.

Concentration (µmol L^{-1})	**NH_4^+**	**SO_4^{2-}**	**NO_3^-**	**Ca^{2+}**	**Mg^{2+}**	**K^+**	**Na^+**	**Cl^-**
Sellegri (2003) [47]	24-150*	4-40*	12-93*					
Aleksic (2009) [25]	67-175*	58-147*	40-99*	2-21*	1-5*	0.8-3*	1-6*	1-8*
Loflund (2002) [26]	29-491*	11-212*	16-320*	2-39*	0,8-42*	1-20*	3-49*	0-45*
Deguillaume (2014) [27]	4-376*	3-218*	1-516*				1-679*	1-394*
Acker (1998) [28]	472°	156°	360°	25°	12°	1.3°	100°	101°
Guo (2012) [29]	1515°	687°	600°	139°	45°	75°	36°	114°

Table 1: Minimum and maximum values (*) or mean values (°) for ions concentration in cloud water.

There are many sources and sinks of inorganic compounds in atmosphere. Nitrate, sulfate and ammonium ions are abundant, as previously observed by Sellegri et al. at the puy de Dome [47] and during other field campaigns [25,26] and they represent an average contribution to the TIC (Total Ionic Current) from 60 to 80% [47] for air masses with anthropogenic influences. Their contribution to the TIC of marine clouds is much lower (25%), due to the relative high concentrations of sodium and chloride.

The principal source of nitrates (NO_3^-) is nitric acid (HNO_3), which comes, in aqueous phase, from the reaction of pernitric acid (HNO_4) and the hydrogenosulfate ion (HSO_3^-) or by the

hydrolysis of N_2O_5 [48], and in gaseous phase from the oxidation of NO_x. Another source of nitrates is the dissolution of aerosols, in particular of ammonium nitrate particles. In cloud aqueous phase nitrates can be reduced to nitrites (NO_2^-) by photochemical or microbiological processes [49]. Sulfate ions (SO_4^{2-}) can come from the dissolution of sea spray aerosol which contains sodium sulfate (Na_2SO_4) crystals or from the oxidation of reduced sulfur gases, primarily dimethylsulfide (DMS), which is produced by biological activity in the oceans, as well as from SO_2. Sulfate ions can also be produced by oxidation of sulfite ions (SO_3^{2-}) in cloud water in the presence of hydrogen peroxide (H_2O_2), HNO_4 or O_3 [50]. Chloride ions (Cl^-) come principally (35% of global emission [45]) from the dissolution of sea spray aerosols which contains NaCl crystals but there are many other secondary sources: for example potassium chloride (KCl) is emitted by biomass combustions, HCl is emitted by volcanic eruptions and industrial processes and CH_3Cl is produced by biological activity in oceans and seas.

Sodium (Na^+) is mostly emitted as sea salt particles (Na_2SO_4 and NaCl) but it can come also from dust produced in soil erosion or by waste incineration. Ammonium (NH_4^+) comes from the dissolution of ammonium based aerosols (NH_4NO_3 and $(NH_4)_2SO_4$ principally) or from gaseous ammonia (NH_3). Ammonia sources are volatilization of fertilizers, biomass burning and microbial decomposition of N-containing organic matter. Potassium (K^+), magnesium (Mg^{2+}) and calcium (Ca^{2+}) ions are emitted as sea salt as KCl, $MgCl_2$ and $CaCl_2$ but they can also come from soil dust and industrial emissions as secondary sources [51].

As observed before, chemical composition is influenced by the sampling site: observations made at the puy de Dôme station are in agreement with those of Gioda et al. [52] and Reyes-Rodriguez et al. [53] who sampled air masses from the Atlantic Ocean in Puerto Rico and showed similar pH and concentrations of inorganic ions while concentrations found by Blas et al. [54] for cloud water sampled at the "Black Triangle", one of Europe's most industrialized regions, are higher (pH difference = 2.5). In France, measurements of cloud chemical composition in the Vosges mountains show high sulfate and nitrate concentrations attributed to an anthropogenic additional source [55,56]. Aleksic et al. [25] sampled at the Whiteface Mountain, in northeastern United States, and observed a lower concentration than the ones found in puy de Dôme and in Puerto Rico, attributed to a different influence of air masses. The authors [25] made a comparison between cloud and rain water and they observe that the same main ions (sulfate, nitrate, hydrogen and ammonium) are less concentrated in rainwater, especially for ammonium. Lin et al. [57] estimated that concentrations of compounds found in rain water are between 2 and 23 times more diluted that the corresponding concentrations in

cloud water. They also observed that trends of main ions in both cloud and rainwater are not linear and an inter-annual oscillation could be observed.

Since it is very difficult to compare absolute concentrations for different measurement sites for the reasons explained before, it can be helpful to consider the ratios of the concentrations of main ions. The nitrate to sulfate equivalent ratio that increases with the distance from the source of pollution, which makes this value an indicator of the remoteness of a site is particularly interesting [58]. This ratio is highest in polluted clouds due to the high nitrate content in polluted air masses.

The ammonium contribution to the TIC is relatively high in air masses of different origins. Therefore, the pH of cloud water is influenced by ammonium related to emissions from agricultural activities. However, the sum of nitrate and sulfate concentrations is much higher than the ammonium concentration for polluted cases, resulting in partial acid neutralization and acidic cloud water.

The concentration of calcium is higher in polluted and continental air masses than in marine air masses, as a result of the higher contribution of its terrestrial source rather than its marine source.

In marine air masses, the average ratio Cl^- / Na^+ is equal to 1.41 and reaches 1.06 for clouds defined as highly marine, a value that is below that of seawater (1.17) [59]. This loss of chlorine may be caused by the deposit of HCl gas on the sea surface before its absorption by the clouds. For polluted air masses, this ratio is 2.54, resulting from the enrichment of chloride that occurs over polluted areas.

Transition metals

Transition metals ions (TMI) are very common constituents of atmospheric droplets. When aerosol particles act as CCN, soluble metals, present as metal oxide, oxo-hydroxide and silicate particles, dissolve into cloud droplets by undergoing thermal and photochemical processes at the surface of the particles. Various field campaigns report concentrations of dissolved trace metals in rainwater and in cloud water samples [60]. Iron (Fe), manganese (Mn) and copper (Cu) are the most abundant transition metals in the atmospheric liquid water as well as in aerosols. The most striking characteristic of the data is the range of concentrations, which covers 3-4 orders of magnitude, from nM to µM and depending on their solubility, on pH or on ionic strenght. Similar results could be presented for other transition metals, though the data would be less extensive [15].

The major effects of transition metals are principally linked to the homogeneous aqueous phase chemistry. Graedel et al. [61] first attempted to explain the complex redox chemistry of transition metals in atmospheric water through the development of a detailed kinetic model. Their results indicated that transition metals (Cu(I) and Cu(II), Fe(II) and Fe(III) and Mn(II) and Mn(III)) could play an important role in the radical chemistry of the atmospheric water phases. This ability is due to the formation of aqua-complex or complex with organic compounds which facilitate the solubilisation of metals and lead to a catalytic activity in redox cycles of organic and inorganic compounds. For example, Graedel et al. predict that photolysis of Fe(III)-complexes should be important in-cloud sources of $HO^{\bullet}$ radicals, and that transition metals should be the most important sinks and sources of hydroperoxide radical and superoxide radical anion ($HO_2^{\bullet}/O_2^{\bullet-}$). Considering these hypotheses, we can argue that their presence can influence the chemical composition of cloud droplets and the oxidative capacity of cloud aqueous phase.

Organic Matter

Within the ongoing discussion on climate change the role of Organic Carbon (OC) in the atmosphere has gained more attention. Organic matter is present in all atmospheric compartments (gaseous phase, aerosols and cloud droplets). It is estimated that only 20% of the organic matter is directly emitted by the Earth's surface [62], due to its high reactivity in the atmosphere through chemical and photochemical transformations: to give an idea of the complexity of its characterization, 10^5 volatile organic compounds (VOCs) are identified in the atmosphere [63].

Dissolved organic carbon (DOC) refers to the hundreds of dissolved compounds found in water that derive from organic materials and is composed of "organic acids", "organic bases" and "neutral groups". The limit between DOC and particulate organic carbon is set at 0.45 µm. DOC is a mixture of simple substances such as carbohydrates, fatty acids and N-containing compounds, and of complex polymeric molecules. They can be present as truly dissolved molecules or as colloids.

Cloud water DOC was quantified to be in the order of 10 mg L^{-1}. Clouds composition has been studied for decades and several low molecular weight organic species have been detected and are believed to be transferred from the gas phase [64] including formic acid, acetic acid [65,66], glyoxal, methylglyoxal, phenol and nitrophenol [67,68]. Many other compounds were observed in clouds, mostly mono and di-carboxylic acids, alcohols and aldehydes [69]. However a large proportion of cloud water DOC is still uncharacterized.

Chapter 2

Cloud aqueous phase oxidant capacity.

Cloud aqueous phase is a complex atmospheric medium where different kinds of reactivity take place: interface and bulk reactivity need to be taken into account but, recently, mainly bulk reactivity was investigated.

Main transformations are initiated by free radicals or oxidant species which can be generated in the presence of light or in dark conditions. In this work, the attention is focused on the photoproduction of radicals and oxidant species by different precursors: these processes, due to solar irradiation during the day, represent the main production pathway of oxidant species. Their importance decreases during the night, when dark reactions become more important.

Although only photo-initiated reactions were considered in this thesis, dark reactions are briefly described in the next paragraph to better understand their importance in the real environment and their possible occurrence also during the day.

Oxidation in dark conditions

In dark conditions the main oxidative processes in cloud water are Fenton reaction and oxidation by ozone.

The oxidation of organic substrates catalyzed both by Fe^{2+} and H_2O_2 is called the "Fenton chemistry". The Fenton reaction can contribute, significantly, to the production of $HO^{\bullet}$ although its reaction rate is weak (about 50 $M^{-1}s^{-1}$ at 25 °C). However, the importance of the Fenton reaction regarding the production of $HO^{\bullet}$ radicals in solution is still subject to controversy. This $HO^{\bullet}$ radical production by the Fenton reaction has been questioned by several studies which suggest that the reaction between H_2O_2 and Fe^{2+} produces the ferryl ion (Fe^{4+}), which is then the active intermediate species in Fenton chemistry [70]. Nevertheless, the reaction could be resumed as follow (R1).

R1) $Fe^{2+} + H_2O_2 \rightarrow Fe^{3+} + HO^{\bullet} + HO^{-}$

Ozone plays a central role in tropospheric chemistry. It is a highly reactive and toxic species and it absorbs both ultraviolet and infrared light contributing to the greenhouse effect and providing protection from the exposure to UV radiations. Even in dark conditions, ozone can oxidize, as reported by Pitts and Lokensgard in the atmospheric oxidation of benzo-a-pyrene [71]. However, ozone solubility is very low and its importance in the bulk of cloud droplets could be negligible. Concerning the surface chemistry of cloud droplets, only a little information is available.

Photochemistry principles

The absorption of sunlight induces photochemistry and generates a variety of high energy species (triplet states and radicals) that drive the chemistry of both the troposphere and the stratosphere. Photochemical reactions are initiated by the absorption of a photon, typically in the ultraviolet wavelength range of 290-400 nm. The energy of an absorbed photon is transferred to the electrons in the molecule which changes its configuration (*i.e.*, from a ground state to an excited state). In chemistry, the most important electron excitations are those resulting in the dissociation of molecular bonds. In order to induce bond breaking, the energy absorbed by the molecule has to be generally higher than 40 kcal mol^{-1}. The radiations containing this amount of energy are essentially the UV radiations which are almost completely absorbed by ozone in the stratosphere. Thought the quantity of UV radiation reaching the lower troposphere and the surface of the Earth is very small compare to the incoming radiation at the top of the atmosphere, this small amount of UV radiation will be the driving force for most of the photochemical reactions in the troposphere [72].

Photophysical processes are processes in which the excited state which is formed in reaction (R2) undergoes radiative transition (R3) or not-radiative transition in which the energy of the excited molecule is converted into collision or vibrational energy and, finally, into heat (R4). Photochemical processes are the processes in which the excited species dissociate (R5), isomerizes, rearranges (R6) or reacts with another molecule (R7). Finally, the electronically excited molecule can also reacts through photosensitized reactions with the surrounding molecules (R8).

R2)	$AB + h\nu \rightarrow AB^*$	Excitation
R3)	$AB^* \rightarrow AB + h\nu$	Light emission (fluorescence/phosphorescence)
R4)	$AB^* + M \rightarrow AB + M$	Energy conversion by collisions
R5)	$AB^* \rightarrow A + B$	Dissociation
R6)	$AB^* \rightarrow AB^{\S}$	Isomerisation or rearrangement
R7)	$AB^* + C \rightarrow AC + B$	Reaction with another molecule
R8)	$AB^* + M \rightarrow AB + M^*$	Photosensitized reaction

Direct photochemistry indicates dissociation, isomerisation or rearrangement of a molecule in an excited state. This is a key process in the production of radicals in atmosphere for both gaseous and condensed phase. Moreover, as mentioned before, an excited molecule can react through photosensitized reactions with other molecules, meaning that the excited molecule induces photochemical reactions in molecules that are not photochemically reactive (they

don’t absorb sunlight). This kind of reactivity is defined as photosensitized reactivity or indirect photolysis.

Many organic compounds are thermodynamically unstable in the presence of oxygen; however, their rate of spontaneous oxidation is slow at room temperature. From a physico-chemical point of view, such reactions are kinetically limited. Molecular oxygen can be photosensitized by a large number of molecules through energy transfer from their triplet state to form $^3O_2$ and finally singlet oxygen ($^1O_2$). For this reason, oxygen is considered as an oxidant even if it absorbs sunlight only at the top of the atmosphere, where wavelengths in the range of 200-240 nm are available.

In condensed phase, the photochemical excitation of a chromophore is often followed by an electron transfer or an H-transfer: this kind of indirect photolysis is theoretically different from photosensization and energy transfer, even if it could be a simultaneous process, and leads to the production of the superoxide radical anion ($O_2^{\bullet-}$), for example.

Photochemistry in cloud water

Homogeneous photochemistry is not limited to gas-phase reactions, but can also take place in the liquid phase. Cloud droplets can undergo chemical changes through photochemical reactions because they receive a considerable amount of sunlight. Organic molecules in the atmosphere, in gas or in condensed phase, are susceptible to undergo chemical or photochemical reaction after their formation or emission. These kinds of reactions include oxidative and not-oxidative pathways which can happen in the gas phase, on aerosol surface or in the aqueous phase. Under natural conditions, where irradiation occurs simultaneously with gas phase oxidation, it is often very difficult to distinguish the part of gas phase photochemistry from the photochemistry in the condensed phases as both are so entwined. The main photosensitizer in natural waters is chromophoric dissolved organic matter (CDOM), while nitrates (NO_3^-), nitrites (NO_2^-) and iron, that are responsible for Fenton and photo-Fenton processes, are other important sources of photogenerated radicals. Degradation of organic compounds in cloud aqueous phase is generally initiated by inorganic radicals or by hydrogen peroxide (H_2O_2) and ozone (O_3) [73]. Many radicals are produced in liquid phase such as ionic radicals: like sulfate (R12), dichlorine (R14−16), dibromine (R17−19), sulphite (R11) and superoxide radical anion ($SO_4^{\bullet-}$, $Cl_2^{\bullet-}$, $Br_2^{\bullet-}$ and $SO_3^{\bullet-}$ and $O_2^{\bullet-}$ respectively). Moreover, neuter radicals, like hydroxyl radical ($HO^{\bullet}$), nitrite radical ($NO_2^{\bullet}$) (R9), nitrate radical ($NO_3^{\bullet}$) (R10) and superoxide radical ($HO_2^{\bullet}$), can diffuse from the gas phase (gas to liquid transfer) or can be produced directly in the aqueous phase. The comparison between

oxidation potentials of each species gives reactivity that increase with the redox potential reported in Table 2.

Radical	E (V)
$HO^{\bullet}$	2.7 [74]
$NO_3^{\bullet}$	2.3 ÷ 2.6 [75]
$SO_4^{\bullet-}$	2.43 [74]
$Cl_2^{\bullet-}$	2.41 [74]
$Br_2^{\bullet-}$	1.69 [74]

Table 2: Redox potential of main oxidant species in the aqueous phase.

The main production pathway of oxidant species is the reaction between $HO^{\bullet}$ and the corresponding inorganic anion.

R9) $HO^{\bullet} + NO_2^- \rightarrow NO_2^{\bullet} + HO^-$ $k_9 = 6.0\times10^9 \div 1.4\times10^{10}\ M^{-1}s^{-1}$ *

R10) $HO^{\bullet} + NO_3^- \rightarrow NO_3^{\bullet} + HO^-$ $k_{10} = 1.1\times10^{10}\ M^{-1}s^{-1}$ *

R11) $HO^{\bullet} + HSO_3^- \rightarrow SO_3^{\bullet-} + H_2O$ $k_{11} = 4.5\times10^9\ M^{-1}s^{-1}$ *

R12) $HO^{\bullet} + HSO_4^- \rightarrow SO_4^{\bullet-} + H_2O$ $k_{12} = 3.5\times10^5 \div 1.7\times10^6\ M^{-1}s^{-1}$ *

R13) $SO_4^{\bullet-} + NO_3^- \rightarrow SO_4^{2-} + NO_3^{\bullet}$ $k_{13} = 5.0\times10^4 \div 2.0\times10^6\ M^{-1}s^{-1}$ *

R14) $HO^{\bullet} + Cl^- \rightleftarrows ClOH^{\bullet-}$ $k_{14} = 3.0 \div 4.3\times10^9\ M^{-1}s^{-1}$ *

R15) $Cl^{\bullet} + H_2O \rightleftarrows ClOH^{\bullet-} + H^+$ $k_{15} = 2.5\times10^5\ M^{-1}s^{-1}$ *

R16) $Cl^{\bullet} + Cl^- \rightarrow Cl_2^{\bullet-}$ $k_{16} = 8.0\times10^9\ M^{-1}s^{-1}$ *

R17) $HO^{\bullet} + Br^- \rightleftarrows BrOH^{\bullet-}$ $k_{17} = 1.1\times10^{10}\ M^{-1}s^{-1}$ *

R18) $Br^{\bullet} + H_2O \rightleftarrows BrOH^{\bullet-} + H^+$

R19) $Br^{\bullet} + Br^- \rightarrow Br_2^{\bullet-}$ $k_{19} = 1.0\times10^{10}\ M^{-1}s^{-1}$ *

* Constants from NIST (National Institute of Standard and Technology) Solution Kinetics Database.

$Br_2^{\bullet-}$ and $Cl_2^{\bullet-}$ have a weak impact due to their low concentrations and reactivity while $SO_4^{\bullet-}$ has an important effect on reaction with transition metal ions (TMI), halogenated and S-containing compounds [30]. In most cases, the second order rate constant between these radicals and organic compounds is lower than the one between $HO^{\bullet}$ and organic compounds (generally one or two orders of magnitude) [76]. $NO_3^{\bullet}$ is a strong oxidant during nighttime while its concentration during the day is very low because it is photolysed in the gas phase [45]. $HO^{\bullet}$ is the main oxidant in the atmosphere, especially during the day, and is the most important way of transforming organic compounds in cloud water [30].

Main oxidants in cloud water

In this chapter, the oxidative capacity of H_2O_2, $NO_3^{\bullet}$ and $HO^{\bullet}$, which are the most important oxidants in cloud water, will be described. Ozone will not be considered in this work because of its low solubility which hinders its transfer from the gas to the liquid phase (K_H = 1.2 × 10^{-2} M atm^{-1}).

Hydrogen peroxide

Sources in gas and liquid phase

Gaseous H_2O_2 is formed from the radical-radical reaction of hydroperoxyl ($HO_2^{\bullet}$) (R20) and/or hydrated hydroperoxyl ($HO_2^{\bullet}$−H_2O) radicals (R21−24), which are produced by the photochemical reactions of atmospheric trace gases such as ozone and volatile organic compounds [77]. Hydrogen peroxide in cloud droplets originates both from gas-to-liquid partitioning of H_2O_2 and $HO_2^{\bullet}$ and from aqueous-phase photo-production. The first situation has traditionally been considered as the predominant source [66] because of the high solubility of H_2O_2 (K_H = 1.0 × 10^5 M atm^{-1}) [78] and of $HO_2^{\bullet}$ (K_H = 2.0±1.0 × 10^3 M atm^{-1}), while other studies support the hypothesis that light absorbing compounds present in cloud droplets can initiate aqueous phase photochemical reactions resulting in the formation of H_2O_2 [79-82]. Several mechanisms have been proposed for the H_2O_2 photoproduction in atmospheric water drops but only on the basis of laboratory experiments. For example the oxidation of transition metal ions (TMI) by radical species leads to the formation of H_2O_2 (R25−27): this is the case of the iron-oxalate complex which is usually used as a model to describe the action of organic iron complexes in cloud aqueous phase. Even if the role of this complex is the subject of debate, the irradiation of cloud water leads to an increase in the concentration of H_2O_2 and Fe(II) [83]. The photolysis of phenolic compounds [79] and biacetyl compounds [84] was also proposed as a source of H_2O_2. Zuo and Deng observed that substantial amounts of H_2O_2 were produced by lightning activities during thunderstorms [85]. Another production pathway is the photolysis of organic peroxides, in particular of the methyl hydroperoxide normally present in water droplets. This photolysis is a source of $HO^{\bullet}$ which leads to the formation of formaldehyde and $HO_2^{\bullet}$ which are sources of H_2O_2 (R28−29).

R20) $HO_2^{\bullet} + HO_2^{\bullet} \rightarrow H_2O_2 + O_2$ $k_{20} = 8.3\times10^5$ $M^{-1}s^{-1*}$

R21) $HO_2^{\bullet} + H_2O \rightarrow (HO_2^{\bullet}{-}H_2O)$ $k_{21} = 9.7\times10^7$ $M^{-1}s^{-1*}$

R22) $HO_2^{\bullet} + (HO_2^{\bullet}{-}H_2O) \rightarrow H_2O_2 + O_2 + H_2O$ $k_{22} = 9.6\times10^7$ $M^{-1}s^{-1*}$

R23) $(HO_2^{\bullet}{-}H_2O) + (HO_2^{\bullet}{-}H_2O) \rightarrow H_2O_2 + O_2 + 2H_2O$ $k_{23} = 9.6\times10^7$ $M^{-1}s^{-1*}$

R24) $HO_2^{\bullet} \rightleftarrows O_2^{\bullet-} + H^+$ $pk_a = 4.88$

R25) $Fe(II) + O_2^{\bullet-} + 2H^+ \rightarrow Fe(III) + H_2O_2$ $k_{25} = 1.2 \div 2.1\times10^6\ M^{-1}s^{-1}$ *

R26) $Fe(II) + O_2 \rightarrow Fe(III) + O_2^{\bullet-}$ pH dependent

R27) $O_2^{\bullet-} + HO_2^{\bullet} + H_2O \rightarrow H_2O_2 + O_2 + HO^-$ $k_{27} = 9.7\times10^7\ M^{-1}s^{-1}$*

R28) $CH_3OOH + h\nu \rightarrow CH_3O^{\bullet} + HO^{\bullet}$

R29) $CH_3O^{\bullet} + O_2 \rightarrow H_2CO + HO_2^{\bullet}$

* Constants from NIST (National Institute of Standard and Technology) Solution Kinetics Database.

Concerning real cloud water, many modeling studies affirm that the main source of $HO^{\bullet}$ comes from the gas phase mass transfer while secondary sources are divided between H_2O_2 photolysis and Fenton like reactions according to the different scenarios.

Steady state concentration

In the gas phase the concentration of H_2O_2 is in the range of 0.1-2 pptv (parts per trillion in volume) but many authors report also higher values [86]. A negative correlation with the concentration of NO_x was found. The half-life time in the gas phase is of 24 h [72] and Valverde Canossa [87] observed a daily cycle, a dependence of the concentration on the actinic radiation. Previous measurements at the puy de Dôme station show that H_2O_2 concentrations in the cloud aqueous phase ranges from 0.3 µM to 20 µM [23], while a study on cloud water sampled in Los Angeles shows concentrations up to 88 µM [88].

Sinks in gas and liquid phase

The main removal mechanisms for H_2O_2 from the gas phase are the photolysis of H_2O_2 ($\lambda <$ 370 nm) (R30), the reaction with $HO^{\bullet}$ (R31) and the gas to liquid phase transfer since H_2O_2 is a very soluble species that readily dissolves in the atmospheric waters. Moreover, all reactions leading to the consumption of $HO_2^{\bullet}$, such as the oxidation of $NO^{\bullet}$ [89] (R32) or the reaction with O_3 (R33−34), can impact on H_2O_2 gaseous concentrations.

R30) $H_2O_2 + h\nu \rightarrow 2HO^{\bullet}$

R31) $H_2O_2 + HO^{\bullet} \rightarrow HO_2^{\bullet} + H_2O$ $k_{31} = 3.2\times10^7\ M^{-1}s^{-1}$*

R32) $HO_2^{\bullet} + NO^{\bullet} \rightarrow NO_2^{\bullet} + HO^{\bullet}$ $k_{32} = 8.8 \times 10^{-12}\ cm^3\ molecules^{-1}\ s^{-1}$ [45]

R33) $HO_2^{\bullet} + O_3 \rightarrow 2O_2 + HO^{\bullet}$ $k_{33} = < 1.0\times10^4\ M^{-1}s^{-1}$*

R34) $HO_2^{\bullet} + O_3 \rightarrow HO_3^{\bullet} + O_2$ $k_{34} = 1.5\times10^9\ M^{-1}s^{-1}$*

* Constants from NIST (National Institute of Standard and Technology) Solution Kinetics Database.

In the gas phase, photolysis leads to a significant loss of peroxides in the troposphere (R30), although the absorption drops rapidly at wavelength above the actinic cutoff of 290 nm. The

quantum yield is of two $HO^{\bullet}$ for each H_2O_2, corresponding to a photodissociation quantum yield of 2 at wavelengths > 222 nm [90]. In condensed phase the quantum yield is lower because the formed radicals have a higher probability of recombining due to the cage solvent effect. Moreover, in cloud aqueous phase, H_2O_2 can be consumed by Fenton processes. Many other inorganic compounds seem to have an impact on the disappearance of H_2O_2: Zuo and Deng found an inverse correlation between H_2O_2 and NO_3^- and SO_4^{2-} concentrations in rainwater and cloud water. This phenomenum is explained by the oxidation of sulfites (S(IV)) to sulfates (S(VI)) and of ammonium (NH_4^+) to nitrates, where the role of H_2O_2 (directly or as a $HO^{\bullet}$ source) is important at typical hydrometeor pH values.

Nitrate radical

Sources in gas phase

The nitrate radical $NO_3^{\bullet}$ is an important intermediary in nighttime chemistry. It is produced in the gas phase by the reaction between $NO_2^{\bullet}$ and O_3 (R35) or between $HO^{\bullet}$ and HNO_3 (R36).

R35) $NO_2^{\bullet}{}_{(g)} + O_{3(g)} \rightarrow NO_3^{\bullet}{}_{(g)} + O_{2(g)}$

R36) $HO^{\bullet}{}_{(g)} + HNO_{3(g)} \rightarrow NO_3^{\bullet}{}_{(g)} + H_2O_{(g)}$

Steady state concentration and sinks

$NO_3^{\bullet}$ absorbs strongly in the red region (620−670 nm) of the visible spectrum, unlike most atmospherically important species which absorb in the UV region. Due to this absorption, during the day it photolyses giving $NO_2^{\bullet}$ or $NO^{\bullet}$ (R37−38).

The spectroscopic proprieties of $NO_3^{\bullet}$ allow a good estimation of its concentration in the dry troposphere during the day (10^4 molecules cm^{-3}) and during the night (10^9 molecules cm^{-3}) [72]. In the case of wet air, $NO_3^{\bullet}$ reacts with $NO^{\bullet}$ to give N_2O_5 which in the presence of water forms HNO_3, responsible for acid fog and rain (sink of nitrate radical by wet deposition) [91]. The exchange of $NO_3^{\bullet}$ with the aqueous−phase was investigated by Thomas et al [92] at room temperature (293 K). From these experiments, the uptake coefficient of $NO_3^{\bullet}$ ($\gamma(NO_3^{\bullet})$) was found to be $\geq 2 \times 10^{-3}$ while the Henry coefficient was estimated to be $K_{H(NO_3^{\bullet})} = 1.8 \pm 3$ M atm^{-1}. Because of its low solubility, the heterogeneous removal of $NO_3^{\bullet}$ is only important under conditions when the dissolved $NO_3^{\bullet}$ is removed quickly from the equilibrium, for example by reactions with Cl^- or HSO_3^- ions (R39−40) in the liquid−phase. Otherwise, heterogeneous removal should mainly proceed via N_2O_5 [92], with production of HNO_3 and consequent inactivation of this radical in condensed phase.

R37) $NO_3^{\bullet} + h\nu < 635\ nm \rightarrow NO_2^{\bullet} + O(^1D)$

R38) $NO_3^{\bullet} + h\nu < 586\ nm \rightarrow NO^{\bullet} + O_2$

R39) $NO_3^{\bullet} + Cl^- \rightarrow Cl^{\bullet} + NO_3^-$ $k_{38} = 1.0 \times 10^7 \div 1.0 \times 10^8\ M^{-1}s^{-1}$ *

R40) $NO_3^{\bullet} + HSO_3^- \rightarrow SO_3^{\bullet -} + NO_3^- + H^+$ $k_{39} = 1.4 \div 2.0 \times 10^9\ M^{-1}s^{-1}$ *

* Constants from NIST (National Institute of Standard and Technology) Solution Kinetics Database.

Hydroxyl radical

The hydroxyl radical drives the daytime chemistry of both polluted and clean atmosphere. The $HO^{\bullet}$ - mediated oxidation of organic compounds in the aqueous phase can lead to the formation of shorter but often multifunctional organic species and, ultimately, to complete mineralization. Complex chemical reactions catalyzed by $HO^{\bullet}$ can also occur in the aqueous phase forming accretion products such as oligomers [62]. These alternative chemical pathways are efficient processes to convert organic compounds into Secondary Organic Aerosols (SOAs).

$HO^{\bullet}$ can be produced in the gas phase and then diffuse to the liquid phase or it can be directly produced in the aqueous phase. On the contrary of what was previously described for the nitrate radical, the hydroxyl radical can diffuse to the aqueous phase after its production in the gas phase ($K_{H(HO\bullet)} = 3.0 \pm 0.2\ M\ atm^{-1}$) [93]. In the following paragraph the main sources are described.

Sources in the gas phase

The hydroxyl radical is produced in the gas phase by photolysis of O_3 and subsequent reaction between $O(^1D)$ (electronically excited singlet atom) and H_2O (R41−42) or by photolysis of HNO_2 (R43) and H_2O_2 (R44). Without light, a very important source is the reaction between $HO_2^{\bullet}$ and $NO^{\bullet}$ (R45). The relative importance of these sources of $HO^{\bullet}$ depends on the species present in the air mass and hence on the location and the time of the day.

R41) $O_3 + h\nu < 340\ nm \rightarrow O(^1D) + O_2$

R42) $O(^1D) + H_2O_{(g)} \rightarrow 2HO^{\bullet}_{(g)}$ $k_{42} = 1.8 \times 10^{10}\ M^{-1}s^{-1}$ [94]

R43) $HNO_{2(g)} + h\nu < 370\ nm \rightarrow NO^{\bullet}_{(g)} + HO^{\bullet}_{(g)}$

R44) $H_2O_{2(g)} + h\nu < 370\ nm \rightarrow 2\ HO^{\bullet}_{(g)}$

R45) $HO_2^{\bullet}{}_{(g)} + NO^{\bullet}_{(g)} \rightarrow OH^{\bullet}_{(g)} + NO_2^{\bullet}{}_{(g)}$ $k_{45} = 9.7 \times 10^{-12}\ cm^3\ molecules^{-1}\ s^{-1}$ [95]

Ozone can react directly on the gas-aqueous interface with $HO_2^{\bullet}$ or with $O_2^{\bullet -}$ to produce $HO^{\bullet}$ [96] following the reactions R46−49. These pathways could be important at the gas-droplet interface.

R46) $O_2^{\bullet-} + H_3O^+ \rightarrow HO_2^{\bullet} + H_2O$ $k_{46} = 5.0 \div 7.2\times10^{10}\ M^{-1}s^{-1*}$ pKa 4.88

R47) $HO_2^{\bullet} + O_3 \rightarrow HO^{\bullet} + 2O_2$ $k_{47} = < 1.0\times10^{4}\ M^{-1}s^{-1*}$

R48) $O_3 + O_2^{\bullet-} \rightarrow O_2 + O_3^{\bullet-}$ $k_{48} = 1.5 \div 1.6\times10^{9}\ M^{-1}s^{-1*}$

R49) $O_3^{\bullet-} + H^+ \rightarrow OH^{\bullet} + O_2$ $k_{49} = 9.0\times10^{10}\ M^{-1}s^{-1*}$

* Constants from NIST (National Institute of Standard and Technology) Solution Kinetics Database.

The concentration in the gas phase in the dry troposphere during the day is estimated to be of the order of 10^6 molecules cm^{-3} [72].

Sources in the aqueous phase

The sources of hydroxyl radicals in the aqueous phase strongly differ from those in the gas phase because of the presence of ionic species and metal ions.

Hydrogen peroxide

An important source is the photolysis of H_2O_2: the reaction (R44) is the same described for the gas phase in the previous paragraph. An estimation of the quantum yield in the range of wavelength between 200 and 400 nm is estimated to be of the order of 0.8-1.2 as shown in Figure 5, as reported by Herrmann and Hoffmann [30].

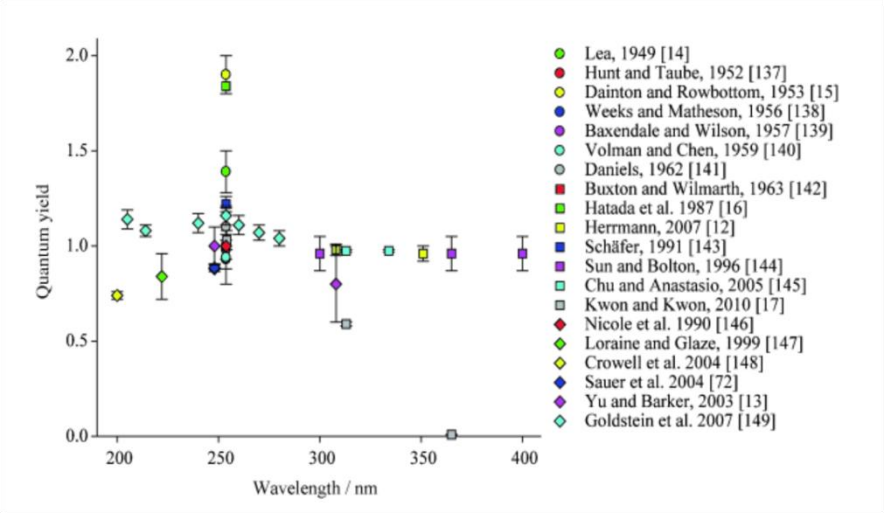

Figure 5: Summary of $HO^{\bullet}$ quantum yields (Φ_{OH}) for H_2O_2 photolysis in aqueous solution at different photolysis wavelengths (from Herrmann and Hoffmann [30]).

Iron photochemistry

Other possible sources of $HO^{\bullet}$ are Fenton or iron photolysis. From an atmospheric point of view, iron is probably the most significant transition metal because of its concentration, which is, in general, much higher than that of other metals. Its concentration is $\sim10^{-6}$ M, but many field experiments indicate that it can vary from 10^{-9} to 10^{-6} M in raindrops and cloud droplets

[61]. The concentration of iron drives the concentration of radicals in cloud droplets, but also partly in the gaseous phase (due to the rate of the mass transfer). In cloud aqueous phase, the redox cycle between Fe(II) and Fe(III) depends on many factors such as the concentration of oxidant, reducing and complexing agents and the intensity of the actinic irradiation. The iron redox cycle is linked to the chemistry of H_xO_y (H_2O_2, $HO^\bullet$, $HO_2^\bullet$/ $O_2^{\bullet-}$), and the main chemical pathways driving the reactivity of the H_xO_y/iron system in cloud water are presented in Figure (left). Iron(III) is present in 3 monomeric forms: Fe^{3+}, $Fe(OH)^{2+}$ and $Fe(OH)_2^{+}$. In cloud droplets, the speciation of iron between its two oxidation states (II and III) is a key parameter of its reactivity in solution and is a function of pH and redox potential, as shown in Figure 6Figure (right). Fe(II) is oxidized by hydrogen peroxide via the Fenton reaction (R51) to form Fe(III) and $HO^\bullet$. Under irradiation, this reaction is in competition with the direct photolysis of H_2O_2 (R44) and the photoreduction of Fe(III) (R50) [97]. Furthermore, as shown in Figure 6, hydroxyl radicals can oxidize iron (reaction D′) and react with hydrogen peroxide to form $HO_2^\bullet$/ $O_2^{\bullet-}$. These radicals can trigger the oxido-reduction of iron (reactions E and E′) and generate H_2O_2. Also iron complexes, like the iron-oxalate complex, can undergo Fenton reaction, as shown in reaction R52. The relevance of iron photochemistry in hydroxyl radical production is high, in particular for air masses of continental origin, but need to be quantified.

R50) $Fe^{(III)}(OH)^{2+} + h\nu \rightarrow Fe^{2+} + HO^\bullet$

R51) $Fe^{(II)}(OH)^{+} + H_2O_2 \rightarrow Fe(OH)^{2+} + HO^\bullet + HO^-$

R52) $Fe^{(II)}(C_2O_4) + H_2O_2 \rightarrow Fe(C_2O_4)^{+} + HO^\bullet + HO^-$

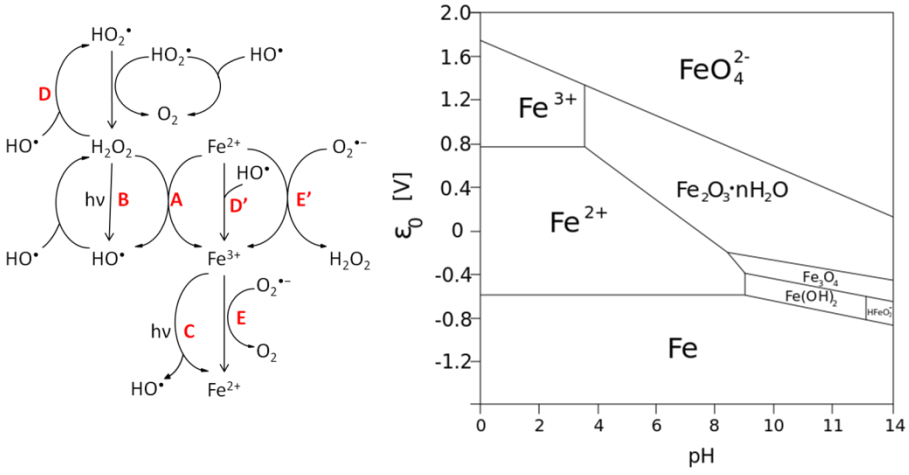

Figure 6: (left) Iron chemistry and photochemistry (adapted from Barbusinski et al. [98])
(right) Pourbaix diagram of iron: speciation is a function of pH and redox potential.

Nitrate and nitrite photolysis

As discussed in Chapter 1, many studies report the concentration of nitrates in cloud water. Nitrate photolysis was firstly investigated in seawater [99]. Nitrates can absorb sunlight and their photolysis gives $NO_2^{\bullet}$ and $O^{\bullet-}$ or $O(^3P)$ (ground state oxygen atom) (R53−56), which is responsible for the formation of $HO^{\bullet}$. $NO_2^{\bullet}$ reacts following many pathways (R57−64) and produces nitrite anions NO_2^-.

R53) $NO_3^- + h\nu \rightarrow NO_2^{\bullet} + O^{\bullet-}$

R54) $NO_3^- + h\nu \rightarrow NO_2^- + O(^3P)$ $\Phi_{305nm} = 1.1 \pm 0.1 \times 10^{-3}$ [100]

R55) $O^{\bullet-} + H_2O \rightarrow HO^- + HO^{\bullet}$

R56) $O(^3P) + H_2O \rightarrow 2HO^{\bullet}$

R57) $NO_2^{\bullet} + HO^{\bullet} \rightarrow HNO_3$

R58) $HNO_3 + h\nu \rightarrow NO_3^- + H^+$

R59) $HNO_3 + h\nu \rightarrow NO_2^{\bullet} + HO^{\bullet}$

R60) $NO_2^{\bullet} + O_2^{\bullet-} \rightarrow NO_2^- + O_2$

R61) $2NO_2^{\bullet} \rightarrow N_2O_4$

R62) $2NO_2^{\bullet} + H_2O \rightarrow NO_2^- + NO_3^- + 2H^+$

R63) $N_2O_4 + H_2O \rightarrow NO_2^- + NO_3^- + 2H^+$

R64) $NO_2^- + HO^{\bullet} \rightarrow NO_2^{\bullet} + HO^-$

Nitrous acid (HNO_2) is a compound normally studied in the gaseous phase because it is strictly connected to the NO_x cycle. Cloud and fog droplet could be sinks of HNO_2 from the gaseous phase because of its high value of Henry's law constant ($K_{H(HNO_2)}$ = 50 M atm^{-1}). Nitrous acid in droplets can undergo photolysis as in the gas phase (R65−67) but, more probably, it follows another reaction pathway: at water droplet pH values, nitrous acid is present in the deprotonated form, nitrite. Even if the concentration is very low (of the order of 0.1 μM), nitrites can absorb sunlight more efficiently than nitrates and they photogenerate $HO^{\bullet}$ following the reactions R68−R70.

R65) $2NO_{2(g)} + H_2O_{(g)} \rightarrow HNO_{2(g)} + HNO_{3(g)}$

R66) $NO_{(g)} + NO_{2(g)} + H_2O_{(g)} \rightarrow 2HNO_{2(g)}$

R67) $HNO_{2(g)} + h\nu \rightarrow NO^{\bullet} + HO^{\bullet}$

R68) $HNO_2 \rightleftarrows H^+ + NO_2^-$ pk_a=3.35

R69) $NO_2^- + h\nu \rightarrow NO^{\bullet} + O^{\bullet-}$

R70) $O^{\bullet-} + H_2O \rightarrow HO^- + HO^{\bullet}$

Main generation and destruction pathways are resumed in Figure 7.

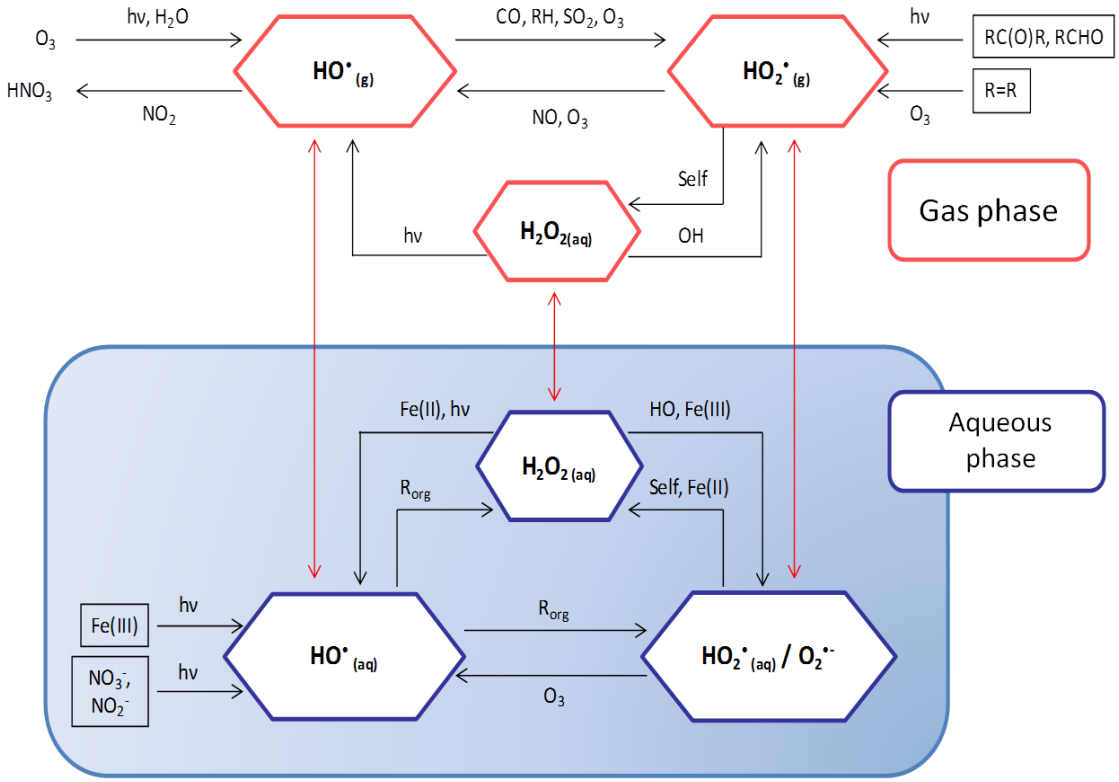

Figure 7: Main hydroxyl radical generation and destruction pathways (with kind permission of Deguillaume).

Reactivity

The reaction of $HO^{\bullet}$ with ions is often described as a simple electron transfer (R71), but such a simple process is unlikely because of the large solvent reorganization energy involved in forming the hydrated hydroxide ion. Instead, it is suggested that an intermediate adduct is formed. Such an adduct is observed in the oxidation of halide and pseudo-halide ions, (R72). Although there are several examples of $HO^{\bullet}$ reacting with inorganic ions at the diffusion controlled rate, rate constants for oxidation of many metal cations seem to be no more than $\sim 3 \times 10^8\ M^{-1}s^{-1}$. A suggested reason for this is that $HO^{\bullet}$ abstracts H from a coordinated water molecule and this is followed by an electron transfer from the metal to the oxidized ligand (R73).

In strongly alkaline solution $HO^{\bullet}$ is rapidly converted into its conjugate base $O^{\bullet-}$, with a pKa value of 11.9 (R74)

In its reactions with organic molecules $HO^{\bullet}$ behaves as an electrophile whereas $O^{\bullet-}$ is a nucleophile and it is generally less reactive. This species is important at pH values higher than 12 and it will not be considered in this work.

R71) $HO^{\bullet} + Fe^{2+} \rightarrow Fe^{3+} + HO^{-}$

R72) $HO^{\bullet} + Cl^{-} \rightleftarrows HClO^{\bullet -}$

R73) $HO^{\bullet} + Fe^{2+} \rightarrow Fe^{2+}HO^{\bullet} \rightarrow Fe^{3+} + OH^{-}$

R74) $HO^{\bullet} + HO^{-} \rightleftarrows O^{-} + H_2O$ pKa = 11.5 [76]

$HO^{\bullet}$ reacts by different pathways (double bond addition, hydrogen abstraction, electron transfer and aromatic ring addition) with organic molecules, as schematized in Figure 8:

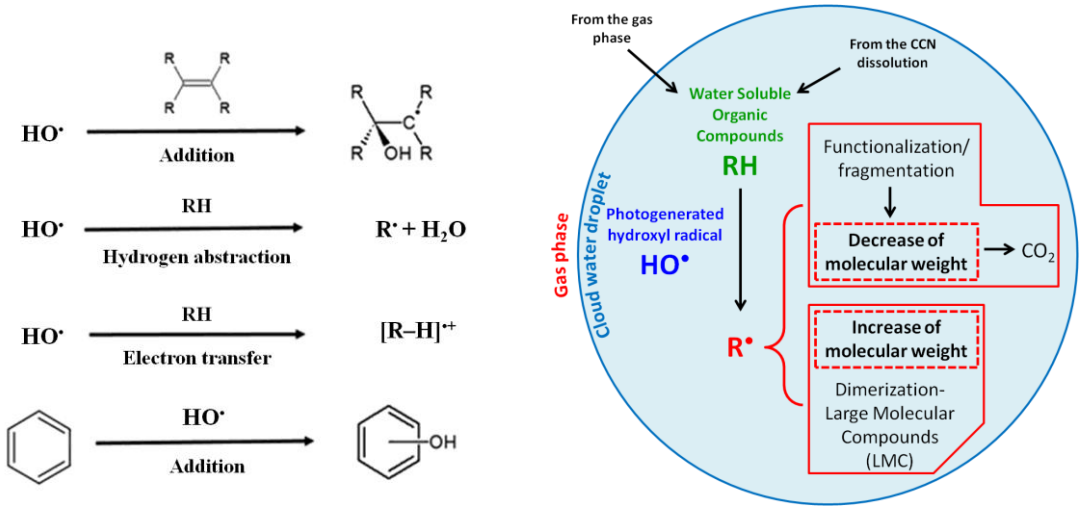

Figure 8: $HO^{\bullet}$ reaction pathway (left) and becoming of organic compounds after reaction (right).

Hydroxyl radical mediated oxidation of organic compounds can lead to the fragmentation or to the formation of oxidized organic species, introducing different functional group, to result in the complete mineralization to CO_2. But another pathway is possible: when water evaporates and solutes become more concentrated, the recombination of organic radicals becomes possible. The result is the formation of dimers, oligomers or, in general, Large Molecular Compounds, as shown in Figure (right). The competition between fragmentation and formation of high weight molecular compounds is well known for oxalic acid that by reacting with hydroxyl radical can mineralize to carbon dioxide or dimerize [101].

Hydroxyl radical sinks

The hydroxyl radical is an important oxidant in atmospheric aqueous phase, where it reacts with both organic and inorganic species. $HO^{\bullet}$ is scavenged in the aqueous phase, primarily by dissolved organic compounds: for example, the $HO^{\bullet}$-mediated oxidation of aqueous glyoxal, glyoxylic acid, and other small, multifunctional organic compounds produces low-volatile secondary organic aerosol species such as oxalic acid and oligomers. The lifetime of an aqueous species "S" considering the reactivity with hydroxyl radical is inversely proportional to the steady-state concentration of $HO^{\bullet}$, generally expressed by the Equation 5:

$$\tau = \frac{1}{k_{S,HO\bullet} \times [HO^{\bullet}]_{ss}}$$

Equation 5: Hydroxyl radical steady state concentration.

where $k_{S,HO\bullet}$ is the bimolecular rate constant between S and $HO^{\bullet}$. Thus, the steady-state concentration of $HO^{\bullet}$ ($[HO^{\bullet}]_{ss}$) is a crucial quantity for understanding the fates of atmospheric pollutants. This concentration is determined by the balance of the $HO^{\bullet}$ sources and sinks, reported in Equation 6

$$[HO^{\bullet}]_{ss} = \frac{P_{HO\bullet}}{k'_{HO\bullet}}$$

Equation 6: Hydroxyl radical mass balance.

where $P_{HO\bullet}$ is the rate of production of $HO^{\bullet}$ and $k'_{HO\bullet}$ is the apparent first-order rate constant for loss of $HO^{\bullet}$ (s^{-1}). Since there are many scavengers for $HO^{\bullet}$, the rate constant for $HO^{\bullet}$ loss is the sum of the individual scavenger contributions, and can be calculated, as reported in Equation 7 as the product of the bimolecular rate constant and the scavenger concentration for each species

$$k'_{HO\bullet} = \sum (k_{S,HO\bullet} \times [S])$$

Equation 7: First-order rate constant for loss of $HO^{\bullet}$ (s^{-1}).

Determining the rate constant for $HO^{\bullet}$ loss in this manner is a herculean task since atmospheric drops and particles can contain on the order of 10^4 individual organic compounds, as well as significant concentrations of poorly characterized, large molecular weight species such as humic-like substances [102]. In contrast, the most sophisticated numerical models of atmospheric waters track the reactions of fewer than 100 individual organic compounds, with none larger than four carbon atoms.

Arakaki et al. found that the $HO^{\bullet}$ sink can be simply estimated by a general carbon rate constant that is applicable both for atmospheric waters as well as surface waters, which allows $k'_{HO\bullet}$ to be estimated by using organic carbon concentrations [103]. Their results show that the scavenging rate constant of $HO^{\bullet}$ by organic species in atmospheric waters can be simply estimated as the product of a robust general rate constant ($k_{DOC,HO\bullet}$) multiplied by the dissolved organic carbon concentration of the sample, as reported in Equation 8.

$$k'_{HO\bullet} = k_{DOC,HO\bullet} \times [DOC]$$

Equation 8: First order rate constant for hydroxyl radical loss as a function of the general second order rate constant between hydroxyl radical and DOC.

In the work of Arakaki et al. [103], $k_{DOC,HO^{\bullet}}$ is estimated to be of the order of 3.8 ± 1.9 × 10^8 L $molC^{-1}$ s^{-1}.

Steady state concentration

Uncertainties in $HO^{\bullet}$ sinks and sources make its concentrations in atmospheric water highly difficult to determine. For this estimation, models describing the multiphase cloud chemistry have been developed and have considered the reactivity in the gas and aqueous phases along with the mass transfer between the two phases [97,104,105]. These numerical tools allow the estimation of the steady−state concentration of $HO^{\bullet}$ ($[HO^{\bullet}]_{ss}$), which is a crucial quantity to understand the fate of atmospheric pollutants [103]. The range of the maximal $HO^{\bullet}$ concentration varies from 10^{-16} to 10^{-12} M, depending on the "chemical scenario" (*i.e.*, emission/deposition and the initial chemical conditions) used in the modeling study, as shown in Table 3, where the estimation of the $HO^{\bullet}$ steady state concentration for different air mass origins is reported. The amounts of organic matter and iron are key parameters controlling the $[HO^{\bullet}]_{ss}$. These models are expected to underestimate the radical sinks because organic scavengers cannot be exhaustively described in the aqueous chemical mechanism [103].

Polluted origin cloud water $[HO^{\bullet}]$ (M)			Remote origin cloud water $[HO^{\bullet}]$ (M)			Marine origin cloud water $[HO^{\bullet}]$ (M)		
mean	max	min	mean	max	min	mean	max	min
3.5×10^{-15}	1.6×10^{-14}	2.9×10^{-16}	2.2×10^{-14}	6.9×10^{-14}	4.8×10^{-15}	2.0×10^{-12}	5.3×10^{-12}	3.8×10^{-14}

Table 3: Calculated $HO^{\bullet}$ radical concentrations in clouds and deliquescent particles using the CAPRAM 3.0 multiphase mechanism. Mean concentrations are averaged values over three simulation days. Data adapted from Herrmann et al. [30].

Chapter 3

Organic matter in clouds

Cloud droplets efficiently scavenge and modify water-soluble compounds and, thus, modify the chemical composition of gas and particle phases. The concentration of DOC in aqueous phase reaches concentrations of the order of 10 mgC L^{-1} [1]. A number of attempts have been made to obtain a mass balance of organic carbon in cloud water but to date no conclusive identification of individual components is available [103]. In addition, the organic carbon in an atmospheric liquid sample is expected to be a very complex mixture [26]. As said before, cloud droplets are formed by condensation of water on CCNs, which contain in most cases a large amount of organic matter that can be dissolved by the liquid phase. Water-soluble organic carbon (WSOC) may comprise up to 70% of the total organic aerosol mass [106] and so a large fraction of the WSOC may partition to the aqueous phase. Moreover, suspended droplets are subject to the gas-liquid equilibrium of volatile compounds and the solid-liquid equilibrium of non-volatile compounds, thus new transport and transformation pathways affecting the composition of DOC may occur [107,108]. For this reason, a considerable number of species, either from the gas phase or the particle phase, can be found in the liquid phase of the droplets. The multiphase environment of the droplets facilitates aqueous phase reactions of the water-soluble species. Several low molecular weight organic species have been studied and are believed to be transferred from the gaseous phase, including formic acid, acetic acid, formaldehyde, glyoxal, methylglyoxal, phenol and nitrophenol [65-68]. Aldheydes and mono and dicarboxylic acids typically comprise a large fraction of DOC because of their high solubility [106] and their behavior is described in the following paragraph. Compounds similar to the high molecular weight organic substances or HULIS found in aerosols were also recently observed in clouds [53,109]. For example, Reyes-Rodriguez et al. [53] observed the high molecular weight organic compounds in cloud samples to be mostly aliphatic and oxygenated, with a small amount of aromatic compounds based on the study of the functional groups. Overall, previous studies either observed several individual compounds or functional groups rather than the complex mixture of the organic compounds on a molecular level.

Carboxylic acids

Determination of the concentration of organic anions gains a lot of importance if we consider that the ion balance of inorganic anions and cations is not equal. An anion deficit was first observed during the HCCT−2010 campaign by van Pinxteren [21] and it ranged up tu 178 µeq

L^{-1}. The inorganic anions missing from this calculation (bicarbonate and sulfite) do not impact the ion balancing.

Only in the last few decades researchers started to investigate cloud water organic composition and its reactivity, especially the formation and transformation of carboxylic acids [101]. For the HCCT−2010 campaign, the concentrations of a large number of organic acids were measured from the bulk of cloud water samples. It was estimated to be in the range of 3-115 μeq L^{-1} and can thus explain a large fraction of the anion deficit. Considering that the DOC fraction is likely to contain many more than the analytically resolved organic acids, it can be assumed that the missing anions are predominantly organic in nature and that organic acidic material had a non negligible impact on cloud water acidity during the HCCT−2010[21]. This result is not an isolated case: similar observations were made during many studies [110,111,112,113].

Such soluble compounds include oxidation products of volatile organic compounds (VOCs) that are emitted from anthropogenic or biogenic sources and are ubiquitous in the atmosphere [114]. The most abundant organic compounds that have been identified in cloud and fog droplets are small volatile carboxylic acids: formic, acetic, oxalic, succinic, malonic, malic and tartaric acids are the most important [5]. Notwithstanding, the composition of DOC is mostly unknown: Loflund at al. [26] correlate the carboxylic acid concentrations to DOC and found that the monocarboxylic acids alone represent 9.3% of DOC. Adding the dicarboxylic acids, this average value increases to 11%.

In a recent work, Deguillaume et al. show that carboxylic acids represent 9 to 12% of the DOC with a preponderance of acetic acid (29-70% of the total of carboxylic acids) and formic acid (15-47%), while malonic succinic and oxalic acids are less concentrated (≈ 20%). In the same work aldehydes are also described and they represent from 0.83 to 1.4% of the DOC, with a prevalence of formaldehyde (from 52 to 73% of the total aldehydes) [27].

Sources

In the atmospheric aqueous phase, carboxylic acids have different sources, such as anthropogenic and biogenic direct emissions in the gas and particulate phases, or chemical transformations from organic precursors [101]. It is quite problematic to distinguish between primary and secondary sources and biogenic and anthropogenic origins and also if they come mostly from the gas phase (high Henry's constant value) or from the dissolution of CCN. Concerning primary emissions, the most important are anthropic sources (fossil fuel combustion) [115], biogenic sources (from vegetation and oceans) [65] and natural sources (wood

combustion) [116]. In gas phase carboxylic acids are produced by degradation of hydrocarbons, for example by oxidation of alkenes by ozone. Also, C1–C3 carbonyl compounds [55,108] were identified in cloud water along with formaldehyde, that represents a final product in the oxidation chain of numerous VOCs, and is the most concentrated. However, difunctional aldehydes, such as glyoxal or methylglyoxal, have higher Henry's law constants than formaldehyde and their concentration are similar to those observed for formaldehyde. Their oxidation pathway is important and lead to the production of oxalic acid [117].

Monocarboxylic acids

Acetic and formic acids represent the most abundant of the carboxylic acids [26]. Regarding their biogenic sources, Khwaya et al [112], Khare et al [118] and Montero et al [119] observe seasonal variation, strictly correlated to the vegetation cycle, and daily variation, correlated to photochemical production. The latter is probably due to the oxidation of monoterpenes and isoprene emitted by vegetation. Concerning anthropic sources, biomass burning leads to the emission in the atmosphere of carboxylic acid and is the most important source of acetic and formic acid in the atmosphere. Incomplete combustion of fossil fuel is also a source of monocarboxylic acids in the atmosphere, especially in densely populated areas. Many authors showed that acetic acid production is more elevated than the formic one [115,120,121].

One source of formic acid in cloud aqueous phase is the oxidation of methanol [122] and formaldehyde [7]. Acetic acid can be produced in the aqueous phase by the oxidation of various alcohols, like ethanol, ethylene glycol or 2-propanol. The transfer from the gas phase is also an important source of formic and acetic acids in the atmospheric aqueous phase, whose Henry's law constants are equal to 5400 and 5300 M atm^{-1} respectively [123]. Sellegri et al [47] showed, during a campaign of measurements at the Puy de Dôme station, that acetic and formic acid are present in the interstitial gaseous phase and that their presence in aqueous phase is due to the gas transfer. Moreover, the presence of acetic and formic acids can also be potentially the result of their production by microorganisms as they are common intermediates in different metabolic pathways [124].

Formic acid concentration in cloud water was evaluated to be of the order of 10 µM during the FEBUKO (II) campaign [21], while Loflund [26] found a concentration of 1 µM. In the same works acetic acid concentration was reported to be of the order of 7 µM and 1 µM respectively.

Dicarboxylic acids

Motor exhausts have been proposed to be primary sources of oxalic, malonic, succinic and glutaric acids. Some of these dicarboxylic acids are also emitted by wood burning, in particular malonic and succinic acids [125]. Glutaric, succinic and adipic acids have been identified as secondary organic aerosols products of the reaction of ozone with cyclohexene, which is emitted naturally from the biosphere.

Oxalic acid is the most abundant carboxylic acid after acetic and formic acids and it is produced through several steps of oxidation. In contrast to acetic and formic acids, oxalic acid in the aqueous phase does not originate from the gas phase, which can probably explain its lower concentration. Together these organic species (acetic, formic and oxalic acids) comprise less than 20% of the organic mass in cloud water [109]. Succinic and malonic acids are the most abundant dicarboxilic acids after oxalic acid. The first is produced principally by pine wood combustion and the second one by oak combustion [125]. Until now, no direct source of malic and tartaric acids has been identified.

Oxalic, malonic, and succinic acid concentrations were evaluated during the FEBUKO (II) campaign [21] and the average concentrations are 1.9, 0.4 and 0.4 μM respectively. Loflund [26] found lower concentrations (0.4, 0.2 and 0.15 μM, respectively).

In Table 4, the concentrations of the main carboxylic acids in cloud aqueous phase during different measurement campaigns are reported.

Carboxylic acid	Concentration (μM)	References
Formic acid	1.3−34.3	Loflund (2002) [26]
	2.1−35.5	Weathers (1988) [126]
	13.9−39.9	Khwaja (1995) [112]
	36.0−51.2	Decesari (2005) [109]
	43.0−167.0	Watanabe (2001) [41]
	3.0−8.4	Leaitch (1996) [127]
	6.4	Vong (1997) [128]
	1.0−11.4	Brantner (1994) [129]
	12.0−103.0	Munger (1989) [130]
	5.5−13.5	Deguillaume (2014) [27]
Acetic acid	4.0−37.8	Loflund (2002) [26]
	0.7−14.4	Weathers (1988) [126]
	5.1−14.7	Khwaja (1995) [112]
	28.3−79.0	Decesari (2005) [109]

	30.0−84.0	Watanabe (2001) [41]
	0.9−4.3	Leaitch (1996) [127]
	2.9	Vong (1997) [128]
	13.1−71.4	Brantner (1994) [129]
	3.0−173.0	Munger (1989) [130]
	4.9−17.7	Deguillaume (2014) [27]
Oxalic acid	0.65−12.65	Loflund (2002) [26]
	1.95−9.65	Khwaja (1995) [112]
	0.02−1.90	Leaitch (1996) [127]
	0.05−15.2	Decesari (2005) [109]
	2.1−4.9	Deguillaume (2014) [27]
Malonic acid	0.70−2.85	Loflund (2002) [26]
	1.95−7.3	Khwaja (1995) [112]
	0.7−1.6	Deguillaume (2014) [27]
Succinic acid	0.85−2.55	Loflund (2002) [26]
	0.6−1.8	Deguillaume (2014) [27]

Table 4: Concentrations of main carboxylic acids in cloud aqueous phase during different measurement campaigns.

Reactivity

Carboxylic acids undergo chemical and photochemical transformations during cloud lifetime. Direct photolysis, as reported in Chapter 2, is an important process only for compounds that absorb actinic radiation. Carboxylic acids present a weak absorption of sunlight and for this reason direct photolysis is negligible in most of the cases. An exception is represented by pyruvate, which undergoes phototransformation under sunlight irradiation [131,132].

The reactivity of organic species in aqueous phase is mainly due to the reaction with the hydroxyl radical. The reactivity of carboxylic acids in the aqueous phase with free radicals is largely investigated and the reactivity constants for the majority of carboxylic acids were measured but the degradation pathway is not clear for many compounds [133]. Kawamura and Kasukabe [134] proposed a photochemical oxidative pathway with a progressive diminution of the carbon chain for carboxylic acids in particulate phase. This could be described by the following pathway (Figure 9).

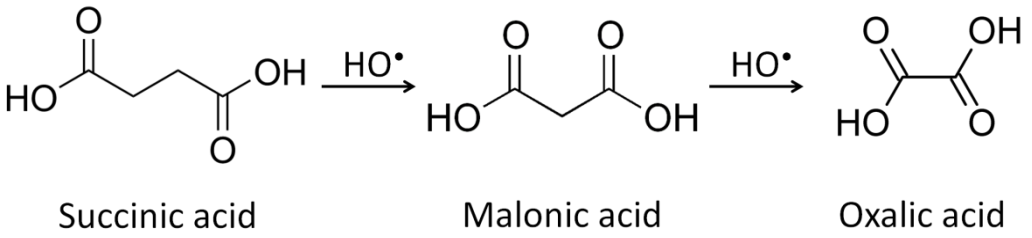

Figure 9: Succinic acid oxidation.

The mechanism of radical reactivity could be summarized as follow:

1) Hydroxyl radical extracts a hydrogen atom from a C−H bond or it is added to a double bond C=C. In each case an alkyl radical $R^{\bullet}$ is generated.
2) In the presence of oxygen, the alkyl radical forms a peroxyl radical $ROO^{\bullet}$.
3) In the aqueous phase the peroxyl radical $ROO^{\bullet}$ with a OH group on the α−carbon undergoes elimination of $HO_2^{\bullet}$/ $O_2^{\bullet-}$. Moreover two peroxyl radicals can react to form a tetraoxyde (ROOOOR) which is unstable and decomposes into more stable products like carbonyls (aldehydes, ketones or carboxylic acids) or alcohols. The peroxyl radical can also give decarboxylation with the liberation of a CO_2 molecule and of other products.

All the transformations described are fast and difficult to study: it is complicated to estimate the degradation rate and the products for each step of the degradation of carboxylic acids.

To better understand the chemical and photochemical behavior of organic matter and, in particular, of carboxylic acids in cloud aqueous phase, many chemical models were developed. The most important ones include the equilibrium with the gas phase and take into account the volatility of the compounds. A detailed and extended chemical mechanism describing tropospheric aqueous phase chemistry is Chemical Aqueous Phase Radical Mechanism (CAPRAM). The mechanism contains extended organic and transition metal chemistry and is formulated on a critical review of the literature [31].

The atmospheric model M2C2 model (Model of Multiphase Cloud Chemistry) was developed by the Lamp laboratory (Laboratoire de Météreologie Physique), in Clermont, and it incorporates explicit treatment of multiphase cloud chemistry. The M2C2 model is composed of two modules which can be coupled together: a multiphase chemistry model and a two–moment warm microphysical scheme module predicting the number concentration of cloud droplets and raindrops and the mixing ratio of cloud water and rainwater categories. The microphysical module has been expanded to consider the process of cloud droplet nucleation and the ice phase formation together with its effect on the budget of trace gases via retention and burial processes. The dynamical framework of the model is an air parcel and the

exchange of chemical species between the gas–phase and the aqueous–phase is parameterized following the mass transfer kinetic formulation previously developed. For the aqueous–phase (cloud and rainwater), the detailed chemistry of HO_x, chlorine, carbonates, NO_y, sulfur, the oxidation of organic volatile compounds (VOCs) with two carbon atoms, the chemistry of transition metal ions for iron, manganese and cooper was included. The pH can also be calculated by solving the electro–neutrality equation as well as photolysis frequencies in the gas–phase and in cloud droplets [50].

Figure 10 reports the degradation pathway for glutaric acid determined experimentally and by CAPRAM model.

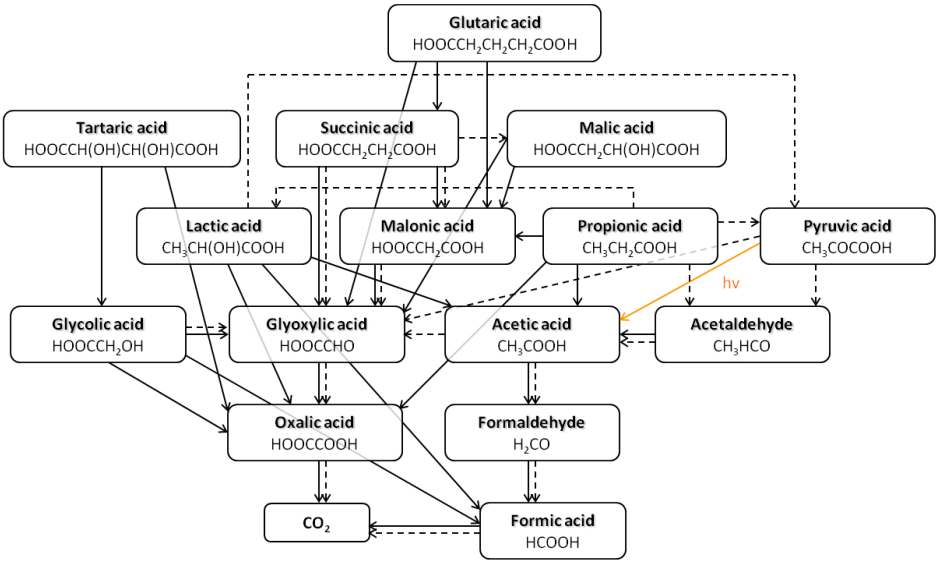

Figure 10: Experimental (solid lines) and modeled (dashed lines) degradation pathway of glutaric acid (from Charbuillot et al. [101]).

These degradations pathways lead to the formation of low weight molecular compounds (from C5 to C1). Despite this, it was observed that the irradiation of formic acid (C1) in the presence of $HO^{\bullet}$ leads to the production of oxalic acid (C2) [101]. This result suggests that mechanisms of radical condensation could be the first step of the formation of organic compounds with high molecular weight, as recently reported by Carlton [135].

Sinks

The principal loss processes for carboxylic acids, other than keto−acids, are dry and wet deposition. Precise quantification of wet *vs* dry removal require the knowledge of carboxylic acid partitioning between liquid and gas phases which depends on the Henry's law constants and the degree of dissociation of these weak acids in cloud droplets. Since low molecular weight carboxylic acids have pKa in the range of 1.3−5.7, they are likely to dissociate in

atmospheric liquid phase, and their degree of dissociation is pH dependent. Quantification of dry deposition rates is not easily achieved because they are expected to vary with season, time of day, temperature, humidity and the ground topology. Wet deposition depends mainly on the rate and frequencies of precipitations, so, its relative importance is different for regions with various pluviometries and for different seasons. Effective residence times of carboxylic acids in the troposphere are not well known. Estimations range from several hours to more than a week, and are due to variable precipitations frequencies in different studies and to uncertainties regarding deposition [120].

Amino acids

Water soluble organic compounds (WSOC) are particularly important in heterogeneous nucleation and the formation of clouds and precipitation. A large proportion of WSOC is still uncharacterized: little is known about the chemical compounds present, their sources, temporal and spatial patterns of variation, and the subsequent impact on climate and environment.

NO_x and their photochemical products are recognized as being centrally important species in the chemistry of the atmosphere. In parallel to the inorganic reactivity, NO_x form also organic nitrates like peroxyacetylnitrate (PAN). Similarly ammonium is the dominant reservoir of nitrogen in the reduced form [86].

A recent study of Zhao et al. [136], concerning the identification of organic matter in clouds using FT−ICR mass spectrometry, shows that there is a large number (about 50%) of CHNO molecular formulas with an Oxygen/Carbon (O/C) ratio lower than 0.7. Generally, these compounds have a large range of Hydrogen/Carbon ratios (H/C) from 0.2 to 2.2. Other studies found an O/C ratio of 0.5 [137,138]. Moreover it was found that compounds with one nitrogen atom represent 40% of CHNO compounds.

Amino acids have an average O/C ratio of 0.6 and a H/C ratio of 0.16, as reported in Table 5, and they could represent a significant contribution to N−containing organic compounds in cloud water.

Amino acid	**Abbreviation**	**Molecular Weight ($g\ mol^{-1}$)**	**%C**	**%N**	**%O**	**%H**	**O/C**	**H/C**
Alanine	ALA	89.08	40.45	15.72	31.44	7.92	0.78	0.20
Arginine	ARG	174.20	41.37	8.04	16.08	8.10	0.39	0.20
Asparagine	ASN	132.12	36.36	21.20	31.80	6.10	0.87	0.17

Aspartate	ASP	133.10	36.10	10.52	42.08	5.30	1.17	0.15
Cysteine	CYS	121.15	29.74	11.56	23.12	5.82	0.78	0.20
Glutamate	GLU	147.13	40.82	9.52	38.07	6.17	0.93	0.15
Glutamine	GLN	146.15	41.09	19.16	28.74	6.90	0.70	0.17
Glycine	GLY	75.07	32.00	18.65	37.31	6.71	1.17	0.21
Histidine	HIS	155.16	46.45	27.07	18.05	5.85	0.39	0.13
Isoleucine	ILE	131.18	54.94	10.67	21.35	9.99	0.39	0.18
Leucine	LEU	131.18	54.94	10.67	21.35	9.99	0.39	0.18
Lysine	LYS	146.19	49.30	19.16	19.16	9.65	0.39	0.20
Methionine	MET	149.20	40.25	9.39	18.77	7.43	0.47	0.18
Phenylalanine	PHE	165.19	65.44	8.48	16.95	6.71	0.26	0.10
Proline	PRO	115.13	52.16	12.16	24.33	7.88	0.47	0.15
Serine	SER	105.09	34.29	13.32	39.97	6.71	1.17	0.20
Threonine	THR	119.12	40.33	11.76	35.27	7.62	0.87	0.19
Tryptophan	TRP	204.23	64.69	13.71	13.71	5.92	0.21	0.09
Tyrosine	TYR	181.19	59.66	7.73	23.18	6.12	0.39	0.10
Valine	VAL	117.15	51.26	11.95	23.91	9.46	0.47	0.18

Table 5: Amino acids: molecular weight. C,O and N percentage and O/C−H/C ratios.

The presence of amino acids in atmospheric precipitation and aerosols has been noted since many years, but no information concerning their occurrence in the atmosphere is reported yet. An important distinction between free and combined forms of amino acids must be distinguished in the analysis of environmental samples. The twenty commons amino acids, that make proteins in living systems, are reported in Table 5. They are normally found in their uncombined forms (as dissolved free amino acids, DFAA) only at low concentrations in the environment. This is due to the fact that they are the favourite form for the uptake of nitrogen compounds by aquatic organisms [139]. In environmental samples amino acids are present as dissolved combined amino acids (DCAA) as proteins and peptides and it is necessary to consider both fractions to describe completely the behaviour of N-containing organic compounds [140].

The interest in amino compounds in the atmosphere is driven by their bioavailability in deposition and their potential role in ecological processes. Amino compounds could have a role in cloud formation, as suggested by the presence of proteinaceous matter in cloud water [141], due to their surface active properties [142,143] and by the fact that L−leucine can act as an ice nucleus [144]. Thus amino compounds could affect the atmospheric water cycle, the radiation balance, and the scavenging of air pollutants.

Sources

In the marine environment, the enrichment of organic matter and proteinaceous material in cloud water is associated with the ubiquitous production of sea salt aerosol caused by air bubbles bursting at the ocean surface [12]. This process is expected to be the main source of combined amino acids in the marine troposphere. Three different sources of proteinaceous matter associated with bubble transport need to be considered: bacteria, phytoplankton and the organic film found in the sea surface microlayer [139].

Proteins generally represent the largest single component of the organic material of many algae and are known to be important extracellular products of blue-green algae. These compounds accumulate at the air-sea interface and are subsequently transported into the aerosol fraction. Tiny aerosol particles contain material from a 2 µm thick portion of the surface microlayer while smaller jet droplets that are suspended in the air carry the material from a 100 µm thick portion of the layer, as shown in Figure 11. In marine aerosol proteinaceous matter is found in a variety of forms: as part of the dissolved organic matter of planktonic and bacterial origin, as particulate organic matter in microorganisms and debris or adsorbed onto inorganic particles [139]. As described before, sea salt aerosol can act as CCN and proteinaceous material could be found in cloud water droplets by solubilisation of WSOC. However, a first oxidation of the proteinaceous matter could happen on the aerosol particle, especially for methionine and tryptophan, which are rapidly transformed during exposure to ozone and sunlight [145].

In the continental environment, proteinaceous matter, including plant debris, pollen, algae and bacteria, has been frequently detected in the atmosphere as aerosols and particles [146,147] and can undergo the same transformations that occur in marine aerosol.

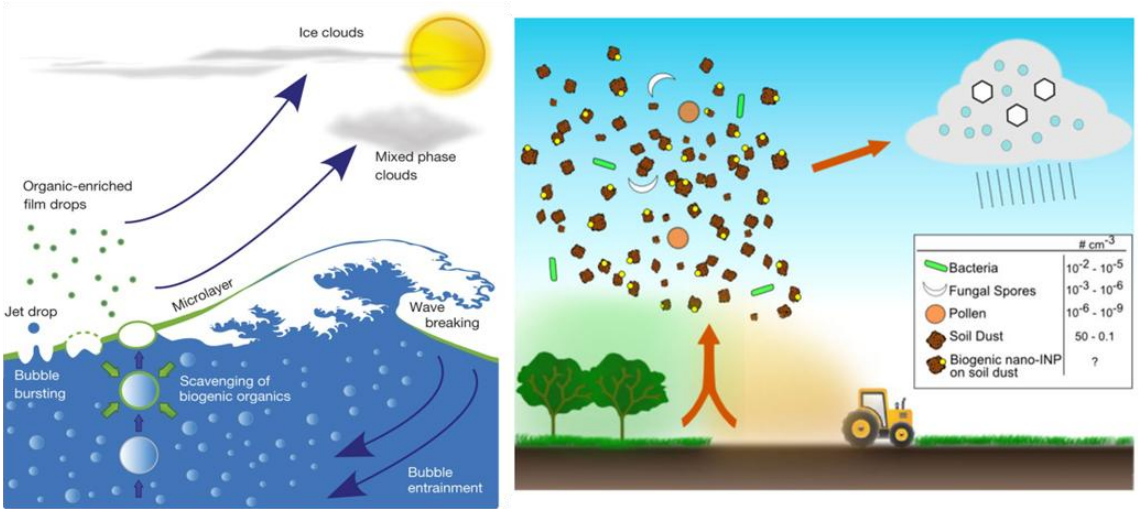

Figure 11: Schematic representation of marine spray (left) and continental biogenic aerosol formation (right).

A crucial point is how proteins and peptides are converted into free amino acids. Aerosols particles and cloud water droplets are known to be unusual chemical systems with highly saline and acidic conditions: however thermal hydrolysis seems not to be a favoured process. The presence of enzymatic hydrolysis in these media is a subject on which little is known, but which cannot be excluded: enzymes are themselves proteinaceous and, if bacteria and other unicellular organisms are found in cloud water droplets, so must be their attendant enzymes. Photochemical transformation would seem most likely except for the drawback that the optical cross sections of peptide and protein fragments are low at sun wavelengths. It is possible that there is a photocatalytic or photosensitized reaction pathway responsible for the hydrolysis step [140].

Reactivity

Direct photolysis

Aqueous solutions of proteins and peptides are decomposed by UV radiation to give a complex series of simpler products. However the direct photolysis of chromophoric amino acids is likely to be a minor process. This is correlated to the low molar extinction coefficient at sun wavelength. The main chromophores are the aromatic amino acids (phenylalanine, tyrosine and tryptophan), with smaller absorbance for histidine [148].

Concerning direct photolysis, the case of tryptophan, which has a weak absorption beyond 300 nm is particularly interesting. Irradiation of TRP leads to its direct photochemical oxidation to N-formylkynureine, which has a strong absorption band in the range of 300-400 nm and can act as a photosensitizer for proteins and peptides that would otherwise be transparent to these wavelengths [149].

Reaction with $HO^{\bullet}$

One plausible reaction pathway of amino acids with the hydroxyl radical leads to the deamination and production of ammonia. This reaction could be very important for the acido-base balance because it leads to the formation of α-keto acids, like pyruvic acid, which is microbiologically transformed in the Krebs cycle to give acetate and other products.

A schematic degradation is reported in R75−76.

R75) $HO^{\bullet} + H_3N^+CH(R)COO^- \rightarrow H_2O + H_3N^+C^{\bullet}(R)COO^-$

R76) $2\ H_3N^+C^{\bullet}(R)COO^- \rightarrow H_3N^+CH(R)COO^- + H_2N^+{=}C(R)COO^-$

At sufficiently high concentrations, some fraction of $H_3N^+C^{\bullet}(R)COO^-$ radicals may dimerize to form α,α'-diamino dicarboxylic acid; its presence has never be detected in aerosols. The

imino acid produced further hydrolyzes following reaction R77 leading to deamination and production of a α-ketoacid.

R77) $H_2N^+=C(R)COO^- + H_2O \rightarrow NH_4^+ + RCOCOO^-$

For the simplest amino acids, such as glycine and alanine, the α-carbonyl radical produced in reaction R75 is expected to react with oxygen to form an imino acid that hydrolyzes as in reaction R77 [150].

For the more complex amino acids the attack of $HO^\bullet$ will no longer take place solely at the C−H bond. $HO^\bullet$ attacks at the side chain C−H bonds of unsaturated α-amino acids such as phenylalanine, histidine and tyrosine and this is an important pathway for aromatic amino acids. Cysteine and methionine are preferentially attacked at the S−H bond [151].

Similarly, the pathways of oxidative degradation of peptides and polypeptides yield amide and keto functions, according to reaction mechanism reported by Milne and Zika [140].

In summary, the photochemical production of ammonia, carbon dioxide, simpler carboxylic acids, amides and amines from the oxidative attack of hydroxyl radical on peptides appears to be a process that may be reasonably expected to take place in cloud water, although the actual extent of these pathways is much harder to determine.

Reactivity with other atmospheric radicals

The reactivity of amino acids with main atmospheric radicals was investigated: scarce information is reported concerning the reactivity with nitrate radicals, which act as one-electron oxidants.

Some works report the reaction between nitrite radical ($NO_2^\bullet$) and cysteine [152].

The reaction of $O_2^{\bullet-}$ with amino acids has been studied and overall amino acids are relatively unreactive with both $O_2^{\bullet-}$ and $HO_2^\bullet$ [153] ($k'' \leq 10^2\ M^{-1}\ s^{-1}$).

Concerning chlorine and bromine radical anions, their selectivity in the reaction with amino acids was investigated by Adams et al. [154]. Methionine, cysteine, tryptophan, tyrosine and phenylalanine show the greatest reactivity which is strongly influenced by pH. Rates of H−abstraction, which appears to be the main mechanistic pathway, are two orders of magnitude lower than the corresponding reaction with $HO^\bullet$.

Second order rate constants of reactions of selected radicals with amino acids are reported in Table 6.

Amino acid	$k_{HO}\bullet(M^{-1}s^{-1})$	$k_{SO_4}\bullet^-(M^{-1}s^{-1})$	$k_{Cl_2}\bullet^-(M^{-1}s^{-1})$	$k_{Br_2}\bullet^-(M^{-1}s^{-1})$
ALA	5.4×10^7	1.0×10^7	1.3×10^5	
ARG	3.5×10^9			
ASN	4.9×10^7			
ASP	7.4×10^7			
CYS	1.5×10^{10}		8.5×10^8	1.8×10^8
GLU	1.6×10^8		2.3×10^5	
GLY	1.7×10^7	9.0×10^6	$< 10^4$	
HIS	5.0×10^9	2.5×10^6	1.4×10^7	1.5×10^7
ILE	2.2×10^9			
LEU	1.7×10^9			
LYS	7.7×10^8			
MET	8.3×10^9	1.1×10^9	4.0×10^9	2.5×10^9
PHE	6.5×10^9		6.0×10^6	$< 1 \times 10^6$
PRO	3.5×10^8			
SER	3.3×10^8	2.3×10^7	1.2×10^5	
THR	4.7×10^8			
TRP	1.2×10^{10}	2.1×10^9	2.6×10^9	7.0×10^8
TYR	1.3×10^{10}	3.2×10^9	2.7×10^8	4.5×10^7
VAL	7.6×10^8			

Table 6: Second order rate constants of reactions of selected radicals with amino acids.

HULIS, TRYLIS and TYLIS

Muller et al. [155] identified by fluorescence spectrophotometry in rainwater three fluorophores: HULIS, TRYLIS and TYLIS.

HUmic−LIke Substances (HULIS) are thought to be present and to originate from aerosol in the atmosphere and are high molecular weight compounds, also called “macromolecular compounds” [156] or “atmospheric humic matter” [157], which are believed to play an important role in cloud formation processes. Although atmospheric HULIS share similar features to terrestrial and aquatic humic substances, they have substantial differences, such as smaller average molecular weight, lower aromatic moiety content, weaker acidic nature, higher aliphatic content and a better surface activity. Atmospheric HULIS are thought to include, in addition to humic and fulvic acids, organic acids and some organic compounds that do not dissociate in aqueous solution such as sugars and peptides [62]. Many authors report that approximately 20−50% of organic carbon in particulate matter can be attributed to HULIS

[158,159]. Potential sources of atmospheric HULIS include primary antropogenic sources (motor vehicle exhaust, tyre and asphalt wear), biomass burning and marine organic material (bubble bursting on ocean surface). Moreover, secondary organic aerosol formation of both higher and lower molecular weight HULIS are correlated to isoprenoid, terpenoid and α−pinene emissions, photochemical reaction of oligomerization of polar low molecular weight degradation products of organic debris and other natural and antropogenic sources. HULIS, as humic substances, present a fluorescence signal: they lie in a similar area of the optical space of humic and fulvic acids identified by Coble [160], even if their precise location can be more blue-shifted. In Table 7 fluorescence excitation and emission wavelengths observed for each fluorophore by Muller et al. are reported [155].

As reported by Muller, visible HULIS, which absorb light in the visible range, are thought to be similar to fulvic acid; they contain amino acid peptides and nucleic acids from original plant matter, including aliphatic carbon, carbohydrates, olephinic, ketonic and aldheydeic carbons, and aromatic and carboxylic carbons, with the latter two providing the fluorescence fraction.

TRYptophan−LIke Substances (TRYLIS) and TYrosine−LIke Substances (TYLIS) were also detected by Muller et al. in rainwater: the authors defined these substances in comparison with the fluorescence signal of tryptophan and tyrosine, respectively, according to the previous quantification of these amino acids in particulate matter and aerosols by Kuznetsova [139] and Zhang and Anastasio [143,145]. Their fluorescence fingerprint is reported in Table 7, while in Figure 12 the Excitation Emission Matrix (EEM) with the optical location for (B) TYLIS, (T) TRYLIS, and (C) 'visible' HULIS is reported.

Substance		**Min**	**Max**	**Mean**
TYLIS	λex (nm)	295	315	301
	λem (nm)	265	285	274
TRYLIS	λex (nm)	335	370	358
	λem (nm)	260	295	275
HULIS	λex (nm)	390	475	414
	λem (nm)	300	340	320

Table 7: Fluorescence excitation and emission wavelengths observed for each fluorophore by Muller et al. [155].

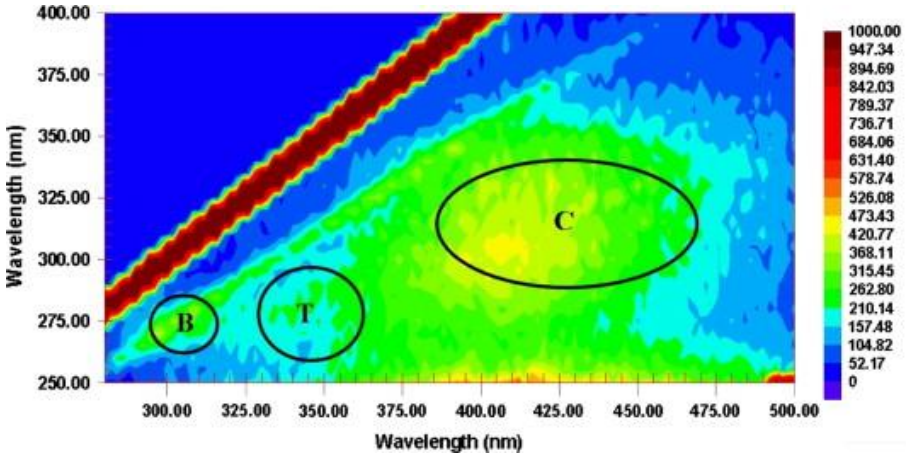

Figure 12: Emission (x)–Excitation (y) Matrix (EEM) chart for a precipitation sample reported by Muller et al [155] showing the approximate optical locations for (B) TYLIS, (T) TRYLIS, and (C) 'visible' HULIS.

Experimental set-ups and methods

Chapter 4

The experimental set-ups and methods used during my PhD will all be described in this chapter. The general set-up and theoretical principles behind the used techniques and methods used will be presented here while the specific analytical methods and experimental details are addressed in the following chapters while dealing with the results.

Sampling site

The cloud sampling was performed at the puy de Dôme atmospheric measurement station (PUY, 45.46°N,°E; 1465 m altitude), in central France.

In pre-Christian Europe, puy de Dôme served as an assembly place for spiritual ceremonies. Temples were built at the summit, including a Gallo-Roman temple dedicated to the God Mercury, the ruins of which were discovered in 1873. In 1648 Blaise Pascal, proved Evangelista Torricelli's theory that barometric observations were caused by the weight of air by measuring the height of a column of mercury at three elevations on puy de Dôme. In 1875, a physics laboratory was built at the summit. A photo of the new observatory is reported in Figure 13.

The station is part of the EMEP (European Monitoring and Evaluation Programme), GAW (Global Atmosphere Watch), and ACTRIS2 (Aerosols, Clouds, and Trace gases Research InfraStructure) networks where atmospheric clouds, aerosols and gases are studied. The PUY station is located on the top of an inactive volcano at an altitude of 1465 m rising above the surrounding area, where fields and forest are dominant.

The main advantage of the site is the high frequency of the cloud occurrence (50% of the time on average throughout the year). Westerly and northerly winds are dominant. Meteorological parameters, including the wind speed and direction, temperature, pressure, relative humidity and radiation (global, UV and diffuse), atmospheric trace gases (O_3, NO_x, SO_2, CO_2) and particulate black carbon (BC) are monitored continuously throughout the year. Long-term studies have been conducted at the site, in particular of aerosol size distribution [161,162], aerosol chemical composition [163,164], aerosol optical properties [165,166], aerosol hygroscopic properties [6], cloud chemistry [27,64] and cloud microphysics [167].

A complete description of the equipment available at the puy de Dome observatory is reported in the recent work of Guyot et al. [168]. To better characterize sampled air masses, cloud water droplet effective radius (r_{eff}) and liquid water content (LWC) were monitored continuously using the instruments described below.

The Particle Volume Monitor (PVM-100, manufactured by Gerber Scientific, Inc., Reston, Virginia) is a ground-based forward-scattering laser spectrometer for particulate volume measurements. It is designed to measure the LWC, the particle surface area (PSA) and to derive the r_{eff}. The PVM-100 (Figure 13, right) measures the laser light (λ = 0.780 µm) scattered in the forward direction by an ensemble of cloud droplets which crosses the probe's sampling volume of 3 cm^{-3}. The light scattered in the 0.25 to 5.2° angle range is collected by a system of lenses and directed through two spatial filters. The first filter converts scattered light to a signal proportional to the particle volume density (or LWC) of droplets; the second filter produces a signal proportional to the particle surface area density (PSA). From the ratio of these two quantities, r_{eff} can be derived (Equation 9):

$$r_{eff} = \frac{LWC}{3\sigma}$$

Equation 9: Calculation of r_{eff}.

Figure 13: Puy de Dome atmospheric measurement station (left) and instruments set up on the roof (PVM100 in detail) (right).

Since 2001, the observation service BEAM (Biophysico-chimie de l'Eau Atmospherique et Modification antropiques) is responsible for studying the chemical and biological composition and microphysical proprieties of cloud water samples collected at the puy de Dome station. Clouds are frequently formed at the top of the site, either during advection of frontal systems or by the orographic rising of moist air. During the winter/spring months, the station lies in the free troposphere and air masses are usually free from the influence of local pollution. Road access to the site was restricted to authorized personnel during all sampling periods. A small military base is located to the north of the station, but fuel combustibles are limited exclusively to winter storm events.

Cloud collector

Cloud water sampling was performed between October 2013 and July 2016. The sampling periods included both warm and super-cooled conditions for cloud droplets. Sampling was restricted to non precipitating clouds with a single-stage cloud collector similar to that described by Marinoni et al. [64].

Droplets are sampled at a flow rate of approximately 80 m^3 h^{-1} and collected by impaction onto a 105 cm^2 rectangular plate. The cloud droplets either freeze upon impact (super-cooled conditions) or are collected directly as a solution. Before each sampling, the collector is cleaned with ultra pure water. The sampling intervals (2 or 3 h) varied and were dependent on the LWC. Cloud water droplets are aspired in the collector, they impact on the collection plate and are accumulated in the collection vessel, as shown in Figure 14. In the case of supercooled conditions, an ice deposit is formed on the collection plate. The droplet sampling efficiency is enhanced with the utilization of a large stagnation plate close to the collector inlet; this plate allows sampling efficiency also for high wind rate. Laboratory tests showed that the cut-off diameter of the collector is approximately 7 µm.

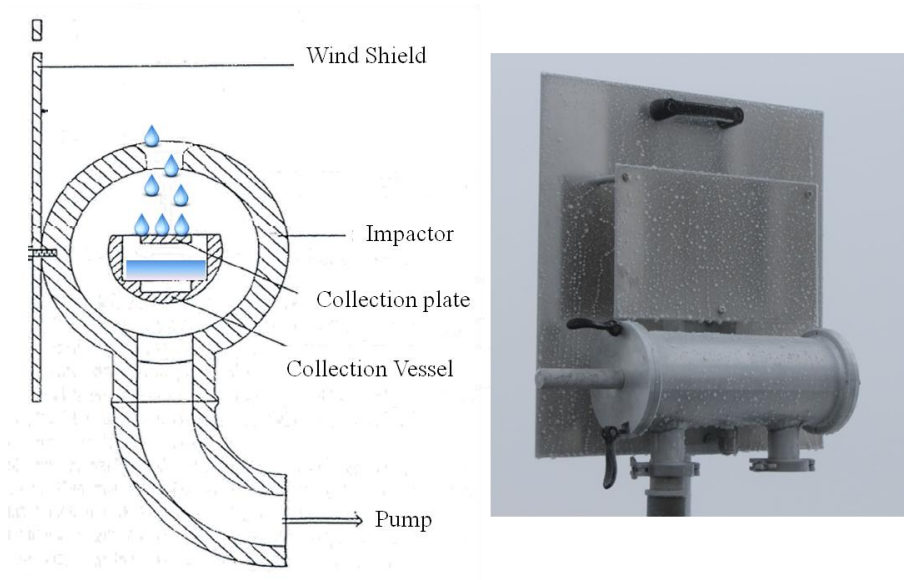

Figure 14: Schema (left) and cloud collector set-up (right) (with kind permission of Deguillaume).

Cloud water samples analysis

Back-trajectory plot

In order to assess the air mass origin, which is correlated to inorganic ions concentration and the oxidative capacity of cloud water, back-trajectory plots were computed for all the collected samples.

The National Oceanic and Atmospheric Administration (NOAA) Air Resources Laboratory's (ARL) Hybrid Single-Particle Lagrangian Integrated Trajectory model (HYSPLIT) is a complete system for computing simple air parcel trajectories as well as complex transport, dispersion, chemical transformation, and deposition simulations. One of the most common model applications is a back-trajectory analysis to determine the origin of air masses and establish source-receptor relationships. The model calculation method is a hybrid between the Lagrangian approach, using a moving frame of reference for the advection and diffusion calculations as the trajectories of air parcels move from their initial location, and the Eulerian methodology, which uses a fixed three-dimensional grid as a frame of reference to compute pollutant air concentrations [169].

Back-trajectories were computed for each cloud event for 72 hours using the option "model of vertical velocity"; in Figure 15 an example is reported.

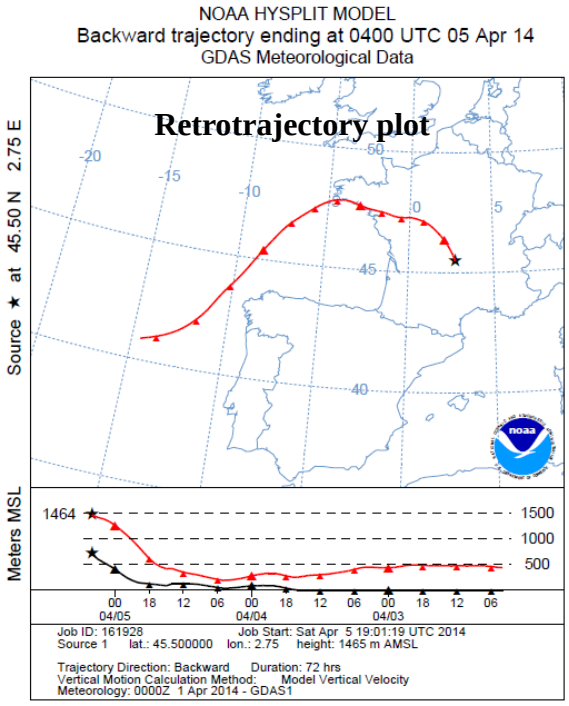

Figure 15: Back-trajectory plot on 72h obtained with the HYSPLIT model.

Irradiation

Irradiation set-ups

Different irradiation set-ups were used during the experimental work:

- **Xenon lamp**: this device is composed of a Xenon lamp (Oriel arc lamp 300 W, solar simulator USHIO UXL-302-O) equipped with a water cooler to avoid the increase of temperature and a mirror to reflect the light vertically (Figure 16). A Pyrex filter was

located before the reactor to filter radiation below 290 nm. Two cylindrical Pyrex reactors, cooled by water circulation to limit thermal reactions, with volume of 40 mL or a 15 mL were used. The solution was continuously stirred with a magnetic stirrer and a Teflon bar to ensure homogeneity.

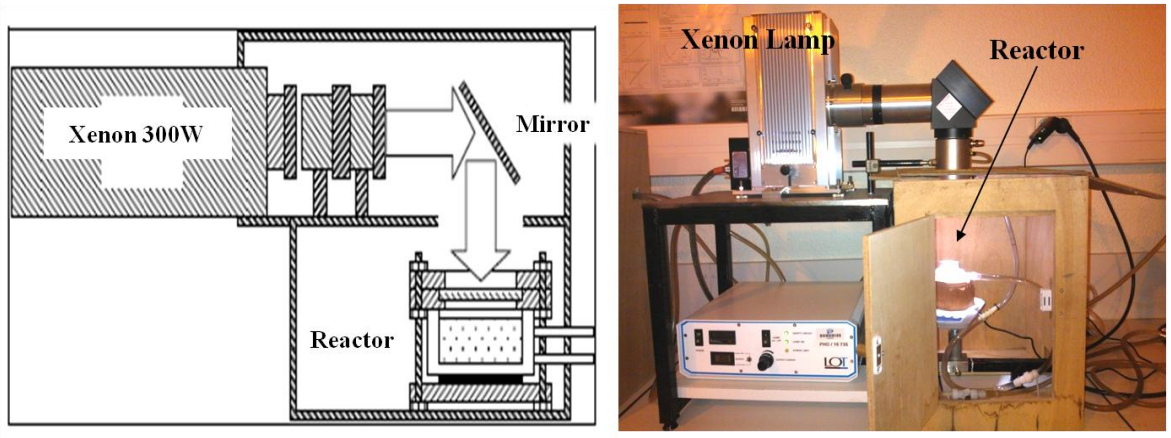

Figure 16: Bulk reactor equipped with a Xenon lamp source.

- **Photoreactor 365 nm and 313 nm**: these set-ups are made up of a cylindrical stainless steel container. Six and four fluorescent lamps (Philips TL D15W/05), whose emission spectrum is centered at 365 and 313 nm respectively (reported in Figure 19), are separately placed in three-two different axes, while the photoreactor, a Pyrex tube of 2.6 cm internal diameter, is placed in the center of the set-up. A schematic representation of this set-up is reported in Figure 17.

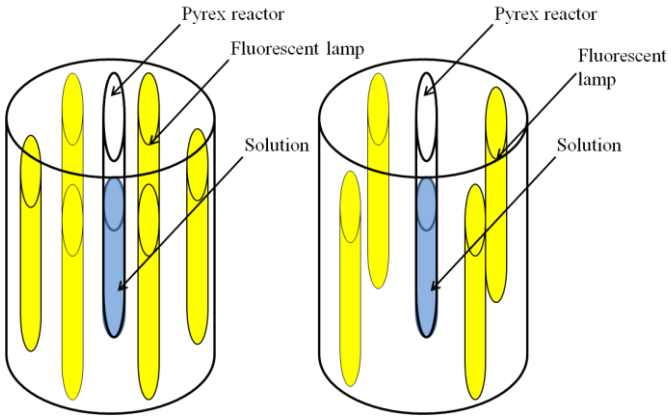

Figure 17: Irradiation devices equipped with neon lamps with emission centered at 365 nm (left) and 313 nm (right).

Actinometry

The emission spectrum of each irradiation system was recorded using a fiber optics coupled with a CCD spectrophotometer (Ocean Optics USD 2000+UV-VIS) calibrated with a UV-Vis-NIR Light source DH2000 from Ocean Optics.

To verify the polychromatic photonic flux of each irradiation system, a chemical actinometry was performed, using the method described by Dulin [170]. A solution 10 µM of p-nitroanisole (PNA) is irradiated in the presence of pyridine 100 µM. The disappearance of PNA is followed by HPLC/PDA using isocratic elution (methanol 60%, MilliQ water 40%) and a Cary Eclipse XDB-C18 column (Agilent, 4.6 × 150 mm, 5 µm). Flow rate was set at 1 mL min^{-1} and PDA at 316 nm.

The disappearance rate of PNA (R_d) is directly correlated to P_{abs}, the radiation absorbed by the solution between 290 and 400 nm, as in Equation 10, where Φ_{PNA} is the quantum yield of PNA, which can be calculated as in Equation 11.

$$\frac{R_d}{\Phi_{\mathrm{PNA}}} = P_{abs}$$

Equation 10.

$$\Phi_{PNA} = 0.44 \times [Pyridine] + 2.8 \times 10^{-4}$$

Equation 11.

The absorbed radiation for each wavelength $P_{abs}(\lambda)$ is correlated to the radiation emitted by the lamp $P_0(\lambda)$ following Equation 12.

$$P_{abs} = \int_{\lambda} P_a(\lambda)\, d(\lambda) = \int_{\lambda} P_0(\lambda)\left(1 - 10^{-A(\lambda)}\right) d(\lambda)$$

Equation 12.

If we consider that $P_0(\lambda)$ is proportional to i_0 measured with the optical fiber by a correction factor k, Equation 13 can be written as follows

$$P_{abs} = \int_{\lambda} k \times I_0(\lambda)\left(1 - 10^{-A(\lambda)}\right) d(\lambda)$$

Equation 13.

And the correction factor k can be calculated by the Equation 14

$$k = \frac{P_{abs}}{\int_{\lambda} I_0(\lambda)\,(1 - 10^{-A(\lambda)}) d(\lambda)}$$

Equation 14.

This factor allows the "calibration" of the spectrum obtained with the optical fiber: in fact, the radiation that reaches the solution can be partially reflected by the reactor. An example is reported in Figure 18.

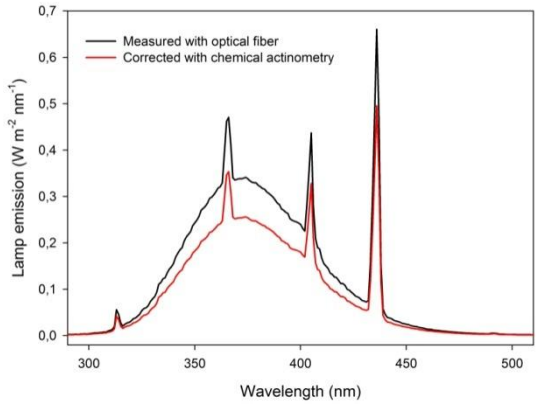

Figure 18: Lamp emission centered at 365 nm measured with optical fiber and corrected by chemical actinometry.

Chemical actinometry was performed for each set-up used and spectra are reported in Figure 19.

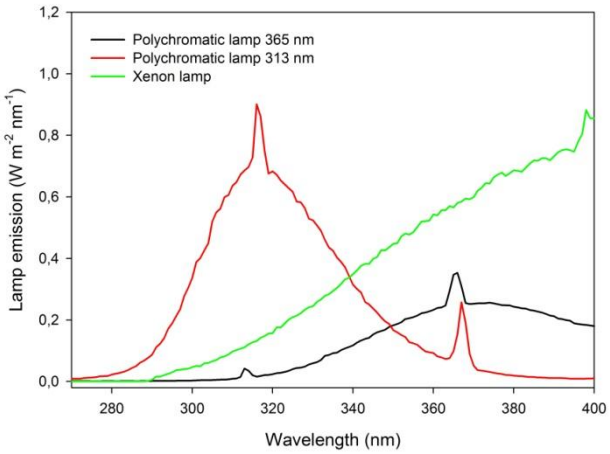

Figure 19: Lamp emission of the three devices used.

Analytical instruments and methods

Physico-chemical parameters

Many physico-chemical parameters were measured: pH, conductivity and redox potential were measured at the puy de Dome station using a Hanna multiparameter instrument. For other experiments, pH was measured with a Cyberscan 510 Eutech instrument pH-meter.

Spectroscopic analysis

Absorption spectra were acquired with a double-ray Varian Cary 300 Scan UV-Visible spectrophotometer in 1 or 5 cm quartz cuvettes. For the cloud water samples' absorption spectra measured at the puy de Dome station, a mono-ray Agilent Technologies Cary 60 UV-Visible spectrophotometer and 1 cm quartz cuvettes were used. Fluorescence spectra and

excitation emission matrix (EEM) were acquired using a Varian Cary Eclipse spectrofluorimeter.

Hydrogen peroxide concentration

Hydrogen peroxide concentration is estimated according to the spectrofluorimetric quantification method described by Miller [171]. Horseradish peroxidase (purchased from Sigma Aldrich, 150-200 units for mg) is dissolved in phosphate buffer at pH 7.4. Two mL of this solution are mixed with 4 mL of 4-hydroxyphenylacetic acid (HPAA) 1×10^{-3} M solution and 60 µL of sample. The formation of the dimer of HPAA, shown in Figure 20, is directly correlated to the concentration of hydrogen peroxide and is detected by fluorescence spectroscopy in 1 cm quartz cuvette setting excitation wavelength at 320 nm and emission wavelength at 408 nm (the fluorescence spectra were acquired between 340 and 500 nm). Considering that the concentration of hydrogen peroxide in cloud water is in the range 1-50 µM, the scan rate was set at 600 nm min^{-1} and the bandpass for excitation and emission were of 10 nm. For other experiments with higher concentrations of H_2O_2 (100 µM ÷ 1 mM), the bandpass were set at 5 nm or the solution was diluted before analysis.

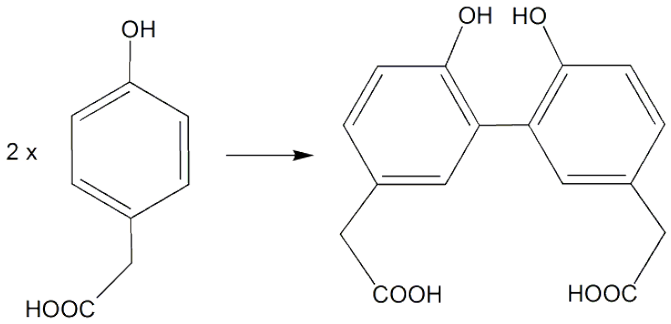

Figure 20: Reaction of formation of the dimer of hydroxyphenylacetic acid (HPAA).

Iron speciation

Fe(II) and Fe(III) concentrations are determined by complexation with FerroZine® (3-(2-Pyridyl)-5,6-diphenyl-1,2,4-triazine-p,p′-disulfonic acid monosodium salt hydrate) (purity > 97%) purchased from Sigma-Aldrich (Figure 21). The spectrophotometric method was adapted from Stookey [172]. Firstly, Fe(II) was determined measuring the absorption at 562 nm of the solution obtained mixing 500 µL of sample and 50µL of FerroZine 20 mM, as shown in Equation 15. The molar absorption coefficient of the complex at 562 nm is 27900 M^{-1} cm^{-1}.

$$[Fe(II)] = \frac{A_{sample} - A_{blank}}{\varepsilon_{562} \times l} \times \frac{V_{tot}}{V_{sample}}$$

Equation 15: Concentration of iron(II).

To determine Fe(III) it is necessary to reduce it to Fe(II): ascorbic acid (purity > 99%, Sigma Aldrich) 0.5 M was used. 500 µL of the sample were mixed with 60 µL of ascorbic acid and, after 10 minutes, with 50 µL of FerroZine solution. Fe(III) is determined by Equation 16, where A_{sample} and A_{blank} are sample and blank absorption, respectively, ε_{562} is the molar extinction coefficient, l is the optic path length, V_{tot} is the total volume (610 µL) and V_{sample} is the sample volume (500 µL). No buffer was used because the signal is stable between pH 4 and 7.

$$[Fe(III)] = \frac{A_{sample} - A_{blank}}{\varepsilon_{562} \times l} \times \frac{V_{tot}}{V_{sample}} - [Fe(II)]$$

Equation 16: Concentration of iron(III).

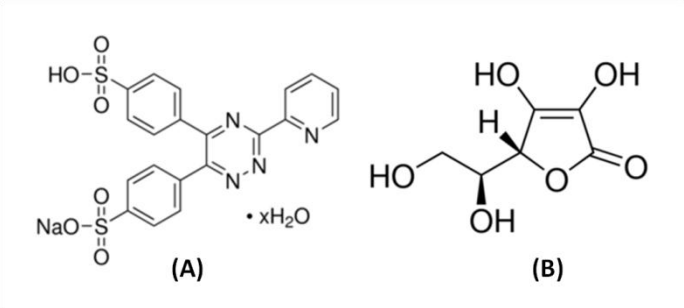

Figure 21: FerroZine (A) and ascorbic acid (B) chemical structure.

Hydroxyl radical formation rate and quantum yield.

Hydroxyl radical formation rate ($R^f_{HO\bullet}$) is determined using terephthalate (TA, purity > 99% purchased from Alfa Aesar) as a probe. Stock solution of disodium terephthalate was added to the sample to have a final TA concentration of 2 mM. The concentration of the probe must be much greater compared with the concentration of organic matter to trap all the photogenerated hydroxyl radicals and to estimate a value for the hydroxyl radical formation rate not affected by depletion by other sinks. This solution was irradiated and at fixed times an aliquot was withdrawn and analyzed using the Varian Cary Eclipse spectrophotometer, setting excitation wavelength at 320 nm and emission wavelength at 420 nm, scan rate of 600 nm min^{-1} and bandpass of 10 or 5 nm. Photogenerated hydroxyl radicals react with TA (not fluorescent) to give fluorescent hydroxyterephthalate (TAOH) and non fluorescent products (Reaction R78). The limit of detection of TAOH is 1 nM.

R78) TA + $HO^\bullet$ → TAOH + products $k = 4.0 \times 10^9$ M^{-1} s^{-1} [76]

The degradation rate of TA (R^d_{TA}) is correlated to the formation rate of TAOH (R^f_{TAOH}) and of $HO^\bullet$ ($R^f_{HO\bullet}$) following the Equation 17.

$$R_{TA}^{d} \propto \frac{R_{TAOH}^{f}}{\gamma} = R_{HO\cdot}^{f}$$

Equation 17.

R^{f}_{TAOH} can be directly determined by the slope of the linear regression of the concentration of TAOH in function of time.

The quantum yield for the photolysis of a molecule in a decomposition reaction is defined as the ratio between the number of molecules decomposed and the number of photons absorbed. In this work the quantum yield was calculated for the photo-generated hydroxyl radical in cloud water samples but also for the photolysis of organic compounds like tryptophan or tartronic acid using different irradiation set-ups.

The quantum yield of hydroxyl radical formation ($\Phi_{\lambda_1-\lambda_2}^{HO\cdot}$) can be calculated by the ratio between R^{f}_{HO}**.** and the number of absorbed photons per unit of time in the overlap range between λ_1 and λ_2 (Equation 18). This value evaluates the photochemical process efficiency independently from the experimental photochemical conditions.

$$\Phi_{\lambda_1-\lambda_2}^{HO\cdot} = \frac{R_{HO\cdot}^{f}}{I_a}$$

Equation 18.

I_a can be calculated from the following Equation 19:

$$I_a = \int_{\lambda_1}^{\lambda_2} I_0(\lambda)\left(1 - 10^{-Abs(\lambda)}\right)d\lambda$$

Equation 19.

$I_0(\lambda)$ is the incident photon flux corresponding to the lamp emission and Abs(λ) is the absorption of the solution, normalized for the optical path.

For the photolysis of organic compounds polychromatic quantum yield is calculated using Equation 20

$$\Phi_{\lambda_1-\lambda_2}^{P} = \frac{R_P^d}{I_a}$$

Equation 20.

Where $\Phi^{P}_{\lambda1-\lambda2}$ is the quantum yield of photolysis of a product P, R^{d}_{P} is the disappearance rate of the compound P and I_a is defined as in Equation 19.

Laser Flash Photolysis

Laser Flash photolysis (LFP), is used for a kinetic study of short lived species, and was developed by George Porter and Ronald Norrish (Nobel Prize 1967). This technique provides direct transient measurement of reactions involving species such as radicals or excited states. In LFP the sample is firstly excited by a strong pulse of monochromatic light from a laser of a nanosecond pulse width. This first pulse starts a chemical reaction or leads to an increased population for energy levels other than the ground state within a sample of atoms or molecules. Differences in absorption compared to the ground state are measured with time resolved spectroscopy.

The set-up used for the experiments is schematized in Figure 22. The third (355 nm) or fourth (266 nm) harmonic of a Quanta Ray GCR 130-01 Nd:YAG laser system instrument was used with a right angle geometry with respect to the monitoring light beam. The single pulses energy was calculated for each experiment and was set in the range of 35-50 mJ. The transient absorbance at the preselected wavelength was monitored by a detection system consisting of a pulsed Xenon lamp (150 W), monochromator and photomultiplier (1P28). A spectrometer control unit was used for synchronizing the pulsed light source and programmable shutters with the laser output. The signal for the photomultiplier was digitized by a programmable digital oscilloscope (HP54522A). A 32 bit RISC-processor kinetic spectrometer workstation was used to analyze the digitized signal.

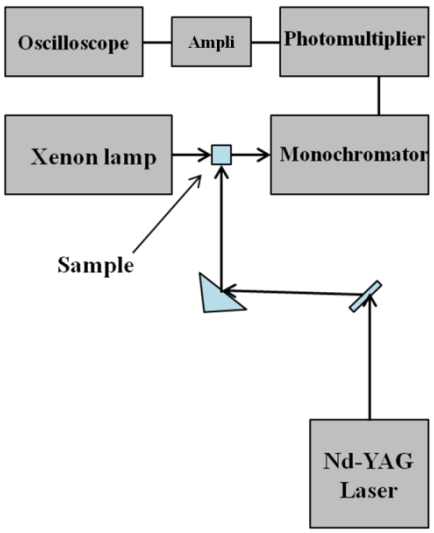

Figure 22: Schematic representation of the Laser Flash Photolysis set-up.

Kinetic approach for the study of the reactivity with hydroxyl radical by LFP.

Laser Flash Photolysis was used for indirect kinetic studies of $HO^{\bullet}$ reactions. Kinetics studies of $HO^{\bullet}$ reactions were carried out by competitive kinetics techniques using the thiocyanate ion

as a reference reactant because hydroxyl radical is not directly detectable due to its low absorption. The formation of the $HO^{\bullet}$ was initiated by photolysis of hydrogen peroxide by the fourth harmonic ($\lambda = 266$ nm) of the Laser set-up described in the previous paragraph. The mean pulse energy was 40-50 mJ and measurements were performed at room temperature.

Solutions were prepared mixing 0.1 M of thiocyanate and 8×10^{-2} M of hydrogen peroxide solutions. The concentration of the hydrogen peroxide stock solution was determined daily by UV-vis spectroscopy. The concentrations of the organic reactant, tartronic acid in particular, were in the range between 2.5 mM and 10 mM. $(NH_4)SCN$, H_2O_2 and the organic reactants were obtained from Merck or Fluka. If necessary, the pH value was adjusted with NaOH and $HClO_4$.

All experiments were carried out under conditions of pseudo-first order kinetics using an excess of the concentrations of the organic reactants in the reaction solution compared to the initial radical concentration. The errors given in the present study represent statistical errors for a confidence interval of 95% as derived from linear regression analysis of the data obtained.

The concentration of the $HO^{\bullet}$ radical was detected by recording the absorbance of the $(SCN)_2^{\bullet-}$ radical anion. The competition kinetics system applied here is based on the following reactions (R78-81):

R78) $H_2O_2 + h\nu$ (266 nm) $\rightarrow 2\ HO^{\bullet}$

R79) $HO^{\bullet} + SCN^{-} \rightarrow SCNHO^{\bullet-}$

R80) $SCNHO^{\bullet-} \rightleftarrows SCN^{\bullet} + HO^{-}$

R81) $SCN^{\bullet} + SCN^{-} \rightleftarrows (SCN)_2^{\bullet-}$

R82) $HO^{\bullet} + R \rightarrow P$

Assuming complete consumption of the initial $HO^{\bullet}$ radicals, it can be concluded that the resulting $(SCN)_2^{\bullet-}$ concentration is equal to the hydroxyl radical initial concentration without R. Calculations based on available data for the reactivity of the $SCNHO^{\bullet-}$and $SCN^{\bullet}$ radicals show that their possible side reactions do not have any influence on the final $(SCN)_2^{\bullet-}$ yield under adopted conditions. By adding a reactant (R) the yield of $(SCN)_2^{\bullet-}$ is reduced by the fraction of $HO^{\bullet}$ consumed by R, following reaction R82. The formation of $(SCN)_2^{\bullet-}$ is inhibited and its signal decreases proportionally to the concentration of R in the solution. An example of the diminution of the absorbance is given in Figure 23.

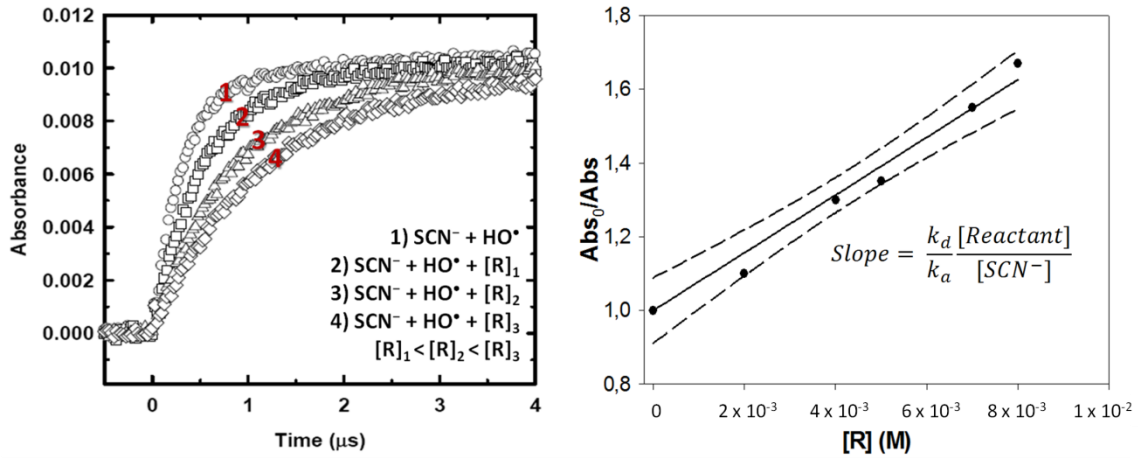

Figure 23: Absorption of thiocyanate radical anion in function of different concentration of reactant R (left) and linear fitting of the ratio Abs_0/Abs in function of the concentration of R to find the second order rate constant (right).

The second order rate constant k_d was obtained from the Equation 21, where Abs_0 is the light intensity absorbed by $(SCN)_2^{\bullet-}$ and *Abs* is the variation of the intensity when the reactant is added to the reaction solution. k_a is the second order rate constant between the hydroxyl radical and thiocyanate (1.10×10^{10} M^{-1} s^{-1} [76]).

$$\frac{Abs_0}{Abs} = 1 + \frac{k_d}{k_a}\frac{[Reactant]}{[SCN^-]}$$

Equation 21.

Ionic Chromatography analysis

Two ionic chromatography systems were used during this study. For inorganic anions (Cl^-, NO_3^-, SO_4^{2-}, PO_4^{3-}) the analysis was performed using a Dionex DX-320 equipped with a guard column IonPac AG11 (4 × 50 mm) and an analytical column IonPac AS11 (5 × 250 mm). Chromatographic analysis was performed employing a KOH gradient and the LOD (limit of detection) of inorganic compounds was estimated to be lower than 0.1 µM. Concentrations of inorganic cations (Na^+, NH_4^+, K^+, Mg^{2+}, Ca^{2+}) were determined using a Dionex ICS-1500 equipped with a guard column IonPac CG16 (4 × 50 mm) and an analytical column IonPac CS16 (5 × 250 mm). A gradient of methansulfonic acid (MSA) was employed. The flow was set at 1 mL min^{-1} for both systems.

Carboxylic acids analysis

The analysis of carboxylic acids (formic, acetic, succinic, tartronic and oxalic) was performed using a Thermo Dionex ICS-5000 equipped with a guard column IonPac AG18 (2 × 50 mm) and an analytical column IonPac AS18 (2 × 250 mm). Chromatographic analysis was

performed using a KOH gradient, reported in Table 8, and the LOD was estimated to be lower than 0.1 µM. In Figure 24 the chromatogram obtained for the analysis of a standard solution 5 µM of carboxylic acids is reported. Samples were analyzed without further purification.

Time (min)	KOH (mM)
0	10.0
4	11.0
11	17.0
21	19.5
23	19.5
23.1	10.0
35	10.0

Table 8:KOH gradient used for the analysis of carboxylic acids.

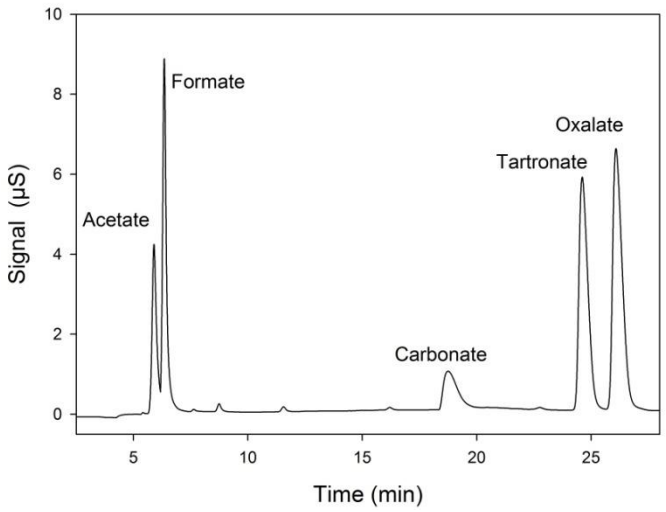

Figure 24: Example of chromatogram obtained for the analysis of carboxylic acids.

HPLC

The HPLC systems used are

- Waters Alliance
- Water Acquity UPLC
- Shimadzu Nexera XR

All the HPLC systems are equipped with photo diode array (PDA) and fluorescence detector (FLR).

Nitrites

Nitrite ion concentration was determined by derivatization with 2,4-dinitrophenylhydrazine (DNPH) (purity > 97%, Sigma Aldrich). The derivatizing solution was prepared mixing 250 mg of DNPH with 6.25 mL of HCl 35%, 3.12 mL of acetonitrile and 15.6 mL of MilliQ water. 50 µL of this solution were added to 3 mL of sample. Nitrites were analyzed by HPLC using isocratic elution (methanol 60%, MilliQ water 40%, $H_3PO_4 \approx 0.1\%$) and a Cary Eclipse XDB-C18 column (Agilent, 4.6 × 150 mm, 5 µm). Flow rate was set at 1 mL min^{-1} and PDA at 307 nm. This method allows the determination of nano molar concentrations of nitrites [173] also in frozen samples. In Figure 25 the reaction between 2,4-dinitrophenylhydrazine and nitrite ions is reported.

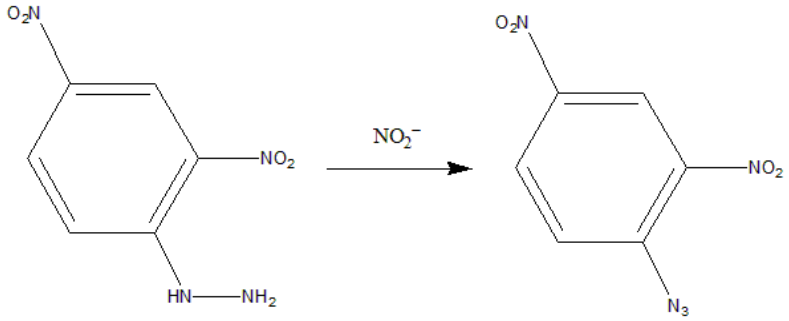

Figure 25: Reaction between 2,4-dinitrophenylhydrazine and nitrite ions.

Detection of amino acids

A lot of derivatization methods have been proposed for detection of amino acids in order to increase sensitivity and selectivity. In this work, samples were pretreated with o-phthalaldehyde (OPA), separated by HPLC and analysed by fluorescence detection.

Primary amino acids with the NH_2 group reacts with OPA to form fluorescent compounds under the presence of a thiol group, in our case of mercaptopropionic acid (MPA). Figure 26 shows the reaction of derivatization.

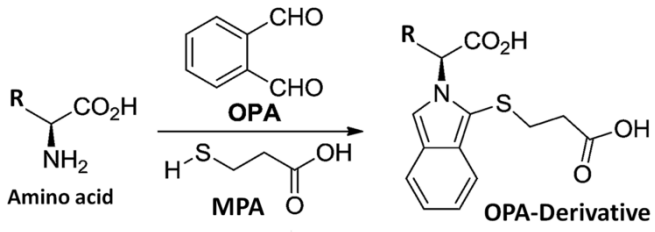

Figure 26: Derivatization of amino acids with o-phthalaldehyde (OPA) in the presence of mercaptopropionic acid (MPA).

OPA 15.0 mM and MPA 7.7 mM were prepared in borate buffer solution 0.1 M and the derivatization is automatically carried on by the HPLC autosampler Shimadzu Nexera SIL-

30AC. For this analysis the HPLC system Shimadzu Nexera and the pretreatement function-equipped autosampler SIL-30AC were used. In an empty vial, 30 µL of MPA, 15 µL of OPA and 5 µL of sample were mixed and after two minutes to complete the derivatization, 1 µL of the solution was injected. Derivatized compounds were separated with HPLC column Shimadzu Shim-pack XR-ODS (3.0 × 100 mm, Ø 2.2 µm, porous particles) using a flow of 0.7 mL min^{-1} following the gradient reported in Table 9. The fluorescence detector RF-20A XS was used with detection at excitation wavelength (λ_{ex})/ emission wavelength (λ_{em}) 350/450 nm.

Time (min)	% Eluent A: 10 mM phosphate buffer, pH 6.8	% Eluent B: CH_3CN:CH_3OH:H_2O 45:45:10
0	90	10
15	25	75
16	0	100
21	0	100
21.5	90	10
25	90	10

Table 9: HPLC gradient for amino acids detection.

A standard solution was prepared by dilution in HCl 0.1 M of an amino acids standard solution (AA S18, 2.5 mM) purchased from Sigma Aldrich, while cloud water samples were analyzed without further treatments. In Figure 27 the chromatogram obtained for the solution 10 µM of the amino acids standard is reported. The limit of detection of the analysis was estimated to be of the order of 25 nM.

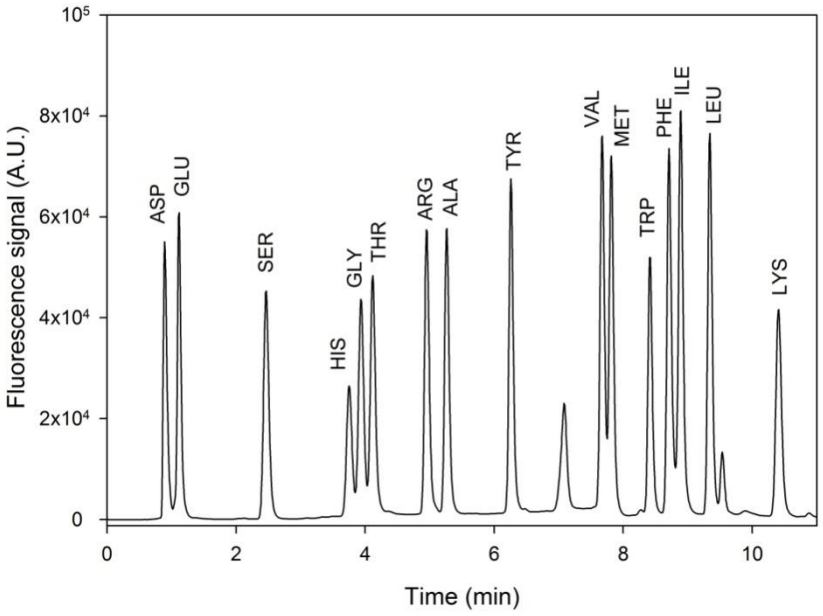

Figure 27: Chromatogram obtained for the solution of the amino acids standard with concentration 10 µM.

Total Organic Carbon

The TOC concentration is determined with a TOC 5050A analyser which uses high temperature catalytic oxidation (HTCO) and is equipped with a non-dispersive infra red detector (NDIR). The limit of detection is of the order of 1 mg L^{-1} and the precision of 0.1 mg L^{-1}.

Results

Chapter 5

Motivation

The following chapter, in the form of a scientific article, published in 2015 in *Atmospheric Chemistry and Physics*, deals with the photochemical production of hydroxyl radicals in cloud water. As described in Chapter 2, organic compounds in cloud aqueous phase react following two competitive pathways: oxidative *vs* accretion. The first part was devoted to the determination of hydroxyl radical photo-formation rate and quantum yield which determine the preferred pathway between oxidation and accretion.

Hydroxyl radical photochemical generation is mainly attributed to the photolysis of inorganic sources like hydrogen peroxide, nitrates, nitrites and iron ions. The second goal of this work was to assess the contribution of inorganic sources to the formation rate and to find the correlation between this parameter and the air mass origin.

The last part of this work concerns the comparison between experimental values and modeled formation rates, calculated by the model of multiphase cloud chemistry (M2C2). This part is the result of collaboration with the LAMP-OPGC (Laboratoire de Météorologie Physique – Observatoire de la Physique du Globe de Clermont-Ferrand) and it enables the adjustment of the contribution of each inorganic source to the hydroxyl radical formation rate in the model.

This work allows, for the first time, the assessment of the role of iron in cloud water oxidant capacity, to date overestimated in atmospheric models.

A better understanding of hydroxyl radical photochemical sources in cloud waters collected at the puy de Dôme station : Experimental *versus* modeled formation rates

A. Bianco[a,b,†], M. Passananti[a,b,†], H. Perroux[c,d], G. Voyard[a,b], C. Mouchel-Vallon[c,d], N. Chaumerliac[c,d], G. Mailhot[a,b], L. Deguillaume[c,d,*], M. Brigante[a,b,*]

[a] *Université Clermont Auvergne, Université Blaise Pascal, Institut de Chimie de Clermont-Ferrand, BP 10448, F-63000 CLERMONT-FERRAND, FRANCE*

[b] *CNRS, UMR 6296, ICCF, F-63171 AUBIERE, FRANCE*

[c] *Université Clermont Auvergne, Université Blaise Pascal, Laboratoire de Météorologie Physique, BP 10448, F-63000 CLERMONT-FERRAND, FRANCE*

[d] *CNRS, UMR 6016, LaMP, F-63171 AUBIERE, FRANCE*

* Corresponding author e-mail:
marcello.brigante@univ-bpclermont.fr
L.Deguillaume@opgc.univ-bpclermont.fr

† These two authors contributed equally to this work

Atmos. Chem. Phys., 15, 9191-9202, 2015

http://www.atmos-chem-phys.net/15/9191/2015/

doi:10.5194/acp-15-9191-2015

Received: 15 Apr 2015 – Published in Atmos. Chem. Phys. Discuss.: 18 May 2015
Revised: 15 Jul 2015 – Accepted: 30 Jul 2015 – Published: 19 Aug 2015

Keywords

cloud water, photochemistry, hydroxyl radical, *in situ* measurements, cloud chemistry model

Abstract. The oxidative capacity of the cloud aqueous phase is investigated during three field campaigns from 2013 to 2014 at the top of the puy de Dôme station (PUY) in France. Forty-one cloud samples are collected, and the corresponding air masses are classified as highly

marine, marine and continental. Hydroxyl radical ($HO^{\bullet}$) formation rates ($R^{f}_{HO\cdot}$) are determined using a photochemical setup (Xenon lamp that can reproduce the solar spectrum) and a chemical probe coupled with spectroscopic analysis that can trap all of the generated radicals for each sample. Using this method, the obtained values correspond to the total formation of $HO^{\bullet}$ without its chemical sinks. These formation rates are correlated with the concentrations of the naturally occurring sources of $HO^{\bullet}$, including hydrogen peroxide, nitrite, nitrate and iron. The total hydroxyl radical formation rates are measured as ranging from approximately 2×10^{-11} to 4×10^{-10} M s^{-1}, and the hydroxyl radical quantum yield formation ($\Phi_{HO\cdot}$) is estimated between 10^{-4} and 10^{-2}. Experimental values are compared with modeled formation rates calculated by the model of multiphase cloud chemistry (M2C2), considering only the chemical sources of the hydroxyl radicals. The comparison between the experimental and the modeled results suggests that the photoreactivity of the iron species as a source of $HO^{\bullet}$ is overestimated by the model, and H_2O_2 photolysis represents the most important source of this radical (between 70 and 99%) for the cloud water sampled at the PUY station (primarily marine and continental).

5.1 Introduction

In the atmosphere, many trace gases are transformed by the hydroxyl radical ($HO^{\bullet}$), which is considered the most efficient environmental oxidant (*e.g.,* Seinfeld et al. [45]). Evaluating the production of this short-lived species is crucial because it determines the fate of many chemical compounds. In atmospheric water drops and aqueous particles, the hydroxyl radical also controls the fate of inorganic and organic species [30]. The $HO^{\bullet}$ - mediated oxidation of organic compounds in the aqueous phase can lead to the formation of shorter but often multifunctional organic species and, ultimately, to complete mineralization [101]. Complex chemical reactions catalyzed by $HO^{\bullet}$ can also occur in the aqueous phase forming accretion products such as oligomers [135,174-178]. These alternative chemical pathways are efficient processes to convert organic compounds into Secondary Organic Aerosols (SOAs) [107].

The sources of hydroxyl radicals in the aqueous phase strongly differ from those in the gas phase because of the presence of ionic species and metal ions. Aqueous phase reactants that produce $HO^{\bullet}$ present high concentrations in water drops and aqueous particles, likely enhancing the $HO^{\bullet}$ photochemical production in the condensed phase. This radical can be generated in the aqueous phase by direct photolysis of hydrogen peroxide (H_2O_2) [30,179], iron

complexes [15], nitrate (NO_3^-) [180] and nitrite ions (NO_2^-) [181]. The other significant source of $HO^\bullet$ in cloud water is the uptake from the gas phase [83]. The relative importance of the different hydroxyl radical sources depends on the chemical composition of the aqueous phase, which is also strongly variable [27]. $HO^\bullet$ is further scavenged in the aqueous phase, primarily by dissolved organic compounds. Evaluation of this sink is difficult because the dissolved organic matter is diverse, complex and poorly characterized [102].

Uncertainties in $HO^\bullet$ sinks and sources make its concentrations in atmospheric water highly difficult to estimate. For this estimation, models describing the multiphase cloud chemistry have been developed and have considered the reactivity in the gas and aqueous phases along with the mass transfer between the two phases [97,104,105]. These numerical tools allow the estimation of the steady-state concentration of $HO^\bullet$ ($[HO^\bullet]_{ss}$), which is a crucial quantity to understand the fate of atmospheric pollutants [103]. The range of the maximal $HO^\bullet$ concentration varies from 10^{-16} to 10^{-12} M, depending on the "chemical scenario" (*i.e.,* emission/deposition and the initial chemical conditions) used in the modeling study. The amounts of organic matter and iron are key parameters controlling the $[HO^\bullet]_{ss}$. These models are expected to underestimate the radical sinks because organic scavengers cannot be exhaustively described in the aqueous chemical mechanism [103].

In this study, we propose the investigation of the hydroxyl radical formation in real cloud water sampled at the puy de Dôme mountain (France). The hydroxyl radical formation rate is quantified for 36 cloud water samples collected during 3 field campaigns (2013-2014). Because the main photochemical sources (hydrogen peroxide, iron, nitrite and nitrate) are also quantified, we can calculate their relative contributions to the production of the hydroxyl radicals. For this purpose, the contribution to the hydroxyl radical formation rate of more concentrated inorganic photochemical sources is investigated separately in synthetic solution. In parallel, the model of multiphase cloud chemistry (M2C2) is used to simulate $HO^\bullet$ formation rates. This model considers explicit aqueous chemical mechanisms, and a "simplified" version of the model is used to reproduce the bulk water irradiation experiments (lamp spectrum) under variable physico-chemical conditions (pH, initial concentrations of $HO^\bullet$ sources) corresponding to the cloud water samples. The comparison between the modeled and experimental $HO^\bullet$ production rates facilitates quantification of the various $HO^\bullet$ sources and enables validation of the model to reproduce the oxidative capacity of the atmospheric aqueous phase.

5.2 Materials and Methods

5.2.1 Chemicals

Hydrogen peroxide (30% in water, not stabilized), sodium nitrate (purity > 99%) and ferrozine (purity > 97%) were obtained from Fluka, while sodium nitrite (purity > 98%) and terephthalic disodium salt (purity > 99%) were purchased from ProLabo and Alfa Aesar, respectively. All of the other chemicals (purity reagent grade) used for the analysis were obtained from Sigma-Aldrich.

Solutions are prepared with deionized ultra-pure aerated milli-Q water from Millipore (resistivity = 18.2 MΩ cm) under a laminar flux hood. Moreover, glass containers and injection material are washed three times with ultra-pure water before use. If necessary, the pH values are adjusted with perchloric acid (1 N) and NaOH (1 N) using a JENWAY 3310 pH-meter within ± 0.01 pH unit. All of the solutions are stored under dark conditions, and the final preparations are performed in a room equipped with a sodium lamp (589 nm emission).

5.2.2 Cloud water sampling

Cloud water is sampled at the puy de Dôme (PUY) station (48°N, 2°E; 1465 m a.s.l.) in the Massif Central region (France). Three campaigns occurred during autumn 2013 from October 14th to November 6th, during spring and autumn 2014 from March 22nd to April 5th and from November 4th to 19th. During these periods, the station was primarily located in the free troposphere; thus, the air masses from various origins were not influenced by the local pollution [182].

The cloud droplet sampling is performed by a one stage cloud droplet impactor [27]. With the air flux used, the lower limit of the aerodynamic diameter is approximately 7 μm [129]. The impactor used for this study is constructed of stainless steel and aluminum, and cloud droplets are collected by impaction onto a rectangular aluminum plate with an average sampling time of two hours. Cloud water samples are filtered using a 0.45 μm PTFE filter within 10 minutes after sampling to eliminate all of the microorganisms and particles that can interfere with the spectroscopic analysis.

Measurements performed immediately after cloud collection are conductivity, redox potential, pH, UV-visible spectroscopy, H_2O_2 and iron concentrations. Ion chromatography (IC), total organic carbon (TOC), and nitrite analysis are determined less than 24 hours after sampling. At each stage, sampling and analyses are performed with the greatest precaution to minimize all possible external contaminations, and the solutions are stored at 277 K under dark

conditions. Hydroxyl radical formation rates ($R_{HO^{\cdot}}^{f}$) and polychromatic quantum yields ($\Phi_{HO^{\cdot}}$) are calculated using polychromatic wavelengths.

5.2.3 Physico-chemical measurements

Different parameters are monitored, including pH, conductivity and redox potential, which are measured using a Hanna multiparameter instrument. The UV-Vis spectrum of the collected cloud water is determined with an Agilent Technologies Cary 60 UV-vis spectrophotometer. The TOC concentration is determined with a TOC 5050A analyzer (Shimadzu). Hydrogen peroxide concentration is estimated using p-hydroxyphenilacetic acid (HPAA, purity > 98%) and horseradish peroxidase (POD) (solid containing 150-200 units per mg), according to the spectrofluorimetric quantification method [183]. The formation of the dimer of HPAA is correlated with the concentration of hydrogen peroxide and is detected using a Varian Cary Eclipse Fluorescence Spectrophotometer setting excitation wavelengths at 320 nm, while emission is registered from 340 and 500 nm. The maximum signal is quantified at 408 nm. The scan rate is 600 nm min^{-1}, and a bandpass of 10 nm is set for excitation and emission. Nitrite ions concentration is determined by derivatization with 2,4-dinitrophenylhydrazine (DNPH) (purity > 97%), in acidic solution (HCl 37%). The UV-absorbing derivative (2,4-dinitrophenilazide) is detected by HPLC. The HPLC system (Waters Alliance) equipped with a diode array detector is used with an Eclipse XDB-C18 column (Agilent, 4.6 × 150 mm, 5 μm), and an isocratic method is adopted, using 40% acidified water (0.1% phosphoric acid) and 60% methanol. The flow rate is 1 mL min^{-1}, and 2,4–dinitrophenilazide is eluted with a retention time of 4.1 min [173] and detected at 307 nm. Fe(II) and Fe(III) concentrations are determined by the spectrophotometric method by complexation with ferrozine (purity > 97%), as described by Stookey [172]. Fe(II) and Fe(III) represent the oxidative state of the iron species. Adopted complexation method allows us to determine all Fe(II) and Fe(III) species present in solution (i.e., considered as free, aquacomplexes and as complex with other organic molecules). Ascorbic acid (purity reagent grade) is used as the reducing agent to determine total iron. The complex absorption is measured with a Varian Cary 300 Scan Spectrophotometer at 562 nm.

It has been previously demonstrated that filtration does not modify the soluble iron quantification in natural cloud water samples [184,185]. It is not possible to measure particulate iron because the ferrozine method cannot solubilize solid phase iron (the contact time between acidic reagents and particulate iron is too short). Moreover, the iron particle is expected to be less reactive than the solubilized iron; consequently, its contribution can be neglected [83].

Ion chromatography (IC) analysis is performed employing a DIONEX DX-320 equipped with an IonPac AG11 (guard-column 4 × 50 mm) and an IonPac AS11 (analytical column 5 × 250 mm) for anions and a DIONEX ICS-1500 equipped with an IonPac CG16 (guard-column 4 × 50 mm) and an IonPac CS16 (analytical column 5 × 250 mm) for cations.

5.2.4 Statistical analysis

Principal component analysis (PCA) and hierarchical clustering analysis (HCA) are performed with R-3.1.2 software [186] using the FactoMineR package (version 1.28, [187]). This statistical analysis provides a synthetic representation of experimental data as a function of the correlations between variables considered and similarities present among the analyzed samples. This technique allows the determination of information contained in a set of multivariate data, summarizing it in a few linear combinations of the variables [188]. HCA data are grouped by similarity, considering all of the information contained in the data set. HCA is a statistical method to qualitatively study the composition of cloud water and can be used to identify the grouping variables that are not well detectable using only PCA.

5.2.5 Irradiation experiments

To evaluate the contribution of each possible photochemical source (nitrate, nitrite or hydrogen peroxide) to the hydroxyl radical formation in cloud water, synthetic solutions doped with a single source of oxidant are irradiated to quantify their contribution to the total generation of hydroxyl radicals in a more complex medium.

The photochemical device is composed of a Xenon lamp equipped with a water cooler to avoid the increase of temperature due to the infrared radiations and a mirror to reflect the light vertically. A Pyrex filter was located before the reactor for filtering of light at wavelengths below than 290 nm, corresponding to the lowest wavelengths of the solar emission spectrum. The reactor is a 40 mL cylindrical Pyrex container cooled by water circulation at a temperature of 278 ± 2 K to limit thermal reactions. Samples are continuously stirred with a magnetic stirrer using a Teflon bar to ensure homogeneity.

In Fig. 1, the emission spectrum of the lamp recorded using fiber optics coupled with a charge-coupled device (CCD) spectrophotometer (Ocean Optics USD 2000+UV-VIS) is reported. The energy was normalized with the actinometry results using a paranitroanisole (PNA)/pyridine actinometer [170]. Over the wavelength range of 290 to 600 nm, a total flux of 157 W m^{-2} is measured. The intensity values of the sun emission under clear sky and cloudy conditions at the puy de Dôme mountain in autumn 2013 are also presented in Fig. 1.

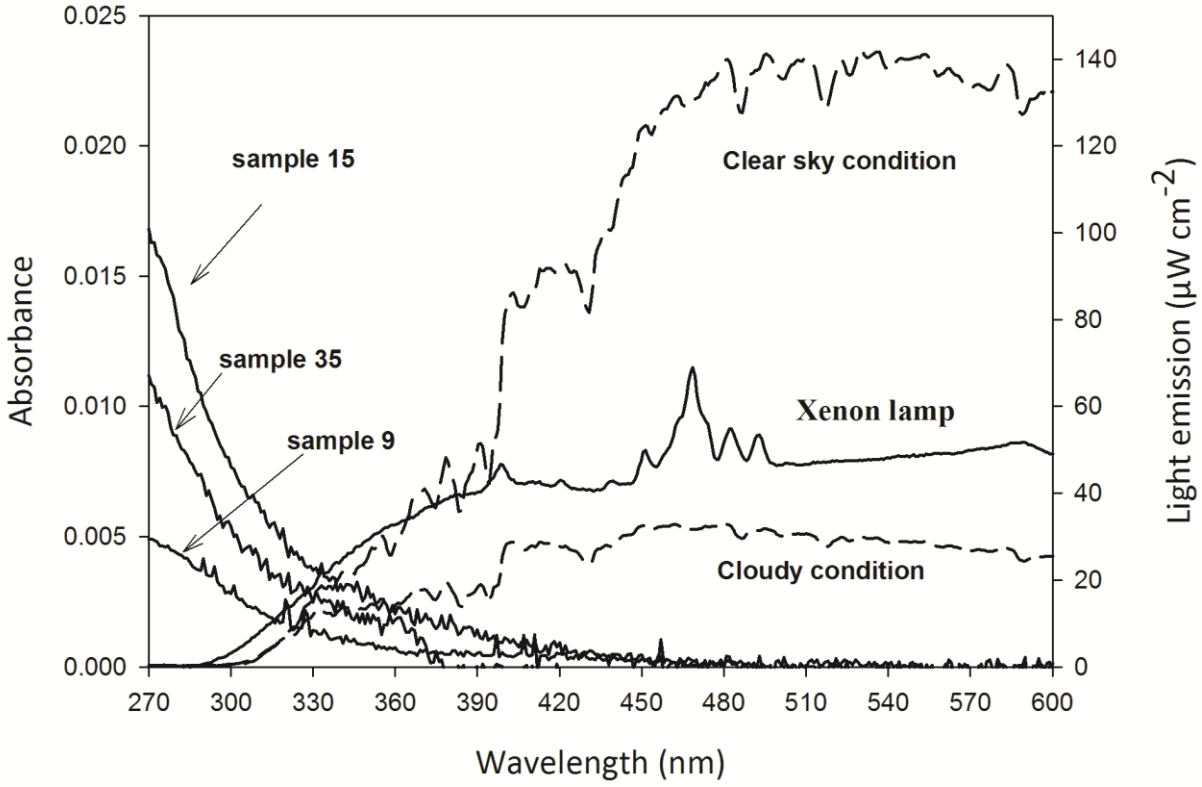

Figure 1: Absorption spectra of different cloud water samples (left axis) and the right-hand axis shows the emission spectrum of the adopted Xenon lamp reaching solutions over the range of 290 to600 nm (total flux intensity = 157 W m^{-2}) compared with the sun emission spectrum (dashed line) for a sunny (353 W m^{-2}) and a cloudy day (90 W m^{-2}) in October 2013.

5.2.6 Hydroxyl radical formation rate and quantum yield determination

The hydroxyl radical formation rate is determined using terephthalate (TA) (terephthalic disodium salt, purity > 99%) as a probe [189]. Formation of hydroxyterephthalate (TAOH) is quantified using a Varian Cary Eclipse Fluorescence Spectrophotometer, setting excitation wavelengths at 320 nm, while the emission maximum is measured at 420 nm. The scan rate is 600 nm min^{-1}, and a bandpass of 10 nm is set for excitation and emission. Terephthalate is a useful probe because it allows the determination of hydroxyl radical formation rates in the presence of fluorescent dissolved organic matter. The concentration of the probe is in a large excess (2 mM) compared with the concentration of organic matter to trap all of the photogenerated hydroxyl radicals and then to estimate a value for the hydroxyl radical formation rate not affected by depletion of $HO^{\bullet}$ by other sinks.

The reaction between TA and the hydroxyl radical leads to the formation of fluorescent TAOH and non fluorescent secondary products (R1), as follows:

(R1) $TA + HO^{\bullet} \rightarrow TAOH + products$

The degradation rate of TA (R_{TA}^{d}) and formation rate of hydroxyl radical ($R_{HO^{\cdot}}^{f}$) and TAOH (R_{TAOH}^{f}) can be expressed as reported in Equation 1 and 2:

$$R_{HO^{\cdot}}^{f} \approx R_{TA}^{d} \approx \frac{R_{TAOH}^{f}}{\gamma}$$

Equation 1.

With

$$R_{TA}^{d} = k_{HO^{\cdot},TA} \times [HO^{\cdot}] \times [TA]$$

Equation 2.

where $k_{HO^{\cdot},TA}$= 4.0 × 10^{9} M^{-1} s^{-1} is the second order rate constant of the reaction between $HO^{\bullet}$ and TA [189], and [TA] is the initial concentration of terephthalate and γ is the TAOH formation yield calculated as a function of solution pH. This value is found to be linearly correlated with the pH value and is estimated between the values of 0.15 and 0.25 over the pH range of 4 to 7.

Other radicals, such as sulfate ($SO_4^{\bullet-}$) or chlorine/dichlorine ($Cl^{\bullet}/Cl_2^{\bullet-}$), can react with TA, leading to the H-abstraction as first chemical reaction. However, their direct generation is nearly exclusively due to the electron transfer reaction from the corresponding anion (*i.e.*, SO_4^{2-} and Cl^{-}, respectively) to the hydroxyl radical. Moreover, considering that the second order rate constant of aromatic compounds with the dichloride radical anion and the sulfate radical is expected to be one or two orders of magnitude lower than that with hydroxyl radical [190], and considering a relatively low concentration of sulfate and dichlorine radicals in our cloud samples, the TA reactivity can be attributed exclusively to the $HO^{\bullet}$.

The quantum yield of hydroxyl radical formation ($\Phi_{290-400\,nm}^{HO^{\cdot}}$) is defined as the ratio between the formation rate of $HO^{\bullet}$ ($R_{HO^{\cdot}}^{f}$) and the number of absorbed photons in Einstein per unit time in the overlap range of 290 to 600 (λ_1 and λ_2) (Equation 3).

This value evaluates the photochemical process efficiency independent of the experimental photochemical conditions.

$$\Phi_{290-400\,nm}^{HO^{\cdot}} = \frac{R_{HO^{\cdot}}^{f}}{I_a}$$

Equation 3.

where I_a can be calculated from the Equation 4:

$$I_a = \int_{\lambda_1}^{\lambda_2} I_0\,(\lambda)\left(1 - 10^{-Abs(\lambda)}\right)d\lambda$$

Equation 4.

where I_0 (photons m^{-2} s^{-1}) is the incident photon flux corresponding to the lamp emission and *Abs* is the absorption of cloud water (normalized considering the optical path length of 5 cm inside of the thermostated reactor).

5.2.7 Back-trajectory plots

Backward trajectories of collected air masses are calculated using the HYSPLIT (hybrid single-particle Lagrangian integrated trajectory) model with the GDAS1 meteorological data archive and the model of vertical velocity (*http://ready.arl.noaa.gov/HYSPLIT.php*). Backward trajectories are calculated for 72 hours [191].

5.2.8 Model description

The M2C2 combines detailed multiphase chemistry along with the parameterization of the microphysics [32,50,192]. Particularly, the detailed chemistry of H_xO_y, chlorine, carbonates, NO_y, sulfur, transition metal ions (iron, copper, manganese) and the oxidation of volatile organic compounds (VOCs) is included. Photolysis rates are calculated in the gaseous and aqueous phases, and the pH is calculated following the H^+ concentration. Numerical results consist of following the time evolution of the concentrations of each chemical species and calculating at each time step the relative contribution of chemical reactions in the production/destruction of chemical compounds.

In this study, a simplified version of the model is used. The cloud chemical mechanism is restricted to inorganic chemistry (H_xO_y, nitrogen, iron) that leads to the $HO^\bullet$ formation (see Table SM1 for details about the considered reactions). The complexation of iron by oxalate is also considered in the model because it can interfere with the $HO^\bullet$ formation rates [97]. Laboratory irradiation experiments are simulated with the M2C2 model considering its chemical module and neglecting microphysical processes and mass transfer parameterizations. Temperature and pH remained constant during the simulation time. We set the pH for each cloud water sample to the values reported in Table SM2, and the temperature is fixed at 278 K, which corresponds to the temperature of the irradiated solutions. The simulated irradiation intensity is held constant and homogenous throughout the experiment. The actinic flux of the experimental lamp is discretized in the tropospheric ultraviolet-visible (TUV) model in 156 non-regular intervals over a wavelength range of 120 to 750 nm [193]. The

photolysis rates of the chemical species are calculated in TUV according to the experimental quantum yields and absorption cross-sections and are indicated in Table SM1. Experimental chemical concentrations (Table SM2) are used to initialize the model (H_2O_2, nitrite, nitrate, iron). Moreover, oxalic acid is considered as an organic complexant during the Fe(II)/Fe(III) cycle. The formation rate of $HO^{\bullet}$ is calculated by the model considering the modeled contribution of each reaction producing $HO^{\bullet}$ during one hour of experiment.

Species		**K_a or K_h**	**-ΔH/R (K)**	**References**
$H_2O_2 \leftrightarrow HO_2^- + H^+$	T(1)	$2.2\ 10^{-12}$	–3730	[194]
$HO_2^{\bullet} \leftrightarrow O_2^{\bullet-} + H^+$	T(2)	$1.6\ 10^{-5}$		[195]
$HNO_2 \leftrightarrow NO_2^- + H^+$	T(3)	$1.6\ 10^{-3}$	1760	[196; 197]
$HNO_3 \leftrightarrow NO_3^- + H^+$	T(4)	$2.2\ 10^{1}$		[198]
$HNO_4 \leftrightarrow NO_4^- + H^+$	T(5)	$1.3\ 10^{-6}$		[199]
$HCl \leftrightarrow Cl^- + H^+$	T(6)	$1.7\ 10^{-6}$	–6890	[200]
$SO_2 + H_2O \leftrightarrow HSO_3^- + H^+$	T(7)	$1.3\ 10^{-2}$	–1960	[201]
$HSO_3^- \leftrightarrow SO_3^{2-} + H^+$	T(8)	$6.4\ 10^{-8}$	–1430	[201]
$H_2SO_4 \leftrightarrow HSO_4^- + H^+$	T(9)	$1.0\ 10^{3}$		[202]
$HSO_4^- \leftrightarrow SO_4^{2-} + H^+$	T(10)	$1.0\ 10^{-2}$		[203]
$Fe^{3+} + H_2O \leftrightarrow [Fe(OH)]^{2+} + H^+$	T(11)	$6.0\ 10^{-3}$		[204]
$[Fe(OH)]^{2+} + H_2O \leftrightarrow [Fe(OH)_2]^+ + H^+$	T(12)	$7.6\ 10^{-4}$		[204]
$CO_2 + H_2O \leftrightarrow HCO_3^- + H^+$	T(13)	$4.2\ 10^{-7}$		[202]
$HCO_3^- \leftrightarrow CO_3^{2-} + H^+$	T(14)	$4.8\ 10^{-11}$		[202]

Table SM1: Chemical mechanism considered in the M2C2 model.

5.3 Results and Discussion

5.3.1 Classification of cloud samples

Recently, physicochemical parameters and concentrations of the major organic and inorganic compounds of cloud samples collected over the last ten years at the puy de Dôme are measured and statistically analyzed by PCA [27]. Along with the corresponding back–trajectory plots, 4 different categories of air masses reaching the summit of the PUY could be distinguished, as follows: polluted, continental, marine and highly marine. Highly marine clouds exhibited high concentrations of Na^+ and Cl^-, and the marine category presented a lower concentration of ions but more elevated pH, while the two remaining clusters, classified as “continental” and “polluted”, are characterized by the second-highest and highest levels of NH_4^+, NO_3^-, and SO_4^{2-}, respectively.

In Table SM2, the measured physico-chemical composition of the cloud water samples is reported for this study. We use the same statistical analysis to classify these cloud water samples as Deguillaume et al. [27]. PCA is performed using the pH and the concentration of sulfate, nitrate, chloride, sodium and ammonium ions as variables. Figure 2 reports the scores plot for samples used for the previously reported classification as a function of the attributed class and for the new samples.

	Date		Origin	Temperature (°C)	pH	Redox potential (mV)	TOC (mg/L)	TC (mg/L)	IC (mg/L)	Anions (µmol/L)						Cations (µmol/L)				
										SO_4^{2-}	Cl^-	Acet	Form	Oxal	Succ	Na^+	NH_4^+	Mg^{2+}	K^+	Ca^{2+}
1	10/14/2013	4PM-6PM	W	6	6.1	NM	NM	NM	2.7	23.0	45.9	8.7	34.8	4.5	3.3	18.5	66.2	33.7	7.2	2.4
2	10/14/2013	6PM-9PM	W	6.5	5.6	NM	NM	NM	0.9	16.7	82.5	3.3	20.4	2.5	3.7	7.6	33.0	6.4	33.1	0.4
3	10/14/2013	9PM-12PM	W	6.7	5.6	NM	1.6	2.2	0.7	18.5	46.2	2.6	11.7	1.8	4.2	11.9	44.6	5.2	20.9	3.8
4	10/29/2013	5AM-8AM	W	2.2	5.0	261	2.8	3.6	0.8	46.8	246.9	21.1	28.5	2.7	4.2	56.3	38.0	NM	4.8	NM
5	10/29/2013	8AM-12AM	W	3.1	5.6	248	3.2	3.3	0.1	55.8	269.5	19.1	25.3	2.8	5.2	76.3	64.0	NM	11.7	NM
6	11/5/2013	2PM-4PM	W	6	5.8	231	2.0	2.7	0.7	8.5	25.0	13.9	25.5	1.9	3.4	7.8	13.5	NM	34.1	NM
7	11/5/2013	4PM-7PM	W	6	5.5	263	1.1	1.7	0.6	4.5	7.2	17.5	12.4	1.3	3.9	3.7	8.9	NM	25.7	NM
8	11/5/2013	7PM-9PM	W	5.8	5.6	313	0.8	1.4	0.56	7.9	16.6	9.3	24.5	1.7	3.0	4.5	17.7	NM	21.9	NM
9	11/5/2013	9PM-12PM	W	5.5	5.0	290	0.6	1.5	0.8	9.8	16.9	5.7	7.2	1.3	2.3	6.5	26.7	NM	22.7	NM
10	11/6/2013	7AM-10AM	W	7.9	5.4	289	1.1	1.9	0.9	6.1	9.7	7.5	17.2	1.3	5.7	6.0	18.0	NM	24.3	NM
11	11/6/2013	10AM-12AM	W	8	5.7	352	1.9	2.6	0.7	6.7	5.8	7.5	9.5	1.5	2.7	3.3	27.0	NM	25.8	NM
12	3/22/2014	7AM-11AM	W	0	6.7	228	2.9	3.5	0.6	34.8	65.7	13.3	48.3	4.1	0.1	20.9	87.6	12.4	2.3	4.7
13	3/22/2014	11AM-2PM	W	0	6.7	264	5.4	6.1	0.7	37.1	133.8	20.4	43.8	5.4	0.2	36.8	108.8	8.7	4.9	6.6
14	3/25/2014	11AM-1PM	W	-2	6.6	240	3.4	3.9	0.5	49.2	228.5	13.8	30.6	3.2	0.1	56.8	73.2	10.3	9.1	7.1
15	3/25/2014	1PM-3PM	NW	0	6.4	228	6.0	6.6	0.5	32.6	153.8	14.0	65.1	3.3	0.2	38.8	79.6	12.5	6.4	6.9
16	3/25/2014	7PM-9PM	NW	-2	6.1	243	8.7	9.0	0.4	14.8	73.0	12.5	65.0	3.8	0.2	20.8	50.2	13.6	4.0	9.4
17	3/26/2014	8AM-9AM	N	-3	5.5	233	6.5	7.0	0.5	56.4	25.2	26.2	38.3	5.9	0.8	9.6	252.4	7.2	2.9	7.9
18	3/26/2014	9AM-11AM	N	-3	5.4	239	8.6	9.2	0.6	45.4	26.5	15.8	34.9	5.3	0.7	8.3	206.0	9.0	2.4	15.6
19	4/4/2014	8PM-10PM	NW	2	6.2	261	1.5	2.0	0.5	13.5	19.4	9.6	23.6	3.4	0.4	5.0	39.6	5.4	7.8	0.0
20	4/4/2014	10PM-12PM	NW	2	6.5	261	1.7	2.1	0.4	18.2	18.2	7.2	24.2	3.8	0.3	3.9	71.4	4.3	7.1	0.0
21	4/5/2014	1PM-4AM	W	2	6.6	250	2.6	3.1	0.5	26.0	29.4	14.3	32.5	4.4	0.3	6.9	124.1	4.4	7.4	0.0
22	4/5/2014	4AM-7AM	W	2	6.9	237	3.9	4.6	0.7	39.8	48.7	25.4	48.8	6.9	0.4	12.6	192.8	4.3	4.8	0.0
23	4/5/2014	7AM-10AM	W	2	6.8	239	4.5	5.3	0.7	67.5	76.1	30.4	63.4	7.4	0.5	18.0	212.7	5.3	4.3	2.0

24	4/11/2014	11AM-1PM	W	1	5.4	207	1.9	1.9	0.0	7.5	14.0	7.6	3.6	5.4	6.2	27.7	NM	NM	31.9	NM
25	5/11/2014	4AM-6PM	W	0.3	4.7	238	1.8	1.8	0.0	58.1	35.4	11.8	3.8	113.2	13.9	51.4	NM	NM	26.0	NM
26	5/11/2014	7AM-9AM	NW	0	4.1	280	1.8	1.8	0.0	139.3	41.7	5.2	3.3	115.7	9.2	43.8	39.7	NM	20.3	NM
27	5/11/2014	9AM-12AM	NW	-0.1	4.1	298	NM	14.9	0.1	247.4	98.0	3.8	3.4	302.2	18.8	99.9	83.9	NM	17.8	NM
28	5/11/2014	12AM-1PM	NW	0.1	4.2	295	3.6	3.6	0.0	202.8	87.0	10.8	3.1	377.2	27.9	116.7	97.37	NM	21.7	NM
29	12/11/2014	3PM-5PM	W	3	5.4	250	4.0	4.0	0.0	38.3	78.9	11.9	5.4	83.2	21.9	83.5	15.1	NM	19.9	NM
30	12/11/2014	5PM-7PM	W	2	5.5	261	2.3	2.4	0.1	28.7	68.2	12.7	4.8	47.1	21.7	72.2	NM	NM	17.6	NM
31	12/11/2014	7PM-9PM	W	2	5.6	254	2.7	2.8	0.1	24.2	68.9	2.9	2.9	32.5	33.0	77.3	NM	NM	21.3	NM
32	12/11/2014	9PM-12PM	W	2	5.4	254	1.7	1.7	0.1	23.4	64.4	5.2	4.5	20.2	13.5	80.1	NM	NM	17.5	NM
33	14/11/2014	5PM-7PM	S	5	5.5	258	2.2	2.2	0.0	11.3	6.0	4.9	3.6	10.4	5.4	15.7	NM	NM	16.3	NM
34	17/11/2014	4PM-6PM	W	1.1	5.6	249	2.2	2.4	0.1	8.8	4.7	7.6	3.9	11.8	5.6	13.1	NM	NM	21.3	NM
35	17/11/2014	7PM-9PM	W	0.7	5.7	245	1.0	1.1	0.0	8.0	2.0	7.3	3.6	10.0	5.8	10.9	NM	NM	19.9	NM
36	17/11/2014	9PM-12PM	W	0.6	5.3	263	1.2	1.2	0.0	11.0	5.3	6.9	3.8	14.3	6.9	14.2	NM	NM	18.5	NM
37	18/11/2014	6AM-8AM	NW	0.1	5.4	258	1.0	0.9	0.0	28.2	16.5	4.2	3.4	32.6	7.2	23.0	NM	NM	19.1	NM
38	18/11/2014	5PM-7PM	NW	1.8	5.7	243	2.3	2.4	0.1	16.4	11.9	8.8	3.6	22.0	7.0	18.3	2.2	NM	20.2	NM
39	18/11/2014	7PM-9PM	NW	1	5.3	257	1.8	1.8	0.0	14.0	7.3	5.6	3.7	14.1	5.6	18.2	NM	NM	20.2	NM
40	18/11/2014	9PM-12PM	NW	1	4.9	284	1.9	1.9	0.1	20.0	18.0	7.0	3.6	16.0	8.3	17.7	NM	NM	18.7	NM
41	19/11/2014	12PM-2AM	NW	1	4.6	306	2.2	2.2	0.0	26.7	36.7	10.3	3.4	34.7	12.3	28.1	NM	NM	17.1	NM

Table SM2: Physico-chemical parameters of sampled clouds. 23 samples have been analyzed corresponding to 6 cloud events. Acet: acetic acid; Form: formic acid, Oxal: oxalic acid, Succ: succinic acid). NM: not measured.

Three types are identified, as follows: (*i*) highly marine, (2 samples) characterized by pH values of 5.0 and 5.6, respectively, high concentration of chloride and sodium and low concentrations of nitrate, nitrite and ammonium; (*ii*) marine cloud waters (28 samples), showing pH values between 4.7 and 7.6 and very low concentrations of anions and cations, and (*iii*) continental samples (11 samples), with pH values from 4.1 to 6.9 and a medium concentration of nitrates, sulfates and ammonium, while sodium and chloride concentrations are very low. No sample could be classified as polluted cloud water because polluted cloud waters have been characterized by concentrations of nitrates, sulfates and ammonium higher than 350, 70 and 330 µM, respectively. This statistical analysis confirms that the majority of the collected samples are of marine origin. This statistical analysis is confirmed by the back-trajectory plots from the HYSPLIT model, showing that most of the air masses reaching the puy de Dôme arises from the west sector *i.e.,* from the Atlantic Ocean.

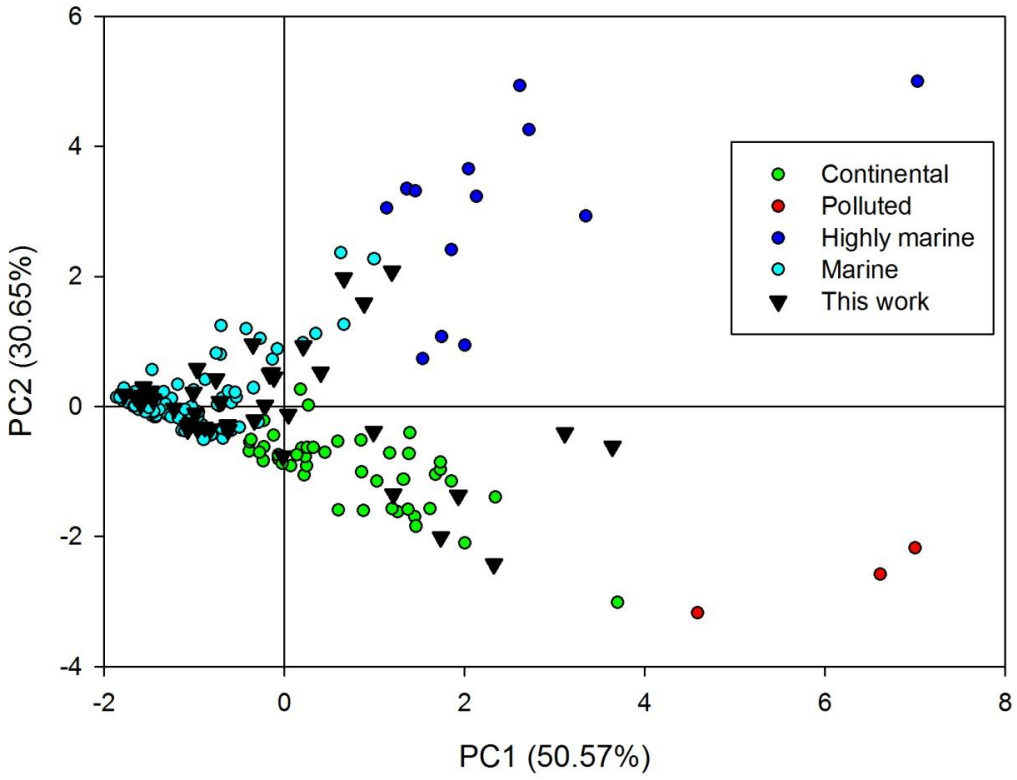

Figure 2. Scores plot obtained by PCA analysis of 137 samples collected before 2013 and grouped in four classes as a function of the previously described classification [27] and 41 samples collected during 2013 and 2014. These new data correspond to 15 cloud events and are indicated in black triangles. Statistical analysis is performed using 6 selected variables (pH, $[Na^+]$, $[Cl^-]$, $[SO_4^{2-}]$, $[NO_3^-]$, and $[NH_4^+]$). The scree plot obtained from autoscaled data shows that two selected principal components (PC) containing a total variance of about 81%.

5.3.2 Determination of the hydroxyl radical formation rates and photolysis rates

The concentration of the main photochemical sources of $HO^{\bullet}$ for each sample is reported in Table 1. Particularly, the Fe(II) and Fe(III) concentrations are below the detection limit (0.01 µM) for the majority of the collected samples. The highest value found for the Fe(II) concentration is 0.7 µM, while it is 0.6 µM for Fe(III), corresponding to typical values found for marine origin cloud waters [184]. The H_2O_2 concentration values range between 6 and 50 µM, nitrate is evaluated between 2 and 220 µM, while the nitrite concentration is between 0 and 1.4 µM.

Sample	Iron (µM)		H_2O_2 (µM)	NO_3^- (µM)	NO_2^- (µM)	Sample	Iron (µM)		H_2O_2 (µM)	NO_3^- (µM)	NO_2^- (µM)
	II	III					II	III			
1	NM	NM	12.3	16.7	0.46	22	BDL	BDL	52.3	131.9	0.72
2	NM	NM	9.0	6.1	1.44	23	BDL	BDL	49.4	133.1	0.95
3	NM	NM	15.1	9.9	0.40	24	BDL	BDL	8.1	7.5	BDL
4	NM	NM	14.0	14.2	0.30	25	0.08	0.02	6.7	21.2	0.15
5	NM	NM	13.0	14.7	0.38	26	0.40	0.20	6.8	39.7	BDL
6	NM	NM	7.8	2.6	BDL	27	0.70	0.20	6.6	75.6	BDL
7	NM	NM	6.2	1.7	BDL	28	0.70	0.30	7.2	73.8	BDL
8	NM	NM	9.7	6.9	BDL	29	0.01	0.10	8.0	24.7	0.27
9	NM	NM	8.2	8.2	BDL	30	BDL	0.16	8.8	19.7	0.52
10	NM	NM	10.2	2.3	BDL	31	BDL	0.45	9.1	20.7	0.61
11	NM	NM	17.2	5.6	BDL	32	BDL	BDL	13.1	21.4	0.07
12	BDL	0.57	18.0	24.7	0.28	33	BDL	0.10	2.1	6.1	BDL
13	BDL	0.12	24.6	23.7	1.10	34	0.09	BDL	8.4	10.3	0.47
14	BDL	0.11	12.0	19.0	BDL	35	BDL	BDL	2.2	15.1	0.51
15	BDL	BDL	14.5	19.0	0.23	36	BDL	0.03	2.1	20.3	BDL
16	BDL	BDL	9.1	21.3	0.10	37	BDL	0.03	2.1	18.5	BDL
17	BDL	0.11	16.2	219.6	0.05	38	0.07	BDL	2.4	13.5	0.34
18	0.10	0.01	16.2	205.6	0.07	39	0.04	BDL	3.1	20.8	BDL
19	BDL	BDL	14.9	20.0	0.12	40	BDL	0.01	5.7	39.1	BDL
20	BDL	BDL	15.7	37.4	0.19	41	BDL	0.02	5.3	46.5	0.16
21	BDL	BDL	22.2	72.6	0.42						

Table 1. Concentration of main sources of hydroxyl radical in sampled clouds. 41 samples have been analyzed. BDL: below detection limit (0.01 µM for iron and 0.05 µM for NO_2^-), NM: not measured.

The $R_{HO\cdot}^{f}$ as measured in pure water doped with different concentrations of hydrogen peroxide, nitrate and nitrite on the same order of magnitude as the collected natural samples. The

conditions were those used for natural cloud samples . A linear correlation between $R_{HO^{\cdot}}^{f}$ and the concentrations of photochemical precursors is found (Figure 3). The photolysis rate (J) (s^{-1}) is then estimated from the slopes and are reported in Table 4. For H_2O_2, the J value is half of the experimental slope because H_2O_2 provides two $HO^{\bullet}$ radicals.

	Modeled photolysis rates J (s^{-1})	**Experimental photolysis rates J (s^{-1})**
$H_2O_2 \xrightarrow{h\nu} 2HO^{\bullet}$	1.52×10^{-6}	$(2.50 \pm 0.11) \times 10^{-6}$
$HNO_2 \xrightarrow{h\nu} HO^{\bullet} + NO^{\bullet}$	6.16×10^{-5}	
$NO_2^- + H_2O \xrightarrow{h\nu} HO^{\bullet} + NO^{\bullet} + HO^-$	9.98×10^{-6}	$(5.15 \pm 0.30) \times 10^{-6}$
$NO_3^- + H_2O \xrightarrow{h\nu} HO^{\bullet} + NO_2^{\bullet} + HO^-$	6.71×10^{-8}	$(1.23 \pm 0.04) \times 10^{-7}$
$Fe^{3+} + H_2O \xrightarrow{h\nu} HO^{\bullet} + Fe^{2+} + H^+$	1.24×10^{-6}	
$Fe(OH)^{2+} \xrightarrow{h\nu} HO^{\bullet} + Fe^{2+}$	2.81×10^{-4}	
$Fe(OH)_2^+ \xrightarrow{h\nu} HO^{\bullet} + Fe^{2+} + HO^-$	3.53×10^{-4}	

Table 4. Modeled photolysis rates calculated by the model *versus* experimental photolysis rates obtained from experiments reported in Figure 3.

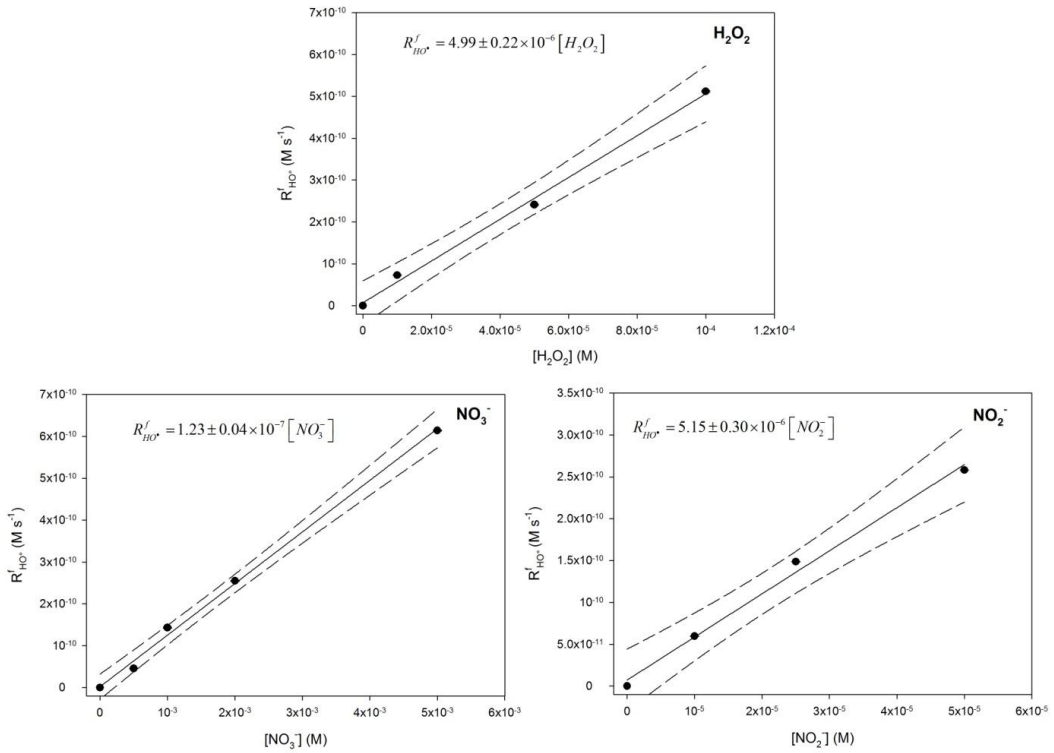

Figure 3. Scatter plot of hydroxyl radical formation rates *vs.* hydrogen peroxide, nitrate and nitrite concentrations using 2 mM of TA at pH 5.0 under Xenon lamp irradiation. The solid line is the linear fit, and dashed lines denote the 90% confidence of the linear fit.

The hydroxyl radical formation rate ($R_{HO^{\cdot}}^{f}$) is determined for 36 samples, and its value is estimated between 3.3 × 10^{-12} and 4.2 × 10^{-10} M s^{-1}. Higher values are obtained for cloud water samples of continental origin, while the values found for marine and highly marine cloud waters are less than 1.4 × 10^{-10} M s^{-1}. The quantum yield of the formation of hydroxyl radicals under polychromatic irradiation between 290 and 400 nm ($\Phi_{290-400\,nm}^{HO^{\cdot}}$, see Equation 3) is estimated as between 10^{-5} and 10^{-2}. (Table 2).

Sample	$R_{HO^{\cdot}}^{f}$ (M s^{-1})	$\Phi_{290-400nm}^{HO^{\cdot}}$	Class	Sample	$R_{HO^{\cdot}}^{f}$ (M s^{-1})	$\Phi_{290-400nm}^{HO^{\cdot}}$	Class
1	(3.30±0.23)×10^{-11}	1.27×10^{-3}	Mar	22	(3.37±0.01)×10^{-10}	2.5×10^{-3}	Cont
2	NM	NM	Mar	23	(4.16±0.01)×10^{-10}	1.8×10^{-3}	Cont
3	NM	NM	Mar	24	(5.10±0.01)×10^{-10}	NM	Mar
4	(1.40±0.01)×10^{-10}	1.0×10^{-2}	H-Mar	25	(2.42±0.08)×10^{-11}	1.9×10^{-4}	Cont
5	(1.24±0.02)×10^{-10}	6.0×10^{-3}	H-Mar	26	(1.41±0.01)×10^{-10}	3.4×10^{-3}	Cont
6	(2.77±0.01)×10^{-11}	1.5×10^{-4}	Mar	27	(4.95±0.01)×10^{-11}	1.5×10^{-4}	Cont
7	(5.60±0.06)×10^{-11}	9.0×10^{-3}	Mar	28	NM	NM	Cont
8	(2.48±0.01)×10^{-11}	2.9×10^{-3}	Mar	29	(8.48±0.04)×10^{-11}	1.3×10^{-4}	Mar
9	(2.20±0.02)×10^{-11}	1.8×10^{-3}	Mar	30	(8.43±0.02)×10^{-11}	1.2×10^{-4}	Mar
10	(2.93±0.02)×10^{-11}	2.4×10^{-3}	Mar	31	(6.11±0.21)×10^{-11}	5.1×10^{-5}	Mar
11	(6.77±0.02)×10^{-11}	2.7×10^{-3}	Mar	32	NM	NM	Mar
12	(6.10±0.19)×10^{-11}	1.7×10^{-4}	Mar	33	(3.27±0.23)×10^{-12}	1.3×10^{-5}	Mar
13	(4.66±0.01)×10^{-11}	1.5×10^{-4}	Mar	34	(2.73±0.01)×10^{-11}	8.5×10^{-4}	Mar
14	(2.81±0.01)×10^{-11}	2.0×10^{-4}	Mar	35	(3.60±0.30)×10^{-11}	6.0×10^{-4}	Mar
15	(1.09±0.04)×10^{-11}	9.0×10^{-5}	Mar	36	(5.97±0.12)×10^{-11}	9.6×10^{-5}	Mar
16	NM	NM	Mar	37	(2.41±0.04)×10^{-11}	8.4×10^{-5}	Mar
17	(6.05±0.44)×10^{-11}	4.1×10^{-5}	Cont	38	(5.76±0.13)×10^{-11}	2.7×10^{-4}	Mar
18	(3.39±0.20)×10^{-11}	3.2×10^{-5}	Cont	39	(2.69±0.04)×10^{-11}	1.1×10^{-4}	Mar
19	(8.11±0.02)×10^{-11}	1.9×10^{-4}	Mar	40	(1.27±0.01)×10^{-10}	2.6×10^{-4}	Cont
20	(8.46±0.01)×10^{-11}	8.4×10^{-3}	Mar	41	(1.09±0.01)×10^{-10}	5.1×10^{-4}	Cont
21	(1.54±0.01)×10^{-10}	1.5×10^{-3}	Cont				

Table 2. Hydroxyl radical formation rate ($R_{HO^{\cdot}}^{f}$ (M s^{-1})) and hydroxyl radical polychromatic quantum yield formation ($\Phi_{290-400\ nm}^{HO^{\cdot}}$) values estimated from cloud water samples. NM: not measured. Mar: Marine, H–Mar: highly marine and Cont: continental influence. The error on $R_{HO^{\cdot}}^{f}$ are derived at the 1–σ level simply from the scattering of experimental data.

To our knowledge, only a scarce number of data are available in the literature concerning measurements of hydroxyl radical formation rates ($R_{HO^{\cdot}}^{f}$) and formation quantum yield ($\Phi_{HO^{\cdot}}$) in real cloud waters (Table 3).

	$R_{HO^{\cdot}}^{f}$ (M s^{-1})	$\Phi_{HO^{\cdot}}$	References
Rain water	2.0 - 6.5 × 10^{-11}		[205]
Cloud water	1.3 - 8.3 × 10^{-10}	4.6 × 10^{-4} - 1.0 × 10^{-2} at 313 nm	[80]
Fog	0.9 - 6.9 × 10^{-10}		
Aqueous extracted aerosol particles	0.4 - 3.8 × 10^{-10}	3.0 × 10^{-4} - 1.7 × 10^{-3}	[206]
Cloud water	3.1 - 6.9 × 10^{-10}		[207]
Cloud water	0.3 - 5.9 × 10^{-10}	5.1 × 10^{-4} - 3.0 × 10^{-3}	[83]
Cloud water at the PUY station	0.2 - 4.2 × 10^{-10}	1.3 × 10^{-5} - 1.0 × 10^{-2} Polychromatic	This work

Table 3. Hydroxyl radical formation rates ($R_{HO^{\cdot}}^{f}$, M s^{-1})and polychromatic quantum yield ($\Phi_{HO^{\cdot}}$) found in literature and in this work.

Faust and Allen [80] measured the photoformation rates of $HO^{\bullet}$ (ranging from 1.3 to 8.3 × 10^{-10} M s^{-1}) under monochromatic light (313 nm) and hydroxyl radical quantum yield (between ~ 5 × 10^{-4} and 10^{-2}) of six continental cloud water samples. Anastasio and McGregor [207] investigated the photoreactivity of two cloud waters from the Tenerife Islands to compare the obtained values with fog waters. The authors found $R_{HO^{\cdot}}^{f}$ ranging between 3.0 and 6.9 × 10^{-10} M s^{-1}. t that are approximately 1 order of magnitude higher than those reported in this study for marine cloud waters, and the differences can be attributed to the air mass origin, as suggested by Faust and Allen [80]. The authors suggested that long-range terrestrial aerosol and gas transport in continental clouds could provide an additional source of hydroxyl radicals compared with other marine or remote clouds.

5.3.3 Modeling the hydroxyl radical formation rates

We simulate the hydroxyl formation rate, $R_{HO^{\cdot}}^{f}$ mod, using the model along with the relative contribution (%) of each chemical source (Table SM3). In Figure 4, the differences between the modeled and experimental $HO^{\bullet}$ formation rates are estimated calculating the bias error (($R_{HO^{\cdot}}^{f}$mod - $R_{HO^{\cdot}}^{f}$exp) / $R_{HO^{\cdot}}^{f}$exp in (%)).

Cloud sample	Relative contribution (%)					$R^{f}_{HO^{\cdot}}$ mod (M s^{-1})	$R^{f}_{HO^{\cdot}}$ exp (M s^{-1})
	H_2O_2 + hν	Fe (II) + H_2O_2	Fe (III) + hν	NO_3^- + hν	HNO_2 + NO_2^- + hν		
1	86.7	0.0	0.0	2.6	10.6	4.3×10^{-11}	3.3×10^{-11}
2	64.9	0.0	0.0	1.0	34.1	4.2×10^{-11}	NM
3	90.7	0.0	0.0	1.3	7.9	5.0×10^{-11}	NM
4	91.2	0.0	0.0	2.0	6.7	4.6×10^{-11}	1.4×10^{-10}
5	89.1	0.0	0.0	2.2	8.6	4.4×10^{-11}	1.2×10^{-10}
6	99.3	0.0	0.0	0.7	0.0	2.4×10^{-11}	2.8×10^{-11}
7	99.4	0.0	0.0	0.6	0.0	1.9×10^{-11}	5.6×10^{-11}
8	98.4	0.0	0.0	1.6	0.0	3.0×10^{-11}	2.5×10^{-11}
9	97.8	0.0	0.0	2.2	0.0	2.5×10^{-11}	2.2×10^{-11}
10	99.5	0.0	0.0	0.5	0.0	3.1×10^{-11}	2.9×10^{-11}
11	99.3	0.0	0.0	0.7	0.0	5.2×10^{-11}	6.8×10^{-11}
12	22.3	21.6	54.2	0.7	1.2	2.4×10^{-10}	6.1×10^{-11}
13	57.3	10.7	22.4	1.2	8.4	1.3×10^{-10}	4.7×10^{-11}
14	52.4	10.7	35.1	1.8	0.0	6.9×10^{-11}	2.8×10^{-11}
15	92.5	0.0	0.0	2.7	4.9	4.7×10^{-11}	1.1×10^{-11}
16	91.8	0.0	0.0	4.8	3.4	3.0×10^{-11}	NM
17	50.2	12.4	21.7	15.1	0.7	9.8×10^{-11}	6.1×10^{-11}
18	51.8	22.3	10.4	14.6	0.9	9.4×10^{-11}	3.4×10^{-11}
19	94.6	0.0	0.0	2.8	2.6	4.8×10^{-11}	8.1×10^{-11}
20	91.4	0.0	0.0	4.8	3.7	5.2×10^{-11}	8.5×10^{-11}
21	88.0	0.0	0.0	6.4	5.6	7.6×10^{-11}	1.5×10^{-10}
22	90.7	0.0	0.0	5.1	4.2	1.7×10^{-10}	3.4×10^{-10}

23	89.0	0.0	0.0	5.3	5.7	1.7×10^{-10}	4.2×10^{-10}
24	98.0	0.0	0.0	2.0	0.0	2.5×10^{-11}	5.1×10^{-11}
25	60.6	29.2	1.1	4.2	4.9	3.4×10^{-11}	2.4×10^{-11}
26	26.2	70.0	1.1	2.6	0.1	1.0×10^{-10}	1.4×10^{-10}
27	19.3	76.8	0.9	3.0	0.1	1.8×10^{-10}	5.0×10^{-11}
28	17.6	79.0	1.0	2.4	0.0	2.2×10^{-10}	NM
29	39.8	40.3	12.7	2.7	4.5	6.2×10^{-11}	8.5×10^{-11}
30	43.4	27.3	18.6	2.2	8.5	6.2×10^{-11}	8.4×10^{-11}
31	21.7	33.0	39.4	1.1	4.8	1.3×10^{-10}	6.1×10^{-11}
32	92.1	1.6	1.3	3.3	1.7	4.3×10^{-11}	NM
33	31.0	10.2	56.8	2.0	0.0	2.3×10^{-11}	3.3×10^{-12}
34	16.6	27.9	52.0	0.5	3.1	1.5×10^{-10}	2.7×10^{-11}
35	24.0	5.5	48.5	3.7	18.4	2.9×10^{-11}	3.6×10^{-11}
36	60.7	7.3	18.9	13.0	0.2	1.1×10^{-11}	6.0×10^{-11}
37	63.5	8.3	15.6	12.4	0.2	1.0×10^{-11}	2.4×10^{-11}
38	47.7	17.3	6.7	5.9	22.4	1.5×10^{-11}	5.8×10^{-11}
39	67.5	14.7	7.7	10.0	0.1	1.4×10^{-11}	2.7×10^{-11}
40	81.6	4.5	1.3	12.4	0.2	2.1×10^{-11}	1.3×10^{-10}
41	47.0	35.9	2.9	9.0	5.3	3.5×10^{-11}	1.1×10^{-10}

Table SM3: Modelled relative contributions of $HO^{\bullet}$ sources for the 41 cloud samples. Modelled and experimental $R_{HO^{\cdot}}^{f}$ are also indicated. NM: not measured.

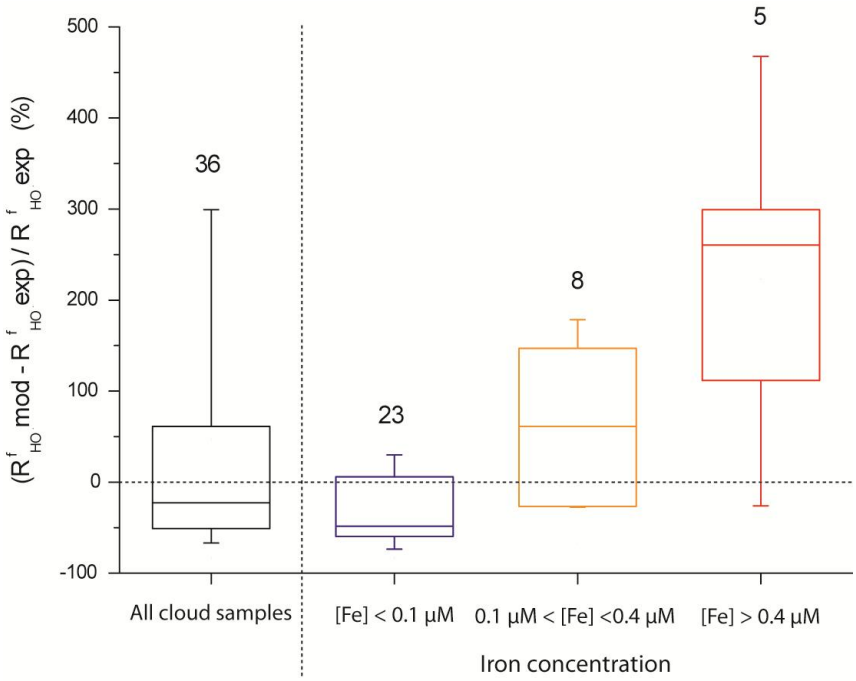

Figure 4. Distribution of the bias error for the whole cloud water samples (black) and for cloud samples discretized as a function of different iron concentration ranges (in color). The bias error is defined by the ratio ($R^f_{HO^\cdot}$mod - $R^f_{HO^\cdot}$exp) / $R^f_{HO^\cdot}$exp in (%). The number of samples analyzed is indicated above each box plot. The bottom and top lines correspond to the 25th and 75th percentiles, respectively. The full line represents the median values. The ends of the whiskers are the 10th and 90th percentiles.

Globally, for the whole cloud water samples (black boxplot), the model can reproduce the range of measured hydroxyl radical formation rates with a slight model underestimation (median of the bias error equal to -23%). However, if the cloud samples are discretized as a function of different iron concentration ranges (boxplots in color), then the model tends to overestimate the hydroxyl radicals formation for iron concentrations (Fe(II) + Fe(III)) more than 0.1 µM. For concentration of iron between 0.1 and 0.4 µM (8 cloud samples), the median of the bias error is 61% whereas for iron concentrations over 0.4 µM (5 cloud samples), the median reaches 260%. For cloud samples in which the iron concentration is 0.4 µM, the modeled contribution to the hydroxyl radical formation of iron (Fenton reaction and photolysis of aqua-complexes) can reach 80% (Table SM3). In the model, Fe(III) is partially complexed with oxalic acid, but the majority of iron for these cloud samples is simulated as aqua-complexes (mainly $Fe(OH)^{2+}$ and $Fe(OH)_2^{+}$). Therefore, iron can act as a significant $HO^\bullet$ source due to its efficient photolysis (Reactions R7, R8, R9, Table SM1) and the Fenton reaction with H_2O_2 (Reactions R11, Table SM1).

However, in atmospheric natural water, the chemical composition of organic matter is still not very well characterized [102]. Part of this organic matter is expected to efficiently complex

metals in cloud water [208]. Due to missing information about the iron speciation and complexation in natural cloud water, the model probably overestimates the free Fe(III). Moreover, iron organic complexes are not expected to directly generate hydroxyl radicals but primarily contribute to the oxidative capacity *via* Fe(II) generation and the Fenton process. To evaluate this hypothesis, we decide to consider the iron as totally complexed by the organic matter present in natural cloud waters. As a first general approximation, we consider iron as not reactive in the model. The new simulations show that the majority of the simulated values (75%) of the hydroxyl radical formation rates are now underestimated by the model (median of the bias error equal to -40%) (Figure 5).

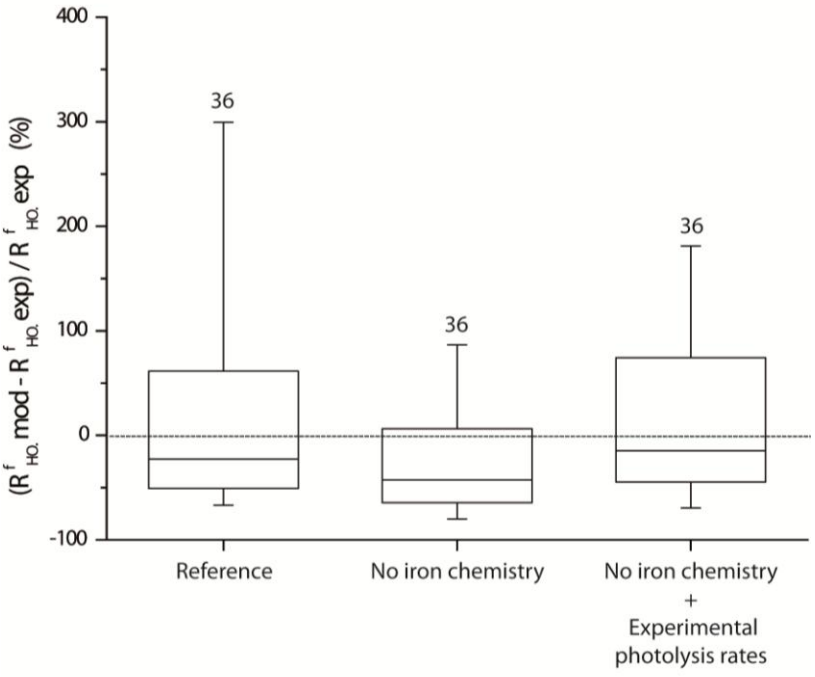

Figure 5**.** Distribution of the bias error for the whole cloud water samples for the reference case and for two sensitivity tests performed with the model: (i) the iron chemistry (photolysis of Fe(III) and the Fenton reaction) is neglected in the model; (ii) the iron chemistry is neglected, and the new photolysis rate constants obtained from experimental measurements are implemented in the model. The bias error is defined by the ratio ($R^f_{HO^\cdot}$mod - $R^f_{HO^\cdot}$exp) / $R^f_{HO^\cdot}$exp in (%).The number of samples analyzed is indicated above each box plot. The bottom and top lines correspond to the 25th and 75th percentiles, respectively. The full line represents the median values. The ends of the whiskers are the 10th and 90th percentiles.

Based on the laboratory irradiation experiments (Figure 3), new photolysis rates from nitrite, nitrate and hydrogen peroxide are previously estimated from the hydroxyl radical formation rates (Table 4). For nitrate and H_2O_2, the values calculated by the model are lower than the experimental ones; the experimental photolysis rates are higher by a factor ~1.5 for H_2O_2 and ~2 for nitrate. For nitrite, the experimental photolysis rate is approximately half of the modeled value. These discrepancies should partially explain the underestimation of $HO^\bullet$

formation by the model. Therefore, we consider the experimental photolysis rates in the model, and a new comparison of modeled $HO^{\bullet}$ formation rates with experimental values is shown in Figure 5. The median of the bias error is -3% with the 25th and 75th percentiles at -50 and 60%, respectively. Table SM4 reports the distribution of the relative contributions of H_2O_2, NO_3^- and NO_2^- photolysis to the modeled $R_{HO\cdot}^f$. While the median value of the nitrite and nitrate contributions is calculated by the model as equal to 1 and 5%, respectively (Figure 6), the main $HO^{\bullet}$ contributor is H_2O_2 photolysis (median value of 93%, with the 25th and 75th percentiles at 85 and 96%, respectively). This result suggests that H_2O_2 is the key compound that drives the oxidative capacity of our cloud water samples when iron concentrations are relatively low or when iron is suggested to be totally complexed by organic matter.

Cloud sample	**Relative contribution (%)**			$R_{HO\cdot}^f$ **mod (M s^{-1})**	$R_{HO\cdot}^f$ **exp (M s^{-1})**
	H_2O_2 + hν	**NO_3^- + hν**	**HNO_2 + NO_2^- + hν**		
1	93.2	3.1	3.7	6.6×10^{-11}	3.3×10^{-11}
2	84.4	1.4	14.2	5.3×10^{-11}	NM
3	95.7	1.6	2.7	7.9×10^{-11}	NM
4	95.3	2.4	2.4	7.3×10^{-11}	1.4×10^{-10}
5	94.4	2.6	3.0	6.9×10^{-11}	1.2×10^{-10}
6	99.2	0.8	0.0	3.9×10^{-11}	2.8×10^{-11}
7	99.3	0.7	0.0	3.1×10^{-11}	5.6×10^{-11}
8	98.3	1.7	0.0	4.9×10^{-11}	2.5×10^{-11}
9	97.6	2.4	0.0	4.2×10^{-11}	2.2×10^{-11}
10	99.4	0.6	0.0	5.1×10^{-11}	2.9×10^{-11}
11	99.2	0.8	0.0	8.6×10^{-11}	6.8×10^{-11}
12	95.2	3.2	1.6	9.4×10^{-11}	6.1×10^{-11}
13	93.4	2.2	4.3	1.3×10^{-10}	4.7×10^{-11}
14	96.2	3.8	0.0	6.2×10^{-11}	2.8×10^{-11}
15	95.3	3.1	1.6	7.6×10^{-11}	1.1×10^{-11}
16	93.5	5.4	1.1	4.8×10^{-11}	NM
17	74.6	25.0	0.4	1.1×10^{-10}	6.1×10^{-11}
18	75.8	23.8	0.5	1.1×10^{-10}	3.4×10^{-11}
19	96.0	3.2	0.8	7.7×10^{-11}	8.1×10^{-11}
20	93.3	5.5	1.2	8.4×10^{-11}	8.5×10^{-11}
21	90.8	7.3	1.8	1.2×10^{-10}	1.5×10^{-10}
22	92.9	5.8	1.4	2.8×10^{-10}	3.4×10^{-10}
23	92.0	6.1	1.9	2.7×10^{-10}	4.2×10^{-10}
24	97.7	2.2	0.0	4.1×10^{-11}	5.1×10^{-11}
25	90.4	7.1	2.6	3.7×10^{-11}	2.4×10^{-11}

26	87.3	12.6	0.1	3.9×10^{-11}	1.4×10^{-10}
27	77.8	22.0	0.2	4.2×10^{-11}	5.0×10^{-11}
28	79.7	20.2	0.2	4.5×10^{-11}	NM
29	89.8	6.8	3.3	4.4×10^{-11}	8.5×10^{-11}
30	89.4	5.0	5.7	4.9×10^{-11}	8.4×10^{-11}
31	88.7	5.0	6.3	5.1×10^{-11}	6.1×10^{-11}
32	95.6	3.8	0.6	6.8×10^{-11}	NM
33	93.3	6.7	0.0	1.1×10^{-11}	3.3×10^{-12}
34	91.8	2.8	5.5	4.6×10^{-11}	2.7×10^{-11}
35	70.6	12.0	17.4	1.6×10^{-11}	3.6×10^{-11}
36	80.7	19.2	0.1	1.3×10^{-11}	6.0×10^{-11}
37	82.0	17.9	0.1	1.3×10^{-11}	2.4×10^{-11}
38	77.6	10.8	11.7	1.5×10^{-11}	5.8×10^{-11}
39	85.7	14.2	0.1	1.8×10^{-11}	2.7×10^{-11}
40	85.4	14.5	0.1	3.3×10^{-11}	1.3×10^{-10}
41	79.5	17.2	3.2	3.3×10^{-11}	1.1×10^{-10}

Table SM4. Modeled relative contributions of $HO^{\bullet}$ sources for the 41 cloud samples considering the new photolysis experimental rates in the model for H_2O_2, nitrite and nitrate and without iron chemistry. Modeled and experimental $R_{HO^{\cdot}}^{f}$ are also indicated. NM: not measured.

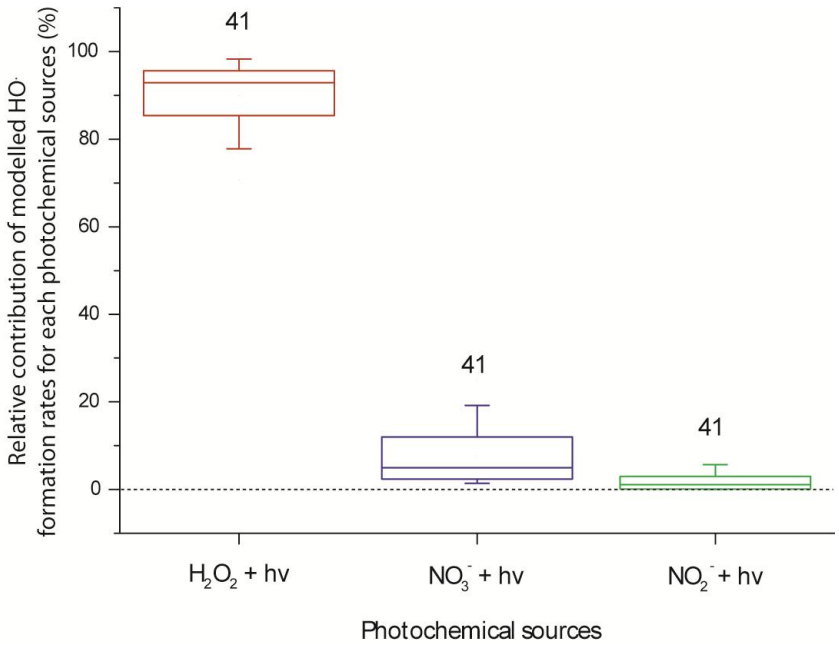

Figure 6. Distribution of relative contributions of modeled $HO^{\bullet}$ formations rates for each photochemical source (H_2O_2, NO_3^- and NO_2^- photolysis) for the whole cloud water samples. Model outputs are obtained from the sensitivity test in which the iron chemistry is not considered, and new photolysis rate constants from experimental measurements are implemented in the model. The number of samples analyzed is indicated above each box plot. The bottom and top lines correspond to the 25th and 75th percentiles, respectively. The full line represents the median values. The ends of the whiskers are the 10th and 90th percentiles.

5.4 Conclusion

In this study, we compare experimental and modeled $HO^{\bullet}$ formation rates for 41 cloud water samples with contrasted chemical compositions depending on the origin of the air masses. This approach helps to elucidate the complex aqueous photoreactivity of natural cloud water that is expected to drive the oxidative capacity. Experimental data are obtained considering only the $HO^{\bullet}$ formation sources with addition of an excess of chemical probe leading to the measurements of total generated $HO^{\bullet}$ radicals. The first comparison with the M2C2 model shows that the model can reproduce the order of magnitude of measured $R_{HO^{\cdot}}^{f}$ (from 1.1 × 10^{-11} to 4.2 × 10^{-10} M s^{-1} and from 1.1 × 10^{-11} to 2.4 × 10^{-10} M s^{-1} for experimental and modeled values, respectively). Some discrepancies appear for samples containing iron concentrations over 0.4 µM in which the model overestimates the contribution of iron(III)-aqua complexes to the $HO^{\bullet}$ production rate. Ultimately, the aqueous chemical mechanism in the model was modified considering new photolysis rates for H_2O_2, nitrite and nitrate estimated by laboratory irradiation experiments. As a sensitivity test, iron reactivity was also suppressed in the model to account for the total complexation of iron. The modeled production rates of $HO^{\bullet}$ with the updated mechanism are closer to the experimental values. This supports the hypothesis that iron could be strongly complexed by the organic matter in natural cloud water. These complexes could be more stable and less photoreactive, leading to less $HO^{\bullet}$ production than that calculated by theoretical models in which only the photochemistry of Fe(III)-carboxylate is considered [209]. In this context, evaluation of the complexation of iron by organic compounds in the cloud aqueous phase and the photoreactivity of these complexes should be pursued in the future. Their photoreactivity provides significant data to understand the specific role of iron species and, more generally, the oxidant capacity of this medium.

Chapter 6

Motivation

This chapter is focused on the photochemical behavior of tartronic acid, a dicarboxylic acid that can be formed by oxidation of sugars in the atmosphere.

This work was carried out considering that many oxidative pathways in atmospheric models lead to the formation of tartronic acid which chemical and photochemical behavior is not completely understood, especially at low concentrations.

The next chapter reports in the first part the results of the spectroscopic investigation on tartronic acid and in the second its reactivity. Direct photolysis and hydroxyl radical photodegradation were performed and the chapter ends with the determination of the second order rate constant between tartronic acid and hydroxyl radical by Laser Flash Photolysis.

This work is still not finished: NMR spectroscopy of irradiated solutions will give us an idea of the reaction's products for both direct and indirect photolysis. Kinetic contants and transformation pathways will be implemented in the model of multiphase cloud chemistry (M2C2).

Photochemical fate of Tartronic acid in cloud waters.

6.1. Introduction

Organic compounds are oxidized in the gas and in the liquid phase of the atmosphere according to their reactivity, as shown in Chapter 2 leading in most cases, to the formation of less volatile products. Scarce information is available about the organic composition of cloud water but it can be assumed that the presence of microorganisms is strictly correlated to the presence of sugars, lipids and other biological molecules. In 1951 Kulka underlined how the metabolism of microorganisms leads to the production of short chain carboxylic acids and, in particular, of tartronic acid:

"... this is the first instance in which tartronic acid has been identified as a product of the dissimilation of glucose by microbiological agency. It is not yet possible to decide whether this production of tartronic acid was affected by living cells of *A.acetosum* or by an enzyme system released from autolysed cells of the organism [*A. acetosum*]..."[210].

Moreover, sugar oxidation was proved to give short chain carboxylic acids like tartronic, tartaric and oxalic acids also in the absence of microrganisms, as recently reported by Smith et al [211]

"The products of the nitric acid oxidation of D-glucose have been identified as D-glucaric acid and its precursors D-gluconic acid along with the byproducts 5-keto-D-gluconic acid, tartaric acid, tartronic acid and oxalic acid".

Despite numerous investigations on the fate of oxalic and tartaric acids, to the best of our knowledge, no data concerning tartronic acid are reported.

Tartronic acid (structure and physico-chemical properties reported in Table 1) was found in PM 10 by van Pixteren et al., who report a concentration of 4 ng m^{-3} for all the sites investigated. Only for one sampling site the concentration reaches the value of 14 ± 13 ng m^{-3} [212]. The same research group found tartronic acid in continental aerosol samples with concentrations of 0.3, 1.9 and 3.8 ng m^{-3} [213]. Neusüss et al [214] found the same average concentrations in marine aerosols.

TARTRONIC ACID	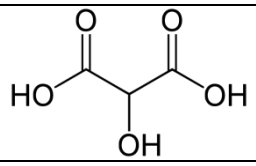
IUPAC name	2-hydroxypropanedioic acid
CAS number	80-69-3
Chemical formula	$C_3H_4O_5$
Molar mass	120.06 g mol^{-1}
Appearance	beige powder

Table 1: Tartronic acid physico-chemical characteristics.

Considering that this compound was found in atmospheric particulate phase, we can suggest the presence of tartronic acid in cloud water due to three different processes: microbiological and chemical oxidation of sugars and also dissolution from aerosols. It could be interesting to understand the chemical and photochemical behaviour of tartronic acid and to implement these data in atmospheric models, where the formation of this compound is predicted but it does not react chemically or photochemically.

6.2. Chemicals

The hydrogen peroxide (solution 30% in water) was purchased from Fluka while the carboxylic acids (tartronic, formic, acetic, oxalic and mesoxalic, were obtained from Sigma Aldrich with a purity ≥ 97%. All the other chemicals (purity reagent grade) used for the analysis were obtained from Sigma-Aldrich.

All the solutions were prepared with deionized ultra pure aerated milli-Q water from Millipore (resistivity = 18.2 MΩ cm) under laminar flux hood. Moreover, all the glass containers and injection material were washed three times with ultra pure water before use. If necessary, the pH values were adjusted with perchloric acid (1 N) and NaOH (1 N) using a JENWAY 3310 pH-meter to ± 0.01 pH unit. During irradiation pH was monitored using a Hanna portable pH-meter. All the solutions were kept in dark conditions and the final preparations were performed in a room equipped with a sodium lamp (589 nm emission).

Fresh solutions of tartronic acid (TAR) were prepared before each experiment from a stock solution (2 mM) stored in the dark at 278 K. The concentration of the stock solution of H_2O_2 in milli-Q water was determined using a molar attenuation coefficient of 38.1± 1.4 M^{-1} cm^{-1} at 240 nm [171].

6.3. Results

6.3.1. Determination of molar extinction coefficient.

TAR UV-vis absorption spectra were recorded with a double beam spectrophotometer Agilent Technologies Cary 60 UV-vis, using a Hellma Analytic 50 mm quartz cuvette. Tartronic solution (1.0 mM) has a natural pH of 3.2; Figure 1 shows on the left the fraction of ionic species (di-anion (T^{2-}), mono-anion (HT^-) and acid (H_2T)) of tartronic in function of pH, considering the pka values of 2.42 and 4.54 reported by Qi et al. [215].

Figure 2 reports on the left the absorbance of a 1 mM solution at different pH values and the emission spectrum of the irradiation device between 200 and 400 nm.

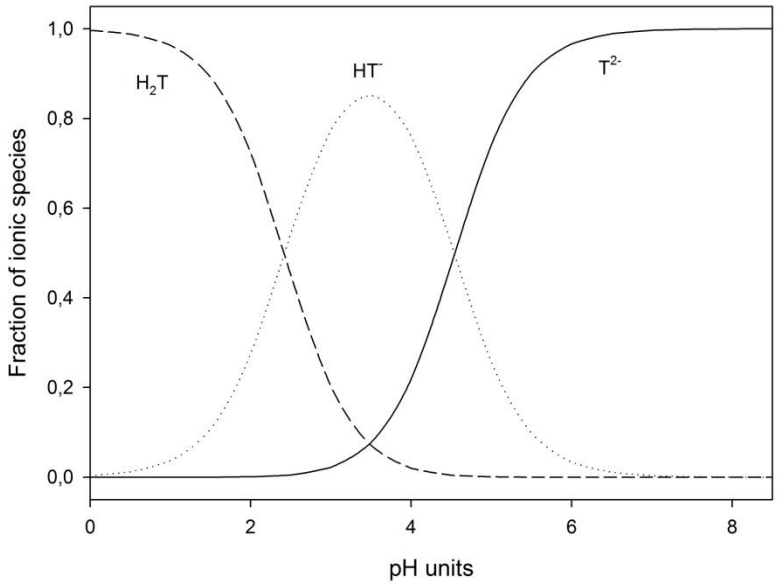

Figure 1: Speciation of tartronic acid in function of pH.

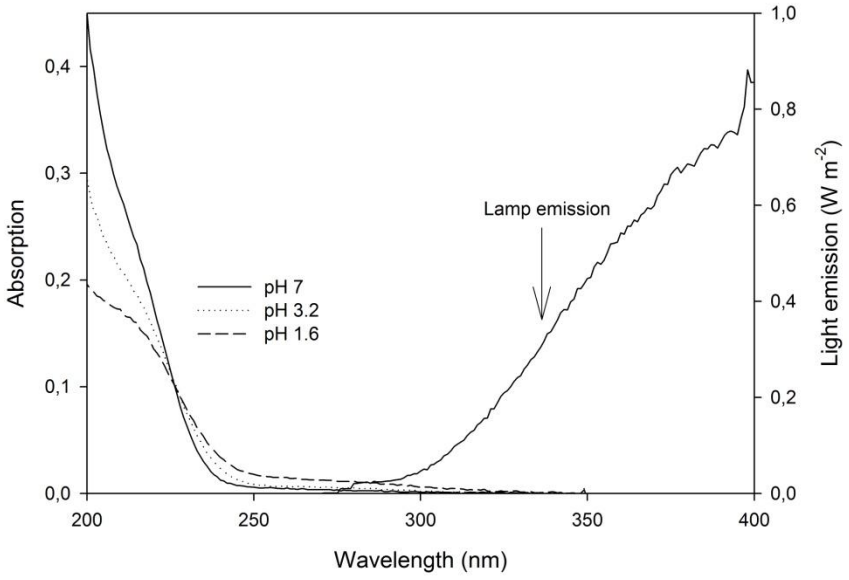

Figure 2: Absorption spectrum of tartronic acid at three pH and lamp emission spectrum.

The molar attenuation coefficient (ε, M^{-1} cm^{-1}) was determined previously by Herrmann et al.[216] for tartronic acid at pH 0.5, with a value of 1160 M^{-1} cm^{-1} at λ = 224 nm, and for the dianionic form at pH 9, with a value of 8470 M^{-1} cm^{-1} at λ = 219 nm. In this work the absorption spectra of tartronic acid were recorded at different pH, from 1 to 11, and the molar extinction coefficient was extrapolated for each form, considering the speciation of the compounds in solution. ε at 219 nm is estimated to be for the dianionic form TAR^{2-} 194 ± 6 M^{-1} cm^{-1}, for the monoanionic form $HTAR^{-}$ 420 ± 20 M^{-1} cm^{-1}. For H_2TAR the UV-vis spectrum of the solution changes in time at pH lower than 2, as shown in Figure 3.

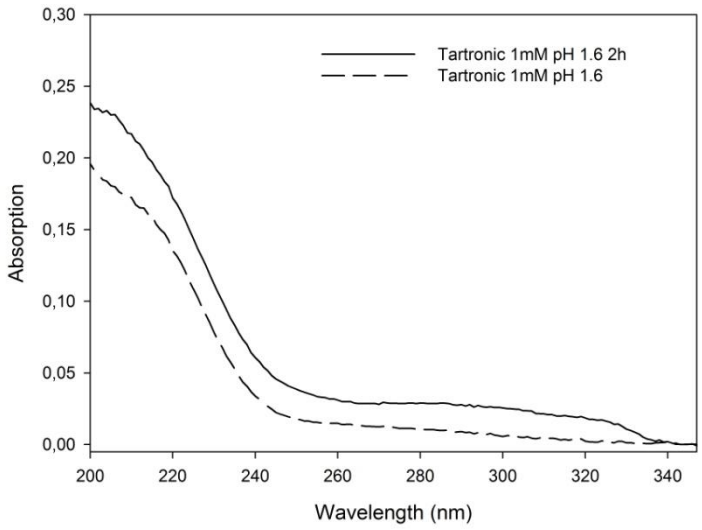

Figure 3: Absorption spectrum of tartronic acid at pH 1.6 before and after 2h.

This is probably due to the protonation of the hydroxyl group on the second carbon in the presence of a large excess of H^+ which leads to the liberation of one water molecule and to the formation of the new species described in Figure 4. This molecule is stabilized by two resonance forms and the conjugated double bond could explain the absorption in the range 260-320 nm. This is only a hypothesis and more computational calculations are needed to prove this degradation pathway. In any case we consider that tartronic acid is not stable at pH lower than 2.

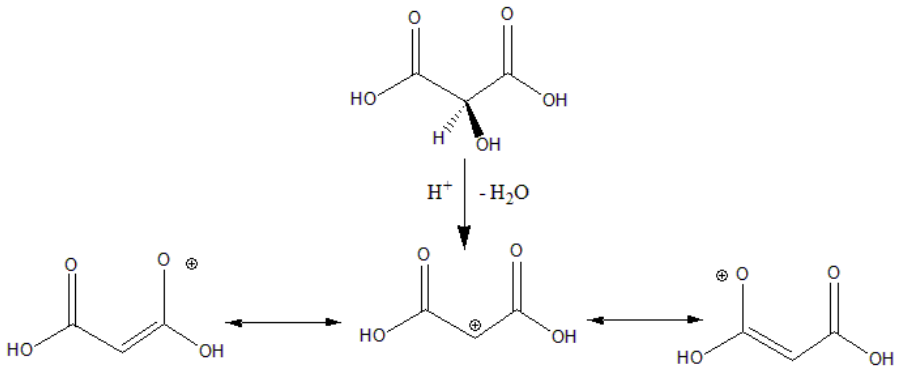

Figure 4: formation of new a species at low pH.

It is very difficult to determine the molar attenuation coefficient (ε) at wavelength of 219 nm because the absorption increases rapidly and the error associated increases exponentially. For this reason we calculated epsilon for the three forms, using the equations reported hereafter.

$$A_{pH\ 7} = \varepsilon_{T^{2-}} \times b \times \chi_{T^{2-}} \times c_{TOT}$$

Equation 1.

$$A_{pH\ 5.2} = \varepsilon_{T^{2-}} \times b \times \chi_{T^{2-}} \times c_{TOT} + \varepsilon_{HT^-} \times b \times \chi_{HT^-} \times c_{TOT}$$

Equation 2.

$$\varepsilon_{T^{2-}} = \frac{A_{pH\ 7}}{b \times \chi_{T^{2-}} \times c_{TOT}}$$

Equation 3.

$$\varepsilon_{HT^-} = \frac{A_{pH\ 5.2} - b \times \chi_{T^{2-}} \times c_{TOT}}{b \times \chi_{HT^-} \times c_{TOT}}$$

Equation 4.

where $A_\lambda(pH\ 7\ or\ 5.2)$ is the absorption measured for each wavelength, c_{TOT} is the concentration (1×10^{-3} M), b represents the optical pathway (1 cm) and $\chi_{T^{2-}}$ and χ_{HT^-} are the fractions of dianionic and monoanionic species respectively. The molar extinction coefficient for the two forms is reported in Figure 5.

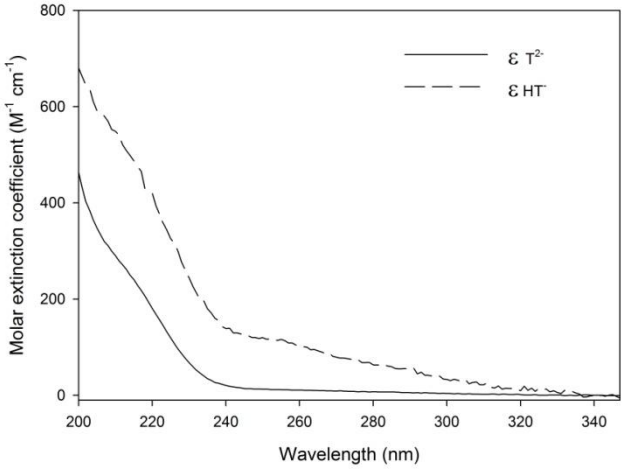

Figure 5: Molar extinction coefficient of tartronic mono and dianionic form.

6.3.2. Irradiation experiments

6.3.2.1. Direct Photolysis

Aqueous solutions of tartronic acid 10 µM were irradiated in the reactor described in Chapter 4. The energy was normalized to the actinometry results using the paranitroanisole (PNA)/pyridine method [170]. A total flux of 44 W m^{-2} reaching the solution was determined in the range 290–400 nm.

Hydrogen peroxide concentration was estimated by using p-hydroxyphenilacetic acid (HPAA, purity > 98%) and peroxydase from horseradish (POD) according with the spettrofluorimetric quantification method described in Chapter 4.

Carboxylic acids quantification was performed using the ion chromatography Thermo Scientific Dionex ICS 5000 described in Chapter 4. The experimental method was modified compared to the one previously reported in Chapter 4 to better separate tartronic acid from oxalic acid. The KOH gradient used is reported in Table 2.

Under these conditions, the retention times of acetate, formate and tartronate are of 6.5, 7.3 and 28.5 min, respectively.

Time (min)	KOH Concentration (mM)
0	10
33	20
35	24
35.5	10

38	10

Table 2: ion chromatography gradient adopted for tartronic analysis.

Results for direct photolysis are reported in Figure 6. At pH 7, 20% of tartronic acid is degraded after 8h of irradiation, while, at pH 4 and 5, 80% of the initial concentration of tartronic acid disappears in the same time. This is clearly a consequence of the higher quantum yield of the form HT^-, which absorbs more than the form H_2T, as reported in Figure 5. Degradation of tartronic acid leads to the production of formate: 1 µM for irradiation at pH 7 and 4 and 5 µM for irradiation at pH 4 and 5 respectively.

The photonic flux reaching the solution was determined using an optical fiber coupled with a CCD spectrophotometer and performing a chemical actinometry, using the method described by Dulin and Mill [170]. Polychromatic quantum yield was estimated as the integral of the superposition of the emission spectrum of the lamp and the absorption spectrum of the solution between 290 and 400 nm. For the dianionic form T^{2-}, at pH 7, polychromatic quantum yield ($\Phi^{pH\ 7}_{290-400\ nm}$) is estimated to be 2.02×10^{-3}. At pH 3.2, where the three forms are present (0.04 T^{2-}, 0.83 HT^- and 0.14 H_2T), the polychromatic quantum yield ($\Phi^{pH\ 3.2}_{290-400\ nm}$) is estimated to be 8.53×10^{-3} between 290 and 400 nm.

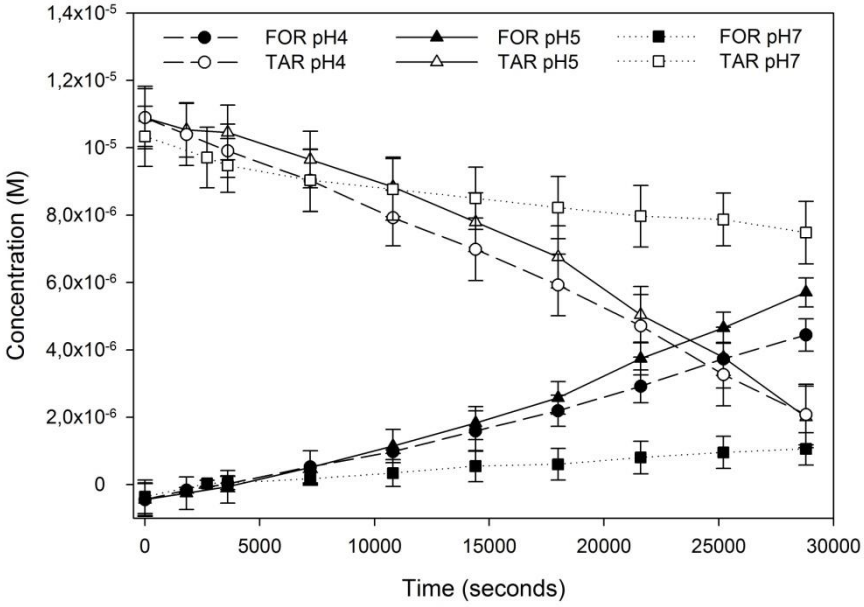

Figure 6: Direct photolysis of tartronic acid (TAR) and formation of formate (FOR).

6.3.2.2. Indirect photolysis

The same experiments were repeated in the presence of H_2O_2 100 µM, which corresponds to the hydroxyl radical formation rate ($R^f_{HO^\cdot}$) of $7.21 \pm 0.05 \times 10^{-10}$ M s^{-1}. The degradation

profile is the sum of direct and indirect photolysis, while the H_2O_2 decrease was estimated to be less than 10% (data not reported). Degradation profiles are reported in Figure 7.

At pH 4 and 5, tartronic acid is completely degraded during 8 h irradiation and the production of formate reaches 6 and 7 µM respectively. At pH 7, 70% of the initial tartronic concentration is degraded after 8h and 4 µM of formate are produced.

These experiments clearly show that tartronic acid reacts with hydroxyl radical and one of the final products is formate. Ionic chromatography does not enable to estabilish if other carboxylic acids are formed during irradiation: acetate, oxalate and mesoxalate were monitored during the analysis but they were not detected. It is possible that mesoxalic acid (H_2M) is produced but its fast reaction with the hydroxyl radical ($k_{HO^{\cdot},H_2M}$ 1.4 × 10^8 M^{-1} s^{-1}, $k_{HO^{\cdot},HM^-}$ 3.2 × 10^8 M^{-1} s^{-1} et $k_{HO^{\cdot},M^{2-}}$ 1.6 × 10^8 M^{-1} s^{-1}) gives formate makes its quantification difficult.

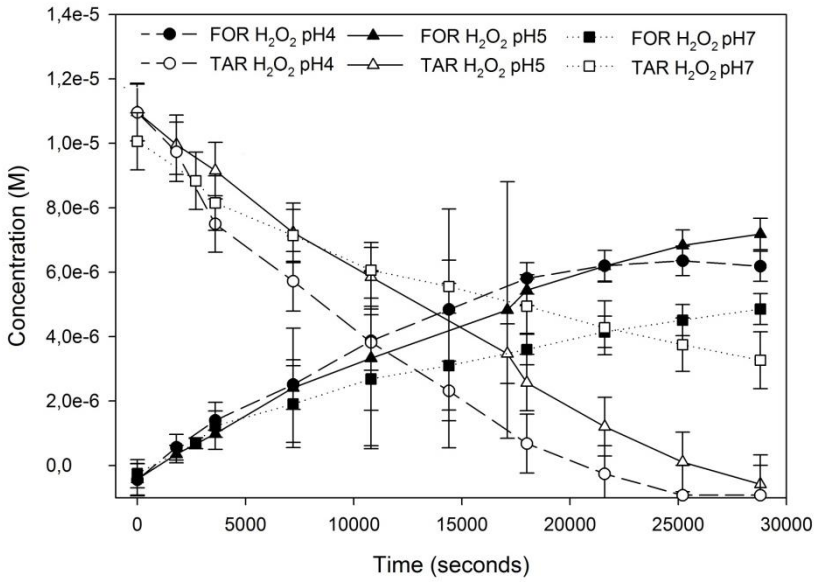

Figure 7: Hydroxyl radical mediated photodegradation of tartronic acid (TAR) and formation of formate (FOR).

6.3.3. LFP experiments

A crucial point is the determination of the second order rate constant with hydroxyl radical. Herrmann et al. previously determined the reactivity by laser flash photolysis at pH 1 but we demonstrated that at low values of pH at least two forms coexist in solution. For this reason we determined the reactivity at different pHs in the range 3-7 to estimate the second order rate constant of each form.

The laser flash photolysis apparatus has been previously described in Chapter 4. Experimental determination of the second order rate constants was performed with the fourth harmonic (λexc = 266 nm) and the excitation energy was set to approximately 45 mJ $pulse^{-1}$. An

appropriate volume of solutions (TAR, H_2O_2, SCN^-) was mixed just before each experiment to obtain the desired mixtures and concentrations. All experiments were performed at ambient temperature (293 ± 2 K) and in aerated solutions.

The concentration of the $HO^\bullet$ radical was detected by recording the absorbance of the $(SCN)_2^{\bullet-}$ radical anion. Kinetic studies of $HO^\bullet$ reactions were carried out by competitive kinetic techniques using the thiocyanate ion as a reference reactant [217]. All experiments were carried out under conditions of pseudo-first order kinetics using an excess of the concentrations of the organic reactants compared to the initial radical concentration.

The second order rate constant k_d was obtained from the Equation 5, where Abs_0 is the light intensity absorbed by $(SCN)_2^{\bullet-}$ and Abs is the variation of the intensity when the reactant is added to the reaction solution. k_a is the second order rate constant between hydroxyl radical and thiocyanate (1.10×10^{10} M^{-1} s^{-1} [76]).

$$\frac{Abs_0}{Abs} = 1 + \frac{k_d}{k_a}\frac{[TAR]}{[SCN^-]}$$

Equation 5

Each value was the average of 4 consecutive laser pulses and the reported error is ± 3σ, which was obtained from the scattering of the experimental data from the fitting line.

Results are reported in Table 3 and clearly show how the monoanionic form of tartronic acid, which is the main form at pH 4 and 5, is the more reactive.

pH	k_{global} **M^{-1} s^{-1}**		k^{II} **M^{-1} s^{-1}**
1.4	3.86×10^8	$k_{HO^\cdot,H_2T}$	3.61×10^8
3.2	6.69×10^8	$k_{HO^\cdot,HT^-}$	5.88×10^8
7.0	5.04×10^8	$k_{HO^\cdot,T^{2-}}$	5.04×10^8

Table 3: Constants between tartronic acid and hydroxyl radical via thyocyanate method. k_{global} is the second order rate constant of at least two different species, while k^{II} is the second order rate constant of a single species.

6.4. Conclusions and perspectives.

In this chapter, I briefly describe our research work concerning the behaviour of tartronic acid. The main results are the determination of the molar absorption coefficient and the estimation of polychromatic quantum yield and second order reactivity constants with hydroxyl radical.

This is only the beginning of a complex work in which the main photoproducts of tartronic acid will be determined by proton nuclear magnetic resonance (H-NMR) and all the results will be implemented in the atmospheric model M2C2 described in Chapter 3.

Chapter 7

Motivation

Cloud water dissolved organic carbon composition is mostly undetermined: as shown in Chapter 3 only aldehydes and main carboxylic acids were determined.

We focused our work on proteinaceous matter that, after enzymatic or hydrolytic action, can be separated into amino acids. In this sense amino acids could constitute the link between microbiological activity and cloud aqueous chemistry and photochemistry. However, they can also come from other sources, as described in Chapter 3.

For this reason, in the work presented in this chapter, we detected and quantified amino acids in cloud water adopting a chromatographic method with pre-column derivatization. We found that the average total concentration of amino acids account for 10% of the DOC. In the second part of this work, we show that amino acids reactivity with the hydroxyl radical is greater than that of carboxylic acids.

For many years, the presence of microorganisms and their activity in cloud water droplet and in the atmosphere in general has been well known but only recently their influence on cloud water dissolved organic carbon speciation has been proved. In particular, it was shown that they transform short chain carboxylic acids. Starting from this assumption, we can easily hypothesize that, during their life in cloud water, microorganisms release organic compounds, mainly in the form of simple carbohydrates (sugars) and proteins. Furthermore, after the death of the cells, the cellular membrane can fissure and all the material contained in cytoplasm (salts, sugars, enzymes, proteins and RNA) pour into the droplet. A general perspective of the work presented could be the correlation between microorganism activity and concentration of amino acids.

Improving the characterization of dissolved organic carbon in cloud water: Amino acids and their impact on the oxidant capacity

Angelica Bianco[a,b], Guillaume Voyard[a,b], Laurent Deguillaume[c,d], Gilles Mailhot[a,b], Marcello Brigante[a,b*]

[a] *Université Clermont Auvergne, Université Blaise Pascal, Institut de Chimie de Clermont-Ferrand, BP 10448, F-63000 CLERMONT-FERRAND, FRANCE*

[b] *CNRS, UMR 6296, ICCF, F-63171 AUBIERE, FRANCE*

[c] *Université Clermont Auvergne, Université Blaise Pascal, OPGC, Laboratoire de Météorologie Physique, BP 10448, F-63000 CLERMONT-FERRAND, FRANCE*

[d] *CNRS, UMR 6016, LaMP/OPGC, BP80026, F-63177 AUBIERE, FRANCE*

* Corresponding author Marcello Brigante: University Blaise Pascal, Institute of Chemistry of Clermont-Ferrand, avenue des Landais 63171 Aubière, France; Phone +33 0473405514 e-mail: marcello.brigante@univ-bpclermont.fr

Article submitted to *Nature Scientific Reports*

Abstract

Improving our understanding of cloud chemistry depends on achieving better chemical characterization (90% of the organic carbon [OC] fraction remains uncharacterized) and, consequently, assessing the reactivity of this complex system. In this manuscript, we report for the first time the concentrations of 16 amino acids (AAs) in 25 cloud water samples. The concentrations of individual AAs ranged from a few nM up to ~2.0 µM, and the average contribution of AAs corresponded to 10% (5.1% to 25.9%) of the dissolved OC (DOC) concentration. Considering their occurrence and concentrations, AAs were expected to represent an important hydroxyl radical ($HO^{\bullet}$) sink in aqueous cloud samples. In this work, we estimated that approximately 20% of the hydroxyl radical-scavenging ability of the DOC could be attributed to the presence of AAs, whereas comparing the AAs suggested that up to 60% of their reactivity with $HO^{\bullet}$ could account for the presence of tryptophan. These results clearly demonstrate that the occurrence and reactivity of AAs must be considered to better estimate the chemical composition and oxidant capacity of the aqueous cloud phase.

7.1. Introduction

The organic carbon (OC) fraction of aerosol accounts for a large portion of air particulate matter and exhibits many complex molecular structures [218]. This organic matter originates from a wide variety of natural and anthropogenic sources; additionally, it undergoes chemical transformations during its atmospheric lifetime [62] and strongly influences the climate and health effects of atmospheric aerosols [219]. In the OC fraction of aerosols, water-soluble OC (WSOC) is especially interesting because it contributes to particles' hygroscopic properties and participates in aqueous cloud chemistry [220]. Some WSOC components are emitted into the air as primary particles (*e.g.*, through biomass burning), and others are produced by reactions in the gas and aqueous phases [221,222]. One major concern is related to the effects of WSOC on the surface tension of particles and their ability to be activated into cloud droplets [223]. However, a large fraction of WSOC remains uncharacterized, and substantial work has focused on quantifying short-chain mono and di-carboxylic acids (CAs) and carbonyl and dicarbonyl compounds [27,102].

Soluble organic matter comprises small volatile molecules associated with larger multifunctional structures containing a substantial fraction of hetero-atoms (*e.g.*, N, S, and O), such as HUmic LIke Substances (HULIS), and polyols, such as sugars, phenols, and polyconjugated species [224,225]. Multiple functionalities, including hydroxyl, carboxyl and carbonyl groups, are present in these molecules. Field measurements have revealed that a large part of this WSOC remains uncharacterized (10% to 50%), despite the application of a variety of analytical approaches.

Among these compounds, the presence of amino acids (AAs) belonging to proteinaceous matter was highlighted in rain, fog waters and aerosols [145,226]. Their effect on the surface tension properties of aerosols and their role as ice nuclei were studied, revealing that AAs could affect the atmospheric water cycle [141,142,144,147]. Proteinaceous matter is injected into the atmosphere by the production of sea salt aerosol when air bubbles burst at the ocean surface. Proteinaceous matter can also be emitted in the atmosphere by the activity of bacteria and phytoplankton or from the injection of organic film into the air at the sea surface [12,139,227]. Over continental areas, proteinaceous matter is injected into the atmosphere as plant debris, pollen, and algae, and this biological fraction has been frequently detected on aerosol particles [146]. The first oxidation of the proteinaceous matter could occur on the aerosol particle, for example, involving methionine and tryptophan, which are rapidly oxidized when exposed to ozone and sunlight [228].

One important difference between the free and combined forms of AAs must be noted when analysing environmental samples (*e.g.*, rain, fog, clouds, and aerosols) [136,139]. The analysis of aerosol and fog samples revealed that AAs were mostly present as dissolved combined AAs (DCAAs), such as proteins, peptides and HULIS [139,229,230]. One crucial question relates to how proteins and peptides are converted into free AAs (dissolved free AAs [DFAAs]). Milne and Zika proposed different hypotheses about aerosol samples, excluding thermal hydrolysis but suggesting that enzymatic hydrolysis could be non-negligible [140]. This hypothesis was corroborated by recent works revealing the presence and impact of AAs on the oxidant capacity and organic speciation of living microorganisms in cloud water [185,231]. The direct photolysis of peptides and photosensitized reaction pathways could be responsible for their fragmentation under actinic radiation [232]. Thus, in environmental samples, both forms of AAs could be detected, but the concentration of DFAAs (uncombined forms) is expected to be lower because this is the preferred form for the uptake of nitrogen compounds by microorganisms [139]. Recent works have showed that AAs dissolved in cloud water could be transformed by solar radiation and reaction with oxidative species (*i.e.*, hydroxyl radicals), leading to the production of different functionalized and oxidized products and short-chain CAs [233,234].

In this manuscript, we report the AA concentrations in 25 cloud water samples obtained at puy de Dôme Mountain (France) during 11 cloud events. Chromatographic separation coupled with chemical complexation and fluorescence detection was used to determine the concentration of DFAAs. To the best of our knowledge, this study reports, for the first time, the concentrations of free AAs in cloud waters. Comparing the reactivities of the AAs with those of naturally occurring CAs and dissolved OC (DOC) suggested that the presence and reactivity of AAs should be considered in the future to better assess the effect of cloud aqueous-phase chemistry on the organic matter transformation mediated by the hydroxyl radical ($HO^{\bullet}$).

7.2. Results and discussions

7.2.1. Quantification of amino acids

The concentrations of 16 AAs were determined in 25 individual samples from 11 cloud events collected during two campaigns in March/April and November 2014 at the top of puy de Dôme mountain (1465 m a.s.l.) in France. The cloud droplet sampling was performed using a one-stage cloud droplet impactor, as previously described [27]. The sampling times ranged from 120 to 180 min depending on the liquid water content, which reflects the mass of water in a cloud in a specified amount of dry air and was in the range of 0.1-0.2 g cm^{-3}. Single-AA concentrations ranged from 5 nM (corresponding to the analytical detection limit) to ~2.0 µM (Supplementary Table S1).

Cloud event	Sample	Sampling period and time (dd/mm/time)	Concentrations (nM)															
			ALA	ARG	ASP	GLU	GLY	HIS	ILE	LEU	LYS	MET	PHE	SER	THR	TRP	TYR	VAL
I	1	22/03 7am-11pm	363 ± 27	31 ± 6	260 ± 21	55 ± 13	278 ± 43	41 ± 5	349 ± 8	93 ± 9	484 ± 43	261 ± 17	287 ± 47	736 ± 63	166 ± 16	686 ± 156	48 ± 5	44 ± 12
II	2	25/03 11am-1pm	271 ± 11	57 ± 8	223 ± 25	61 ± 20	197 ± 5	38 ± 6	312 ± 78	79 ± 7	82 ± 54	108 ± 26	385 ± 48	526 ± 44	150 ± 29	797 ± 189	30 ± 5	56 ± 14
III	3	26/03 8am-9am	170 ± 5	36 ± 5	130 ± 14	40 ± 12	176 ± 5	75 ± 20	1174 ± 327	111 ± 5	162 ± 81	84 ± 7	507 ± 169	268 ± 6	147 ± 9	1318 ± 367	21 ± 5	61 ± 5
IV	4	26/03 9am-11am	638 ± 50	27 ± 5	168 ± 19	86 ± 15	250 ± 8	84 ± 8	1142 ± 289	102 ± 7	129 ± 41	64 ± 17	564 ± 177	298 ± 18	202 ± 26	1497 ± 421	24 ± 5	67 ± 10
	5	04/04 8pm-10pm	231 ± 5	54 ± 5	242 ± 16	85 ± 12	151 ± 5	41 ± 5	353 ± 12	108 ± 4	57 ± 32	93 ± 5	246 ± 38	319 ± 5	195 ± 20	671 ± 100	34 ± 5	56 ± 6
V	6	04/04 10pm-12pm	185 ± 5	35 ± 5	137 ± 16	45 ± 11	144 ± 10	49 ± 10	434 ± 5	99 ± 5	95 ± 28	31 ± 5	350 ± 23	276 ± 8	166 ± 29	898 ± 125	20 ± 5	31 ± 5
	7	04-05/04 1pm-4am	106 ± 21	38 ± 5	87 ± 18	38 ± 12	300 ± 48	217 ± 98	278 ± 7	38 ± 5	80 ± 31	71 ± 12	226 ± 10	223 ± 5	123 ± 54	1378 ± 18	19 ± 5	58 ± 6
	8	05/04 4am-7am	167 ± 5	40 ± 6	152 ± 22	44 ± 15	259 ± 5	71 ± 12	1569 ± 42	167 ± 5	148 ± 30	80 ± 11	254 ± 20	237 ± 6	72 ± 14	2034 ± 530	29 ± 5	72 ± 5
	9	05/04 7am-10am	277 ± 15	22 ± 6	211 ± 11	63 ± 13	449 ± 21	80 ± 22	1881 ± 16	226 ± 5	282 ± 81	174 ± 91	481 ± 31	498 ± 26	447 ± 16	1758 ± 614	23 ± 4	63 ± 24
VI	10	04/11 11am-1pm	603 ± 11	310 ± 24	314 ± 15	182 ± 13	330 ± 15	134 ± 13	169 ± 5	173 ± 5	269 ± 85	169 ± 12	310 ± 51	639 ± 4	198 ± 12	307 ± 49	90 ± 5	152 ± 5
VII	11	05/11 4am-6pm	253 ± 12	165 ± 26	205 ± 18	59 ± 10	350 ± 14	129 ± 14	295 ± 21	111 ± 8	107 ± 65	119 ± 5	274 ± 50	629 ± 46	186 ± 32	534 ± 160	62 ± 5	91 ± 14
	12	05/11 7am-9am	256 ± 5	153 ± 23	200 ± 13	83 ± 9	207 ± 5	88 ± 18	341 ± 10	91 ± 12	347 ± 85	97 ± 6	414 ± 6	330 ± 5	85 ± 6	771 ± 228	38 ± 5	62 ± 5
	13	05/11 9am-12am	561 ± 12	132 ± 24	458 ± 46	71 ± 11	889 ± 76	196 ± 13	498 ± 5	242 ± 5	259 ± 112	213 ± 10	748 ± 43	1694 ± 83	512 ± 20	1095 ± 245	135 ± 5	111 ± 9
VIII	14	12/11 5pm-7pm	87 ± 6	339 ± 33	165 ± 14	47 ± 9	79 ± 10	92 ± 15	251 ± 8	66 ± 5	190 ± 78	131 ± 8	253 ± 20	126 ± 9	81 ± 5	684 ± 171	47 ± 5	37 ± 5
	15	12/117pm-9pm	56 ± 6	210 ± 27	119 ± 11	35 ± 10	57 ± 12	62 ± 14	240 ± 10	61 ± 5	123 ± 64	102 ± 7	228 ± 41	95 ± 10	51 ± 5	568 ± 121	25 ± 5	33 ± 5
	16	12/11 9pm-12pm	410 ± 5	430 ± 22	989 ± 58	361 ± 20	206 ± 5	271 ± 26	489 ± 23	294 ± 5	325 ± 103	172 ± 5	394 ± 46	484 ± 5	762 ± 9	491 ± 98	409 ± 6	243 ± 13
IX	17	14/11 5pm-7pm	118 ± 5	126 ± 24	147 ± 15	39 ± 10	139 ± 7	45 ± 9	171 ± 8	55 ± 5	96 ± 28	55 ± 5	100 ± 51	210 ± 11	77 ± 6	455 ± 11	30 ± 5	25 ± 5
X	18	17/11 4pm-6pm	79 ± 5	57 ± 6	109 ± 15	31 ± 11	66 ± 5	30 ± 5	275 ± 77	29 ± 5	67 ± 36	26 ± 5	66 ± 9	134 ± 5	72 ± 24	446 ± 93	22 ± 5	18 ± 5
	19	17/11 7pm-9pm	79 ± 5	90 ± 7	128 ± 12	33 ± 11	73 ± 11	42 ± 5	200 ± 32	50 ± 5	162 ± 52	86 ± 21	159 ± 29	136 ± 11	59 ± 7	349 ± 12	27 ± 5	42 ± 16
	20	17/11 9pm-12pm	71 ± 5	51 ± 5	91 ± 13	28 ± 9	60 ± 11	34 ± 12	191 ± 27	59 ± 5	100 ± 52	53 ± 5	209 ± 47	116 ± 9	66 ± 18	531 ± 101	25 ± 5	15 ± 5
	21	18/11 6am-8am	143 ± 6	44 ± 5	127 ± 17	39 ± 11	113 ± 5	30 ± 5	199 ± 5	58 ± 5	183 ± 46	59 ± 5	155 ± 41	270 ± 16	145 ± 25	433 ± 93	32 ± 5	31 ± 7
	22	18/11 5pm-7pm	188 ± 5	47 ± 6	188 ± 12	37 ± 10	173 ± 5	31 ± 5	218 ± 7	57 ± 5	196 ± 74	64 ± 7	182 ± 35	374 ± 7	157 ± 6	571 ± 98	33 ± 5	30 ± 5
	23	18/11 7pm-9pm	88 ± 5	37 ± 5	106 ± 10	39 ± 13	55 ± 8	22 ± 5	197 ± 5	49 ± 5	110 ± 29	54 ± 5	193 ± 43	127 ± 6	51 ± 7	504 ± 93	22 ± 5	21 ± 5
XI	24	18/11 9pm-12pm	126 ± 5	43 ± 5	171 ± 17	38 ± 9	91 ± 5	25 ± 6	226 ± 5	55 ± 5	168 ± 52	79 ± 10	198 ± 26	205 ± 5	92 ± 31	614 ± 137	31 ± 5	31 ± 6
	25	19/11 12pm-2am	226 ± 5	63 ± 5	176 ± 12	49 ± 11	220 ± 5	44 ± 6	201 ± 7	71 ± 5	173 ± 41	109 ± 7	201 ± 42	353 ± 10	216 ± 16	459 ± 34	35 ± 5	69 ± 5

Table S1: Amino acids concentrations in each cloud water sample. Number of cloud events is given in Roman. Errors are given considering 2 separates injections.

Figure 1 illustrates the concentrations of each AA in the cloud samples, showing that the average concentrations of ALA, ILE, PHE, SER and TRP exceeded 0.25 μM (see Table 1 for the AA abbreviations and relative concentrations). Specifically, ALA, PHE and SER were categorized as hydrophilic and amphiphilic compounds and can alter the surface activity and surface tension [235], which are important properties involved in cloud drop activation [236,237].

Compound	**Abbreviation**	**Number of Carbons**	**Molecular weight (g mol^{-1})**	**Average concentration (nM)**	**Carbon average concentration (μg C L^{-1})**
Alanine	ALA	3	89.0	230 ± 11	8.3 ± 0.4
Arginine	ARG	6	174.2	106 ± 10	7.6 ± 0.7
Aspartate	ASP	4	133.1	212 ± 11	10.2 ± 0.5
Glutamate	GLU	5	147.1	68 ± 3	4.1 ± 0.2
Glycine	GLY	2	75.1	212 ± 18	5.1 ± 0.4
Histidine	HIS	6	155.2	79 ± 19	5.7 ± 1.4
Isoleucine	ILE	6	131.2	466 ± 83	33.6 ± 6.0
Leucine	LEU	6	131.2	102 ± 3	7.3 ± 0.2
Lysine	LYS	6	146.2	176 ± 25	12.7 ± 1.8
Methionine	MET	5	149.2	102 ± 18	6.1 ± 1.1
Phenylalanine	PHE	9	165.2	295 ± 41	31.9 ± 4.4
Serine	SER	3	105.1	372 ± 21	13.4 ± 0.8
Threonine	THR	4	119.1	179 ± 12	8.6 ± 0.6
Tryptophan	TRP	11	204.2	791 ± 157	104.4 ± 20.7
Tyrosine	TYR	9	181.2	52 ± 1	5.6 ± 0.1
Valine	VAL	5	117.2	61 ± 6	3.7 ± 0.4
Total				**3504**	**268**

Table 1: Average single-AA concentration (nM) and corresponding average carbon concentration expressed in μg C L^{-1}. Values are presented with the standard deviation determined by analysing 25 samples.

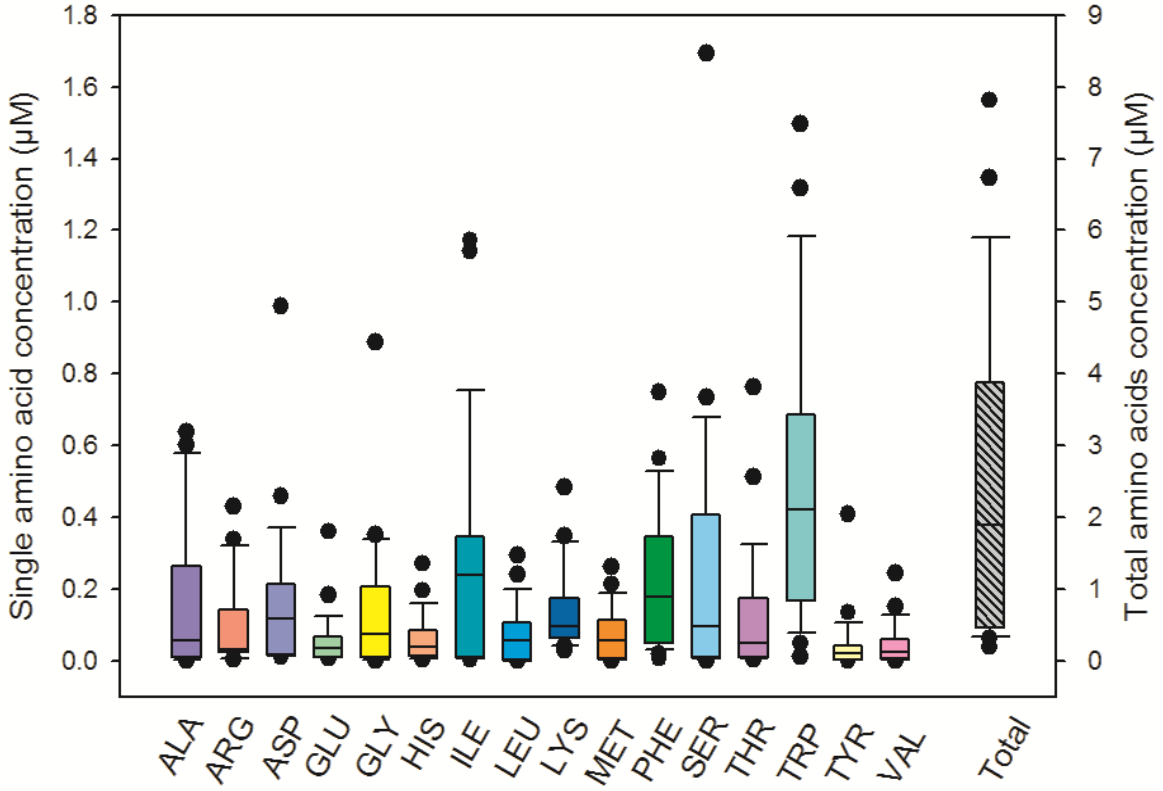

Figure 1: Distribution of each AA in the cloud samples. The bottom and top lines of the box correspond to the 25th and 75th percentiles, respectively. The middle line represents the median. The ends of the whiskers are the 10th and 90th percentiles, and the filled circle is an outlier. The y-right scale shows the total AA concentration.

Simulations and laboratory experiments also confirmed the role of AAs as effective cloud condensation nuclei (CCNi) [236,238]. The median values of the single-AA concentrations were lower than 0.5 µM, and TRP's concentration was the highest: 2 µM. The total AA concentration, defined as the median value of the sum of the AA concentration in each sample, ranged from 0.5 µM to 4 µM. The average concentrations of AA in cloud water samples were lower than those measured in fog water by Zhang et al. [145] (2.6-99 µM, mean ± 1σ = 20 ± 27 µM) and in dew water samples in Germany by Scheller [239] (0.5-110 µM, mean = 22.5 µM). The concentrations found here were relatively similar to those reported in rainwater by Gorzelska et al. [240] (≈ 0.4 µM) and Mopper and Zika [237] (6.5 µM). Fog and dew water were expected to be more concentrated than cloud water because they are influenced relatively strongly by local sources. The sampling procedure may also have contributed to this difference because of the potential evaporation of the liquid sample. The high TRP concentration cannot be directly correlated to the hydrolysis of proteinaceous matter. However, TRP was recently demonstrated to be strongly correlated with the formation of high-molecular-weight compounds with spectroscopic characteristics similar to those of

HULIS, which can also be considered as a potential TRP reservoir [233,241]. Muller et al. [242] evaluated TRYptophan LIke Substances (TRYLIS) in rain using fluorescence emission. These authors found that the TRP concentration was higher in samples from marine origins, suggesting that the presence of TRYLIS promoted the development of ice-precipitation at 'warmer' temperatures. Nevertheless, the detection of this compound in the fluorescence matrix was not suitable for the discrimination of free and combined TRP.

The proportion of AAs to the DOC ranged from 5.1% to 25.9% of the total carbon (with an average value of 10%) in 25 samples, corresponding to an average estimated concentration of ~ 268 µg C L^{-1} (see Table 1 for the average AA concentrations). Deguillaume et al. suggested that the characterization of the organic matter in cloud water remains incomplete because approximately 11% and 1% of the DOC is represented by short-chain CAs (formate, acetate, oxalate, malonate and succinate) and aldehydes, respectively [27]. In Figure 2 the average contributions of CAs, aldehydes and AAs to the DOC are presented, and the second pie plot reports the proportion of each AA.

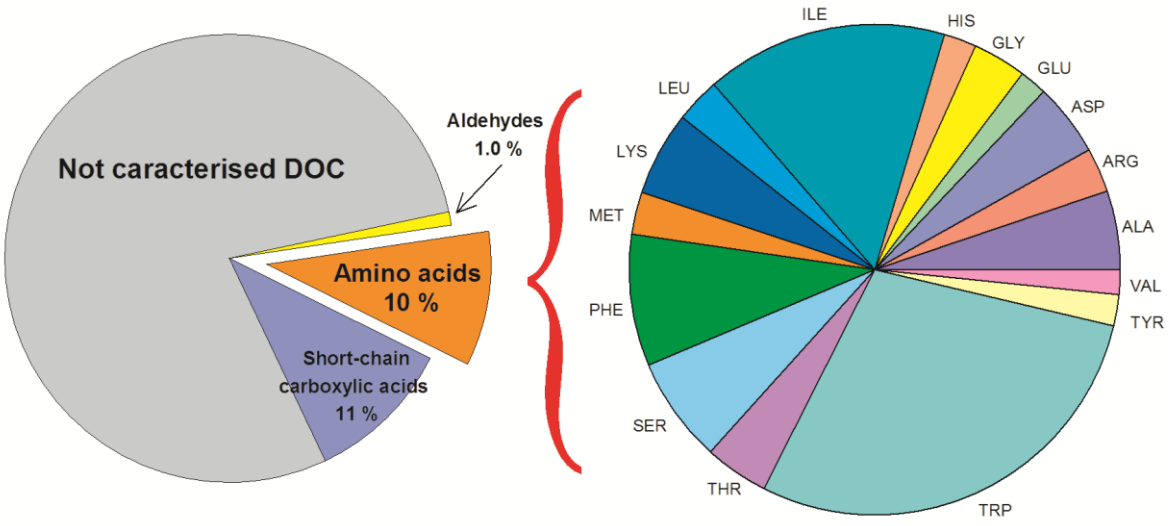

Figure 2: Pie plot showing the distributions of AAs, aldehydes and the most relevant short-chain CAs (formate, acetate, oxalate, malonate and succinate) relative to the total DOC in cloud water samples. The percentages were calculated based on the average concentrations of individual AAs, aldehydes, CAs and DOC in mgC L^{-1}. The second plot shows the distribution of a single AA relative to the total distribution.

Reactivity with $HO^{\bullet}$: Competition among AAs, CAs and DOC

The reactivity of AAs with hydroxyl radicals can be calculated and compared with those of most relevant short-chain CAs (formate, acetate, oxalate, malonate and succinate) always measured in the aqueous cloud phase [26,27,111]. This competition ($C_{AA/AC}$) can be evaluated by

considering the ratios between the scavenging rate constants of HO$^\bullet$ by AA ($k'_{HO^\cdot,AA}$) and CA ($k'_{HO^\cdot,CA}$)) using Equation 1:

$$C_{AA/AC} = \frac{k'_{HO^\cdot,AA}}{k'_{HO^\cdot,CA}}$$

Equation 1.

where $k'_{HO^\cdot,AA}$and $k'_{HO^\cdot,CA}$ are determined as the product of the second-order rate constant of HO$^\bullet$ with single AAs and CAs ($k'_{HO^\cdot,AA}$ or $k'_{HO^\cdot,CA}$) and their concentrations, respectively. Based on the average CA concentration in the aqueous cloud phase reported by Deguillaume et al. [27] (Supplementary Table S2) and the AA concentrations determined in each sample, $C_{AA/AC}$can be calculated by considering the contribution (or not) of formate to the CAs and a pH of 5.0 (see Supplementary Tables S3 and S4 for the pKa values and HO$^\bullet$ reactivities of each species and the DOC concentrations in each cloud sample, respectively).

Compounds	**Concentrations (µM)**
Formate	17.5
Acetate	6.5
Oxalate	3.0
Malonate	0.6
Succinate	0.4

Table S2: Concentrations of carboxylic acids considered for the calculation of competition with amino acids. Data are taken from the average concentrations reported by Deguillaume et al[27].

Compounds	**pKa**	$\boldsymbol{k_{HO^\cdot}}$ $(\boldsymbol{M^{-1}s^{-1}})$
ALA	2.3	7.7×10^{9}
ARG	2.2	3.5×10^{9}
ASP	2.2	7.5×10^{7}
GLU	2.2	2.3×10^{8}
GLY	2.3	1.7×10^{7}
HIS	1.8	5.0×10^{9}
ILE	2.4	1.8×10^{9}
LEU	2.4	1.7×10^{9}
LYS	2.2	3.5×10^{8}

MET	2.3	8.5×10^{9}
PHE	1.8	6.9×10^{9}
SER	2.2	3.2×10^{8}
THR	2.6	5.1×10^{8}
TRP	2.4	1.3×10^{10}
TYR	2.2	1.3×10^{10}
VAL	2.3	8.5×10^{8}
Formate	3.76	3.2×10^{9} (A^{-}); 1.3×10^{8} (HA)
Acetate	4.75	8.5×10^{7} (A^{-}); 1.6×10^{7} (HA)
Oxalate	1.25-4.23	7.7×10^{6} (A^{2-}); 4.7×10^{7} (HA^{-}); 1.4×10^{6} (H_2A)
Succinate	4.23-5.64	5.0×10^{8} (A^{2-}); 5.0×10^{8} (HA^{-}); 1.1×10^{8} (H_2A)
Malonate	2.8-5.6	3.0×10^{8} (A^{2-}); 6.0×10^{7} (HA^{-}); 2.0×10^{7} (H_2A)

Table S3: Second order rate constant with $HO^{\bullet}$ ($k_{HO^{\cdot}}$ ($M^{-1}s^{-1}$)) of amino acids and carboxylic acids (values are taken from literature [76,133,243]). For amino acids the value is given for the deprotonated form while, for carboxylic acids the values are given for deprotonated and protonated forms.

Sample	**DOC (mgC L^{-1})**	$\frac{k'_{HO^{\cdot},AA}}{k'_{HO^{\cdot},CA}} = \frac{\sum_i k'_{HO^{\cdot},AA}\,[AA]_i}{\sum_i k'_{HO^{\cdot},CA}\,[CA]_i}$	
		Without Formate	With Formate
1	2.9	21.0 ± 3.3	0.34 ± 0.05
2	3.4	17.9 ± 4.1	0.29 ± 0.07
3	6.5	28.6 ± 8.1	0.46 ± 0.13
4	8.6	31.1 ± 8.6	0.50 ± 0.14
5	1.5	14.9 ± 2.1	0.24 ± 0.03
6	1.7	18.5 ± 2.3	0.30 ± 0.04
7	2.6	24.8 ± 1.4	0.40 ± 0.02
8	3.9	37.6 ± 8.1	0.60 ± 0.13
9	4.5	38.7 ± 10.6	0.62 ± 0.17
10	1.9	15.3 ± 2.2	0.25 ± 0.04
11	1.8	15.3 ± 3.6	0.25 ± 0.06
12	1.8	20.0 ± 4.3	0.32 ± 0.07
13	NM	31.6 ± 5.1	0.51 ± 0.08
14	2.3	17.8 ± 3.6	0.29 ± 0.06

15	2.7	14.0 ± 2.8	0.23 ± 0.05
16	1.7	26.5 ± 3.0	0.43 ± 0.05
17	2.2	10.4 ± 1.0	0.17 ± 0.02
18	2.2	9.1 ± 2.0	0.15 ± 0.03
19	1.0	10.0 ± 1.2	0.16 ± 0.02
20	1.2	11.8 ± 2.4	0.19 ± 0.04
21	1.0	11.0 ± 2.1	0.18 ± 0.03
22	2.3	13.4 ± 2.5	0.22 ± 0.04
23	1.8	11.2 ± 2.0	0.18 ± 0.03
24	1.9	13.9 ± 2.8	0.22 ± 0.04
25	2.2	12.4 ± 1.3	0.20 ± 0.02

Table S4: DOC value for each cloud water sample. $\frac{k'_{HO^{\cdot},AA}}{k'_{HO^{\cdot},CA}} = \frac{\sum_i k'_{HO^{\cdot},AA}[AA]_i}{\sum_i k'_{HO^{\cdot},CA}[CA]_i}$ are used to determine the HO$^{\bullet}$ scavenge competition between amino acids (AA) and carboxylic acids (CA). NM: not measured

As shown in Figure 3, for the comparison without formate, the AA contribution was between ~9 and 40 times larger than that of the CAs. Interestingly, for all samples, the scavenging abilities of the AAs were at least one order of magnitude higher than those of the short-chain CAs. In terms of the proportion of formate among the short-chain CAs, the $C_{AA/AC}$ value ranged from 0.15 to 0.5. These findings seem reasonable given the high reactivity of formate with HO$^{\bullet}$ ($k''_{HO^{\cdot},formate} = 3.2 \times 10^9\ M^{-1}s^{-1}$). Nevertheless, at lower pH values, the contribution of formate was expected to be relatively small; indeed, at pH 4.0, approximately 37% of formate exists as its acidic form (i.e., formic acid, pKa = 3.76), which is less reactive towards HO$^{\bullet}$ ($k''_{HO^{\cdot},formic\ acid} = 1.3 \times 10^8\ M^{-1}s^{-1}$).

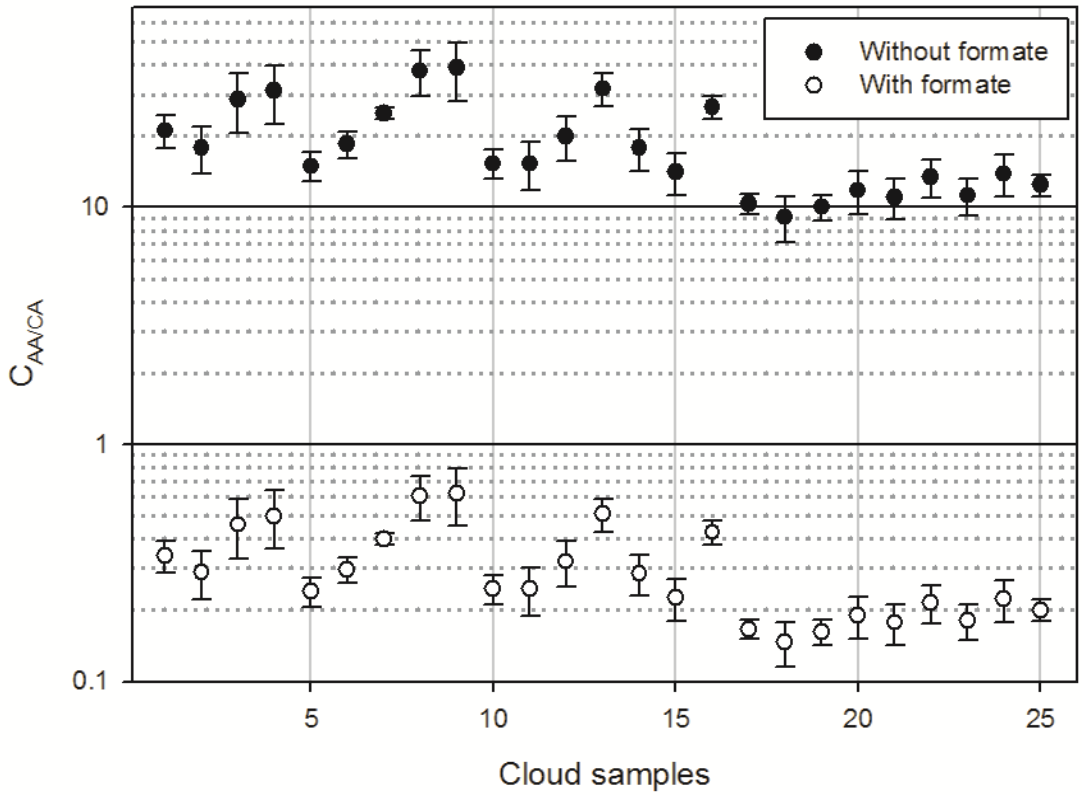

Figure 3: Ratio of the scavenging rate constants of HO• (expressed in s^{-1}) with AAs and short-chain CAs ($C_{AA/CA}$) without (filled circles) and with (empty circles) formate (calculated using equation 1). The error bars were determined by considering the uncertainties associated with AA quantification in each sample.

Figure 4 shows the contributions of all AAs, TRP and DOC to the scavenging rate constant of the hydroxyl radical in terms of their average concentrations. Up to 60% of the total reactivity of HO•, which is expressed as $k'_{HO^\bullet,AA_i}$, was attributable to TRP ($k'_{HO^\cdot,TRP}$ ~9.5 × 10^3 s^{-1}) among all AAs ($k'_{HO^\cdot,AA}$ ~1.7 × 10^4 s^{-1}). Interestingly the concentration of TRP was expected to be lower than those of other AAs because of its high reactivity with HO• ($k''_{HO^\cdot,TRP} = 1.3 \times 10^{10} M^{-1}s^{-1}$), suggesting the presence of a possible source in cloud water [231]. Moreover, as recently reported, the oxidation of TRP in cloud waters led to the formation of formate and acetate in 20% yields, with other nitrogen derivatives also likely produced (up to 60% of the uncharacterized carbon) [233]. These findings demonstrated that TRP oxidation could be responsible for a large fraction of the HO• scavenged in natural samples.

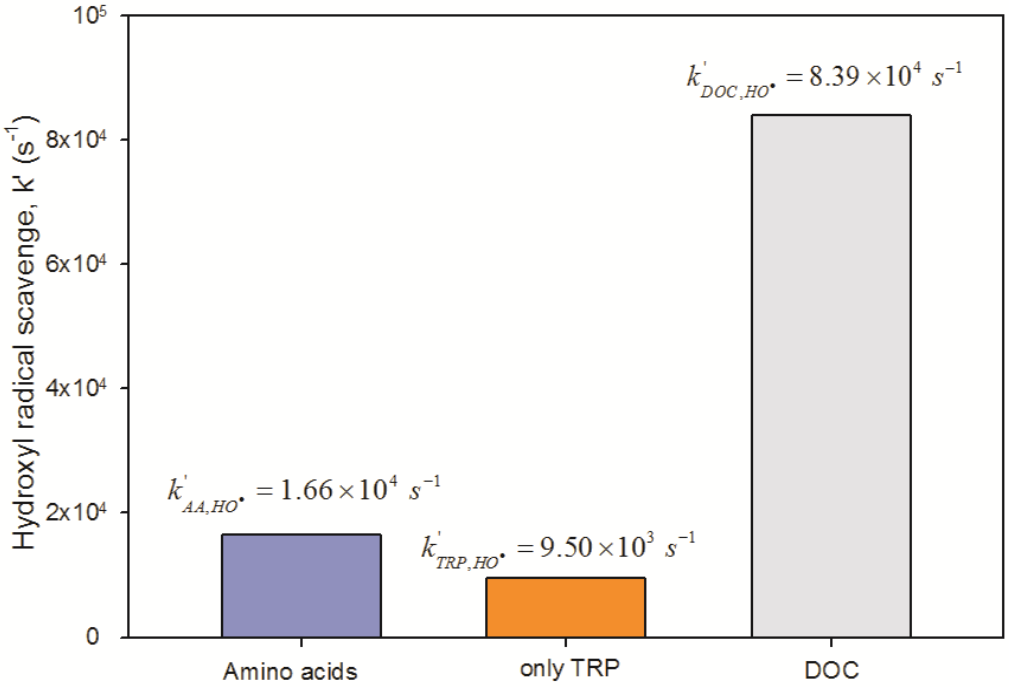

Figure 4: HO• scavenging rates (k') of AAs, TRP and DOC. These values were determined based on the average values of $\sum_i k''_{HO^{\cdot},AA}\,[AA]_i$, $\sum_i k''_{HO^{\cdot},TRP}\,[TRP]_i$ and $\sum_i k''_{HO^{\cdot},DOC}\,[DOC]_i$ using the concentrations and second-order rate constants reported in Tables S1 and S3. The $k''_{HO^{\cdot},DOC}$ value was taken from Arakaki et al.[103]

Moreover, the relative contributions of AAs to the DOC's reactivity with HO• can be estimated using Equation 2:

$$k'_{HO^{\cdot},DOC} = k''_{HO^{\cdot},DOC}\,[DOC]$$

Equation 2.

where $k''_{HO^{\cdot},DOC}$ and $[DOC]$ are the second-order rate constant between HO• and DOC estimated by Arakaki et al. [103] to be 3.8 × 10^8 L (mol C) $^{-1}$ s^{-1}) and the concentration of DOC, which varied from 1.0 mgC L^{-1} to 8.6 mgC L^{-1}, with an average of 2.65 mgC L^{-1} (Supplementary Table S4). In our samples, $k'_{HO^{\cdot},DOC}$ was in the range 0.14–2.72 × 10^5 s^{-1}. These values are similar to those previously determined by Arakaki and Faust, who reported a HO• scavenging rate range of 0.95 – 4.2 × 10^5 s^{-1} in 7 cloud water samples collected from Whiteface Mountain [83]. Comparing the reactivity of hydroxyl radicals and AAs in each cloud sample revealed that 10% to 43% of the total hydroxyl radicals scavenged by DOC were attributable to the presence of AAs (see Supplementary Table S5 for the calculations performed for each cloud sample).

Finally, AAs constituted a large fraction of the OC in cloud waters and play an important role in the scavenging of generated hydroxyl radicals. The origins of these AAs remain somewhat

unknown, and their concentrations could not be explained by considering only particle dissolution during cloud droplet formation. This observation suggests the presence of *in-situ* sources (*i.e.,* macromolecule oxidation or microorganism metabolism) that should be investigated in the future. However, our findings implied that the oxidant capacity of this medium (mainly related to $HO^{\bullet}$ reactivity) was strongly influenced by the presence of AAs, which can both act as sinks but modify the hydroxyl radical photogeneration processes *via,* for example, iron (Fe^{2+}/Fe^{3+}) complexation in cloud water. Finally, we demonstrated that the presence of AAs in cloud waters must be accounted for to facilitate predicting the cloud water oxidizing capacity using multiphase chemistry models.

7.3. Experimental Materials and methods

7.3.1. AA analysis

Cloud water samples were filtered immediately after collection using a 0.45-µm polytetrafluoroethylene (PTFE) filter to eliminate any microorganisms or particles. The solutions were stored at 255 K in the dark before analysis. The derivatization adopted was based on a previous method described by Ishida et al. [244] and adapted to the cloud water analysis of primary AAs. Essentially, the $-NH_2$ groups of primary AAs react with *o*-phthalaldehyde (OPA) to form a fluorescent derivative in the presence of a thiol group (here, mercaptopropionic acid [MPA]), which acts as a reaction catalyst. Secondary AAs were previously reported to be unreactive with OPA. After reacting with OPA, the cloud water samples were analysed by high-performance liquid chromatography (HPLC; Shimadzu Nexera equipped with an autosampler/pretreatment unit (SIL-30AC). For this purpose, 30 µL of MPA (7.7 mM in 0.1-M borate buffer), 15 µL of OPA (15.0 mM in 0.1-M borate buffer) and 5 µL of sample were mixed in a vial, and after 35 min, which is the length of time required for complete complexation, 20 µL of the solution was injected. Chemicals were purchased from Sigma-Aldrich and all solutions were prepared using MilliQ water (≥ 18.2 MΩ cm). The derivatized compounds were separated with an HPLC column (Shimadzu Shim-pack XR-ODS; 3.0 × 100 mm, Ø 2.2 µm, porous particles) and eluted at a flow rate of 0.7 mL min^{-1} using a gradient program with two eluents: eluent A (10-mM phosphate buffer, pH 6.8) and eluent B (acetonitrile, methanol and water 45:45:10 v/v/v). The gradient elution was as follows: initially, 10% of (B); a linear gradient to 75% (B) within 15 min; a faster increase of (B) to 100% in 1 min (corresponding to 16 min of elution); and constant (B) for an additional 5 min. A fluorescence detector (RF-20A XS) was used to detect AA-OPA

derivatives at an excitation wavelength (λ_{ex})/emission wavelength (λ_{em}) 350/450 nm (Figure 5 shows the HPLC chromatograms of samples 2 and 9).

The standard solution was prepared by diluting the AA-S-18 AA standard solution (Sigma Aldrich) in 0.1 M HCl (Supplementary Figure S1). Cloud water samples were analysed without further pre-treatment.

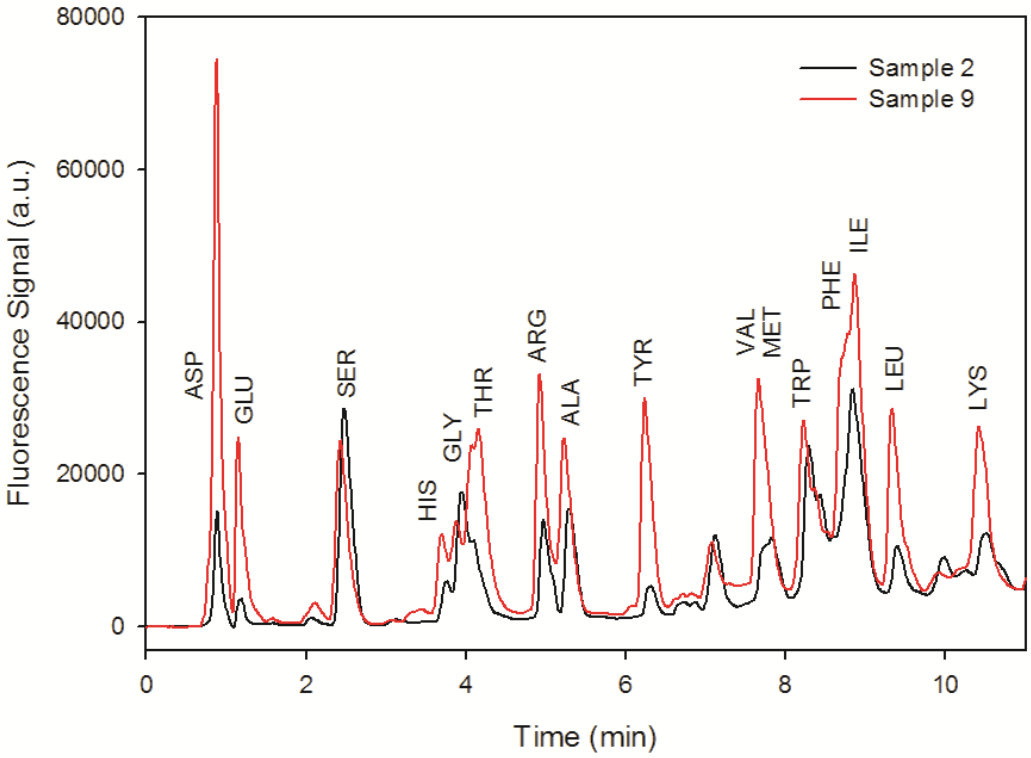

Figure 5: Example HPLC chromatograms obtained from samples 2 and 9.

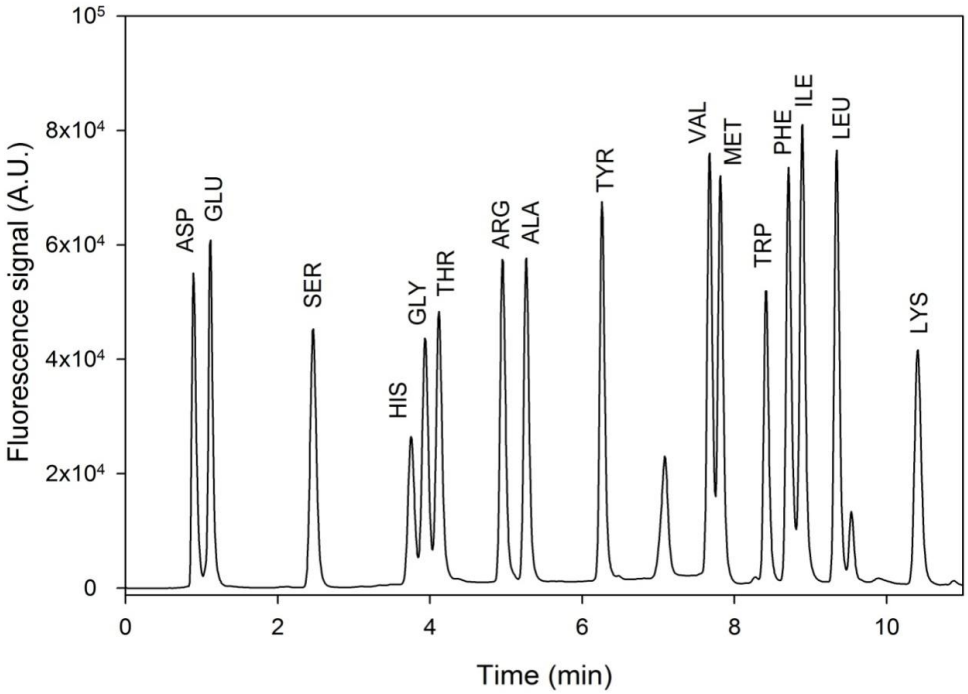

Figure S1: Chromatogram obtained for a standard solution (10 µM of each amino acid injection volume of 1 µL).

Each analysis was evaluated and monitored in terms of the reproducibility of the peak retention times and peak heights and the linearity of the calibration curve. The method's limit of detection (LOD) was estimated to be on the order of 5 nM with the injection of 20 µL of sample. Blank experiments (MilliQ water subjected to the entire derivatization process) were performed and confirmed that the AA concentration in water was always lower than the LOD. In this work, only the DFAA concentration was quantified. The samples were subjected to acidic hydrolysis according to the method described by Fountoulakis et al. [245] (1.5 mL of sample combined with 6 M HCl in an ampoule and then heated at 100 °C for 60 min). However, both the combined and dissolved AAs were hydrolysed, and the concentration was below the LOD. No significant differences in the AA concentration were found using filtered vs. unfiltered samples or before and after freezing.

Chapter 8

Motivation

It was previously reported in Chapter 3 that atmospheric water contains three principal fluorophores, identified as similar to humic substances (HULIS), to tyrosine (TYLIS) and to tryptophan (TRYLIS). These compounds are very important in the atmosphere because they can act as cloud condensation nuclei due to their hygroscopicity and surface tension activity. In addition they could represent a large fraction of dissolved organic matter but this parameter is difficult to evaluate because their physico-chemical proprieties are poorly characterized.

In this work, presented as a published article in *Atmospheric Environment*, we performed spectroscopic analysis of cloud water samples and we identified TRYLIS and HULIS and we quantified tryptophan by HPLC-FLR. In addition we irradiated tryptophan in distilled water and synthetic cloud water, mimicking cloud water composition, in the presence and in the absence of hydroxyl radical inorganic sources, in order to investigate direct and indirect photolysis of this compound.

The last part of this work reports the comparison between tryptophan and of dissolved organic carbon in hydroxyl radical scavenging.

Tryptophan and tryptophan-like substances in cloud water: occurrence and photochemical fate

Angelica Bianco[a, b], Monica Passananti[a, b], Laurent Deguillaume[c, d], Gilles Mailhot[a, b], Marcello Brigante[a, b*]

[a] *Université Clermont Auvergne, Université Blaise Pascal, Institut de Chimie de Clermont-Ferrand, BP 10448, F-63000 CLERMONT-FERRAND, FRANCE*

[b] *CNRS, UMR 6296, ICCF, F-63171 AUBIERE, FRANCE*

[c] *Université Clermont Auvergne, Université Blaise Pascal, OPGC, Laboratoire de Météorologie Physique, BP 10448, F-63000 Clermont-Ferrand (France)*

[d] *CNRS, UMR 6016, LaMP/OPGC, BP80026, F-63177 Aubière*

* Corresponding author E-mail: marcello.brigante@univ-bpclermont.fr

Atmos. Env., 137, 53 - 61, 2016

doi:10.1016/j.atmosenv.2016.04.034

Received 9 March 2016
Received in revised form 22 April 2016
Accepted 24 April 2016

Highlights

Tryptophan and tryptophan-like substances were quantified in cloud water sampled at the puy de Dôme station.

The fate of tryptophan was investigated in the cloud aqueous phase under sun-simulated conditions.

The hydroxyl radical-mediated transformation of tryptophan in cloud water can be considered to be a source of carboxylic and *N*-functionalized compounds.

Keywords

cloud water; photochemistry; organic matter; amino acids

Abstract

This work investigates the occurrence and photochemical behaviour of tryptophan (TRP) in the cloud aqueous phase. The concentrations of tryptophan, TRYptophan LIke Substances

(TRYLIS) and HUmic LIke Substances (HULIS) in real cloud water, collected between October 2013 and November 2014 at the top of the puy de Dôme station, were determined using the Excitation-Emission-Matrix (EEM) technique. The amount of free and complexed tryptophan (TRP) up to 10^{-7} M in cloud aqueous phase was quantified by HPLC-UV-fluorescence analysis, and its photoreactivity under sun-simulated conditions was investigated in synthetic water samples mimicking cloud aqueous phase compositions (oceanic and continental origins). TRP undergoes direct photolysis, and its degradation is enhanced in the presence of naturally occurring species able to photo-generate hydroxyl radicals ($HO^{\bullet}$). The polychromatic quantum yield of TRP ($\Phi^{TRP}_{290-340\,nm}$) is estimated to be 8.37×10^{-4} between 290 and 340 nm, corresponding to the degradation rate (R^{d}_{TRP}) of 1.29×10^{-11} M s^{-1} under our irradiation conditions. The degradation is accelerated up to 3.65×10^{-10} and 8.26×10^{-10} M s^{-1} in synthetic oceanic and continental cloud water samples doped with 100 µM hydrogen peroxide, respectively.

Hydroxyl radical-mediated transformation leads to the generation of different functionalized and oxidized products, as well as small carboxylic acids, such as formate and acetate. Moreover, fluorescent signals of irradiated solutions indicate the formation of HULIS.

8.1. Introduction

In the atmosphere, Primary Biological Aerosols (PBA) are ubiquitous and are comprised of either biological particles, including dead or live cells, or cell fragments [246-248]. They are able to nucleate cloud droplets and ice particles *via* physical processes [249-251]. PBA are mainly made up of organic substances and contribute to aerosol masses (organic carbon fraction, OC), and the organic fraction resulting from PBA components is made of biological compounds such as proteins and/or amino acids. These amino compounds were found to account for a significant fraction of fine particulate matter [252]. For example, [253] showed that amino acids can represent between 1.6 and 14% of the $PM_{2.5}$ mass at Davis in California. Several sources can be responsible for the atmospheric amino acid content; over a continental area, the biological compounds are produced by plants, pollen, algae, fungi and bacteria spores [145,254-256]. Human activities can also lead to the input of amino acids into the atmosphere. Zhang and Anastasio [145] identified livestock farming as the most important source of amino acids over the Californian region. These compounds are also present on anthropogenic coarse particles; soil and desert dust are also probably important sources of amino acids [257]. Moreover, marine emissions can also influence the atmospheric concentrations of amino acids [226], as confirmed by Weydan and Preston [258] over the southern

Atlantic Ocean. Finally, amino acids can be ejected into the atmosphere by volcanoes [259] or by biomass burning [254,260].

Amino acids can influence the microstructure of aerosol particles and consequently their water uptake, thus modifying cloud formation [261-263]. They can also act as ice-forming nuclei due to their hygroscopicity [258], leading to the formation of new particles in the atmosphere [264]. These compounds belong to the Water-Soluble Organic Compounds (WSOC) and consequently dissolve into the atmospheric aqueous phase. Several studies have reported concentrations of amino acids in the condensed phase of aerosols [145,265-267] as well as in rainwater and fog [268]. For example, the total amino acids have been evaluated to account for 13% of the Dissolved Organic Carbon (DOC) in fog waters and approximately 10% of the WSOC in $PM_{2.5}$ [145]. Amino acids should also be present in cloud water and could contribute to the dissolved organic content of cloud water that is currently still not well characterized [269,270].

In atmospheric water and aerosols, amino acids have been classified into the following different categories: DFAA (Dissolved Free Amino Acids), which indicates the free amino acids, and DCAA (Dissolved Combined Amino Acids), which indicates peptides, proteins and free amino acids that are also constituents of humic and fulvic acids [139]. Another classification distinguishes between FAC (Free Amino Compounds), which are comprised of amino acids and alkyl amines, and CAC (Combined Amino Compounds) if they are free or combined in proteins, peptides or HULIS substances [145].

Amino acids, and more particularly TRP, present in atmospheric water can directly absorb sun radiation or react with oxidants leading to the formation of inorganic and organic products [145,234,255,271,272]. Their reactivity can therefore modify the chemical composition of dissolved organic matter changing the chemical properties of water droplets and thus of aerosol particles.

Currently, scarce data are present in the literature on the occurrence and fate of amino acids or amino compounds in atmospheric water. To our knowledge, only Muller and co-workers [155] have previously reported the presence of TRYptophan LIke Substances (TRYLIS) in rainwater. In our work, we quantified the TRP concentration and detected the presence of TRYLIS and HUmic-LIke-Substances (HULIS) in cloud water samples collected at the puy de Dôme mountain station (France). To assess the possible impact on the aqueous organic chemical composition, TRP solutions are irradiated under sun-simulated conditions and transformation products are characterized. Oxidation processes occur and lead to the formation of carboxylic acids, as well as HULIS, which are followed during our experiments.

8.2. Materials and Methods

8.2.1 Sampling method

A total of 23 cloud samples were collected during two field campaigns in October and November 2013 and in March and April 2014 at the top of puy de Dôme mountain (1465 m a.s.l.) in France that belongs to the GAW (Global Atmosphere Watch) stations network. Cloud samples are spread among the following three classes: marine, highly marine and continental following the statistical analysis from Deguillaume et al. [27].

The cloud droplet sampling was carried out by a one stage cloud droplet impactor. The sampling times ranged from 120 to 180 minutes depending on the Liquid Water Content (LWC), which was in the range of 0.1-0.2 g cm^{-3}.

8.2.2 Chemical analysis

In order to characterize the main physicochemical properties of the sampled solution, the following physico-chemical measurements are performed immediately after cloud sampling and filtration: conductivity, redox potential, pH, UV-visible spectrum, and Excitation Emission Matrix (EEM) are carried out in less than one hour, while ion chromatography, quantification of the nitrite concentration and determination of the Total Organic Carbon (TOC) were performed on frozen samples. Analyses on frozen samples (kept at 255 K) are carried out in less than 48 hours after sampling. The results of the physico-chemical analysis are reported in Bianco et al. [273].

8.2.3 Irradiation experiments

One hundred millilitre aliquots of TRP solutions are irradiated in a photoreactor placed in a cylindrical stainless steel container. Six fluorescent lamps (Philips TL D15W/05), whose emission spectrum ranges from 290 to 500 nm, are separately placed along three different axes, while the photoreactor, a Pyrex tube with a 2.6 cm internal diameter, is placed in the centre of the setup. All of the experiments are carried out at 278 ± 2 K. An aliquot of the solution (3 mL) is withdrawn from the reactor and used for analysis at fixed times. In Figure 1, the emission spectrum of the lamp recorded using fibre optics coupled with a CCD spectrophotometer (Ocean Optics USD 2000+UV-VIS) is reported. The energy has been normalized to the actinometry results using paranitroanisole (PNA)/pyridine actinometer [274]. Over the UV region (wavelength range 290-400 nm), a total flux of 15.8 W m^{-2} is measured. The adopted intensity was close to the intensity measured between 290 and 400 nm at the top of puy de Dôme mountain during a late-autumn cloudy day at 11:00 am (see Figure 1).

Moreover, the absorption spectrum of TRP in water at a pH of 6.0 is reported in Figure 1, showing an overlap with the emission spectrum of the irradiation setup.

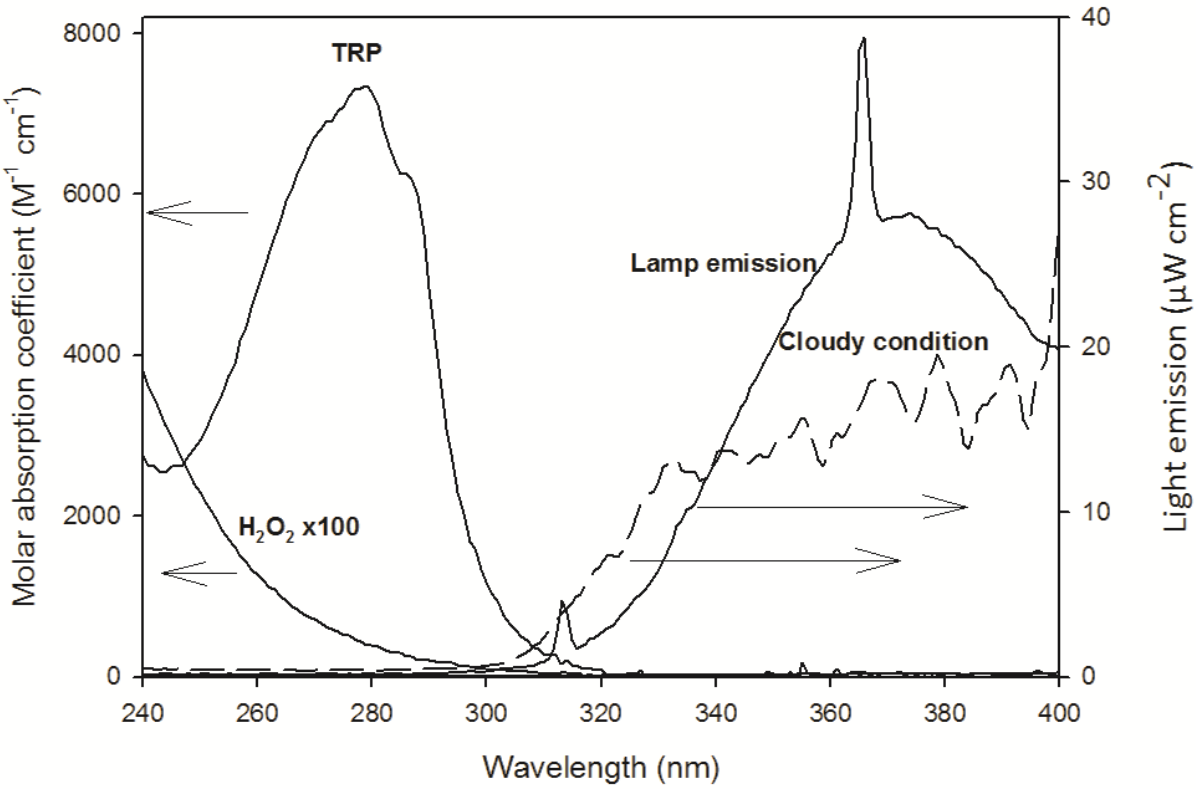

Figure 1: Left axis: absorption spectra of TRP and H_2O_2 (×100) aqueous solutions. Right axis: emission spectrum of the fluorescent lamps reaching solutions over the range of 290–400 nm (total flux intensity of 2039 µW cm^{-2}) compared with the sun emission spectrum (dashed line) for a cloudy day (1580 µW cm^{-2}) in October 2013.

TRP (10 µM) is irradiated in pure Milli-Q water and in synthetic water samples mimicking the chemical composition of cloud water doped with H_2O_2 (from 100 µM to 10 mM). Two different synthetic water samples are prepared; the first one is representative of marine cloud water and the second is a solution of continental cloud water (see Table SM1 for the chemical composition).

Anion	***Oceanic***	***Continental***
SO_4^{2-}	200 µM	800 µM
Cl^-	500 µM	500 µM
NO_3^-	200 µM	1000 µM
NO_2^-	0.5 µM	4 µM
pH	5.6	4.5

Table SM1**:** Chemical composition of synthetic cloud waters.

8.2.4 Fluorescence characterization of samples

Fluorescence chromophores are identified in real cloud water samples on the basis of previously reported data [160,275] using an Excitation Emission Matrix (EEM).

EEM are recorded with a Varian Cary Eclipse Fluorescence Spectrophotometer with 5 nm intervals for excitation wavelengths from 200 to 500 nm and emission from 220 to 600 nm with scan rate of 600 nm min^{-1} and bandpass of 10 nm for both excitation and emission. Standard solutions of TRP (between 1×10^{-9} and 5×10^{-7} M) were used to calibrate the fluorescence signal. The following two signals are considered: the first one at λ_{ex} 225 nm and λ_{em} 330 nm and the second one at λ_{ex} 275 nm and λ_{em} 340 nm. Many other compounds could present fluorescence emission at λ_{ex} 225 nm; for this reason, the second signal at λ_{ex}/ λ_{em} 275/330 nm is considered for calibration. The limit of detection of this method is estimated to be 5×10^{-10} M according to the signal/noise ratio of the instrument.

8.2.5 Chromatographic analysis and kinetics

The TRP concentration was determined in cloud water samples and in synthetic solutions prepared with Milli-Q water. Quantification was performed with a Waters Acquity Ultra Performance LC equipped with Water Acquity Photo Diode Array detector and fluorescence detector. Compound separation was performed using a Waters Acquity UPLC C18 column (100 mm x 2.1 mm x 1.7 µm) and isocratic elution with 90% acetate buffer (2.5 mM) and 10% methanol. The eluent flow rate was 0.3 mL min^{-1}, and the retention time of TRP is 2.7 min. Fluorescence detection is performed with λ_{ex} = 225 nm and λ_{em} = 340 nm.

The initial rates of TRP degradation were determined by fitting the experimental data with the pseudo-first order decay equation of the form $[TRP]_t = [TRP]_0 \times e^{-k^d_{TRP}\times t}$, where $[TRP]_0$ and $[TRP]_t$ are the concentrations of TRP at the initial time and time t, respectively, and k^d_{TRP} is the pseudo-first order decay constant. The TRP degradation rate (R^d_{TRP}, M s^{-1}) could then be obtained from $k^d_{TRP} \times [TRP]_0$.

The polychromatic degradation quantum yield ($\Phi^{TRP}_{290-340\,nm}$) is also calculated. $\Phi^{TRP}_{290-340\,nm}$ is defined as the ratio between the number of molecules transformed and the number of photons absorbed in the same period of time (Equation 1):

$$\Phi^{TRP}_{290-340\,nm} = \frac{R^d_{TRP}}{I_a}$$

Equation 1.

where R_{TRP}^{d} is the TRP degradation rate (M s^{-1}) and I_a is the absorbed photon flux per unit of surface and unit of time. The latter was calculated from Equation 2:

$$I_a = \int_{\lambda} I_0(\lambda)(1 - 10^{-\varepsilon(\lambda) d [TRP]_0})$$

Equation 2.

where I_0 is the incident photon flux, ε the molar absorption coefficient of TRP, d the optical path length inside the cell and $[TRP]_0$ is the initial TRP concentration.

8.2.6 Transformation product identification

With the objective of detecting the photoproducts, more concentrated TRP solutions (200 µM) are irradiated in the presence and absence of hydrogen peroxide (1 mM) and analysed by LC-MS with ESI (Electro Spray Ionization) in the positive mode, followed by detection by tandem mass spectrometry using a qTOF (quadrupole time of flight) detector. A resolution of 5000 was used for the TOF-MS analyses.

SM: Identification of tryptophan transformation products .

A LC-MS system (Agilent 1100 Series, binary pump) equipped with an ESI ion source (MSD VL) is used to identify TRP transformation products. All transformation products are identified in the positive mode.

Electrospray mass spectra and tandem mass spectra are acquired with a Q-TOF (Micromass, Manchester, UK). The capillary needle voltage is 3 kV, and the source temperature is maintained at 100°C. Nitrogen is used as the nebulizer gas. The cone voltage is 35 V for MS. The resulting product ions are determined by the TOF analyser. Data acquisition is carried out with a Micromass MassLynx 4.1 data system.

Water acidified with 0.1% of formic acid/methanol 50/50 is used as the solvent system to move the sample to the electrospray source, and the signal is acquired for 5 minutes.

Ion Chromatography (IC) analyses are performed using a DIONEX DX-320 equipped with an IonPac AG18 (guard column, 2 × 50 mm) and an IonPac AS18 (analytical column 2 × 250 mm). Elution is performed with a gradient of 10 mM potassium hydroxide to 20 mM in 30 minutes and with a prior stabilization for 5 minutes at 10 mM. The injection loop volume is fixed to 750 µL. Under these conditions, the retention times of acetate and formate are of 6.5 and 7.3 min, respectively.

8.3. Results and Discussion

8.3.1 Fluorescence characterization of cloud aqueous phase samples

In Figure 2, the EEM spectra of cloud aqueous phase samples 4 and 9 (see Table 1) are reported for illustration. In both spectra (Figure 2, graphics 4-A and 9-A) obtained using an intensity range scale from 0 to 50 or 60, different peaks can be observed. The first peak is centred at $\lambda_{ex}/\lambda_{em}$ 225/340 nm with a high intensity signal, and the other two peaks can be detected using a lower intensity scale (from 0 to 20) at $\lambda_{ex}/\lambda_{em}$ 275/330 nm and $\lambda_{ex}/\lambda_{em}$ 310/410 nm (see Figure 2, graphics 4-B and 9-B).

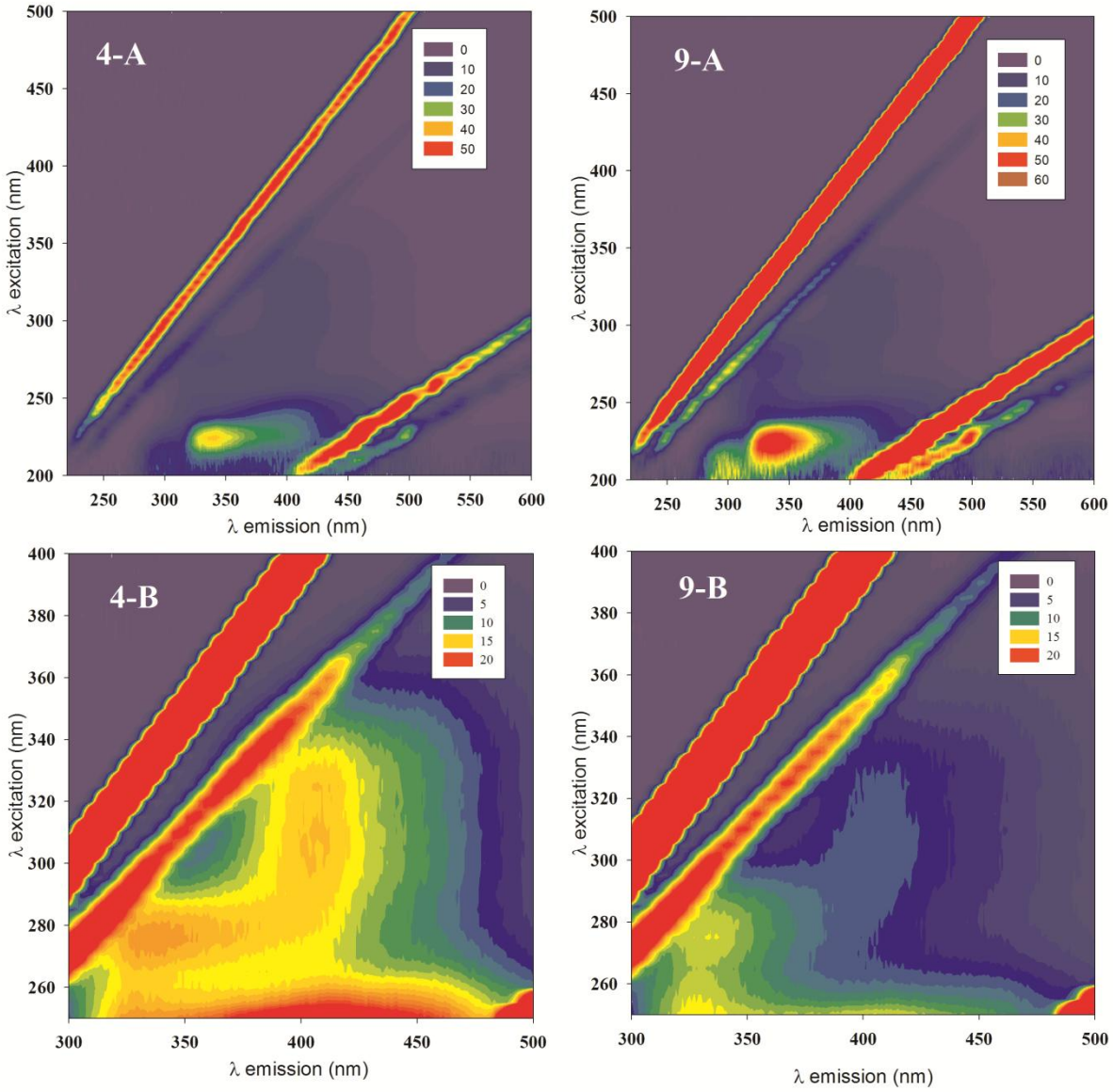

Figure 2: EEM (as contour plot) of samples 4 and 9. For 4-**A** and 9-**A**, excitation ranges from 200 to 500 nm and emission from 220 to 600 nm. The intensity is scaled from 0 to 50 or 60. For 4-**B** and 9-**B**, excitation ranges from 250 to 400 nm and emission from 300 to 500 nm. Intensity is scaled from 0 to 20. The linear features (in red) are Rayleigh scattering in water.

Sampling			Tryptophan-like signal (M)*	Tryptophan *UPLC-FLR*	HULIS signal (A.U.)
Period (dd/mm/yyyy)	**Sampling time**	**Sample number**			***λ_{ex} = 340 nm λ_{em} = 420 nm***
14/10/2013	4 PM-6 PM	1	1.1×10^{-7}	$2.4\pm0.7 \times 10^{-8}$	29.8
14/10/2013	6 PM-9 PM	2	6.1×10^{-8}	ND	12.3
14/10/2013	9 PM-12 PM	3	1.4×10^{-7}	ND	20.7
29/10/2013	5 AM-8 AM	4	3.6×10^{-7}	$1.7\pm0.2 \times 10^{-7}$	52.8
29/10/2013	8 AM-12 AM	5	1.1×10^{-7}	ND	15.9
05/11/2013	2 PM-4 PM	6	8.4×10^{-8}	ND	13.1
05/11/2013	4 PM-7 PM	7	2.6×10^{-7}	ND	25.8
05/11/2013	7 PM-9 PM	8	1.6×10^{-8}	$9.4\pm0.5 \times 10^{-8}$	2.8
05/11/2013	9 PM-12 PM	9	1.6×10^{-7}	ND	15.3
06/11/2013	7 AM-10 AM	10	2.5×10^{-7}	ND	20.6
06/11/2013	10 AM-12AM	11	1.8×10^{-7}	ND	21.3
22/03/2014	7 AM-11 AM	12	1.1×10^{-7}	$2.7\pm0.5 \times 10^{-8}$	15.5
22/03/2014	11 AM-2 PM	13	1.0×10^{-7}	ND	14.0
25/03/2014	11 AM-1 PM	14	2.8×10^{-7}	ND	22.2
25/03/2014	1 PM-3 PM	15	3.9×10^{-7}	$1.6\pm0.5 \times 10^{-8}$	25.5
25/03/2014	7 PM-9 PM	16	4.4×10^{-7}	$1.5\pm0.5 \times 10^{-8}$	22.2
26/03/2014	8 AM-9 AM	17	1.1×10^{-7}	ND	27.9
26/03/2014	9 AM-11 AM	18	1.2×10^{-7}	ND	15.3
01/04/2014	8 PM-10 PM	19	1.1×10^{-7}	ND	7.7
01/04/2014	10 PM-12 PM	20	1.1×10^{-7}	ND	10.0
01/04/2014	1 PM-4 AM	21	1.2×10^{-7}	ND	9.6
01/04/2014	4 AM-7 AM	22	9.3×10^{-8}	ND	10.8
01/04/2014	7 AM-10 AM	23	1.3×10^{-7}	ND	11.7

Table 1: TRP-like concentrations and emission intensities of HULIS taken normalizing the Raman signal (350 nm) at 500 A.U. ND: quantification not determined because the signal was lower than the detection limit of 1 nM. * the value was estimated considering the fluorescence signal of pure TRP solution

The TRP signal in pure water is reported in Figure SM1, where two EEM peaks are present at $\lambda_{ex}/\lambda_{em}$ 225/360 nm and $\lambda_{ex}/\lambda_{em}$ 275/360 nm.

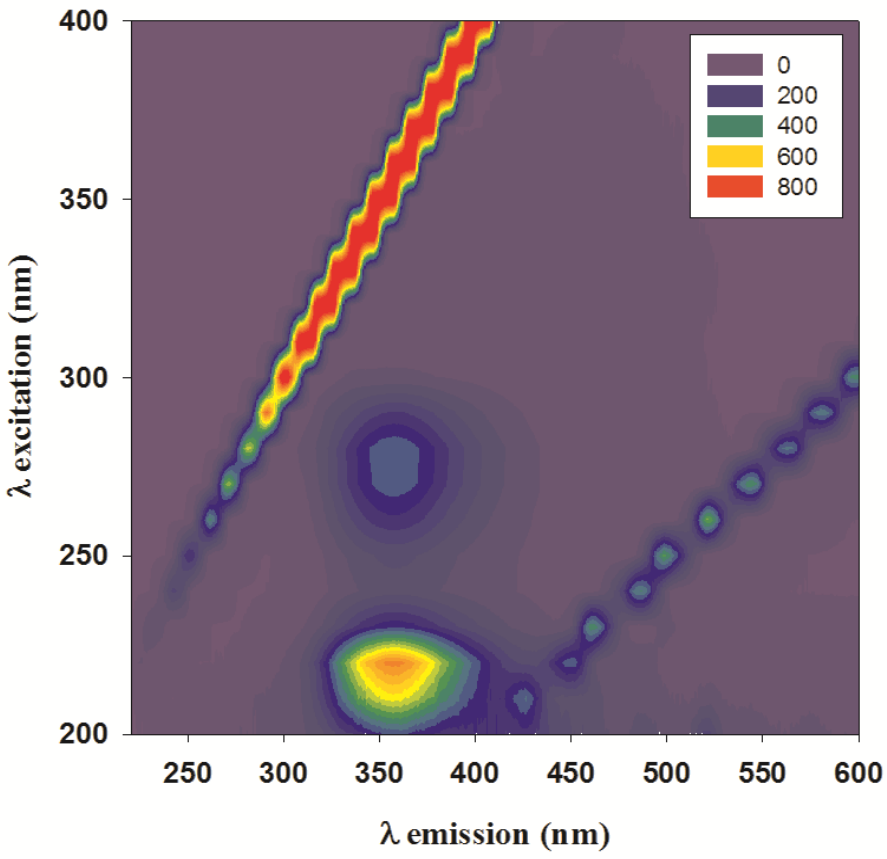

Figure SM1**:** 3D fluorescence excitation-emission matrix (as contour plot) of 10µM tryptophan M in milli-Q water. Fluorescence intensity is scaled from 0 to 800 intensity units. The linear feature (in red) is the Raman signal.

Tryptophan-like substances are detected in our samples from the signal intensity at λ_{ex} = 225 nm and λ_{em} = 330 nm (see Table 1). The fluorescence signal is normalized for the Raman intensity peak at 350 nm, and the concentration is calculated with the calibration reported in Figure SM2.

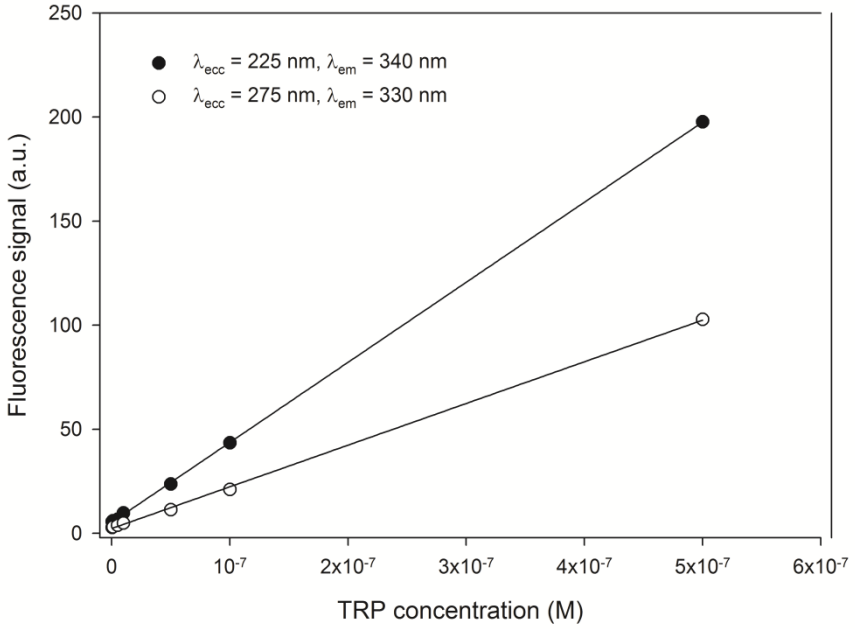

Figure SM2: Dependence of the intensity of fluorescence signal at $\lambda_{ex}/\lambda_{em}$ 225/340 and $\lambda_{ex}/\lambda_{em}$ 275/330 on TRP concentration. Lines show linear fit of data and 95% confidence range.

TRYLIS signals in the cloud aqueous phase present a blue-shift emission as reported when amino acids are combined. Fluorescence in the natural environment may be different to that observed in the laboratory under controlled conditions using pure amino acid solutions. Protein fluorescence resembles that of amino acids, as observed by Mayer et al. [275]. Most of the intrinsic fluorescence emission is due to the excitation of TRP residues (quantum yield of fluorescence of 0.20), with some emission due to tyrosine (TYR, with a fluorescence quantum yield of 0.14) or phenylalanine (PHE, with a fluorescence quantum yield of 0.04). TRP fluorescence emission is dominant over the weaker signals of TYR and PHE. The signal of TRP is influenced by the proximity of other amino acid residues; the signal could be shifted or quenched, especially by aspartate (ASP) or glutamate (GLU) residues [276]. Many authors found a blue shift to shorter emission wavelengths due to differences in the behaviour of amino acids in the different microenvironments present within proteins. Determann and co-workers [277] detect TRP and TRYLIS in seawater with $\lambda_{ex}/\lambda_{em}$ 230/350 nm, and Hudson and co-workers [278] show that there are two signals with the first one at λ_{ex} 225–237 nm and λ_{em} 340–381 nm and the less intense second signal at $\lambda_{ex}/\lambda_{em}$ 275/310 nm.

Many compounds could present a fluorescent signal with excitation at λ_{ex} 225 nm, and the concentration could be overestimated. For this reason, TRP is detected and quantified in EEM from the signal intensity at $\lambda_{ex}/\lambda_{em}$ 275/330 nm. The concentration is calculated with the

calibration reported in Figure SM2. The average concentration of TRP is 1.7 ± 1.1 × 10^{-7} M. The EEM method is not able to distinguish between free and combined TRP, so the reported concentration values correspond to the total concentration of TRP. We quantified free TRP by UPLC-FLR, and the data are shown in Table 1. The limit of detection (LOD), based on the signal/noise ratio of the instrument, allows the determination of concentrations up to 5 × 10^{-9} M. TRP is not detected in all of the samples; however, when TRP is detected, the average concentration is 5.8 ± 6.2 × 10^{-8} M. Considering that the concentration of the sum of free and combined TRP is estimated to be approximately 1.7 × 10^{-7} M, free TRP represents less than 37% of the total TRP in cloud water.

8.3.2 TRP photoreactivity

Different irradiation experiments using 10 µM TRP solutions were performed in Milli-Q and synthetic cloud water doped with H_2O_2 (used as photochemical source of hydroxyl radicals) in order to investigate the photoreactivity and fate of TRP. Under direct photolysis, TRP undergoes slow degradation, with up to 5% disappearance after 4 h of irradiation, and the polychromatic quantum yield between 290 and 350 nm ($\Phi^{TRP}_{290-340\,nm}$) is estimated to be 8.37 × 10^{-4}.

In the presence of different H_2O_2 concentrations (100 µM, 1 mM and 10 mM), TRP degradation rates increase from 1.29 × 10^{-11} M s^{-1} in pure water to 4.32 × 10^{-10} M s^{-1} in the presence of H_2O_2 (10 mM) corresponding to a hydroxyl radical formation rate of $R^{f}_{HO^{\cdot}}$ = 2.78 ± 0.01 × 10^{-8} M s^{-1} (see Figure SM2). Under our experimental conditions, a fraction of the photogenerated hydroxyl radicals also reacts with the source (H_2O_2). It is then possible to quantify the fraction of hydroxyl radicals reacting with TRP for each experimental condition considering the initial concentration of H_2O_2 in the solution and the related second order rate constants with HO$^{\bullet}$ ($k_{HO^{\cdot},H_2O_2}$= 2.7 × 10^{7} M^{-1} s^{-1}) [76].

SM: HO$^{\bullet}$ formation rate quantification.

The TRP degradation in the presence of hydroxyl radical photochemical sources (S) can be estimated to be the sum of contributions of direct photolysis ($R^{d}_{TRP,h\nu}$) and hydroxyl radical mediated degradation ($R^{d}_{TRP,HO^{\cdot}}$):

$$R^{d}_{TRP} = R^{d}_{TRP,HO^{\cdot}} + R^{d}_{TRP,h\nu}$$

Equation 1 SM.

Regarding the chemical reactions, the source can absorb the radiation leading to the formation of hydroxyl radical (R1) that can reacts with TRP (R2) and the source (R3):

R1) S + hν → HO$^{\bullet}$ $R^{f}_{HO^{\cdot}}$ (M s^{-1})

R2) HO$^{\bullet}$ + TRP → products$_1$ $k_{TRP,HO^{\cdot}}$=1.3×10^{10} M^{-1} s^{-1} [76]

R3) $HO^{\bullet}$ + S → $products_2$ $k_{S,HO^{\cdot}}$

In the presence of a high scavenger concentration, we can argue that $R_{HO^{\cdot}}^{f}$ can be estimated to be equal to the R_{TRP}^{d} .

TRP degradation can be quantitatively attributed to the hydroxyl radical as shown in Figure 3, where a linear correlation between R_{TRP}^{d} and the hydroxyl radical formed (making the radicals available to react with TRP) is found.

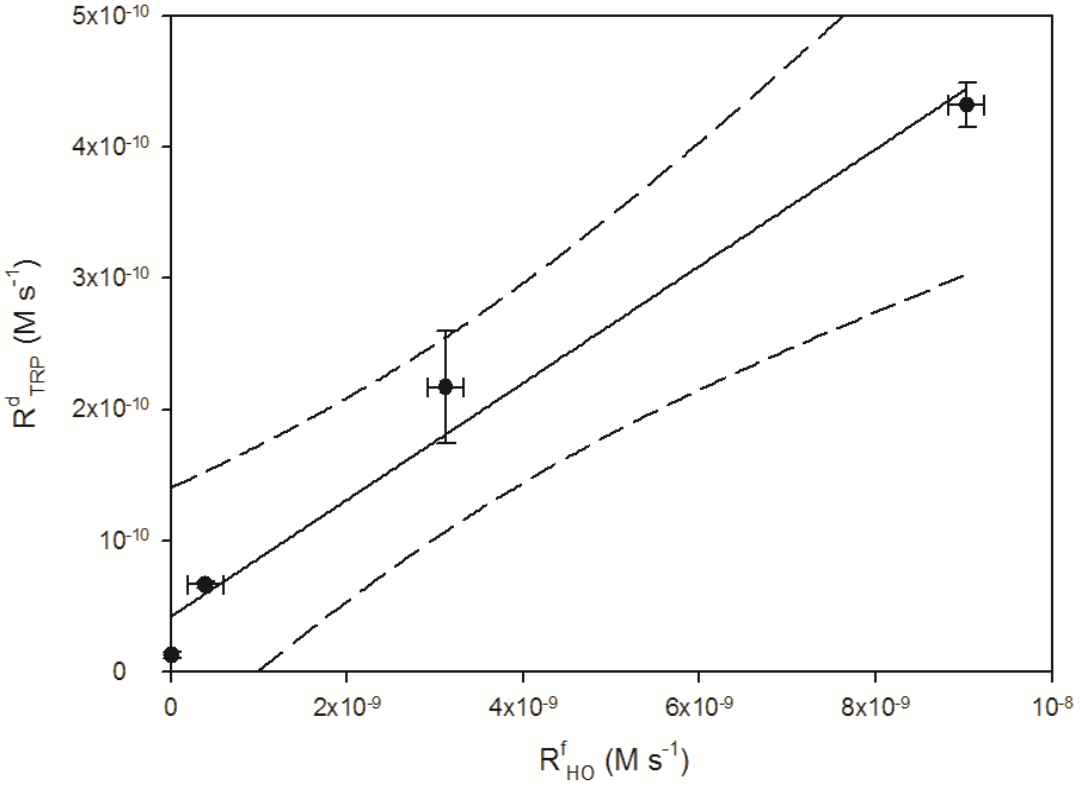

Figure 3: Correlation between the initial transformation rate of TRP (R_{TRP}^{d}, M s^{-1}) and the formation rate of hydroxyl radicals ($R_{HO^{\cdot}}^{f}$, M s^{-1}). The experiment was performed using an initial TRP concentration of 10 µM and varying the H_2O_2 concentration between 0 and 10 mM. The error bars represent the 3σ based on the linear fit of experimental data, and dashed lines denote the 95% confidence of the linear fit.

In order to better understand the behaviour of TRP in cloud water, synthetic water samples are prepared on the basis of the concentrations of anions found in real cloud water [273] (see Table SM1). To maintain the same ratio between TRP and the inorganic compounds, the average concentration of anions is multiplied by a factor 10.

Figure 4 reports the kinetic profiles for 10 µM TRP in the presence of Milli-Q and synthetic cloud water samples doped with 100 µM of H_2O_2. In the oceanic and continental synthetic water samples, TRP degradation is increased by approximately 3.5 and 10 times, respectively, compared to the value with an initial concentration of 100 µM H_2O_2 in pure water. This trend

can be explained by considering the presence of nitrates (NO_3^-) and nitrites (NO_2^-) that provide an additional source of $HO^\bullet$ [273].

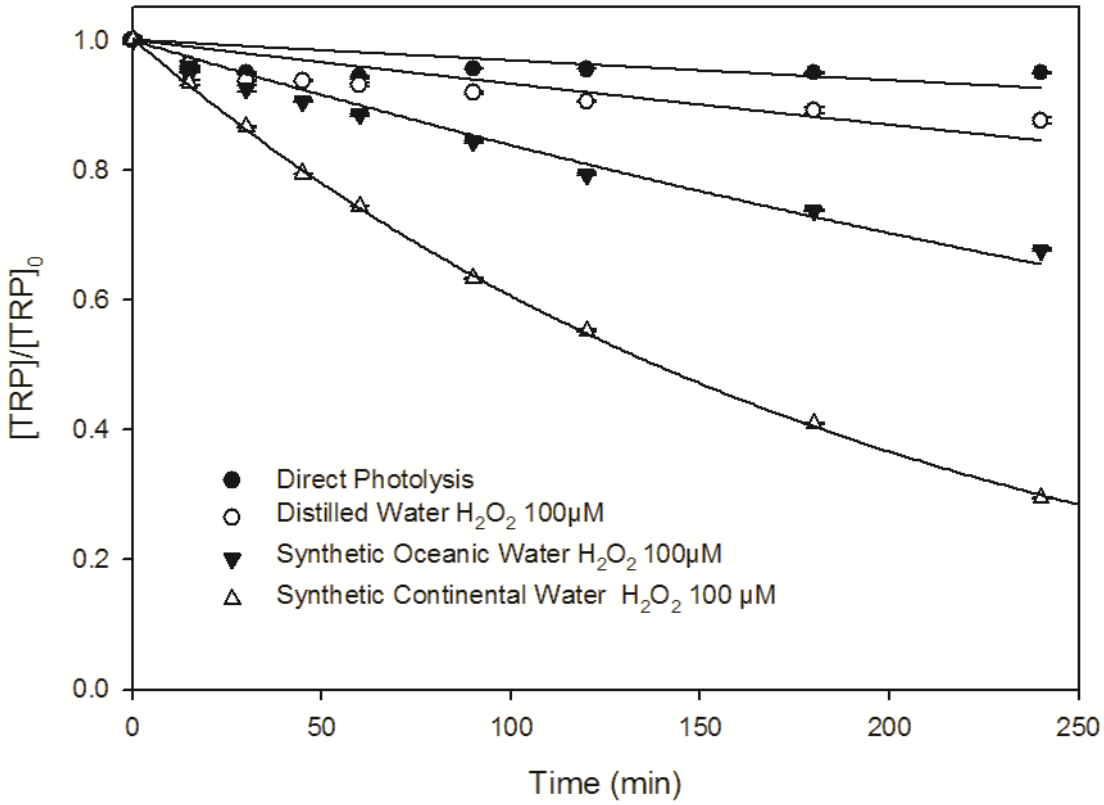

Figure 4: Irradiation time-dependent concentration of TRP (10 µM) under polychromatic irradiation in the presence of H_2O_2 (100 µM) in distilled water or in synthetic cloud water mimicking the continental or oceanic origin scenario. The pH was set to 4.5 for the continental and 5.6 for the marine synthetic water samples, and the temperature was 288 ± 3 K.

8.3.3 Transformation mechanism

TRP (10 µM) is irradiated in the presence of 1 and 10 mM hydrogen peroxide. Irradiated solutions are analysed by Ion Chromatography for quantification of the carboxylic acid concentrations and by HPLC-fluorescence analysis for estimation of the fate of TRP (Figure 5). After 4 h of irradiation and with 1 mM H_2O_2, TRP disappearance leads to the formation of 0.74 µM acetate and 0.37 µM formate. In the presence of 10 mM hydrogen peroxide, a complete disappearance of TRP is reported, leading to the formation of 2.0 µM acetate and formate (Figure 5). After 4 h of irradiation, acetate and formate concentrations represent less than 10% of the initial carbon concentration (mgC L^{-1}), and thus the carbon gap indicates the formation of other organic compounds.

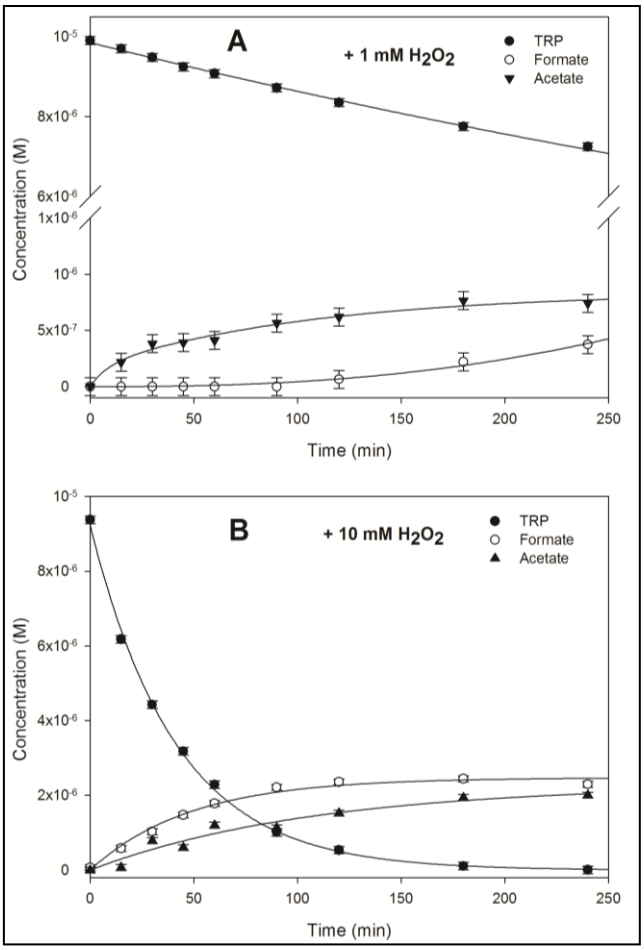

Figure 5: Disappearance of TRP (10 µM) in the presence of H_2O_2 1 mM (**A**) and 10 mM (**B**) and the formation of formate and acetate under polychromatic irradiation in water at a pH of approximately 5.5 and T = 288 ± 3 K.

A plausible interpretation of the photochemical and $HO^{\bullet}$-induced transformation of TRP is reported in Figure 6. TRP can undergo the following two different transformation pathways: hydroxyl radical addition (*i* and *ii*) and hydrogen abstraction (*iii*). Hydroxyl radical addition (*i*) can lead to the formation of mono- and di-hydroxylate derivatives detected by LC-MS at $[M+H]^+$ = 221 m/z and at $[M+H]^+$ = 237 m/z, respectively. The hydroxylation of tryptophan occurs in different positions of the molecule yielding several possible hydroxytryptophan isomers. Unfortunately, in this case mass spectrometry does not allow understanding of which position on the aromatic ring the hydroxyl functional group is located [279].

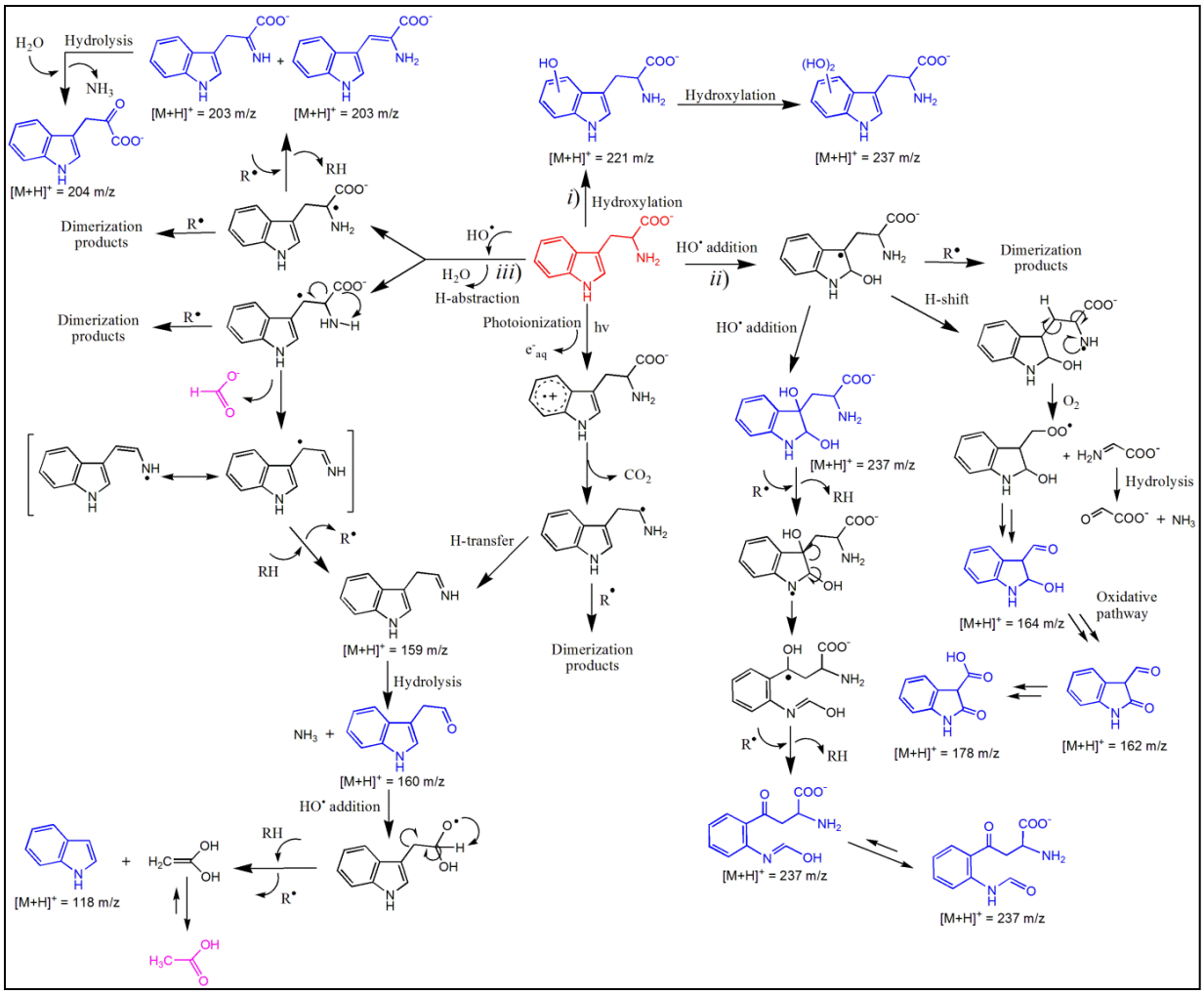

Figure 6: Suggested transformation mechanism of TRP (red) in aqueous solution. In blue are the chemical structures proposed for products detected by MS-ESI, and in violet are the carboxylic acids detected by ion chromatography.

The addition of HO$^{\bullet}$ (*ii*) could take place on the pyrrolic ring, and the oxidative opening of the five-membered ring can lead to *N*-formylkynurenine ([M+H]$^+$ = 237 m/z). The oxidative opening of the pyrrolic ring has been previously observed for other indole derivatives [280]. Formation of *N*-formylkynurenine from TRP oxidation has been previously reported [279]. The reactivity of molecular oxygen, after HO$^{\bullet}$ addition, can occur as previously suggested for several amino acids [255] and could lead to the formation of 2-hydroxyindoline-3-carbaldehyde ([M+H]$^+$ = 164 m/z). This product could undergo further oxidation to form 2-oxoindoline-3-carbaldehyde and 2-oxoindoline-3-carboxylic acid detected by MS at [M+H]$^+$ = 162 m/z and [M+H]$^+$ = 178 m/z, respectively [281].

Hydrogen abstraction (pathway *iii*) can take place on the α-carbon, and the generated radical could be reduced to an unsaturated compound with a double bond between carbons in the α and β positions. The chemical structures of these compounds have been previously proposed [279]. The radical at the α-carbon could also undergo oxidative deamination (through imine) and

produce a ketoacid ($[M+H]^+$ = 204 m/z) [255]. The hydrogen abstraction could also take place at the β-carbon, leading to the formation of formic acid and a resonance-stabilized radical intermediate; this intermediate could lead to an imine by H-transfer. The imine can be easily hydrolysed in water to form an aldehyde detected by MS at $[M+H]^+$ = 160 m/z. The further oxidation of the aldehyde by a hydroxyl radical could lead to fragmentation of the carbon chain with the production of acetic acid and formation of indole detected by ion chromatography and mass spectrometry, respectively.

The formation of carboxylic acids by the photo-oxidation of amino acids has also been suggested by Milne and Zika [255]. Tryptophan can absorb UV-light, and therefore, it can undergo direct photolysis. We have shown that the photolysis process in the presence and absence of hydrogen peroxide leads to the formation of the same products but with a prevalence of hydroxylated products in the case of irradiation in the presence of hydrogen peroxide. In the absence of photogenerated hydroxyl radicals, TRP could undergo photoionization, as reported in the literature for TRP and other indole derivatives [271,282], leading to a radical intermediate. The decarboxylation of this intermediate followed by H-transfer could produce the same imine produced in presence of $HO^{\bullet}$ [282]. The radicals produced during TRP irradiation could lead to a radical chain reaction with the formation of oxidized products and small carboxylic acids, as observed with hydrogen peroxide.

High molecular weight products are also detected at $[M+H]^+$ = 332 m/z and 334 m/z, with the ion at 334 m/z most likely being an adduct of tryptophan with 3-methyl indole. The ion at $[M+H]^+$ = 332 m/z corresponds to the reduced form of this adduct with a double bond between the α and β carbons of the tryptophan molecule [279]. Moreover, the product with a mass of $[M+H]^+$ = 409 m/z can be attributed to the dimer of TRP.

8.3.4 Fluorescence spectra of irradiated solutions

Figure 7 reports the EEM spectra of a 10 µM TRP solution before (Figure 7A) and after 4 h of irradiation in the presence of 100 µM H_2O_2 (Figure 7B). In the presence of H_2O_2 under irradiation, the intensity of the TRP signal decreases, while another signal appears at λ_{ex} 330 nm and λ_{em} 425 nm (see the difference between 7B and 7A in Figure 7).

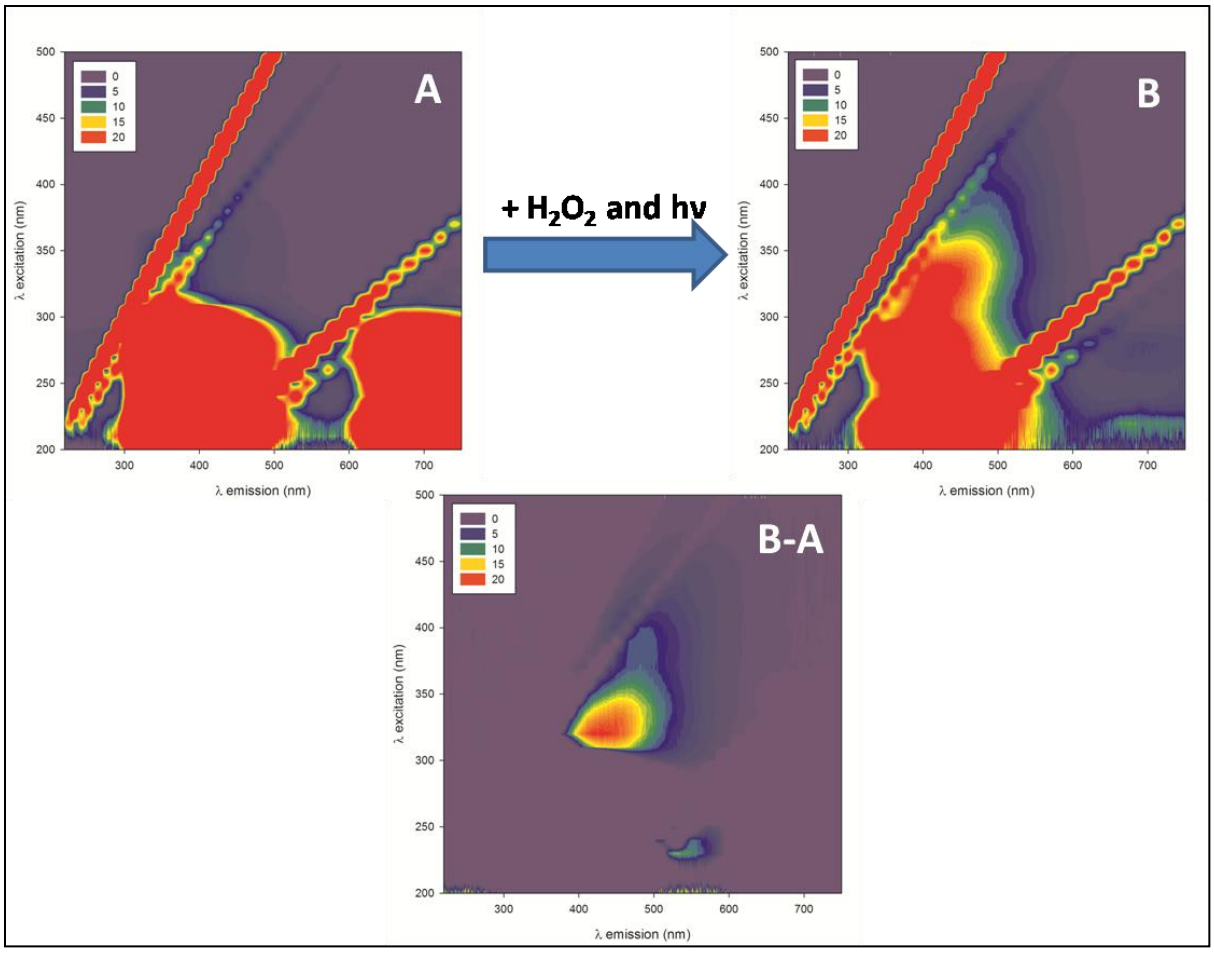

Figure 7: EEM (as a contour plot) of 10 µM TRP (**A**) and an irradiated solution for 4 hours in the presence of 100 µM H_2O_2 (**B**). The difference between the two EEM normalized for the TRP concentration is reported as **B**-**A**.

This signal is classified by Coble [160] as the fluorescence signal of HUmic LIke Substances. Domingues et al. [279] show for the first time that the oxidation of TRP leads to the formation of compounds at higher molecular weights, as well as their hydroxylation products. The same fluorescent signal was previously reported under UV irradiation using a mM level of TRP in aqueous solution [241]. It could not be excluded that the fluorescence signal at λ_{ex} = 330 nm and λ_{em} = 425 nm is due to these species, for which the molecular weight and oxidation could be compared to the spectroscopic signature of HULIS or FULIS. Under direct photolysis (Figure SM3), no signal corresponding to HULIS formation is detected.

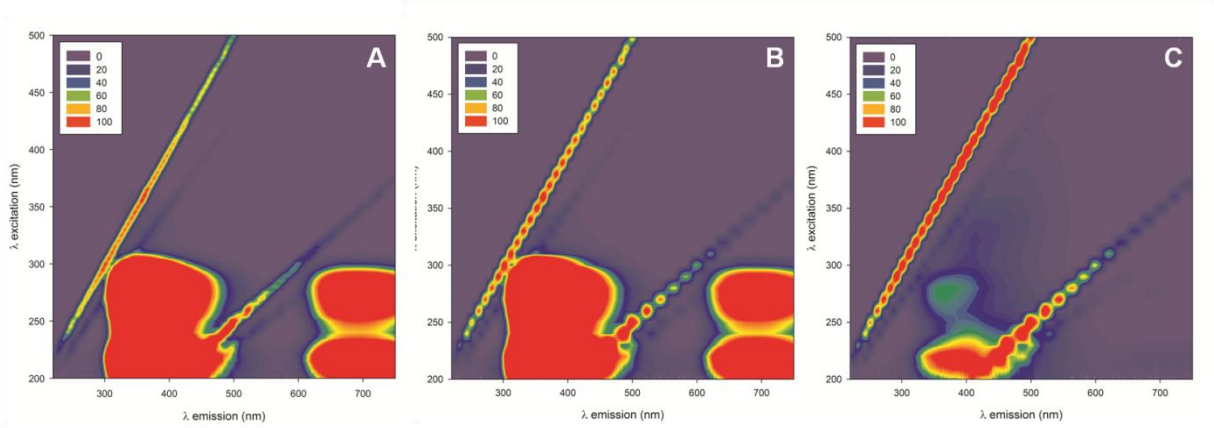

Figure SM3**:** Excitation Emission Matrix of TRP 10 µM (A), of TRP 10 µM irradiated for 4h (B) and of TRP 10 µM irradiated for 4h in the presence of H_2O_2 100 µM (C).

8.4 Atmospheric Relevance and Conclusions

TRP is found in cloud water from oceanic and continental origin, and its concentration is estimated to be on the order of 10^{-7} to 10^{-8} M. Considering the second order rate constant between TRP and HO$^\bullet$ ($k_{HO^\cdot,TRP}$) of 1.3 × 10^{10} M^{-1} s^{-1} [76], we can compare the hydroxyl radical scavenging ability of TRP with those of other relevant short-chain carboxylic acids, such as acetic, oxalic and succinic acids, that are generally found in concentrations of a few micromolar in cloud water. This value can be correlated to the fraction of HO$^\bullet$ scavenged by DOC (Dissolved Organic Matter), considering the $k_{HO^\cdot,DOC}$ of 3.8 × 10^8 L $molC^{-1}$ s^{-1} [103]. The HO$^\bullet$ inhibition ($I_{HO^\cdot}$, %) for TRP and selected carboxylic acids can be estimated for each cloud water sample using Equation 3:

$$I_{HO^\cdot}\,(\%) = \frac{[A] \times k_{HO^\cdot,A}}{[DOC] \times k_{HO^\cdot,DOC}} \times 100$$

Equation 3.

where [A] and $k_{HO^\cdot,A}$ are the concentration and second order rate constant with HO$^\bullet$ of the considered species *A*, and $[DOC] \times k_{HO^\cdot,DOC}$ is determined considering the DOC concentration of each sample (see Table SM2). In Figure 8, the contributions are reported considering a pH of 6.0 and the relative concentrations of the acidic and basic forms of species thereafter (see SM).

SM: HO$^\bullet$ inhibition.

The HO$^\bullet$ inhibition was determined considering the chemical species speciation calculated at a pH of 6.0 as reported in Table SM2 and following the second order rate constant with the hydroxyl radical.

The reaction rate constants with HO$^\bullet$ are 1.6 ×10^7 M^{-1} s^{-1} (acetic acid), 8.5 ×10^7 M^{-1} s^{-1} (acetate), 4.7×10^7 M^{-1} s^{-1} (oxalate mono-anion), 7.7 ×10^6 M^{-1} s^{-1} (oxalate di-anion), 1.1 ×10^8 M^{-1} s^{-1} (succinic acid), 5.0 ×10^8 M^{-1} s^{-1} (succinate mono-anion), 5.0 × 10^8 M^{-1} s^{-1} (succinate di-anion) , 3.8 × 10^8 L $molC^{-1}$ s^{-1} (DOC) [76,103,133,243].

Sample / Chemical	1	4	8	12	15	16
	Concentration (M)					
Acetic acid	4.35×10^{-7}	1.06×10^{-6}	4.66×10^{-7}	6.67×10^{-7}	6.99×10^{-7}	6.25×10^{-7}
Acetate	8.27×10^{-6}	2.01×10^{-5}	8.84×10^{-6}	1.27×10^{-5}	1.33×10^{-5}	1.19×10^{-5}
Oxalate (mono-anion)	9.00×10^{-8}	5.34×10^{-8}	3.40×10^{-8}	8.26×10^{-8}	6.62×10^{-8}	7.50×10^{-8}
Oxalate (di-anion)	4.41×10^{-6}	2.62×10^{-6}	1.67×10^{-6}	4.05×10^{-6}	3.24×10^{-6}	3.68×10^{-6}
Succinic acid	3.32×10^{-8}	4.18×10^{-8}	3.04×10^{-8}	1.40×10^{-9}	1.60×10^{-9}	1.90×10^{-9}
Succinate (mono-anion)	9.96×10^{-7}	1.25×10^{-6}	9.12×10^{-7}	4.20×10^{-8}	4.80×10^{-8}	5.70×10^{-8}
Succinate (di-anion)	2.29×10^{-6}	2.88×10^{-6}	2.10×10^{-6}	9.66×10^{-8}	1.10×10^{-7}	1.31×10^{-7}
TOC (mgC L^{-1})	5.0*	2.8	0.9	2.9	6.0	8.7

* Average value

Table SM2: Concentration for each acidic and basic form determined at a pH of 6.0. Values are reported by Bianco et al. [273].

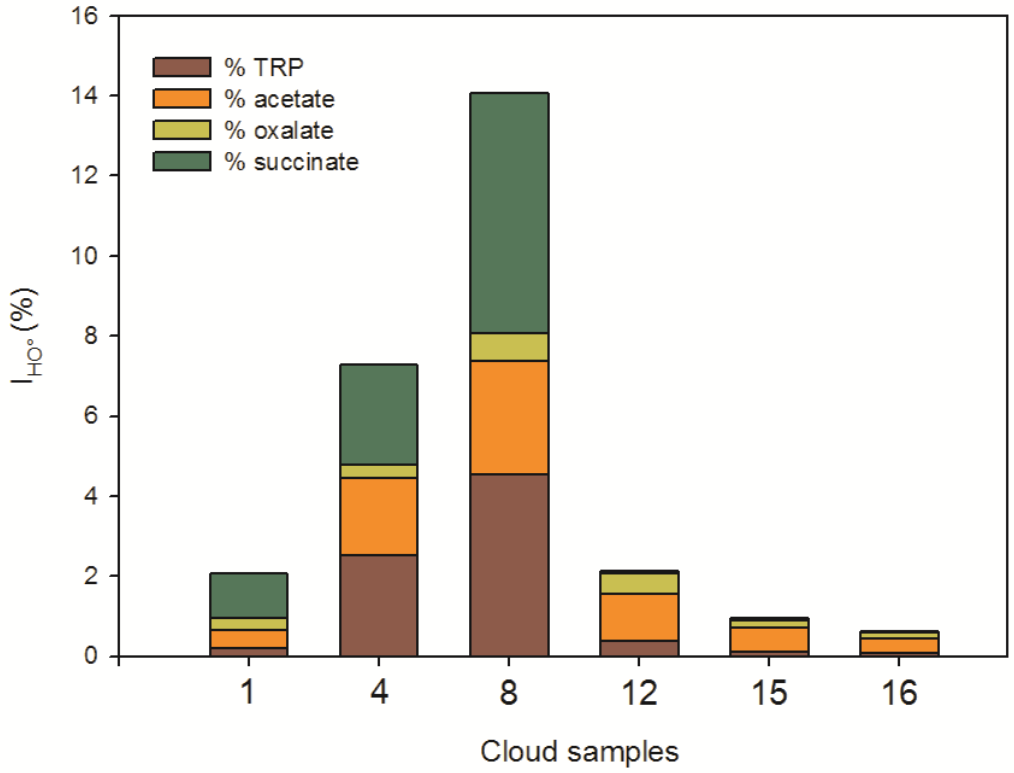

Figure 8: HO$^\bullet$ inhibition ($I_{HO^\cdot}$, %) by TRP, acetate, oxalate and succinate. Values are estimated considering a pH of 6.0. The relative concentration of each species is reported in the SM.

The contribution of TRP is between 0.07 and 0.38% for samples n° 1, 12, 15 and 16, while the concentrations for cloud water samples n° 4 and 8 rise up to 2.50 and 4.55%, respectively. Moreover, considering that TRP is only one of the essential amino acids, we can argue that investigating the concentrations of amino acids and their transformation is crucial to better assess the organic matter composition and hydroxyl radical reactivity in cloud water.

In this work, we demonstrated that TRP reactivity with hydroxyl radicals occurs following different reactivity pathways: *1*) formation of hydroxylated products, *2*) formation oligomeric compounds with similar fluorescence characteristics to those reported for HULIS, *3*) formation of decarboxylated compounds such as N-formylkynurenine and *4*) formation of short chain carboxylic acids. The phototransformation of TRP (direct and $HO^{\bullet}$-mediated) in cloud water can be considered to be a new source of short chain organic compounds and HULIS. These results highlight the importance of the complementary approach (*i.e.*, characterization and reactivity assessment) in improving the understanding of photochemical and hydroxyl radical-driven transformations in this medium. Certainly, the real impact of proteinogenic amino acid transformation depends on their concentrations and on the oxidative properties of the cloud aqueous phase.

Chapter 9

Motivation

During my PhD I had the opportunity to participate to the redaction of an invited divulgatif publication concerning the work of our research group that is composed by three main teams, working in chemistry/photochemistry, microbiology and physics/microphysics. The following chapter is an invited review in french that will be soon published on *Revue belge des questions scientifiques*. It shows how the reactivity in cloud water is influenced not only by chemical and photochemical processes but also by microbial activity, which has an impact on the organic composition and on radical activity as sinks of radicals and of their precursors.
For this review, my main contribution focuses on the description of the sampling site and of the analysis performed on cloud water. In addition I summarized our knowledge concerning cloud water oxidant capacity and composition.
In this chapter it is reported how microorganisms interact with chemical and photochemical processes and it is introduced a new research work on the combined impact of microorganisms and light on accurately characterized chemical compounds such as iron, carboxylic acids and amino acids.

This work clearly demonstrates that, for a better understanding of cloud water composition and reactivity, we need to investigate the interactions between chemical, photochemical, microphysical and microbiological processes and not only their contribution.

Les microorganismes: acteurs oubliés de la chimie des nuages. Compétition avec les voies de phototransformation

Anne-Marie DELORT, Angelica BIANCO et Marcello BRIGANTE

Université Clermont Auvergne, Université Blaise Pascal, Institut de Chimie de Clermont-Ferrand, BP 10448, F-63000 CLERMONT-FERRAND, FRANCE
A-Marie.Delort@univ-bpclermont.fr

Résumé

On sait depuis longtemps que la phase aqueuse des nuages est le siège de réactions radicalaires et notamment photochimiques de tels que le peroxyde d'hydrogène, les nitrates et les complexes de Fer. Ces précurseurs peuvent former des espèces très réactives telles que les radicaux hydroxyles, espèces chimiques considérées comme oxydants majeurs et transformer la matière organique dans la goutte d'eau nuageuse.
Cependant la découverte très récente de la présence de microorganismes métaboliquement actifs dans les nuages implique qu'ils sont capables d'utiliser des composés carbonés présents dans ce milieu comme nutriment ou interagir avec des espèces oxydantes. Les microorganismes peuvent donc être considérés comme des biocatalyseurs, acteurs potentiels de la chimie atmosphérique en compétition avec la chimie radicalaire.
Le travail de notre groupe au sein de l'Institut de Chimie de Clermont-Ferrand porte sur une meilleure compréhension et l'évaluation du rôle joué par les microorganismes dans le chimie nuageuse qui reste très complexe.

9.1. Introduction

9.1.1. La chimie des nuages

Les nuages ont toujours suscité la curiosité de l'homme et ont étés objet de définitions et classifications à partir d'Aristote (IV siècle a J.-C.). Cependant, l'étude scientifique au sens moderne a commencée seulement au début du XX siècle pour faire face à des situations de crise, comme les pluies acides, l'effet de serre ou le trou dans la couche d'ozone. Dans un premier temps, les efforts se sont concentrés principalement sur la photochimie et plus généralement la chimie en phase gazeuse. Pourtant, étant donné leur capacité à capter et dissoudre une grande partie des composés gazeux et particulaires, les gouttelettes des nuages

sont un des milieux les plus concentrés et réactifs de l'atmosphère et donc un lieu privilégié d'interaction entre les constituants les plus divers. La gouttelette de nuage peut être considérée comme un réacteur chimique extrêmement efficace où ont lieu des nombreuses réactions chimiques [270]. Toutefois, le rôle central des nuages dans la composition chimique de l'atmosphère planétaire est encore mal connu et reste une des principales incertitudes dans les modèles de prévision du climat et plus particulièrement de l'estimation du réchauffement climatique terrestre [283].

Dans ce contexte, les chercheurs de l'Institut de Chimie de Clermont-Ferrand (ICCF) travaillent depuis plus de 10 ans sur les phénomènes photochimiques et microbiologiques présents dans la phase aqueuse des nuages, le but étant d'évaluer les impacts sur la composition chimique et sur la capacité oxydante de l'atmosphère pour répondre aux problématiques liées plus généralement à la pollution atmosphérique et aux changements climatiques. Les études sont menées parallèlement en laboratoire mais aussi sur site à travers des prélèvements de la phase aqueuse des nuages effectués au sommet du puy de Dôme. Ce site, qui reste unique en France, est géré par l'Observatoire de Physique du Globe de Clermont-Ferrand (OPGC) et il a reçu le label Global GAW (Global Atmosphere Watch). (Figure 1)

Figure 1 : Le site de prélèvement d'eau nuageuse du puy de Dôme.

Photo P. Amato.

Depuis 2001, la phase aqueuse des nuages prélevée au sommet du puy de Dôme est analysée et caractérisée par la mesure de paramètres physico-chimiques (pH, conductivité, potentiel d'oxydoréduction) et de la concentration d'espèces inorganiques et organiques ainsi que du carbone organique total (TOC) [27]. Les prélèvements sont effectués avec un impacteur à nuage qui permet d'aspirer les gouttelettes de nuage qui sont collectées dans un réservoir, en collaboration avec les chercheurs du Laboratoire de Météorologie Physique.

L'eau du nuage présente souvent un caractère acide (> 3,8), mais les valeurs de pH peuvent aller jusqu'à 7,6. Parmi les composés inorganiques les plus abondants on peut citer les anions nitrate (NO_3^-), chlorure (Cl^-) et sulfate (SO_4^{2-}) et les cations ammonium (NH_4^+) et sodium (Na^+) dont les concentrations peuvent dépasser les 100 µM. Les composés organiques sont quantifiés par mesure de la concentration en carbone organique total (COT). La valeur de COT est typiquement de quelque mg de carbone par litre (mgC L^{-1}), mais peut atteindre 25 mgC L^{-1} pour des nuages très pollués. En termes de spéciation, les composés organiques majoritaires qui ont été identifiés sont des acides carboxyliques (acétique, formique, oxalique, succinique et malonique, du plus concentré au moins concentré) [27], et, à un degré moindre en termes de concentration, des aldéhydes (principalement la formaldéhyde) [284]. Cependant, il est important de noter que la contribution des acides carboxyliques et des aldéhydes représente seulement en moyenne environ 11% et un peu plus de 1% du carbone organique total respectivement. Le constat que plus de 80% du carbone organique n'est pas identifié montre la complexité de la phase aqueuse des nuages et donc la présence d'une multitude d'autres composés organiques non identifiés de manière récurrente. Tous ces composés qui peuvent conduire à la formation d'acides carboxyliques par oxydation, restent difficiles à identifier à cause de leur nombre important, des très faibles concentrations et des différentes techniques analytiques permettant leur détection.

La gouttelette d'eau de nuage est exposée à la radiation solaire qui peut induire des réactions photochimiques sur les composées organiques et inorganiques (photolyse) et donc conduire à leur transformation. La photolyse des nitrates (NO_3^-) [285] et du peroxyde d'hydrogène (H_2O_2) [286] mène, par exemple, à la formation du radical hydroxyle ($HO^\bullet$), qui est appelé le détergent de l'atmosphère à cause de sa forte réactivité. Le radical hydroxyle est majoritairement impliqué dans la photochimie de la phase aqueuse atmosphérique et peut donc être considéré comme le principal oxydant responsable de la transformation de la matière organique présente dans ce milieu [103,287].

9.1.2. Les microorganismes des nuages

Pendant très longtemps seuls des processus chimiques et physiques ont été considérés dans les nuages, ce n'est que récemment qu'il a été mis en évidence la présence de microorganismes (bactéries, champignons, levures, etc.) et leur rôle potentiel comme acteurs de la chimie atmosphérique [288]. Ces microorganismes sont aérosolisés à partir de la surface de la Terre par des mécanismes de «bubbling» (formation des embruns marins), l'action du vent (poussières) ou de la pluie (surface des feuilles). Comme toute particule de quelques microns, les

microorganismes peuvent condenser de l'eau à leur surface en tant que CCN (Cloud Condensation Nuclei) et être ainsi intégrés aux nuages sous forme de gouttelettes. Ils peuvent ensuite retourner sur Terre après un temps de résidence de 2 a 10 jours dans l'atmosphère notamment lors de précipitations [289]. La concentration microbienne dans les nuages est de l'ordre de 10^5 cellules mL^{-1} pour les bactéries et 10^4 cellules mL^{-1} pour les levures et champignons [290-292]. La biodiversité de cette communauté microbienne reste encore assez méconnue, ceci est principalement dû à la difficulté d'échantillonner des nuages et aussi au fait que la plupart des études sont basées sur des méthodes culturales. Les genres bactériens cultivables majeurs sont les genres *Pseudomonas* (γ-Proteobacteria), S*phingomonas* (α-Proteobacteria), *Streptomyces* (Actinobacteria), *Rhodococcus* (Actinobacteria), et *Bacillus* (Firmicutes), et pour les levures ce sont les genres *Dioszegia* (Basidimycota), *Udeniomyces* (Basidimycota) et *Crytococcus* (Basidimycota) [292-294]. Des analyses moléculaires récentes confirment la présence de ces genres tout en rapportant la présence d'autres microorganismes d'intérêt tels que des Cyanobacteria, et des classes bactériennes comme les *Methylobacteriacae* et *Oxalobacteraceae* [295-297].

Le milieu nuage semble *a priori* un environnement particulièrement hostile pour les microorganismes, d'une part parce que ce milieu est très instable d'un point de vue microphysique, d'autre part parce qu'il contient des molécules toxiques. Cependant les microorganismes ont développé des stratégies pour se protéger des stress atmosphériques dans les zones troposphériques: *i*) la présence de pigments (près de 50% des souches isolées des nuages sont pigmentées), [292] *ii*) la synthèse de polymères, dits EPS (ExoPolymeric Substances, [298] *iii*) la présence de spores (*Bacillus*, levures, champignons). Récemment, Joly et al. [299] ont mesuré le taux de survie de microorganismes modèles isolés de nuages, exposés à différents stress: la présence d'H_2O_2 et l'exposition aux rayons UV (stress oxydant); des cycles d'évaporation-condensation (choc osmotique), de congélation–décongélation (stress multiple combinant choc au froid/ stress oxydant/ choc osmotique). Les résultats montrent que le stress le plus important est celui du cycle congélation–décongélation et qu'il est souche dépendant, la réponse aux chocs osmotiques est relativement efficace, les oxydants et la lumière ont très peu d'effet sur les microorganismes.

La capacité des microorganismes à survivre dans le milieu nuage fait que ceux-ci sont métaboliquement actifs. Sattler et al. [300] ont été les premiers à montrer que les microorganismes pouvaient intégrer des molécules marquées au ^3H dans des gouttelettes de nuage en surfusion. Amato et al. [301] ont démontré que les microorganismes présents dans de l'eau de nuage incubée en laboratoire pouvaient se développer en utilisant des substrats

carbonés et azotés du milieu nuage. Cette activité métabolique a été largement confirmée en mesurant le contenu en ATP (Adenosine-5'-triphosphate) directement *in situ* dans de l'eau de nuage [290,292], l'ATP est considérée comme molécule référence de l'état énergétique des cellules. En utilisant une autre approche basée sur l'intégrité des membranes cellulaires, Hill et al. [302] ont démontré que 76% des bactéries étaient vivantes dans des eaux nuageuses.

Au final, le point le plus important de la découverte de la présence de microorganismes dans les nuages est qu'ils sont métaboliquement actifs. Ceci implique qu'ils sont capables d'utiliser des composés présents dans ce milieu comme nutriment, dans des conditions extrêmes (exposition aux oxydants, aux UV, aux basses températures, etc…). Les microorganismes peuvent donc être considérés comme des biocatalyseurs, acteurs potentiels de la chimie atmosphérique en compétition avec la chimie radicalaire (et notamment la photochimie). Notre équipe a joué un rôle pionnier dans cette découverte et dans l'étude de la contribution des microorganismes à la chimie nuageuse.

9.2. Le nuage, siège de transformations chimiques et microbiologiques

Au sein de la phase aqueuse des nuages de nombreuses interactions existent entre oxydants, microorganismes et matière organique. Ces interactions très complexes sont schématisés dans la Figure 2, elles conduisent au final à la transformation de la matière organique dans l'eau du nuage. Ainsi les espèces photo générées (radicaux, voie a) ainsi que les enzymes du métabolisme carboné des microorganismes (voie b) transforment directement les composés organiques. De plus les microorganismes peuvent interagir directement sur les sources de radicaux (H_2O_2 ou Fer, voie c) et agir indirectement sur la transformation de la matière organique.

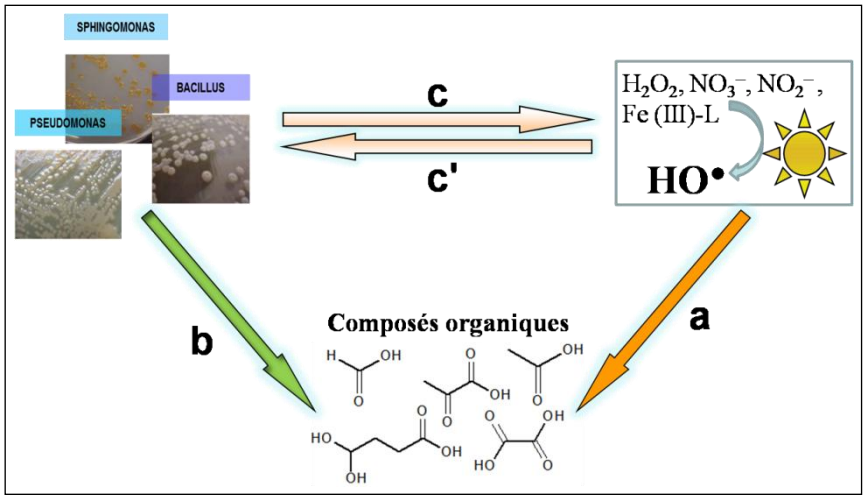

Figure 2: Schéma des interactions microorganismes / espèces oxydantes / composés organiques **a** : voies photochimiques et radicalaires ; **b** : métabolisme du carbone ; **c** et **c'** : interactions oxydants / microorganismes.

9.2.1. Voies photochimique et radicalaires

La première voie de réaction des composés dissous est l'interaction avec la lumière. Les rayons UV du spectre solaire sont les plus énergétiques et peuvent induire la scission des liaisons chimiques des molécules organiques. On appelle ce phénomène, photolyse. Un exemple est le cas du pyruvate, un acide carboxylique à 3 atomes de carbone, qui est aussi un des métabolites cellulaires. Il a été montré que l'acide pyruvique absorbe la lumière solaire et sa photolyse conduit à la formation de molécules de plus grande taille ou à sa fragmentation en molécules plus petites telles que l'acide lactique et l'acide acétique [303,304].

La lumière peut aussi induire la transformation de la matière organique par voie indirecte. En effet, la radiation lumineuse peut agir *via* la photolyse de précurseurs comme le peroxyde d'hydrogène (H_2O_2) ou les ions nitrate (NO_3^-) et nitrite (NO_2^-), la formation d'espèces très oxydantes comme le radical hydroxyle ($HO^\bullet$) (voir réactions R1, R2 et R3) [287]. De plus, la photolyse des complexes de Fer(III) (Fe^{III}-L) conduit à la formation de Fe^{2+} (R4) qui réagissant avec le peroxyde d'hydrogène (réaction de Fenton), est source de radicaux hydroxyles (R5) [97]. Ces processus sont très importants pour les composés organiques qui n'absorbent pas la radiation solaire. La transformation de la matière organique dans la gouttelette est fortement reliée à la quantité de ce radical qui, à son tour, dépend de la concentration des sources et de l'intensité de la radiation solaire. Un des travaux réalisés par notre équipe a porté à la quantification de la vitesse de formation du radical hydroxyle à partir des sources chimiques présentes dans l'eau du nuage sous irradiation solaire simulée, en utilisant une sonde chimique, l'acide téréphtalique (TA) qui permet de piéger $HO^\bullet$ pour le quantifier grâce à la spectroscopie de fluorescence.[189].

R1) $H_2O_2 \xrightarrow{h\nu} 2\,HO^\bullet$

R2) $NO_3^- + H^+ \xrightarrow{h\nu} {}^\bullet NO_2 + HO^\bullet$

R3) $NO_2^- + H^+ \xrightarrow{h\nu} {}^\bullet NO + HO^\bullet$

R4) $Fe^{III} - L \xrightarrow{h\nu} Fe^{II} + L_{ox}$

R5) $Fe^{II} + H_2O_2 \rightarrow Fe^{III} + HO^- + HO^\bullet$

Nous avons mesuré, par exemple, que les vitesses de formation des radicaux hydroxyles peuvent varier entre 0,1 et 6,5 × 10^{-10} M s^{-1}. Nous avons estimé la contribution du peroxyde d'hydrogène et des ions nitrate/nitrite dans la formation totale des radicaux hydroxyles, montrant que ces sources expliquent en grande partie la production totale des $HO^\bullet$. De plus, la contribution du fer est fortement liée à sa complexation avec la matière organique [287].

La transformation de plusieurs composés chimiques a été étudiée dans la phase aqueuse des nuages. Du fait de leur concentration la plus abondante parmi les nombreux composés chimiques identifiés dans ce milieu, les principaux efforts se sont focalisés sur le devenir des acides carboxyliques, eux-mêmes résultant vraisemblablement de l'oxydation par $HO^{\bullet}$ d'autres molécules plus grandes comme les hydrocarbures ou les alcools.

Plusieurs travaux se sont focalisés sur la compréhension des voies de formation/dégradation des acides carboxyliques à courte chaine [105,305,306]. Notre équipe à contribué a ces travaux avec l'étude du devenir de 13 acides carboxyliques en présence des radicaux hydroxyles dans le milieu nuageux. Nous avons constaté que la dégradation des acides carboxyliques conduit très majoritairement à la formation d'autres acides carboxyliques avec une chaîne carbonée plus courte (fragmentation) [189]. Ce processus de raccourcissement de chaîne est particulièrement observé avec les acides dicarboxyliques. Cependant il est important de noter que l'expérience avec l'acide formique (HCOOH) conduit à la transformation en CO_2 mais aussi à la formation d'acide oxalique (plus grand) qui représente 1% de l'acide formique dégradé. Même si cette voie ne représente qu'un faible pourcentage, cela suggère la possible formation de composés de plus haut poids moléculaire *via* des mécanismes de condensation radicalaire comme cela a été déjà montré dans différentes études) [307] (Figure 3).

En ce qui concerne les irradiations d'eau de nuage, elles ont conduit systématiquement à la formation d'acide acétique et d'acide formique qui sont les deux acides carboxyliques les plus abondants présents dans ce milieu, composés quasi-terminaux des voies d'oxydation de la matière organique. Cette formation est donc très probablement due à l'oxydation des composés organiques de plus haut poids moléculaire et plus généralement de la matière organique présente dans ce milieu qui reste encore peu caractérisée.

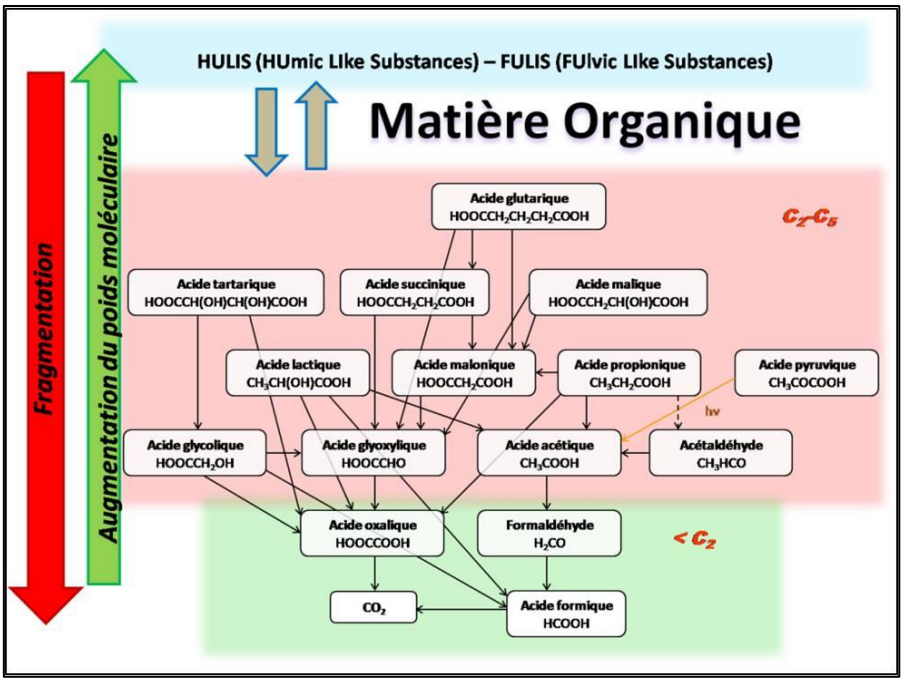

Figure 3: Représentation schématique des possibles voies de fragmentation (en acides carboxyliques et puis minéralisation en CO_2) et augmentation de la taille (jusqu'à la formation de substances type humiques, HULIS et FULIS) de la matière organique présente dans le nuage suite à la réaction avec les radicaux hydroxyles.

9.2.2. Métabolisme du carbone

Comme tout organisme vivant, les microorganismes tirent leur énergie en bio-transformant la matière organique, et plus particulièrement les composés carbonés, grâce à de très nombreuses voies métaboliques [308]. En ce qui concerne la chimie atmosphérique, encore peu de voies ont été explorées; elles se limitent aux voies des composés en C1 (méthanol, formaldéhyde), et aux voies impliquant des acides mono- ou di-carboxyliques à courte chaine.

La mise en évidence de l'implication de ces voies métaboliques s'est faite en construisant des microcosmes de plus en plus complexes pour mimer au plus près l'environnement nuageux. Trois grandes approches ont été utilisées :

- Incubation d'une souche microbienne pure isolée des nuages en présence d'un composé pur, dans un tampon phosphate.
- Incubation d'une souche microbienne pure isolée des nuages dans un milieu «nuage artificiel» contenant les principaux composés carbonés, azotés et inorganiques.
- Incubation d'échantillons «d'eau de nuage réel» contenant toute la biodiversité microbienne et complexité chimique.

Métabolisme des composés en C1

Comme le montre la Figure 4, le formaldéhyde est au centre du métabolisme des composés en C1, il est formé par oxydation du méthanol. Ce composé peut être considéré comme toxique et éliminé par la cellule par une voie dite de «dissimilation» conduisant à la formation de CO_2. Cette voie est soit directe *via* la formation de formiate, soit indirecte *via* le RuMP cycle qui redonne du ribulose-5P et du CO_2. Chez certains microorganismes le formaldéhyde est aussi une source de carbone et peut être intégré dans le métabolisme de la cellule par une voie «d'assimilation». Ainsi la voie du RuMP conduit à la production de frucose-6P qui entre dans la voie classique de la glycolyse et du métabolisme central. Alternativement, le formaldéhyde peut rentrer dans le cycle de la serine (acide aminé) relié au cycle de Krebs et des acides gras.

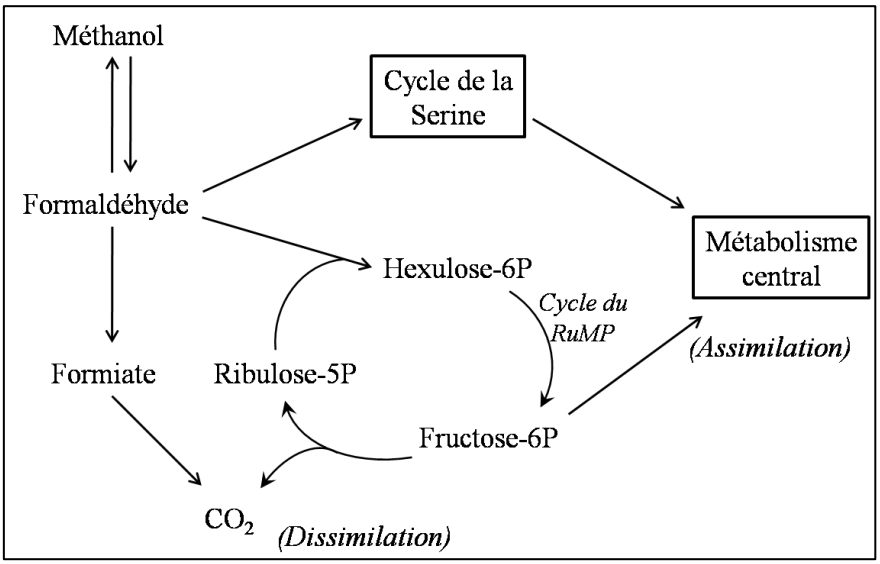

Figure 4: Métabolisme des composés en C1 (adapté de Schrader J. *et al*.)[309].

Il est à noter que contrairement aux voies radicalaires le formaldéhyde peut être réduit en méthanol et peut servir à construire des molécules à plus haut poids moléculaire.

Amato et al.[301] ont réalisé un large screening de 60 souches (bactéries et levures) isolées d'eau de nuage au puy de Dôme (1465m) pour leur capacité à transformer le formaldéhyde et le méthanol. Ils ont montré que toutes dégradaient activement le formaldéhyde alors que la transformation du méthanol dépendait des souches ($Gram^-$, $Gram^+$ et levures). Une étude approfondie a été menée sur une de ces souches, *Bacillus* sp 3B6, en utilisant la spectroscopie RMN du ^{13}C *in vivo* [310]. Cette souche peut transformer le formaldéhyde en méthanol, en formiate et CO_2 mais peut aussi utiliser la voie de la serine et conduire à la production de glycérol, de 1,2- et 1,3-propanediol.

Biodégradation d'acides mono- ou di-carboxyliques à courte chaine

La voie la plus connue de la dégradation des acides carboxyliques est le cycle de Krebs encore appelé TCA (TriCarboxylic Acid) cycle. Ce cycle permet la transformation successive de l'acide acétique en acide citrique, puis succinique, fumarique et malique [311]. Ce cycle constitue le métabolisme central des microorganismes et est relié à de très nombreuses autres réactions. On peut citer le métabolisme de l'acide pyruvique, de l'acide glycolique, d'acide di-carboxyliques, la glycolyse, le métabolisme des acides aminés, etc…

Pour ce qui est des acides di-carboxyliques, l'équipe d'Aryia a montré que les acides succiniques, maloniques, glutariques, adipique, pimélique et piniques étaient dégradées efficacement par des souches fongiques isolées de l'atmosphère [312,313]. Notre équipe a également montré la dégradation de l'acide succinique par de très nombreuses souches isolées des nuages soit avec des souches pures soit dans l'eau réelle de nuage [185,301,314,315]. Ces deux groupes de recherche ont démontré que, dans leurs conditions, l'oxalate n'était pas dégradé.

Pour les acides mono-carboxyliques, Herlily et al. [316] furent les premiers à montrer la dégradation de l'acide formique et acétique dans l'eau de pluie. Amato et al.[301] ont pour leur part montré qu'un panel de 60 souches microbiennes isolées d'eau de nuage pouvait dégrader l'acide formique, acétique et lactique. Certains intermédiaires de dégradation ont été mis en évidence comme le pyruvate et le fumarate, montrant que le métabolisme microbien pouvait servir à la fois de puits mais aussi de source pour les composés carbonés de la phase aqueuse du nuage. D'autres expériences menées en microcosmes de plus en plus proches du milieu nuage ont confirmé le potentiel des microorganismes des nuages à dégrader l'acide formique et acétique [185,314,315]. Une étude très récente a également montré le potentiel d'une souche de *Shingomonas aerolata* aérosolisée dans un tunnel à intégrer de l'acide acétique dans son métabolisme [317]. Cette étude est intéressante car elle élargit la problématique du rôle des microorganismes dans la chimie atmosphérique en phase aqueuse à la chimie en phase gaz.

9.2.3. Interaction microorganismes / oxydants

Métabolisme du stress oxydant

Les microorganismes qui vivent dans les nuages sont de type aérobie, ils utilisent l'oxygène comme accepteur d'électrons lors de la respiration (Figure 5). En réalité l'oxygène qui diffuse à travers la membrane plasmique est très vite transformé en ion superoxyde qui est très toxique pour les cellules. Cette molécule est donc convertie de manière extrêmement efficace en H_2O_2 par la SOD (superoxyde dismutase), ensuite le peroxyde d'hydrogène est transformé

en oxygène et eau par des catalases [318]. En dehors de ces enzymes spécifiques (SOD et catalases) qui combattent la formation des radicaux intracellulaires, les cellules sont capables de synthétiser des molécules anti-oxydantes très puissantes qui sont des pièges à radicaux. Ce sont principalement des vitamines (acide ascorbique, β-tocophérol..), du gluthation ou des pigments (caroténoïdes) [319,320]. Comme déjà indiqué la majorité des microorganismes sont pigmentés dans l'atmosphère (50% dans les nuages et 80% dans l'air) [290,292,321,322]. L'ensemble de cette machinerie mise en place pour lutter contre les espèces réactives oxydantes (Reactive Oxygen Species en anglais, ROS), que sont H_2O_2, $HO_2^{\bullet}/O_2^{\bullet-}$, $HO^{\bullet}$ est appelé «métabolisme du stress oxydant». Ce métabolisme permet éviter des dommages cellulaires comme l'attaque des protéines, des lipides et des acides nucléiques, constituants clés de la cellule [323].

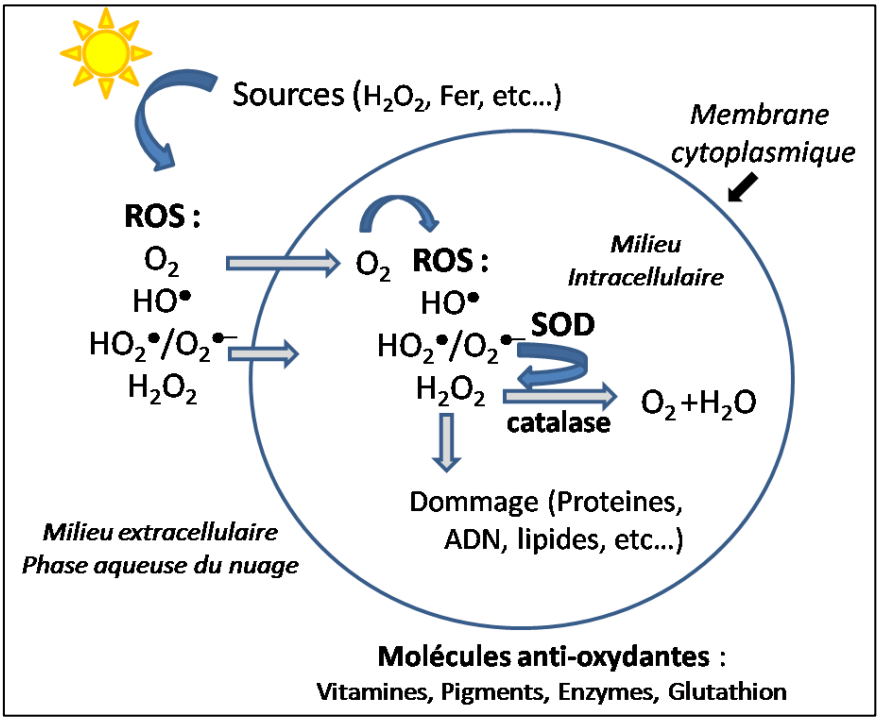

Figure 5: Metabolisme du stress oxydant. SOD : superoxyde dismutase ; ROS : reactive oxygen species.

On comprend alors que les microorganismes des nuages sont naturellement équipés pour résister aux ROS produits *via* des réactions chimiques atmosphériques: tout d'abord H_2O_2 qui peut diffuser dans la cellule et être dégradé par des catalases, ensuite les radicaux formés lors de réaction de Fenton et Photo-Fenton (voir section 2.1) qui pourront être neutralisés par la SOD ou des molécules anti-oxydantes (Figure 5).

Des expériences récentes menées dans notre laboratoire ont confirmé la très grande résistance des microorganismes de nuages à ces stress oxydants. Tout d'abord Joly et al (2015) ont montré que différentes souches modèles caractéristiques des genres majeurs de bactéries et de

levures pouvaient survivre même à une concentration aussi élevée que 1mM de H_2O_2 ; la concentration maximale de H_2O_2 dans les nuages au puy de Dôme est de l'ordre de quelques dizaines de 30 µM [324]. D'autre part Vaitinlingom et al.[185] ont montré que la flore endogène microbienne des nuages pouvait dégrader H_2O_2 présente dans l'eau de nuage. Dans ce même article, la mesure du rapport ATP/ADP, marqueur de l'énergétique cellulaire, reste inchangé en présence de radicaux, ce qui démontre que les microorganismes résistent à la présence de ces ROS.

Ces résultats sont très importants et novateurs car ils ont mis en lumière pour la première fois l'impact potentiel des microorganismes sur la capacité oxydante du nuage.

Interaction avec le Fer :

Comme expliqué précédemment, le fer joue un rôle important dans la chimie atmosphérique (voir section 2.1). Les réactions de Fenton qui impliquent le Fe^{2+} et H_2O_2 ainsi que la photolyse des complexes de Fer(III) sont considérés comme une source de radicaux. Actuellement seuls les complexes de Fer-oxalate sont considérés dans les modèles de chimie atmosphérique, cependant des études récentes de Bianco et al [287] suggèrent que la production de $HO^{\bullet}$ est surestimée par ce type de réactions. Se pose donc la question de la complexation du fer de la part de la matière organique dans les nuages. Dans l'océan comme dans l'eau de pluie la présence de sidérophores a été démontrée [325,326]. Les sidérophores sont des complexants très puissants du Fe(III) (log K>20), leur structures chimiques sont très variées mais ils possèdent des fonctions chantantes communes de type catéchol, hydroxamate ou carboxylates. Ces composés sont produits par les microorganismes, exportés hors de la cellule pour complexer le fer présent dans le milieu puis internalisés dans la cellule. Le fer est un élément essentiel de la vie des microorganismes car il intervient dans de nombreuses réactions d'oxydo-réduction et il est présent dans le site actif d'enzymes. Notre hypothèse est que les microorganismes présents dans les nuages pourraient produire des sidérophores et être donc en compétition avec l'oxalate pour complexer le fer. De plus les mécanismes de photolyse de ces complexes peuvent varier en fonctions du complexant organique (oxalate, sidérophores, etc…). Des expériences sont en cours pour valider cette hypothèse.

9.3. Compétition chimie radicalaire vs métabolisme microbien

Si la capacité des microorganismes à transformer des composés organiques ou à interagir avec des oxydants est maintenant acquise, le grand challenge est d'évaluer la contribution réelle de

ces réactions biologiques par rapport à la chimie radicalaire. Plusieurs stratégies ont été utilisées pour aborder cette compétition entre chimie radicalaire et métabolisme microbien:

Approche indirecte: cette première approche consiste à mesurer expérimentalement des vitesses de biodégradation de composés présents dans les nuages par des microorganismes (souche isolée ou population endogène) et de les comparer avec des vitesses théoriques calculées sur la base de la réactivité des principaux radicaux tels que les $HO^{\bullet}$ et $NO_3^{\bullet}$ sur ces mêmes composés.

Approche directe: cette deuxième approche vise à comparer les vitesses de biodégradation et de photodégradation de composés atmosphériques d'intérêt, mesurées expérimentalement dans des photo-bioréacteurs. Là encore souches pures ou population microbiennes complexes peuvent être étudiées dans des milieux nuages artificiels ou naturels.

9.3.1. Approche indirecte

En ce qui concerne les composés en C1, Husarova et al. [310] ont étudié la biodégradation du méthanol et du formaldéhyde par 4 souches isolées d'eau nuageuse au puy de Dôme. Les vitesses de biodégradation mesurées à 5°C (température moyenne du site de prélèvement) ont été comparées aux vitesses de transformation de ces mêmes composés par les radicaux $HO^{\bullet}$ et $NO_3^{\bullet}$. Ceci permet d'appréhender la contribution de l'activité microbienne pendant le jour où les deux types de radicaux sont présents et pendant la nuit où seul $NO_3^{\bullet}$ intervient. De plus deux scénarios ont été considérés, l'un où les nuages sont considérés comme pollués ($[NO_3^{\bullet}]$ élevée), l'autre comme non pollués ($[NO_3^{\bullet}]$ faible). Dans tous scénarios les radicaux $HO^{\bullet}$ sont les plus actifs pendant le jour. La nuit, l'activité des microorganismes domine sauf pour le méthanol en milieu pollué où les radicaux $NO_3^{\bullet}$ restent plus actifs.

Pour les acides dicarboxyliques (acides maloniques, succiniques, adipiques, pimeliques et pineliques), Aryia et al [312] ont montré que les vitesses de biodégradation par une souche fongique de *Geotrichum* sp isolée de l'air étaient du même ordre de grandeur que celles de transformation par $HO^{\bullet}$ mais beaucoup plus rapides (de 70 à 1000 fois) que les transformations induites par O_3 ou $HO_2^{\bullet}$.

Vaïtilingom et al [315] ont mené une étude exhaustive en considérant 17 souches isolées au puy de Dôme. Les incubations ont été réalisées dans des milieux artificiels mimant l'eau des nuages et contenant 4 acides organiques représentatifs (oxalate, succinate, acétate et formiate). En dehors de l'oxalate qui n'est pas dégradé biologiquement, les autres composés sont dégradés plus rapidement par les microorganismes que par les radicaux $HO^{\bullet}$ et $NO_3^{\bullet}$ pendant la nuit. Les microorganismes restent très compétitifs le jour lorsque les calculs sont

faits avec des concentrations en radicaux de 10^{-14} M (Figure 6A). Le même résultat est obtenu si on incube un échantillon de nuage réel contentant toute la biodiversité et complexité chimique (Figure 6B).

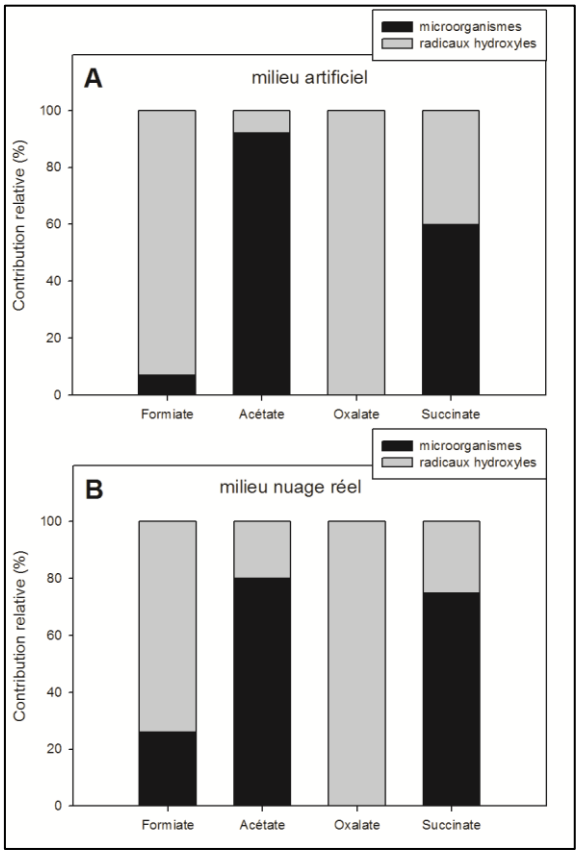

Figure 6: Contribution relative de l'activité microbienne (en noir) sur la dégradation d'acides organiques par rapport à l'action des radicaux HO• (gris clair). L'activité microbienne a été mesurée en laboratoire en milieu artificiel ou en milieu nuage réel. L'activité radicalaire a été calculée avec des concentrations de HO• de 10^{-14}M.

9.3.2. Approche directe

L'approche utilisée précédemment s'est révélée très utile pour comparer activités radicalaires et microbiennes, cependant elle est fortement dépendante de la concentration en radicaux utilisée dans les calculs. Or cette concentration est issue de calculs de modélisation ce qui conduit à des incertitudes extrêmes. Ainsi par exemple la concentration en HO• varie de 10^{-12} M à 10^{-16} M. L'alternative pertinente est donc de comparer directement des vitesses de dégradations biotiques et abiotiques mesurées dans les mêmes conditions expérimentales dans des photo-bioréacteurs.

Une première série d'expériences menées en nuage artificiel avec 17 souches microbiennes pures, avec ou sans lumière, ont confirmé les résultats obtenus par calcul décrits précédemment.[315]

Une autre expérience beaucoup plus complète a été réalisée avec 3 échantillons de nuages différents prélevés au sommet du puy de Dôme.[185] L'oxalate n'est dégradé qu'en présence de lumière, le formiate (c'est aussi vrai pour l'acétate et le succinate) sont surtout biodégradés par les cellules. Enfin le cas du formaldéhyde est intéressant puisqu'il est photo-produit alors qu'il est dégradé par les microorganismes. Dans cette même expérience les auteurs ont montré que les microorganismes dégradaient H_2O_2 de manière majoritaire la nuit (78%) et de manière substantielle le jour (18%).

9.4. Conclusion

La compréhension du rôle des microorganismes dans la chimie du nuage représente un défi majeur pour comprendre les voies de transformation dans ce milieu très complexe. Le double rôle de synergie et compétition avec les voies photochimiques reste un sujet encore très peu étudié, notre équipe est une des seules au monde à s'y consacrer. A l'avenir de nombreuses pistes sont à explorer: Tout d'abord la transformation d'autres composés organiques tels que les sucres ou les acides aminés doivent être étudiés, leur comportement photochimique est peu connu et ils sont de très bons substrats pour les microorganismes. Un autre aspect concerne la formation de molécules de plus haut poids moléculaires. Une activité scientifique importante s'est développée autour de la synthèse d'aérosols organiques secondaires (OAS) par voie radicalaire, les microorganismes peuvent aussi former des macromolécules ou des métabolites secondaires (sidérophores, biosurfactants, substances exopolymériques...). Enfin même si les études de photo et biotransformation de composés organiques ont montré que les microorganismes pouvaient être des acteurs efficaces de la chimie atmosphérique, les études réalisées, même en milieu nuage réel, restent limitées à des expériences en laboratoire. Seul des modèles numériques de chimie atmosphérique peuvent rendre compte de la complexité du système multiphasique du nuage intégrant de très nombreuses réactions et des transferts entre phase aqueuse -phase gazeuse. Ces modèles ne prennent pas en compte la composante biologique, notre équipe travaille en étroite collaboration avec le Laboratoire de Météorologie Physique qui développe actuellement cette nouvelle approche. Le développement de modèles plus performants devrait conduire à terme à une meilleure prévision du climat.

Conclusions and perspectives

In my PhD work the attention was firstly focused on hydroxyl radical photogeneration: hydroxyl radical formation rate and polychromatic quantum yield were estimated for clouds with different geographic origin and characterized by peculiar chemical composition and pH values. These two parameters were correlated with the concentrations of inorganic precursors such as hydrogen peroxide, nitrates, nitrites and iron (Fe^{2+}/Fe^{3+}) and the main result was that the photolysis of hydrogen peroxide is the predominant source of hydroxyl radical, while nitrates and nitrites have a secondary importance. Concerning the production of hydroxyl radical by iron chemistry and photochemistry, our results show that iron is a minor source in disagreement with literature data.

Experimental results were compared with modeled hydroxyl radical formation rates, calculated with the M2C2 model. This model can reproduce the order of magnitude of experimental values but some discrepancies appear in the case of high concentration of iron or hydrogen peroxide. For this reason, iron chemistry was not considered and the photolysis of hydrogen peroxide was determined experimentally. The modeled production rates of hydroxyl radical with the updated mechanism are closer to the experimental values, supporting the hypothesis that iron could be strongly complexed by organic ligands and it is less photoreactive in this form.

This study provides significant data on the oxidant capacity of cloud aqueous phase.

Subsequently, the attention was focused on the chemical and photochemical behavior of tartronic acid, a dicarboxylic acid, in cloud water. This work is still not finished but spectroscopic properties of this compound and direct and indirect photolysis were presented in the manuscript. Moreover, the second order rate constants of the three forms of tartronic acid with hydroxyl radical were determined experimentally by Laser Flash Photolysis. The results will be implemented in the M2C2 model to better understand the reactivity of C3 functionalized compounds in cloud aqueous phase.

Another crucial point of this thesis was the development of a chromatographic method with precolumn derivatization and fluorescence detection for the quantification of free amino acids at low concentration. 16 amino acids were detected and quantified in cloud water samples and their concentration ranges from few nM up to 2 µM. The average contribution of amino acids to the cloud water DOC was for the first time estimated and it is of 10%, with maximum value of 25%.

This result represents an important step in the characterization of cloud water composition, especially if we consider that up to now only 11% of the DOC was described as composed by carboxylic acids and aldehydes. Furthermore, amino acids contribution to the hydroxyl radical scavenge ranges from 10% up to 30% with an average value around 20%.

Tryptophan was found to be the most concentrated amino acid. It can also be detected, as the sum of free and combined form, by fluorescence spectroscopy (EEM, Excitation Emission Matrix) and, in the free form, by a chromatographic method coupled with fluorescence detection. Using these two methods, tryptophan and TRYLIS (TRYptophan LIke Substances) were detected in cloud water from oceanic and continental origin.

Tryptophan photoreactivity under sun simulated conditions was investigated in distilled water and in synthetic water samples mimicking cloud aqueous phase composition. Irradiated solutions were analyzed by ion chromatography, mass spectrometry and fluorescence spectroscopy and it was found that hydroxyl radical-mediated transformation leads to the generation of different functionalized and oxidized products, as well as small carboxylic acids, such as formate and acetate. In addition fluorescent signals of irradiated solutions indicate the formation of HULIS. This finding improve our comprehension of the reactivity of organic compounds in cloud water: in parallel to the oxidation and the diminution of molecular weight, reactions of formation of high weight molecular compounds by dimerization or aggregation processes have been demonstrated.

This is a crucial subject that needs to be deeply investigated to understand and predict the behavior of organic compounds in cloud water by atmospheric models.

In the last part of this manuscript, I have choosen to present an article that will be published in a divulgatif review: it describes how microorganisms, naturally present in cloud water, could impact cloud water oxidant capacity, acting as sinks of hydroxyls radicals but also as inhibitors of their formation. They could also impact carboxylic acids and amino acids concentration and speciation in function of their production and consumption.

This article indicates a perspective of the work presented: the interaction between microbiological activity and light need to be investigated, especially concerning hydroxyl radical formation rate and steady state concentration and amino acids behavior. Many questions rise to mind: “do microorganisms inhibit significantly hydroxyl radical formation rate?”, “is the concentration of amino acids influenced by the presence of microorganisms?”, “does microorganisms really influence chemical and photochemical processes?”…

Cloud water chemistry can have a relevant repercussion on the comprehension of atmospheric chemistry and on climate change. At this stage, more work is needed to fully understand the natural processes, to investigate their universality and their impact on tropospheric chemistry.

References

(1) Ervens, B.; Wang, Y.; Eagar, J.; Leaitch, W. R.; Macdonald, A. M.; Valsaraj, K. T.; Herckes, P. *Atmos. Chem. Phys.* **2013**, *13*, 5117-5135.

(2) Education, T. H.; Cartoon showing different cloud types and levels., Ed., 2007.

(3) Daum, P. H.; Schwartz, S. E.; Newman, L. "Studies of the gas-and aqueous-phase composition of stratiform clouds," Brookhaven National Lab., Upton, NY (USA), 1982.

(4) Heikes, B.; Lazrus, A.; Kok, G.; Kunen, S.; Gandrud, B.; Gitlin, S.; Sperry, P. *J. Geophys. Res., Oceans.* **1982**, *87*, 3045-3051.

(5) Jacob, D. J. *J. Geophys. Res., Atmos.* **1986**, *91*, 9807-9826.

(6) Bank, S.; Castillo, R. *Geophys. Res. Lett.* **1987**, *14*, 210-212.

(7) Chameides, W. L.; Davis, D. D. *Nature* **1983**, *304*, 427-429.

(8) Allen, M. R.; Ingram, W. J. *Nature* **2002**, *419*, 224-232.

(9) Fischer, J.; Bohn, M. *Mol. Phys.* **1986**, *58*, 395-399.

(10) Chuang, P. Y.; Charlson, R. J.; Seinfeld, J. H. *Nature* **1997**, *390*, 594-596.

(11) Gill, P. S.; Graedel, T. E.; Weschler, C. J. *Rev. Geophys.* **1983**, *21*, 903-920.

(12) Blanchard, D. C. *Science* **1964**, *146*, 396-397.

(13) Husar, R. B.; Shu, W. R. *Thermal Analyses of the Los Angeles Smog Aerosol*; American Meteorological Society, 1975.

(14) Feingold, G.; Chuang, P. Y. In *Journal of the Atmospheric Sciences*; American Meteorological Society, 2002; Vol. 59.

(15) Deguillaume, L.; Leriche, M.; Desboeufs, K.; Mailhot, G.; George, C.; Chaumerliac, N. *Chem. Rev.* **2005**, *105*, 3388-3431.

(16) Schwartz, S. E.; Potter, T. D.; Colman, B. R. *Handbook of Weather, Climate, and Water: Cloud chemistry*; Wiley Interscience, 2003.

(17) van Breemen, N.; Burrough, P. A.; Velthorst, E. J.; van Dobben, H. F.; de Wit, T.; Ridder, T. B.; Reijnders, H. F. R. *Nature* **1982**, *299*, 548-550.

(18) Daum, P. H.; Kelly, T. J.; Schwartz, S. E.; Newman, L. *Atmos. Environ.* **1984**, *18*, 2671-2684.

(19) Elbert, W.; Hoffmann, M. R.; Kramer, M.; Schmitt, G.; Andreae, M. O. *Atmos. Environ.* **2000**, *34*, 1109-1122.

(20) Moller, D.; Acker, K.; Wieprecht, W. *Atmos. Res.* **1996**, *41*, 321-335.

(21) van Pinxteren, D.; Fomba, K. W.; Mertes, S.; Muller, K.; Spindler, G.; Schneider, J.; Lee, T.; Collett, J.; Herrmann, H. *Atmos. Chem. Phys. Discuss.* **2015**, *2015*, 24311-24368.

(22) Ogren, J. A.; Heintzenberg, J.; Zuber, A.; Noone, K. J.; Charlson, R. J. *Tellus B* **1989**, *41B*, 24-31.

(23) Marinoni, A.; Parazols, M.; Brigante, M.; Deguillaume, L.; Amato, P.; Delort, A.-M.; Laj, P.; Mailhot, G. *Atmos. Res.* **2011**, *101*, 256-263.

(24) Monod, A.; Carlier, P. *Atmos. Environ.* **1999**, *33*, 4431-4446.

(25) Aleksic, N.; Roy, K.; Sistla, G.; Dukett, J.; Houck, N.; Casson, P. *Atmos. Environ.* **2009**, *43*, 2709-2716.

(26) Loflund, M.; Kasper-Giebl, A.; Schuster, B.; Giebl, H.; Hitzenberger, R.; Puxbaum, H. *Atmos. Environ.* **2002**, *36*, 1553-1558.

(27) Deguillaume, L.; Charbouillot, T.; Joly, M.; Vaitilingom, M.; Parazols, M.; Marinoni, A.; Amato, P.; Delort, A. M.; Vinatier, V.; Flossmann, A.; Chaumerliac, N.; Pichon, J. M.; Houdier, S.; Laj, P.; Sellegri, K.; Colomb, A.; Brigante, M.; Mailhot, G. *Atmos. Chem. Phys.* **2014**, *14*, 1485-1506.

(28) Acker, K.; Möller, D.; Wieprecht, W.; Kalaß, D.; Auel, R. *Fresenius. J. Anal. Chem.* **1998**, *361*, 59-64.

(29) Guo, J.; Wang, Y.; Shen, X.; Wang, Z.; Lee, T.; Wang, X.; Li, P.; Sun, M.; Collett Jr, J. L.; Wang, W.; Wang, T. *Atmos. Environ.* **2012**, *60*, 467-476.

(30) Herrmann, H.; Hoffmann, D.; Schaefer, T.; Bräuer, P.; Tilgner, A. *ChemPhysChem* **2010**, *11*, 3796-3822.

(31) Ervens, B.; George, C.; Williams, J. E.; Buxton, G. V.; Salmon, G. A.; Bydder, M.; Wilkinson, F.; Dentener, F.; Mirabel, P.; Wolke, R.; Herrmann, H. C. *J. Geophys. Res., Atmos.* **2003**, *108*, 4426.

(32) Leriche, M.; Voisin, D.; Chaumerliac, N.; Monod, A.; Aumont, B. *Atmos. Environ.* **2000**, *34*, 5015-5036.

(33) Deguillaume, L.; Tilgner, A.; Schrödner, R.; Wolke, R.; Chaumerliac, N.; Herrmann, H. *J. Atmos. Chem.* **2009**, *64*, 1-35.

(34) Albrecht, B. A.; Fairall, C. W.; Thomson, D. W.; White, A. B.; Snider, J. B.; Schubert, W. H. *Geophys. Res. Lett.* **1990**, *17*, 89-92.

(35) Junge, C. E. *Air chemistry and radioactivity*; New York and London. Academic Press, 1963.

(36) Sinner, T.; Hoffmann, P.; Ortner, H. *Contrib. Atmos. Phys.* **1994**, *67*, 353-357.

(37) Cini, R.; Prodi, F.; Santachiara, G.; Porci, F.; Bellandi, S.; Stortini, A. M.; Oppo, C.; Udisti, R.; Pantani, F. *Atmos. Res.* **2002**, *61*, 311-334.

(38) Kawamura, K.; Steinberg, S.; Ng, L.; Kaplan, I. R. *Atmos. Environ.* **2001**, *35*, 3917-3926.

(39) Behar, S. *Testing the Waters: Chemical and Physical Vital Signs of a River*; River Watch Network, 1996.

(40) Collett Jr, J. L.; Bator, A.; Sherman, D. E.; Moore, K. F.; Hoag, K. J.; Demoz, B. B.; Rao, X.; Reilly, J. E. *Atmos. Res.* **2002**, *64*, 29-40.

(41) Watanabe, K.; Takebe, Y.; Sode, N.; Igarashi, Y.; Takahashi, H.; Dokiya, Y. *Atmos. Res.* **2006**, *82*, 652-662.

(42) Castillo, R. A.; Jiusto, J. E.; McLaren, E. *Atmos. Environ.* **1983**, *17*, 1497-1505.

(43) Fowler, D.; Pilegaard, K.; Sutton, M. A.; Ambus, P.; Raivonen, M.; Duyzer, J.; Simpson, D.; Fagerli, H.; Fuzzi, S.; Schjoerring, J. K.; Granier, C.; Neftel, A.; Isaksen, I. S. A.; Laj, P.; Maione, M.; Monks, P. S.; Burkhardt, J.; Daemmgen, U.; Neirynck, J.; Personne, E.; Wichink-Kruit, R.; Butterbach-Bahl, K.; Flechard, C.; Tuovinen, J. P.; Coyle, M.; Gerosa, G.; Loubet, B.; Altimir, N.; Gruenhage, L.; Ammann, C.; Cieslik, S.; Paoletti, E.; Mikkelsen, T. N.; Ro-Poulsen, H.; Cellier, P.; Cape, J. N.; Horvath, L.; Loreto, F.; Niinemets, U.; Palmer, P. I.; Rinne, J.; Misztal, P.; Nemitz, E.; Nilsson, D.; Pryor, S.; Gallagher, M. W.; Vesala, T.; Skiba, U.; Bruggemann, N.; Zechmeister-Boltenstern, S.; Williams, J.; O'Dowd, C.; Facchini, M. C.; de Leeuw, G.; Flossman, A.; Chaumerliac, N.; Erisman, J. W. *Atmos. Environ.* **2009**, *43*, 5193-5267.

(44) Monks, P. S.; Granier, C.; Fuzzi, S.; Stohl, A.; Williams, M. L.; Akimoto, H.; Amann, M.; Baklanov, A.; Baltensperger, U.; Bey, I.; Blake, N.; Blake, R. S.; Carslaw, K.; Cooper, O. R.; Dentener, F.; Fowler, D.; Fragkou, E.; Frost, G. J.; Generoso, S.; Ginoux, P.; Grewe, V.; Guenther, A.; Hansson, H. C.; Henne, S.; Hjorth, J.; Hofzumahaus, A.; Huntrieser, H.; Isaksen, I. S. A.; Jenkin, M. E.; Kaiser, J.; Kanakidou, M.; Klimont, Z.; Kulmala, M.; Laj, P.; Lawrence, M. G.; Lee, J. D.; Liousse, C.; Maione, M.; McFiggans, G.; Metzger, A.; Mieville, A.; Moussiopoulos, N.; Orlando, J. J.; O'Dowd, C. D.; Palmer, P. I.; Parrish, D. D.; Petzold, A.; Platt, U.; Poschl, U.; Prevot, A. S. H.; Reeves, C. E.; Reimann, S.; Rudich, Y.; Sellegri, K.; Steinbrecher, R.; Simpson, D.; ten Brink, H.; Theloke, J.; van der Werf, G. R.; Vautard, R.; Vestreng, V.; Vlachokostas, C.; von Glasow, R. *Atmos. Environ.* **2009**, *43*, 5268-5350.

(45) Seinfeld, J. H.; Pandis, S. N. *Atmospheric Chemistry and Physics: From Air Pollution to Climate Change, 2nd Edition*; Wiley Interscience, 2006.

(46) Barth, M. C. *Atmos. Res.* **2006**, *82*, 294-309.

(47) Sellegri, K.; Laj, P.; Marinoni, A.; Dupuy, R.; Legrand, M.; Preunkert, S. *Atmos. Chem. Phys.* **2003**, *3*, 1509-1522.

(48) Leriche, M.; Deguillaume, L.; Chaumerliac, N. C. *J. Geophys. Res., Atmos.* **2003**, *108*, 4433.

(49) Suslick, K. S.; Watson, R. A. *Inorg. Chem.* **1991**, *30*, 912-919.

(50) Deguillaume, L.; Leriche, M.; Monod, A.; Chaumerliac, N. *Atmos. Chem. Phys.* **2004**, *4*, 95-110.

(51) Lee, D. S.; Pacyna, J. M. *Atmos. Environ.* **1999**, *33*, 1687-1697.

(52) Gioda, A.; Mayol-Bracero, O. L.; Morales-García, F.; Collett, J.; Decesari, S.; Emblico, L.; Facchini, M. C.; Morales-De Jesús, R. J.; Mertes, S.; Borrmann, S.; Walter, S.; Schneider, J. *Water, Air, Soil Pollut.* **2008**, *200*, 3-14.

(53) Reyes-Rodriguez, G. J.; Gioda, A.; Mayol-Bracero, O. L.; Collett Jr, J. *Atmos. Environ.* **2009**, *43*, 4171-4177.

(54) Blas, M.; Sobik, M.; Twarowski, R. *Atmos. Res.* **2008**, *87*, 224-231.

(55) Herckes, P.; Hannigan, M. P.; Trenary, L.; Lee, T.; Collett Jr, J. L. *Atmos. Res.* **2002**, *64*, 99-108.

(56) Lammel, G.; Metzig, G. *Fresenius. J. Anal. Chem.* **1991**, *340*, 564-574.

(57) Lin, N.-H.; Peng, C.-M. *Terr. Atmos. Ocean. Sci.* **1999**, *10*, 693-704.

(58) Wang, Y.; Guo, J.; Wang, T.; Ding, A.; Gao, J.; Zhou, Y.; Collett Jr, J. L.; Wang, W. *Atmos. Res.* **2011**, *99*, 434-442.

(59) Holland, H. D. *The chemistry of the atmosphere and oceans, Wiley interscience*; Wiley interscience, 1978.

(60) Anastasio, C.; Jordan, A. L. *Atmos. Environ.* **2004**, *38*, 1153-1166.

(61) Graedel, T. E.; Mandich, M. L.; Weschler, C. J. *J. Geophys. Res., Atmos.* **1986**, *91*, 5205-5221.

(62) Kanakidou, M.; Seinfeld, J. H.; Pandis, S. N.; Barnes, I.; Dentener, F. J.; Facchini, M. C.; Van Dingenen, R.; Ervens, B.; Nenes, A.; Nielsen, C. J.; Swietlicki, E.; Putaud, J. P.; Balkanski, Y.; Fuzzi, S.; Horth, J.; Moortgat, G. K.; Winterhalter, R.; Myhre, C. E. L.; Tsigaridis, K.; Vignati, E.; Stephanou, E. G.; Wilson, J. *Atmos. Chem. Phys.* **2005**, *5*, 1053-1123.

(63) Goldstein, A. H.; Galbally, I. E. *Environ. Sci. Technol.* **2007**, *41*, 1514-1521.

(64) Marinoni, A.; Laj, P.; Sellegri, K.; Mailhot, G. *Atmos. Chem. Phys.* **2004**, *4*, 715-728.

(65) Keene, W. C.; Mosher, B. W.; Jacob, D. J.; Munger, J. W.; Talbot, R. W.; Artz, R. S.; Maben, J. R.; Daube, B. C.; Galloway, J. N. *J. Geophys. Res., Atmos.* **1995**, *100*, 9345-9357.

(66) Laj, P.; Fuzzi, S.; Facchini, M. C.; Lind, J. A.; Orsi, G.; Preiss, M.; Maser, R.; Jaeschke, W.; Seyffer, E.; Helas, G.; Acker, K.; Wieprecht, W.; Muller, D.; Arends, B. G.; Mols, J. J.; Colvile, R. N.; Gallagher, M. W.; Beswick, K. M.; Hargreaves, K. J.; Storeton-West, R. L.; Sutton, M. A. *Atmos. Environ.* **1997**, *31*, 2589-2598.

(67) Luttke, J.; Levsen, K. *Atmos. Environ.* **1997**, *31*, 2649-2655.

(68) Luttke, J.; Scheer, V.; Levsen, K.; Wunsch, G.; Neil Cape, J.; Hargreaves, K. J.; Storeton-West, R. L.; Acker, K.; Wieprecht, W.; Jones, B. *Atmos. Environ.* **1997**, *31*, 2637-2648.

(69) Charbouillot, T.; Brigante, M.; Deguillaume, L.; Mailhot, G. *J. Photochem. Photobiol.* **2012**, *88*, 32-37.

(70) Walling, C. *Acc. Chem. Res.* **1998**, *31*, 155-157.

(71) Pitts, J. N.; Lokensgard, D. M.; Ripley, P. S.; Van Cauwenberghe, K. A.; Van Vaeck, L.; Shaffer, S. D.; Thill, A. J.; Belser, W. L. *Science* **1980**, *210*, 1347-1349.

(72) Finlayson-Pitts, B. J.; Pitts, J. N. *Chemistry of the upper and low atmosphere. Academic Press, San Diego*, 2000.

(73) Herrmann, H.; Tilgner, A.; Barzaghi, P.; Majdik, Z.; Gligorovski, S.; Poulain, L.; Monod, A. *Atmos. Environ.* **2005**, *39*, 4351-4363.

(74) Huie, R. E.; Clifton, C. L.; Neta, P. *Int. J. Radiat. Appl. Instrum. C Radiat. Phys. Chem.* **1991**, *38*, 477-481.

(75) Schuchmann, H. P.; Deeble, D. J.; Olbrich, G.; Sonntag, C. v. *Int. J. Radiat. Biol. Relat. Stud. Phys. Chem. Med.* **1987**, *51*, 441-453.

(76) Buxton, G. V.; Greenstock, C. L.; Helman, W. P.; Ross, A. B. *J. Phys. Chem. Ref. Data* **1998**, *17*, 513-886.

(77) Finlayson, B. J.; Pitts, J. N. *Atmospheric chemistry: Fundamentals and experimental techniques*; John Wiley and Sons Inc.,New York, NY, 1986.

(78) Lind, J. A.; Kok, G. L. *J. Geophys. Res., Atmos.* **1986**, *91*, 7889-7895.

(79) Arakaki, T.; Anastasio, C.; Shu, P. G.; Faust, B. C. *Atmos. Environ.* **1995**, *29*, 1697-1703.

(80) Faust, B. C.; Allen, J. M. *Environ. Sci. Technol.* **1993**, *27*, 1221-1224.

(81) Faust, B. C.; Anastasio, C.; Allen, J. M.; Arakaki, T. *Science* **1993**, *260*, 73-75.

(82) Anastasio, C.; Faust, B. C.; Allen, J. M. *J. Geophys. Res., Atmos.* **1994**, *99*, 8231-8248.

(83) Arakaki, T.; Faust, B. C. *J. Geophys. Res.* **1998**, *103*, 3487-3504.

(84) Faust, B. C.; Powell, K.; Rao, C. J.; Anastasio, C. *Atmos. Environ.* **1997**, *31*, 497-510.

(85) Zuo, Y.; Deng, Y. *Geochim. Cosmochim. Acta* **1999**, *63*, 3451-3455.

(86) Finlayson-Pitts, B. J.; Pitts Jr, J. N. *Chemistry of the upper and lower atmosphere: theory, experiments, and applications*; Academic press, 1999.

(87) Valverde-Canossa, J.; Wieprecht, W.; Acker, K.; Moortgat, G. K. *Atmos. Environ.* **2005**, *39*, 4279-4290.

(88) Richards, L. W.; Anderson, J. A.; Blumenthal, D. L.; McDonald, J. A.; Kok, G. L.; Lazrus, A. L. *Atmos. Environ.* **1983**, *17*, 911-914.

(89) Atkinson, R.; Baulch, D. L.; Cox, R. A.; Hampson, R. F.; Kerr, J. A.; Rossi, M. J.; Troe, J. *J. Phys. Chem. Ref. Data* **1997**, *26*, 1329-1499.

(90) Vaghjiani, G. L.; Turnipseed, A. A.; Warren, R. F.; Ravishankara, A. R. *J. Chem. Phys.* **1992**, *96*, 5878-5886.

(91) Wayne, R. P.; Barnes, I.; Biggs, P.; Burrows, J.; Canosa-Mas, C.; Hjorth, J.; Le Bras, G.; Moortgat, G.; Perner, D.; Poulet, G. *Atmos. Environ. A-Gen.* **1991**, *25*, 1-203.

(92) Thomas, K.; Volz-Thomas, A.; Mihelcic, D.; Smit, H. G. J.; Kley, D. *J. Atmos. Chem.*, *29*, 17-43.

(93) Hanson, D. R.; Burkholder, J. B.; Howard, C. J.; Ravishankara, A. R. *J. Phys. Chem.* **1992**, *96*, 4979-4985.

(94) Biedenkapp, D.; Hartshorn, L. G.; Bair, E. J. *Chem. Phys. Lett.* **1970**, *5*, 379-381.

(95) Bohn, B.; Zetzsch, C. *J. Phys. Chem. A* **1997**, *101*, 1488-1493.

(96) Jans, U.; Hoigné, J. *Atmos. Environ.* **2000**, *34*, 1069-1085.

(97) Long, Y.; Charbouillot, T.; Brigante, M.; Mailhot, G.; Delort, A.-M.; Chaumerliac, N.; Deguillaume, L. *Atmos. Environ.* **2013**, *77*, 686-695.

(98) Barbusinski, K. *Ecological Chemistry and Engineering. S* **2009**, *16*, 347-358.

(99) Zafiriou, O. C.; True, M. B. *Mar. Chem.* **1979**, *8*, 33-42.

(100) Warneck, P.; Wurzinger, C. *J. Phys. Chem.* **1988**, *92*, 6278-6283.

(101) Charbouillot, T.; Gorini, S.; Voyard, G.; Parazols, M.; Brigante, M.; Deguillaume, L.; Delort, A.-M.; Mailhot, G. *Atmos. Environ.* **2012**, *56*, 1-8.

(102) Herckes, P.; Valsaraj, K. T.; Collett Jr, J. L. *Atmos. Res.* **2013**, *132-133*, 434-449.

(103) Arakaki, T.; Anastasio, C.; Kuroki, Y.; Nakajima, H.; Okada, K.; Kotani, Y.; Handa, D.; Azechi, S.; Kimura, T.; Tsuhako, A.; Miyagi, Y. *Environ. Sci. Technol.* **2013**, *47*, 8196-8203.

(104) Ervens, B.; Sorooshian, A.; Lim, Y. B.; Turpin, B. J. *J. Geophys. Res.* **2014**, *119*, 3997-4016.

(105) Tilgner, A.; Herrmann, H. *Atmos. Environ.* **2010**, *44*, 5415-5422.

(106) Saxena, P.; Hildemann, L. M. *J. Atmos. Chem.* **1996**, *24*, 57-109.

(107) Ervens, B.; Turpin, B. J.; Weber, R. J. *Atmos. Chem. Phys.* **2011**, *11*, 11069-11102.

(108) Collett Jr, J. L.; Herckes, P.; Youngster, S.; Lee, T. *Atmos. Res.* **2008**, *87*, 232-241.

(109) Decesari, S.; Facchini, M. C.; Fuzzi, S.; McFiggans, G. B.; Coe, H.; Bower, K. N. *Atmos. Environ.* **2005**, *39*, 211-222.

(110) Straub, D. J.; Hutchings, J. W.; Herckes, P. *Atmos. Environ.* **2012**, *47*, 195-205.

(111) Hegg, D. A.; Gao, S.; Jonsson, H. *Atmos. Res.* **2002**, *62*, 1-10.

(112) Khwaja, H. A. *Atmos. Environ.* **1995**, *29*, 127-139.

(113) Collett, J.; Daube, B.; Munger, J. W.; Hoffmann, M. R. *Atmos. Environ.* **1989**, *23*, 999-1007.

(114) Kesselmeier, J.; Staudt, M. *J. Atmos. Chem.* **1999**, *33*, 23-88.

(115) Khare, P.; Kumar, N.; Kumari, K. M.; Srivastava, S. S. *Rev. Geophys.* **1999**, *37*, 227-248.

(116) Gaeggeler, K.; Prevot, A. S. H.; Dommen, J.; Legreid, G.; Reimann, S.; Baltensperger, U. *Atmos. Environ.* **2008**, *42*, 8278-8287.

(117) Warneck, P. *J. Atmos. Chem.* **2005**, *51*, 119-159.

(118) Khare, P.; Satsangi, G. S.; Kumar, N.; Maharaj Kumari, K.; Srivastava, S. S. *Atmos. Environ.* **1997**, *31*, 3867-3875.

(119) Montero, L.; Vasconcellos, P. C.; Souza, S. R.; Pires, M. A. F.; Sanchez-Ccoyllo, O. R.; Andrade, M. F.; Carvalho, L. R. F. *Environ. Sci. Technol.* **2001**, *35*, 3071-3081.

(120) Chebbi, A.; Carlier, P. *Atmos. Environ.* **1996**, *30*, 4233-4249.

(121) Kawamura, K.; Kaplan, I. R. *Environ. Sci. Technol.* **1987**, *21*, 105-110.

(122) Deguillaume, L.; Tilgner, A.; Schrödner, R.; Wolke, R.; Chaumerliac, N.; Herrmann, H. *J. Atmos. Chem.*, *64*, 1-35.

(123) Johnson, B. J.; Betterton, E. A.; Craig, D. *J. Atmos. Chem.* **1996**, *24*, 113-119.

(124) Amato, P.; Demeer, F.; Melaouhi, A.; Fontanella, S.; Martin-Biesse, A. S.; Sancelme, M.; Laj, P.; Delort, A. M. *Atmos. Chem. Phys.* **2007**, *7*, 4159-4169.

(125) Rogge, W. F.; Hildemann, L. M.; Mazurek, M. A.; Cass, G. R. *Environ. Sci. Technol.* **1998**, *32*, 13-22.

(126) Weathers, K. C.; Likens, G. E.; Bormann, F. H.; Bicknell, S. H.; Bormann, B. T.; Daube, B. C.; Eaton, J. S.; Galloway, J. N.; Keene, W. C.; et al. *Environ. Sci. Technol.* **1988**, *22*, 1018-1026.

(127) Leaitch, W. R.; Banic, C. M.; Isaac, G. A.; Couture, M. D.; Liu, P. S. K.; Gultepe, I.; Li, S. M.; Kleinman, L.; Daum, P. H.; MacPherson, J. I. *J. Geophys. Res., Atmos.* **1996**, *101*, 29123-29135.

(128) Vong, R. J.; Baker, B. M.; Brechtel, F. J.; Collier, R. T.; Harris, J. M.; Kowalski, A. S.; McDonald, N. C.; McInnes, L. M. *Atmos. Environ.* **1997**, *31*, 1991-2001.

(129) Brantner, B.; Fierlinger, H.; Puxbaum, H.; Berner, A. *Water, Air, Soil Pollut.* **1994**, *74*, 363-384.

(130) Munger, J. W.; Collett, J.; Daube, B. C.; Hoffmann, M. R. *Tellus B* **1989**, *41B*, 230-242.

(131) Atkinson, R. *Atmos. Environ.* **2007**, *41*, 200-240.

(132) Grosjean, D. *Atmos. Environ.* **1983**, *17*, 2379-2382.

(133) Herrmann, H. *Chem. Rev.* **2003**, *103*, 4691-4716.

(134) Kawamura, K.; Kasukabe, H.; Barrie, L. A. *Atmos. Environ.* **1996**, *30*, 1709-1722.

(135) Carlton, A. G.; Turpin, B. J.; Altieri, K. E.; Seitzinger, S.; Reff, A.; Lim, H.-J.; Ervens, B. *Atmos. Environ.* **2007**, *41*, 7588-7602.

(136) Zhao, Y.; Hallar, A. G.; Mazzoleni, L. R. *Atmos. Chem. Phys.* **2013**, *13*, 12343-12362.

(137) Wozniak, A. S.; Bauer, J. E.; Sleighter, R. L.; Dickhut, R. M.; Hatcher, P. G. *Atmos. Chem. Phys.* **2008**, *8*, 5099-5111.

(138) Mazzoleni, L. R.; Ehrmann, B. M.; Shen, X.; Marshall, A. G.; Collett, J. L. *Environ. Sci. Technol.* **2010**, *44*, 3690-3697.

(139) Kuznetsova, M.; Lee, C.; Aller, J. *Mar. Chem.* **2005**, *96*, 359-377.

(140) Milne, P. J.; Zika, R. G. *J. Atmos. Chem.* **1993**, *16*, 361-398.

(141) Saxena, V. K. *J. Phys. Chem.* **1983**, *87*, 4130-4134.

(142) Facchini, M. C.; Mircea, M.; Fuzzi, S.; Charlson, R. J. *Nature* **1999**, *401*, 257-259.

(143) Zhang, Q.; Anastasio, C. *Atmos. Environ.* **2001**, *35*, 5629-5643.

(144) Szyrmer, W.; Zawadzki, I. *Bull. Am. Meteorol. Soc.* **1997**, *78*, 209-228.

(145) Zhang, Q.; Anastasio, C. *Atmos. Environ.* **2003**, *37*, 2247-2258.

(146) Zhang, Q.; Anastasio, C.; Jimenez-Cruz, M. *J. Geophys. Res., Atmos.* **2002**, *107*.

(147) O'Sullivan, D.; Murray, B. J.; Ross, J. F.; Whale, T. F.; Price, H. C.; Atkinson, J. D.; Umo, N. S.; Webb, M. E. *Sci. Rep.* **2015**, *5*, 8082.

(148) Edelhoch, H. *Biochemistry* **1967**, *6*, 1948-1954.

(149) Pirie, A. *Biochem. J.* **1972**, *128*, 1365-1367.

(150) Bonifacic, M.; Stefanic, I.; Hug, G. L.; Armstrong, D. A.; Asmus, K.-D. *J. Am. Chem. Soc.* **1998**, *120*, 9930-9940.

(151) Xu, G.; Chance, M. R. *Chem. Rev.* **2007**, *107*, 3514-3543.

(152) Forni, L. G.; Mora-Arellano, V. O.; Packer, J. E.; Willson, R. L. *J. Chem. Soc., Perkin Trans. 2* **1986**, 1-6.

(153) Bielski, B. H.; Shiue, G. G. In *Oxygen free radicals and tissue damage*; CIBA Foundation Symposium, Ed., 1979.

(154) Adams, G. E.; Aldrich, J. E.; Bisby, R. H.; Cundall, R. B.; Redpath, J. L.; Willson, R. L. *Radiat. Res.* **1972**, *49*, 278-289.

(155) Muller, C. L.; Baker, A.; Hutchinson, R.; Fairchild, I. J.; Kidd, C. *Atmos. Environ.* **2008**, *42*, 8036-8045.

(156) Kiss, G.; Tombacz, E.; Varga, B.; Alsberg, T.; Persson, L. *Atmos. Environ.* **2003**, *37*, 3783-3794.

(157) Zappoli, S.; Andracchio, A.; Fuzzi, S.; Facchini, M. C.; Gelencser, A.; Kiss, G.; Krivacsy, Z.; Molnar, Ã.; Meszaros, E.; Hansson, H. C.; Rosman, K.; Zebuhr, Y. *Atmos. Environ.* **1999**, *33*, 2733-2743.

(158) Havers, N.; Burba, P.; Lambert, J.; Klockow, D. *J. Atmos. Chem.* **1998**, *29*, 45-54.

(159) McFiggans, G.; Alfarra, M. R.; Allan, J.; Bower, K.; Coe, H.; Cubison, M.; Topping, D.; Williams, P.; Decesari, S.; Facchini, C.; Fuzzi, S. *Faraday Discuss.* **2005**, *130*, 341-362.

(160) Coble, P. G. *Mar. Chem.* **1996**, *51*, 325-346.

(161) Venzac, H.; Sellegri, K.; Villani, P.; Picard, D.; Laj, P. *Atmos. Chem. Phys.* **2009**, *9*, 1465-1478.

(162) Rose, C.; Boulon, J.; Hervo, M.; Holmgren, H.; Asmi, E.; Ramonet, M.; Laj, P.; Sellegri, K. *Atmos. Chem. Phys.* **2013**, *13*, 11573-11594.

(163) Freney, E. J.; Sellegri, K.; Canonaco, F.; Boulon, J.; Hervo, M.; Weigel, R.; Pichon, J. M.; Colomb, A.; Prevot, A. S. H.; Laj, P. *Atmos. Chem. Phys.* **2011**, *11*, 13047-13059.

(164) Bourcier, L.; Sellegri, K.; Chausse, P.; Pichon, J. M.; Laj, P. *J. Atmos. Chem.* **2012**, *69*, 47-66.

(165) Hervo, M.; Sellegri, K.; Pichon, J.; Roger, J.; Laj, P. *Atmos. Chem. Phys.* **2014**, *14*, 27731-27767.

(166) Asmi, E.; Freney, E.; Hervo, M.; Picard, D.; Rose, C.; Colomb, A.; Sellegri, K. *Atmos. Chem. Phys.* **2012**, *12*, 11589-11607.

(167) Mertes, S.; Schwarzenback, A.; Laj, P.; Wobrock, W.; Pichon, J.-M.; Orsi, G.; Heintzenberg, J. *Atmos. Res.* **2001**, *58*, 267-294.

(168) Guyot, G.; Gourbeyre, C.; Febvre, G.; Shcherbakov, V.; Burnet, F.; Dupont, J. C.; Sellegri, K.; Jourdan, O. *Atmos. Meas. Tech.* **2015**, *8*, 4347-4367.

(169) Stein, A. F.; Draxler, R. R.; Rolph, G. D.; Stunder, B. J. B.; Cohen, M. D.; Ngan, F. *Bull. Am. Meteorol. Soc.* **2015**, *96*, 2059-2077.

(170) Dulin, D.; Mill, T. *Environ. Sci. Technol.* **1982**, *16*, 815-820.

(171) Miller, W. L.; Kester, D. R. *Anal. Chem.* **1988**, *60*, 2711-2715.

(172) Stookey, L. L. *Anal. Chem.* **1970**, *42*, 779-781.

(173) Kieber, R. J.; Seaton, P. J. *Anal. Chem.* **1995**, *67*, 3261-3264.

(174) Altieri, K. E.; Seitzinger, S. P.; Carlton, A. G.; Turpin, B. J.; Klein, G. C.; Marshall, A. G. *Atmos. Environ.* **2008**, *42*, 1476-1490.

(175) Perri, M. J.; Seitzinger, S.; Turpin, B. J. *Atmos. Environ.* **2009**, *43*, 1487-1497.

(176) Tan, Y.; Lim, Y. B.; Altieri, K. E.; Seitzinger, S. P.; Turpin, B. J. *Atmos. Chem. Phys.* **2011**, *12*, 801-813.

(177) Ervens, B.; Volkamer, R. *Atmos. Chem. Phys.* **2010**, *10*, 8219-8244.

(178) De Haan, D. O.; Tolbert, M. A.; Jimenez, J. L. *Geophys. Res. Lett.* **2009**, *36*, L11819.

(179) Yu, X.-Y.; Barker, J. R. *J. Phys. Chem. A* **2003**, *107*, 1325-1332.

(180) Zellner, R.; Exner, M.; Herrmann, H. *J. Atmos. Chem.* **1990**, *10*, 411-425.

(181) Zafiriou, O. C.; Bonneau, R. *J. Photochem. Photobiol.* **1987**, *45*, 723-727.

(182) Hervo, M., Etude des propriétés optiques et radiatives des aérosols en atmosphère réelle : impact de l'hygroscopicité. Blaise Pascal University, 2013.

(183) Miller, W. L.; Kester, D. R. *Anal. Chem.* **2002**, *60*, 2711-2715.

(184) Parazols, M.; Marinoni, A.; Amato, P.; Abida, O.; Laj, P.; Mailhot, G. *J. Atmos. Chem.* **2006**, *54*, 267-281.

(185) Vaitilingom, M.; Deguillaume, L.; Vinatier, V.; Sancelme, M.; Amato, P.; Chaumerliac, N.; Delort, A.-M. *Proc. Natl. Acad. Sci.* **2013**, *110*, 559-564.

(186) R Core Team Vienna, Austria, 2013.

(187) Lê, S.; Josse, J.; Husson, F. *J. Stat. Softw.* **2008**, *25*, 1-18.

(188) Deming, S. N.; Michotte, Y.; Massart, D. L.; Kaufman, L.; Vandeginste, B. G. M. *Chemometrics: A textbook, 1st Edition*; Elsevier Science, 1988.

(189) Charbouillot, T.; Brigante, M.; Mailhot, G.; Maddigapu, P. R.; Minero, C.; Vione, D. *J. Photochem. Photobiol., A* **2011**, *222*, 70-76.

(190) Neta, P.; Huie, R. E.; Ross, A. B. *J. Phys. Chem. Ref. Data* **1988**, *17*, 1027-1284.

(191) Draxler, R. R.; Rolph, G. D., 2012.

(192) Leriche, M.; Chaumerliac, N.; Monod, A. *Atmos. Environ.* **2001**, *35*, 5411-5423.

(193) Madronich, S.; Flocke, S. In *Environmental Photochemistry*; Boule, P., Ed.; Springer Berlin Heidelberg, 1999; Vol. 2 / 2L.

(194) Smith, R. M.; Martell, A. E. *Critical Stability Constants, Volume 4: Inorganic Complexes*: New York, 1976.

(195) Bielski, B. H. J.; Cabelli, D. E.; Arudi, R. L.; Ross, A. B. *J. Phys. Chem. Ref. Data* **1985**, *14*, 1041-1100.

(196) Park, J. Y.; Lee, Y. N. *J. Phys. Chem.* **1988**, *92*, 6294-6302.

(197) Riordan, E.; Minogue, N.; Healy, D.; O'Driscol, P.; Sodeau, J. R. *J. Phys. Chem. A* **2005**, *109*, 779-786.

(198) IUPAC SC-Database: A comprehensive database of published data on equilibrium constants of metal complexes and ligands

(199) Goldstein, S.; Czapski, G. *Inorg. Chem.* **1997**, *36*, 4156-4162.

(200) Marsh, A. R. W.; McElroy, W. J. *Atmos. Environ.* **1985**, *19*, 1075-1080.

(201) Maash, H. G. In *Heterogenous Atmospheric Chemistry*, *Geophys. Monogr. Ser.*; Schryer, D. R., Ed.; AGU: Washington, D. C., 1982; Vol. 6.

(202) Cotton, F. A.; Wilkinson, G. *Advanced inorganic chemistry: a comprehensive text*; 4th ed.; John Wiley & Sons: New York, 1980.

(203) Eigen, M.; Krause, W.; Maash, H. G.; Demaeyer, L. In *Progress in reaction kinetics*; Porter, G., Ed.; Macmillan: N. J., 1964; Vol. 2.

(204) Brandt, C.; van Eldik, R. *Chem. Rev.* **1995**, *95*, 119-190.

(205) Albinet, A.; Minero, C.; Vione, D. *Sci. Total Environ.* **2010**, *408*, 3367-3373.

(206) Arakaki, T.; Kuroki, Y.; Okada, K.; Nakama, Y.; Ikota, H.; Kinjo, M.; Higuchi, T.; Uehara, M.; Tanahara, A. *Atmos. Environ.* **2006**, *40*, 4764-4774.

(207) Anastasio, C.; McGregor, K. G. *Atmos. Environ.* **2001**, *35*, 1079-1089.

(208) Okochi, H.; Brimblecombe, P. *Sci. World. J.* **2002**, *2*, 767-786.

(209) Weller, C.; Tilgner, A.; Brauer, P.; Herrmann, H. *Environ. Sci. Technol.* **2014**, *48*, 5652-5659.

(210) Kulka, D.; Hall, A. N.; Walker, T. K. *Nature* **1951**, *167*, 905-906.

(211) Smith, T. N.; Hash, K.; Davey, C.-L.; Mills, H.; Williams, H.; Kiely, D. E. *Carbohydr. Res.* **2012**, *350*, 6-13.

(212) van Pinxteren, D.; Neusus, C.; Herrmann, H. *Atmos. Chem. Phys.* **2014**, *14*, 3913-3928.

(213) Herrmann, H.; Wolke, R.; Muller, K.; Bruggemann, E.; Gnauk, T.; Barzaghi, P.; Mertes, S.; Lehmann, K.; Massling, A.; Birmili, W.; Wiedensohler, A.; Wieprecht, W.; Acker, K.; Jaeschke, W.; Kramberger, H.; Svrcina, B.; Bachmann, K.; Collett Jr, J. L.; Galgon, D.; Schwirn, K.; Nowak, A.; van Pinxteren, D.; Plewka, A.; Chemnitzer, R.; Rud, C.; Hofmann, D.; Tilgner, A.; Diehl, K.; Heinold, B.; Hinneburg, D.; Knoth, O.; Sehili, A. M.; Simmel, M.; Wurzler, S.; Majdik, Z.; Mauersberger, G.; Muller, F. *Atmos. Environ.* **2005**, *39*, 4169-4183.

(214) Neusüss, C.; Pelzing, M.; Plewka, A.; Herrmann, H. *J. Geophys. Res., Atmos.* **2000**, *105*, 4513-4527.

(215) Qi, J.; Xin, L.; Chadderdon, D. J.; Qiu, Y.; Jiang, Y.; Benipal, N.; Liang, C.; Li, W. *Appl. Catal., B* **2014**, *154-155*, 360-368.

(216) Herrmann, H.; Barzaghi, P.; Hesper, J. In *Kinetic and spectroscopic investigations of OH radical reactions with tropospheric relevant compounds in aqueous solution*, 2000, Poster.

(217) Zellner, R.; Exner, M.; Herrmann, H. *Journal of Atmospheric Chemistry* **1990**, *10*, 411-425.

(218) Fuzzi, S.; Baltensperger, U.; Carslaw, K.; Decesari, S.; Denier Van Der Gon, H.; Facchini, M.; Fowler, D.; Koren, I.; Langford, B.; Lohmann, U. *Atmos. Chem. Phys.* **2015**, *15*, 8217-8299.

(219) Poschl, U. *Angew. Chem.* **2005**, *44*, 7520-7540.

(220) Saxena, P.; Hildemann, L. M.; McMurry, P. H.; Seinfeld, J. H. *J. Geophys. Res., Atmos.* **1995**, *100*, 18755-18770.

(221) Miyazaki, Y.; Kondo, Y.; Takegawa, N.; Komazaki, Y.; Fukuda, M.; Kawamura, K.; Mochida, M.; Okuzawa, K.; Weber, R. *J. Geophys. Res., Atmos.* **2006**, *111*, D23.

(222) Kondo, Y.; Miyazaki, Y.; Takegawa, N.; Miyakawa, T.; Weber, R.; Jimenez, J.; Zhang, Q.; Worsnop, D. *J. Geophys. Res., Atmos.* **2007**, *112*, D1.

(223) Shulman, M. L.; Jacobson, M. C.; Carlson, R. J.; Synovec, R. E.; Young, T. E. *Geophys. Res. Lett.* **1996**, *23*, 277-280.

(224) Kiss, G.; Varga, B.; Galambos, I.; Ganszky, I. *J. Geophys. Res., Atmos.* **2002**, *107* 8339.

(225) Sullivan, A.; Weber, R.; Clements, A.; Turner, J.; Bae, M.; Schauer, J. *Geophys. Res. Lett.* **2004**, *31*, L13105.

(226) Matsumoto, K.; Uematsu, M. *Atmos. Environ.* **2005**, *39*, 2163-2170.

(227) Bigg, E. K.; Leck, C. *J. Geophys. Res., Atmos.* **2008**, *113*, D11209.

(228) Sharma, V. K.; Graham, N. J. *Ozone: Sci. Eng.* **2010**, *32*, 81-90.

(229) Lin, P.; Rincon, A. G.; Kalberer, M.; Yu, J. Z. *Environ. Sci. Technol.* **2012**, *46*, 7454-7462.

(230) Hawkins, L. N.; Lemire, A. N.; Galloway, M. M.; Corrigan, A. L.; Turley, J. J.; Espelien, B. M.; De Haan, D. O. *Environ. Sci. Technol.* **2016**, *50(14)*, 7443-7452.

(231) Vaitilingom, M.; Amato, P.; Sancelme, M.; Laj, P.; Leriche, M.; Delort, A.-M. *Appl. Environ. Microbiol.* **2009**, *76*, 23-29.

(232) McLaren, A.; Gentile, P.; Kirk, D. C.; Levin, N. A. *J. Polym. Sci.* **1953**, *10*, 333-344.

(233) Bianco, A.; Passananti, M.; Deguillaume, L.; Mailhot, G.; Brigante, M. *Atmos. Environ.* **2016**, *137*, 53-61.

(234) McGregor, K. G.; Anastasio, C. *Atmos. Environ.* **2001**, *35*, 1091-1104.

(235) Mulligan, C. N.; Sharma, S. K.; Mudhoo, A. *Biosurfactants: research trends and applications*; CRC Press, 2014.

(236) Li, X.; Hede, T.; Tu, Y.; Leck, C.; Agren, H. *Tellus B* **2013**, *65*.

(237) Mopper, K.; Zika, R. G. *Nature* **1987**, *325*, 246-249.

(238) Kristensson, A.; Rosenorn, T.; Bilde, M. *J. Phys. Chem. A* **2009**, *114*, 379-386.

(239) Scheller, E. *Atmos. Environ.* **2001**, *35*, 2179-2192.

(240) Gorzelska, K.; Galloway, J. N.; Watterson, K.; Keene, W. C. *Atmos. Environ. A-Gen.* **1992**, *26*, 1005-1018.

(241) Bianco, A.; Minella, M.; De Laurentiis, E.; Maurino, V.; Minero, C.; Vione, D. *Chemosphere* **2014**, *111*, 529-536.

(242) Muller, C. L.; Kidd, C.; Fairchild, I. J.; Baker, A. *Atmos. Res.* **2010**, *96*, 241-255.

(243) Ervens, B.; Gligorovski, S.; Herrmann, H. *Phys. Chem. Chem. Phys.* **2003**, *5*, 1811-1824.

(244) Ishida, Y.; Fujita, T.; Asai, K. *J. Chromatogr., A* **1981**, *204*, 143-148.

(245) Fountoulakis, M.; Lahm, H.-W. *J. Chromatogr., A* **1998**, *826*, 109-134.

(246) Deguillaume, L.; Leriche, M.; Amato, P.; Ariya, P. A.; Delort, A. M.; Poschl, U.; Chaumerliac, N.; Bauer, H.; Flossmann, A. I.; Morris, C. E. *Biogeosciences* **2008**, *5*, 1073-1084.

(247) Després, V. R.; Huffman, J. A.; Burrows, S. M.; Hoose, C.; Safatov, A. S.; Buryak, G.; Frohlich-Nowoisky, J.; Elbert, W.; Andreae, M. O.; Poschl, U.; Jaenicke, R. *Tellus B* **2012**, *64*, 15598.

(248) Zhu, C.; Kawamura, K.; Kunwar, B. C. J. D. *J. Geophys. Res. Atmos.* **2015**, *120*, 5504-5523.

(249) Möhler, O.; DeMott, P. J.; Vali, G.; Levin, Z. *Biogeosciences* **2007**, *4*, 1059-1071.

(250) Morris, C. E.; Conen, F.; Alex Huffman, J.; Phillips, V.; Pöschl, U.; Sands, D. C. *Glob. Change Biol.* **2014**, *20*, 341-351.

(251) Spracklen, D. V.; Heald, C. L. *Atmos. Chem. Phys.* **2014**, *14*, 9051-9059.

(252) Ge, X.; Wexler, A. S.; Clegg, S. L. *Atmos. Environ.* **2011**, *45*, 524-546.

(253) Zhang, Q.; Anastasio, C.; Jimenez-Cruz, M. *J. Geophys. Res. Atmos.* **2002**, *107*, AAC 3-1-AAC 3-9.

(254) Mace, K. A.; Artaxo, P.; Duce, R. A. C. *J. Geophys. Res. Atmos.* **2003**, *108*.

(255) Milne, P.; Zika, R. *J. Atmos. Chem.* **1993**, *16*, 361-398.

(256) Scheller, E. *Atmos. Environ.* **2001**, *35*, 2179-2192.

(257) Mace, K. A.; Kubilay, N.; Duce, R. A. C. *J. Geo. Res. Atmos.* **2003**, *108*.

(258) Wedyan, M. A.; Preston, M. R. *Atmos. Environ.* **2008**, *42*, 8698-8705.

(259) Scalabrin, E.; Zangrando, R.; Barbaro, E.; Kehrwald, N. M.; Gabrieli, J.; Barbante, C.; Gambaro, A. *Atmos. Chem. Phys.* **2012**, *12*, 10453-10463.

(260) Chan, M. N.; Choi, M. Y.; Ng, N. L.; Chan, C. K. *Environ. Sci. Technol.* **2005**, *39*, 1555-1562.

(261) Hock, N.; Schneider, J.; Borrmann, S.; Rompp, A.; Moortgat, G.; Franze, T.; Schauer, C.; Poschl, U.; Plass-Dulmer, C.; Berresheim, H. *Atmos. Chem. Phys.* **2008**, *8*, 603-623.

(262) McFiggans, G.; Artaxo, P.; Baltensperger, U.; Coe, H.; Facchini, M. C.; Feingold, G.; Fuzzi, S.; Gysel, M.; Laaksonen, A.; Lohmann, U.; Mentel, T. F.; Murphy, D. M.; O'Dowd, C. D.; Snider, J. R.; Weingartner, E. *Atmos. Chem. Phys.* **2006**, *6*, 2593-2649.

(263) Schwier, A. N.; Viglione, G. A.; Li, Z.; Faye McNeill, V. *Atmos. Chem. Phys.* **2013**, *13*, 10721-10732.

(264) De Haan, D. O.; Corrigan, A. L.; Tolbert, M. A.; Jimenez, J. L.; Wood, S. E.; Turley, J. J. *Environ. Sci. Technol.* **2009**, *43*, 8184-8190.

(265) Barbaro, E.; Zangrando, R.; Vecchiato, M.; Piazza, R.; Cairns, W. R. L.; Capodaglio, G.; Barbante, C.; Gambaro, A. *Atmos. Chem. Phys.* **2015**, *15*, 5457-5469.

(266) Mandalakis, M.; Apostolaki, M.; Tziaras, T.; Polymenakou, P.; Stephanou, E. G. *Atmos. Environ.* **2011**, *45*, 1003-1009.

(267) Mochizuki, T.; Kawamura, K.; Aoki, K. *Aerosol Air Qual. Res.* **2016**, *16*, 632-639.

(268) Zhang, Q.; Anastasio, C. *Atmos. Environ.* **2001**, *35*, 5629-5643.

(269) Herckes, P.; Valsaraj, K. T.; Collett Jr, J. L. *Atmos. Res.* **2013**, *132-133*, 434-449.

(270) Herrmann, H.; Schaefer, T.; Tilgner, A.; Styler, S. A.; Weller, C.; Teich, M.; Otto, T. *Chem. Rev.* **2015**, *115*, 4259-4334.

(271) Creed, D. *Photochem. Photobiol.* **1984**, *39*, 537-562.

(272) Suzuki, J.; Ueki, T.; Shimizu, S.; Uesugi, K.; Suzuki, S. *Chemosphere* **1985**, *14*, 493-500.

(273) Bianco, A.; Passananti, M.; Perroux, H.; Voyard, G.; Mouchel-Vallon, C.; Chaumerliac, N.; Mailhot, G.; Deguillaume, L.; Brigante, M. *Atmos. Chem. Phys.* **2015**, *15*, 13923-13955.

(274) Dulin, D.; Mill, T. *Environ. Sci. Technol.* **1982**, *16*, 815-820.

(275) Mayer, L. M.; Schick, L. L.; Loder Iii, T. C. *Mar. Chem.* **1999**, *64*, 171-179.

(276) Vivian, J. T.; Callis, P. R. *Biophys. J.* **2001**, *80*, 2093-2109.

(277) Determann, S.; Lobbes, J. M.; Reuter, R.; Rullkotter, J. *Mar. Chem.* **1998**, *62*, 137-156.

(278) Hudson, N.; Baker, A.; Reynolds, D. *River Res. Appl.* **2007**, *23*, 631-649.

(279) Domingues, M. R. M.; Domingues, P.; Reis, A.; Fonseca, C.; Amado, F. M. L.; Ferrer-Correia, A. J. V. *J. Am. Soc. Mass Spectrom.* **2003**, *14*, 406-416.

(280) Turjanski, A. G.; Rosenstein, R. E.; Estrin, D. A. *J. Med. Chem.* **1998**, *41*, 3684-3689.

(281) Hinman, R. L.; Lang, J. *Biochemistry* **1965**, *4*, 144-158.

(282) Temussi, F.; Cermola, F.; DellaGreca, M.; Iesce, M. R.; Passananti, M.; Previtera, L.; Zarrelli, A. *J. Pharm. Biomed. Anal.* **2011**, *56*, 678-683.

(283) Intergovernmental Panel on Climate Change, http://www.ipcc.ch/.

(284) Houdier, S. p.; Barret, M.; Dominé, F.; Charbouillot, T.; Deguillaume, L.; Voisin, D. *Anal. Chim. Acta* **2011**, *704*, 162-173.

(285) Zellner, R.; Exner, M.; Herrmann, H. *J. Atmos. Chem.* **1990**, *10*, 411-425.

(286) Yu, X.-Y.; Barker, J. R. *J. Phys. Chem. A* **2003**, *107*, 1313-1324.

(287) Bianco, A.; Passananti, M.; Perroux, H.; Voyard, G.; Mouchel-Vallon, C.; Chaumerliac, N.; Mailhot, G.; Deguillaume, L.; Brigante, M. *Atmos. Chem. Phys.* **2015**, *15*, 9191-9202.

(288) Delort, A.-M.; Vaitilingom, M.; Amato, P.; Sancelme, M.; Parazols, M.; Mailhot, G.; Laj, P.; Deguillaume, L. *Atmos. Res.* **2010**, *98*, 249-260.

(289) Burrows, S. M.; Elbert, W.; Lawrence, M. G.; Poschl, U. *Atmos. Chem. Phys.* **2009**, *9*, 9263-9280.

(290) Amato, P.; Menager, M.; Sancelme, M.; Laj, P.; Mailhot, G.; Delort, A.-M. *Atmos. Environ.* **2005**, *39*, 4143-4153.

(291) Amato, P.; Parazols, M.; Sancelme, M.; Laj, P.; Mailhot, G.; Delort, A.-M. *FEMS Microbiol. Ecol.* **2007**, *59*, 242-254.

(292) Vaitilingom, M. l.; Attard, E. O.; Gaiani, N.; Sancelme, M.; Deguillaume, L.; Flossmann, A. I.; Amato, P.; Delort, A.-M. *Atmos. Environ.* **2012**, *56*, 88-100.

(293) Ahern, H. E.; Walsh, K. A.; Hill, T. C. J.; Moffett, B. F. *Biogeosciences* **2007**, *4*, 115-124.

(294) Fuzzi, S.; Mandrioli, P.; Perfetto, A. *Atmos. Environ.* **1997**, *31*, 287-290.

(295) DeLeon-Rodriguez, N.; Lathem, T. L.; Rodriguez-R, L. M.; Barazesh, J. M.; Anderson, B. E.; Beyersdorf, A. J.; Ziemba, L. D.; Bergin, M.; Nenes, A.; Konstantinidis, K. T. *Proc. Natl. Acad. Sci.* **2013**, *110*, 2575-2580.

(296) Kourtev, P. S.; Hill, K. A.; Shepson, P. B.; Konopka, A. *Atmos. Environ.* **2011**, *45*, 5399-5405.

(297) Santl-Temkiv, T.; Finster, K.; Dittmar, T.; Hansen, B. M.; Thyrhaug, R.; Nielsen, N. W.; Karlson, U. G. *PLoS One* **2013**, *8*, e53550.

(298) Matulova, M.; Husarova, S.; Capek, P.; Sancelme, M.; Delort, A.-M. *Environ. Sci. Technol.* **2014**, *48*, 14238-14247.

(299) Joly, M.; Amato, P.; Sancelme, M.; Vinatier, V.; Abrantes, M.; Deguillaume, L.; Delort, A.-M. *Atmos. Environ.* **2015**, *117*, 92-98.

(300) Sattler, B.; Puxbaum, H.; Psenner, R. *Geophys. Res. Lett.* **2001**, *28*, 239-242.

(301) Amato, P.; Demeer, F.; Melaouhi, A.; Fontanella, S.; Martin-Biesse, A. S.; Sancelme, M.; Laj, P.; Delort, A. M. *Atmos. Chem. Phys.* **2007**, *7*, 4159-4169.

(302) Hill, K. A.; Shepson, P. B.; Galbavy, E. S.; Anastasio, C.; Kourtev, P. S.; Konopka, A.; Stirm, B. H. C. D. *Journal of Geophysical Research: Atmospheres* **2007**, *112*.

(303) Charbouillot, T.; Gorini, S.; Voyard, G.; Parazols, M.; Brigante, M.; Deguillaume, L.; Delort, A.-M.; Mailhot, G. *Atmos. Environ.* **2012**, *56*, 1-8.

(304) Griffith, E. C.; Carpenter, B. K.; Shoemaker, R. K.; Vaida, V. *Proc. Natl. Acad. Sci.* **2013**, *110*, 11714-11719.

(305) Ervens, B.; Feingold, G.; Frost, G. J.; Kreidenweis, S. M. *J. Geophys. Res.* **2004**, *109*, D15205.

(306) Warneck, P. *Atmos. Environ.* **2003**, *37*, 2423-2427.

(307) Tan, Y.; Carlton, A. G.; Seitzinger, S. P.; Turpin, B. J. *Atmos. Environ.* **2010**, *44*, 5218-5226.

(308) <http://www.genome.jp/kegg/pathway.html>.

(309) Schrader, J.; Schilling, M.; Holtmann, D.; Sell, D.; Filho, M. V.; Marx, A.; Vorholt, J. A. *Trends Biotechnol.* **2009**, *27*, 107-115.

(310) Husarova, S.; Vaitilingom, M.; Deguillaume, L.; Traikia, M.; Vinatier, V.; Sancelme, M.; Amato, P.; Matulova, M.; Delort, A.-M. *Atmos. Environ.* **2011**, *45*, 6093-6102.

(311) http://www.genome.jp/kegg-bin/show_pathway?rn00020+R00342.

(312) Ariya, P. A.; Nepotchatykh, O.; Ignatova, O.; Amyot, M. C. *Geophys. Res. Lett.* **2002**, *29*, 34-1-34-4.

(313) Côté, V.; Kos, G.; Mortazavi, R.; Ariya, P. A. *Sci. Total Environ.* **2008**, *390*, 530-537.

(314) Vaïtilingom, M.; Amato, P.; Sancelme, M.; Laj, P.; Leriche, M.; Delort, A.-M. *Appl. Environ. Microbiol.* **2010**, *76*, 23-29.

(315) Vaitilingom, M.; Charbouillot, T.; Deguillaume, L.; Maisonobe, R.; Parazols, M.; Amato, P.; Sancelme, M.; Delort, A. M. *Atmos. Chem. Phys.* **2011**, *11*, 8721-8733.

(316) Herlihy, L. J.; Galloway, J. N.; Mills, A. L. *Atmos. Environ.* **1987**, *21*, 2397-2402.

(317) Krumins, V.; Mainelis, G.; Kerkhof, L. J.; Fennell, D. E. *Environ. Sci. Technol. Lett.* **2014**, *1*, 376-381.

(318) Vorob'eva, L. I. *Appl. Biochem. Microbiol.* **2004**, *40*, 217-224.

(319) Dieser, M.; Greenwood, M.; Foreman, C. M. *Arct., Antarc., Alp. Res.* **2010**, *42*, 396-405.

(320) Tong, Y.; Lighthart, B. *FEMS Microbiol. Ecol.* **1998**, *26*, 311-316.

(321) Fahlgren, C.; Hagstrom, Ã.; Nilsson, D.; Zweifel, U. L. *Appl. Environ. Microbiol.* **2010**, *76*, 3015-3025.

(322) Zweifel, U. L.; Hagstrom, Ã. k.; Holmfeldt, K.; Thyrhaug, R.; Geels, C.; Frohn, L. M.; Skjeth, C. A.; Karlson, U. G. *Aerobiologia* **2012**, *28*, 481-498.

(323) Davey, M.; O'toole, G. *Microbiol. Mol. Biol. Rev.* **2000**, *64*, 847-867.

(324) Marinoni, A.; Parazols, M.; Brigante, M.; Deguillaume, L.; Amato, P.; Delort, A.-M.; Laj, P.; Mailhot, G. *Atmos. Res.* **2011**, *101*, 256-263.

(325) Cheize, M.; Sarthou, G. r.; Croot, P. L.; Bucciarelli, E.; Baudoux, A.-C.; Baker, A. R. *Anal. Chim. Acta* **2012**, *736*, 45-54.

(326) Gledhill, M.; Buck, K. N. *Front. Microbiol.* **2012**, *3*.

UNIVERSITE BLAISE PASCAL

U.F.R. Sciences et Technologies

ECOLE DOCTORALE DES SCIENCES FONDAMENTALES

Résumé de THESE

Présenté pour obtenir le grade de

DOCTEUR D'UNIVERSITE

Spécialité : Chimie Physique

Angelica BIANCO

Formation photoinduite du radical hydroxyle dans la phase aqueuse du nuage : impact sur les acides carboxyliques et les acides aminés.

Le cycle de l'eau vise à stocker de l'eau et à la déplacer sur, dans et au-dessus de la Terre. Les transformations chimiques et photochimiques dans les eaux de surface et souterraines ont réveillé l'intérêt de la communauté scientifique pour la raison que l'eau est un des besoins les plus primordiaux de l'humanité et de formes de vie sur la Terre. Bien que l'atmosphère ne puisse pas être un grand entrepôt d'eau, c'est la voie la plus rapide de déplacement de l'eau autour du globe. Pour avoir une vision complète du devenir des composés, il faut considérer aussi les transformations dans l'eau en phase vapeur : pour cette raison il est nécessaire d'étudier la composition de phase aqueuse atmosphérique et sa réactivité, dans le but de comprendre comment les émissions naturelles et anthropogéniques peuvent influencer la déposition de polluants et le cycle des nuages. Ma thèse est donc centrée sur l'étude de l'eau de nuage.

Pourquoi étudier l'eau de nuage ? On commence par le cycle de l'eau : l'eau s'évapore des océans et plus généralement des eaux de surface, se condense, forme les nuages puis précipite sous formes de pluie, de neige ou de grêle. Mais ce cycle n'est pas si simple : nous n'aurions pas les nuages sans la présence de noyaux de condensation, des petites particules qui facilitent la formation des gouttelettes, que nous appelons en anglais CCN (cloud condensation nuclei). De plus, les émissions naturelles ou anthropogéniques sous forme de particules, d'aérosols ou de gaz, peuvent être englobés dans les gouttelettes des nuages où elles sont transformés chimiquement, photochimiquement ou bien subissent des transformations microbiologiques ou des redistribution en fonction de la microphysique. Les composés transformés peuvent subir une déposition sèche ou humide (sous forme de pluie) ou, si l'eau s'évapore, rester dans l'atmosphère. Ces transformations peuvent avoir un impact sur la pollution de l'atmosphère si elles rendent ces composés plus polluants. Ce n'est pas le seul effet car l'eau peut s'évaporer de la gouttelette et le noyau solide, ou liquide concentré, appelé aérosol secondaire (SOA, Secondary organic aerosol) peut agir à son tour comme noyau de condensation. Les émissions ont un impact sur la formation d'aérosol, sur le cycle de nuage et, plus globalement, un impact sur le cycle de l'eau.

La première étude concernant les nuages a été publiée en 1922 par Bergeron, qui a découvert l'importance des CCN. Ensuite, pendant plus de 60 ans, il y a eu un développement impressionnant des recherches au sujet de la microphysique des nuages. D'un point de vue chimique, l'intérêt scientifique pour l'étude de l'atmosphère a commencé avec les phénomènes de pollution du dernier siècle, comme le smog de Londres (1952). En premier lieu les chercheurs se sont occupés de la phase gazeuse, de sa composition et réactivité. Seulement à partir de 1982 on assiste au développement des études sur la chimie de l'eau de

nuage : sur la composition chimique, sur les oxydants majeurs et sur la caractérisation de la matière organique. A partir de 1990 on a le plein développement de la recherche sur ces sujets.

Le nuage est un milieu atmosphérique très complexe : il y a environ 100 gouttelettes d'eau et de mille à cent mille particules d'aérosol par centimètre cube, en fonction de la propreté de l'air. C'est un milieu dynamique et gouverné par la microphysique où la gouttelette d'eau est en équilibre entre évaporation et condensation et son temps de vie est très court (de quelques secondes à quelques minutes).

La première question que les chercheurs se sont posé est : « quelle est la composition de l'eau de nuage ? ». Les composés présents dans l'eau des nuages peuvent provenir de la dissolution de la fraction soluble du CCN au moment de la formation de la gouttelette ou par le transfert de la phase gaz à la phase liquide. Le camembert en Figure 1 présente les principaux ions inorganiques, dont la concentration varie de 10 à 200 µM. La valeur de pH est de 5,2 en moyenne mais peut varier entre 4 et 7. Plusieurs oxydants sont présents, comme le peroxyde d'hydrogène, avec une concentration allant jusqu'à 50 µM. Si les composants inorganiques et leur concentration sont désormais bien connus, la matière organique est beaucoup moins caractérisée : 1% environ d'aldéhydes, 10% d'acides carboxyliques et 89 % est inconnu à ce jour.

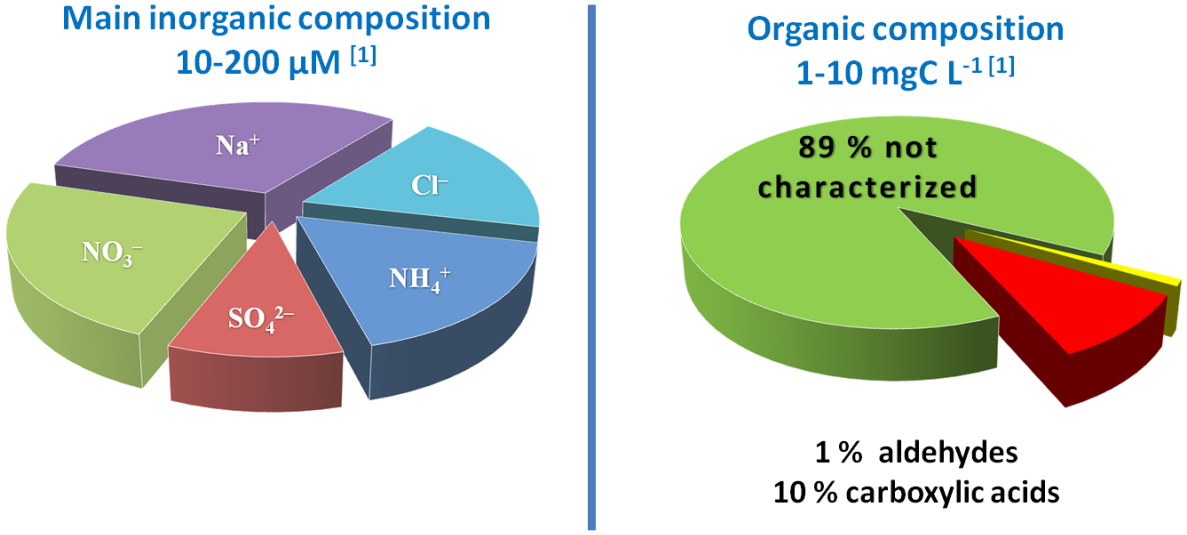

Figure 1: Composition organique et inorganique de la phase aqueuse du nuage.

[1] Deguillaume, L. et al., *Atmos. Chem. Phys.* 2014, *14*, (3), 1485-1506.

Si la composition est peu connue, la réactivité l'est moins encore : la plupart des études concernent la phase liquide alors que la réactivité à l'interface n'a jamais été étudiée. A l'obscurité, on peut avoir la réaction de Fenton et de l'ozone, même si celui-ci est limité par la

faible solubilité du gaz. La majorité des réactions sont de type photochimique : on peut avoir la photolyse directe du composé, comme observé par l'acide pyruvique qui donne l'acide lactique, l'acide acétique et l'acétoïne. Seulement peu de composés peuvent absorber la radiation solaire : de ce fait la photolyse directe est rarement observée et la majorité des réactions est de type « photolyse indirecte ». Des espèces réactives sont produites par photolyse directe de précurseurs tels que le peroxyde d'hydrogène, les nitrates et les nitrites et ces espèces réagissent avec les composés organiques. L'espèce la plus réactive est le radical hydroxyle ($HO^{\bullet}$) qui réagit selon différentes voies : par addiction sur les doubles liaisons, extraction d'hydrogène, transfert d'électron ou addition sur anneau aromatique. Chaque composé absorbe différemment la lumière et réagit différemment avec le radical hydroxyle. Pour ce motif, c'est bien difficile de comprendre les chemins de dégradation des composés.

Cette introduction permet de comprendre que l'eau de nuage est un milieu peu connu mais très important d'un point de vu chimique, pour la transformation chimique des composés mais aussi pour leur déposition sèche ou humide sur la surface terrestre ou, encore pour leur transport. De plus, les nuages sont responsables de l'effet serre de notre planète et la formation d'aérosol secondaire peut potentiellement amener à un changement de la quantité/fréquence des nuages, qui peut impacter la température terrestre. Pour ce motif, il est nécessaire d'étudier l'eau de nuage, en particulier sa composition organique et sa réactivité. Ma thèse se développe sur trois axes principaux : la capacité oxydante de l'eau de nuage, à travers l'étude de la photogeneration du radical hydroxyle et de la corrélation entre sa vitesse de formation et la concentration des sources inorganiques ; la caractérisation de la composition organique de l'eau de nuage, a travers la détection et quantification du tryptophane et de 16 acides aminés ; J'ai ensuite étudié la réactivité par photolyse directe et indirecte de l'acide tartronique, un acide à trois atomes de carbone qui peut être considéré un proxy de plusieurs composés dans l'atmosphère, et du tryptophane. La Figure 2 schématise les axes principaux de mon travail : l'étude de la capacité oxydante, en bleu, la caractérisation, en vert, et la réactivité, en rouge.

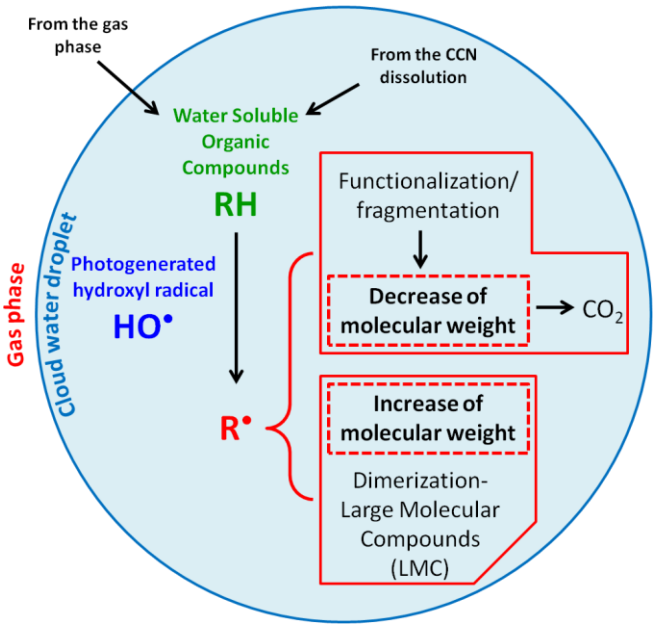

Figure 2: Schématisation des mécanismes dans la gouttelette de l'eau de nuage.

Le travail sur l'eau de nuage implique forcement un échantillonnage. Contrairement à ce qu'on pense, l'échantillonnage du nuage est très difficile : il faut avoir un bon site et le matériel approprié. L'eau de nuage est prélevée sur le toit de l'observatoire au sommet du puy de Dôme, où plusieurs paramètres comme la température, le contenu en eau liquide, le rayon des gouttelettes et le contenu en eau liquide sont mesurés en continu. L'eau de nuage est prélevée grâce à l'impacteur à nuage, composé d'une pompe d'aspiration et d'un impacteur montré en Figure 3.

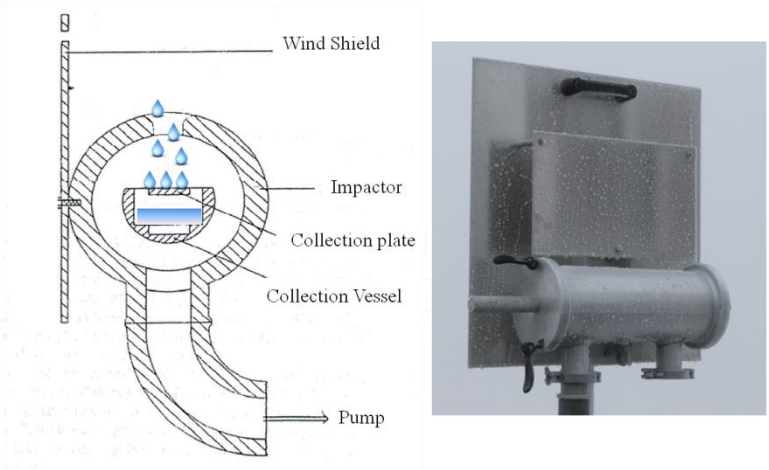

Figure 3: Impacteur à nuage.

Le vent impacte sur la plaque de l'impacteur et les gouttelettes de nuage sont aspirées par la fente. Elles impactent sur la plaque de collection et sont récoltées sous forme de solution dans le collecteur. L'eau de nuage est ensuite filtrée et caractérisée spectroscopiquement par matrice de fluorescence (EEM, Excitation Emission Matrix) et par spectre UV-Visible. On

mesure également des parametres physico-chimiques (la température, le potentiel redox, le pH), la composition chimique à travers la concentration des principaux cations et anions et le carbone organique dissout, et la concentration des oxydants majeurs (H_2O_2, fer, nitrites). De plus, pendent la thèse on a commencé à mesurer la vitesse et le rendement quantique polychromatique de formation du radical hydroxyle. En parallèle, à l'aide du modèle de retrotrajectoire HYSPLIT (NOAA), on évalue la provenance de la masse d'air sur 72h. L'analyse de composantes principaux (ACP) sur certains paramètres nous permet de corréler la composition de l'échantillon avec l'origine de la masse d'air en tenant en compte que, l'origine différente est liée à une composition différente et à une réactivité différente.

La mesure de la vitesse de formation du radical hydroxyle et de son rendement quantique nous a amené à l'étude de la capacité oxydante de l'eau de nuage et à sa corrélation avec la concentration des sources.

Le radical hydroxyle est l'oxydant principal dans l'eau de nuage. Il est généré par l'interaction de la lumière avec des précurseurs comme le peroxyde d'hydrogène, les nitrates, les nitrites et le fer. La matière organique, représentée en Figure 2 comme RH, réagit avec le radical hydroxyle pour former un radical R point qui peut suivre deux chemins en compétition : l'oxydation accompagné de formation des composés à poids moléculaire moins élevé, ou l'oligomérization/accretion, avec formation des composées à poids moléculaire plus élevé. La vitesse de formation du radical hydroxyle est un paramètre fondamental pour déterminer le chemin préférentiel. Dans la littérature, peu de données sont disponibles sur la vitesse de formation d'$HO^{\bullet}$ et encore moins sur le rendement quantique polychromatique.

Si on compare le spectre d'absorption des échantillons d'eau de nuage avec le spectre d'emission solaire, on peut facilement voir que le recouvrement entre les spectres peut donner lieu à des réactions de photolyse, directe et indirecte, dont la photogeneration des radicaux hydroxyles. La vitesse de formation du radical hydroxyle a été mesurée grâce à une sonde chimique, l'acide téréphthalique, non fluorescent, qui réagit avec $HO^{\bullet}$ pour former l'acide hydroxytéréphthelique, fluorescent, dont on peut mesurer la vitesse de formation. Cette vitesse est corrélée à celle de formation d'$HO^{\bullet}$ par le paramètre gamma, dépendent de la température et du pH. Le rendement quantique polychromatique est calculé comme rapport entre la vitesse de formation u radical hydroxyle et l'intensité de radiation absorbée par la solution.

41 échantillons ont été analysés et la vitesse de formation d' $HO^{\bullet}$ présente des valeurs comprises entre 10^{-12} et 10^{-10} M s^{-1} tandis que le rendement quantique est de l'ordre de 10^{-5} à 10^{-3}. Les valeurs changent en fonction de la provenance de la masse d'air et, pour la vitesse de

formation d' HO•, sont plus élevés pour un nuage d'origine continentale que pour un nuage d'origine océanique ou désertiques. La question qu'on s'est posée est: Existe-t-il une corrélation entre la vitesse de formation d' HO• et la concentration des sources inorganiques ?

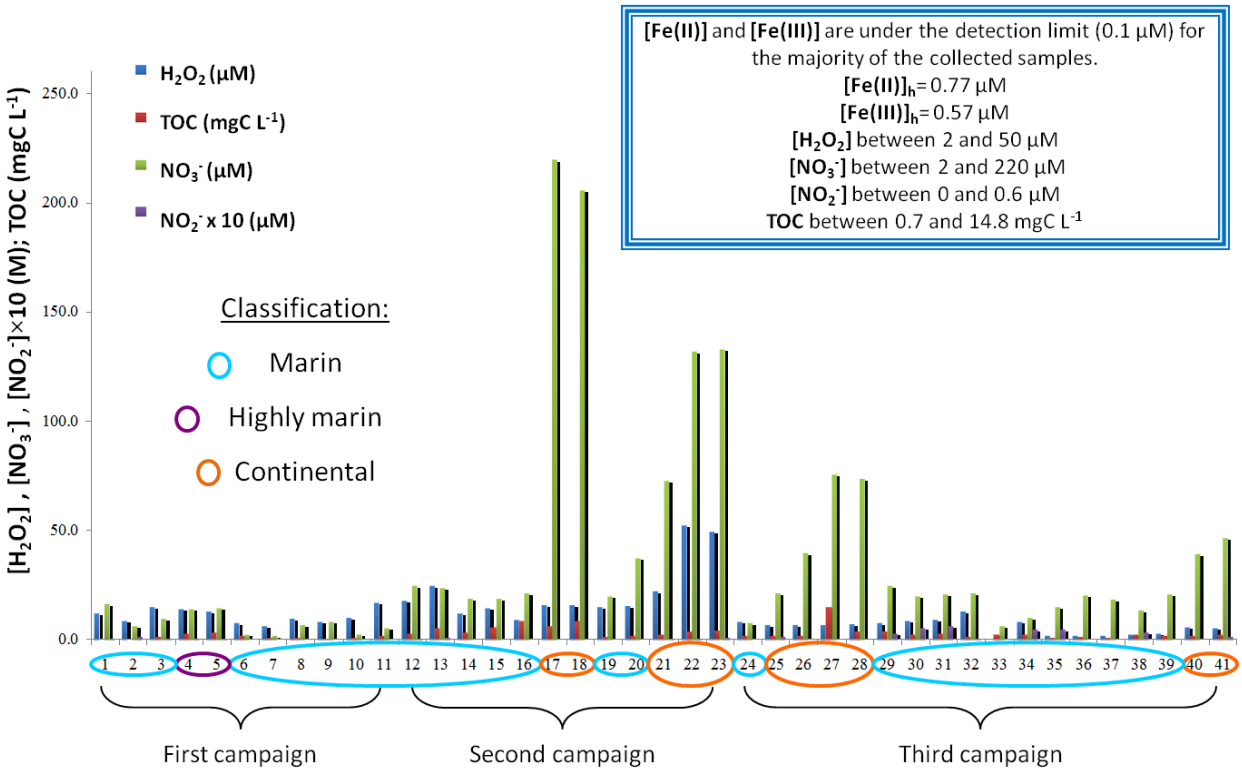

Figure 4: Hydrogen peroxide, nitrate, nitrite and TOC concentrations in cloud samples collected during three campaigns in 2013-2014.

La Figure 4 montre en ordonné la concentration des sources d' HO• telle que le peroxyde d'hydrogène, les nitrates et les nitrites, dans les échantillons analysés. Il y a aussi la valeur de TOC (principal piège d' HO•). En abscisse le numéro d'échantillon. Le fer est sous la limite de détection pour la plupart des échantillons, le peroxyde d'hydrogène est entre 2 et 50 µM, les nitrates : entre 2 et 220 µM, les nitrites : entre 0 et 0,6 µM et la TOC a une valeur moyenne de 3 mgC L^{-1}. En couleur la classification des échantillons en marin (bleu clair), fortement marin (violet) et continentaux (orange). On peut bien voir que la concentration des sources est plus élevée pour les nuages d'origine continentale.

Pour trouver expérimentalement la corrélation entre la vitesse de formation d'HO• et la concentration des sources, on a cherché la corrélation entre le paramètre $R^{f}_{HO•}$ et la concentration des sources en eau ultrapure. Nous avons pu remarquer que les pentes pour le peroxyde et pour le nitrite sont quasi équivalentes, alors que les nitrates ont une pente beaucoup plus faible (production de radicaux moins élevée). Tout se joue donc sur la concentration: vu que le peroxyde d'hydrogène est plus concentré, on peut estimer que sa

photolyse est la source principale de radicaux hydroxyles. Pour mieux comprendre le rôle du fer et des ions nitrite et nitrate j'ai collaboré avec le LaMP qui a mis au point un modèle de chimie de nuage M2C2 (Model of Multiphase Cloud Chemistry). Les vitesses de formation d' $HO^{\bullet}$ ont été calculées théoriquement avec le modèle M2C2 en fonction de la concentration des sources, de la température, du pH et du spectre de la lampe Xénon.

Le modèle M2C2 arrive à reproduire l'ordre de grandeur de la vitesse de formation d' $HO^{\bullet}$ mais il y a quelques divergences pour les échantillons contenant du fer. Pour ce motif, les vitesses expérimentales de photolyse de peroxyde d'hydrogène, nitrate et nitrite ont été introduites dans le modèle et la réactivité du fer a été supprimée. Finalement, avec les nouvelles conditions, le modèle estime des valeurs de vitesse de formation d' $HO^{\bullet}$ plus proches des valeurs expérimentales. On trouve donc que la vitesse de formation d' $HO^{\bullet}$ est due en moyenne pour 90% au peroxyde d'hydrogène, 5 % au nitrate et 2% au nitrite, comme montré en Figure 5.

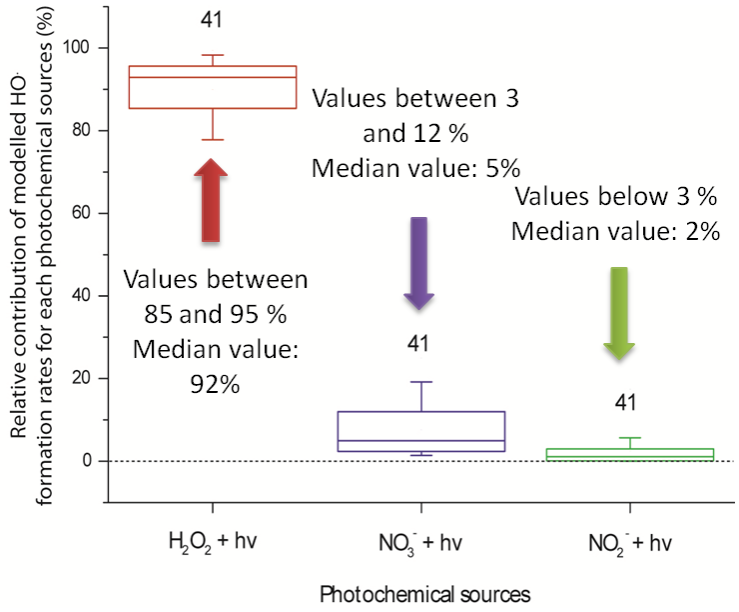

Figure 5: Distribution de la contribution relative de chaque source photochimique à la vitesse de formation du radical hydroxyle pour la totalité des échantillons d'eau de nuage.

En conclusion, la vitesse et le rendement quantique de formation photoinduite du radical hydroxyle ont été estimés pour plusieurs échantillons d'eau de nuage. La formation du radical $HO^{\bullet}$ est principalement due à la photolyse du peroxyde d'hydrogène alors que les nitrates et les nitrites contribuent pour moins de 10 % à la vitesse totale. Le rôle du fer pour les échantillons analysés est négligeable. Les résultats ont été comparés avec la sortie du modèle M2C2 et le modèle à été calibré avec des données expérimentales pour mieux décrire la

corrélation entre la vitesse de formation d' $HO^{\bullet}$ et les sources inorganiques. L'ensemble de ces résultats ont été publiés dans la revue Atmospheric Chemistry and Physics en 2015.

Le radical hydroxyle est donc un des acteurs principaux de la chimie atmosphérique avec la lumière solaire. Pour mieux comprendre leur impact sur le devenir des composés organique on a étudié l'acide tartronique.

L'acide tartronique est un acide à trois atomes de carbone et il a été détecté dans différent milieu atmosphériques comme le PM10 et l'aérosol continental et marin. Il est produit par dégradation chimique et microbiologique des sucres, comme le glucose, de la dissolution du CCN et de l'oxydation d'acides carboxyliques comme l'acide lactique et malonique. Il peut potentiellement se trouver dans l'eau de nuage et produire par photolyse directe et indirecte de l'oxalate, du formiate et du dioxyde de carbone. Ce composé a été peu caractérisé d'un point de vue de sa réactivité et de ses propriétés spectroscopiques. De plus, dans les modèles atmosphériques, comme M2C2, il y a que des hypothèses de réactivité basées sur les relations structure-activité. Ce travail expérimental vise à confirmer ces hypothèses en passant par l'étude des propriétés spectroscopiques, l'effet du pH, le rendement quantique de photolyse, la réactivité, les intermédiaires de réaction et les rapports de branchement. Ce travail, en cours, est mené en collaboration avec le LaMP.

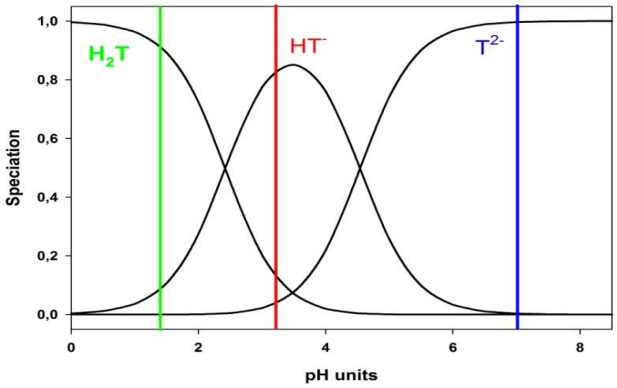

Figure 6: Speciation de l'acide tartronique.

La Figure 6 montre la spéciation de l'acide tartronique en fonction du pH. A pH 7 la forme di-anionique est prévalente, à pH 3.2 on a un mélange des trois formes avec une dominance de la forme mono-anionique, enfin, à pH 1.6 on a majoritairement la forme protonée. A valeurs de pH inferieurs à 1.6 le spectre évolue en fonction du temps, comme montré dans notre étude. Le pH de l'eau de nuage étant normalement supérieur à 3, la forme protonée n'a pas été considérée dans cette étude. On a calculé le coefficient d'extinction molaire pour les deux formes anioniques, montrés en graphique, et le rendement quantique polychromatique à pH 7 et 3.2.

Ensuite on a irradié, avec l'enceinte montrée pour l'étude de la capacité oxydante, des solutions de tartronique de concentration 10 µM à pH 4 et 7 et elles ont été analysées par chromatographie ionique, comme montré en Figure 7.

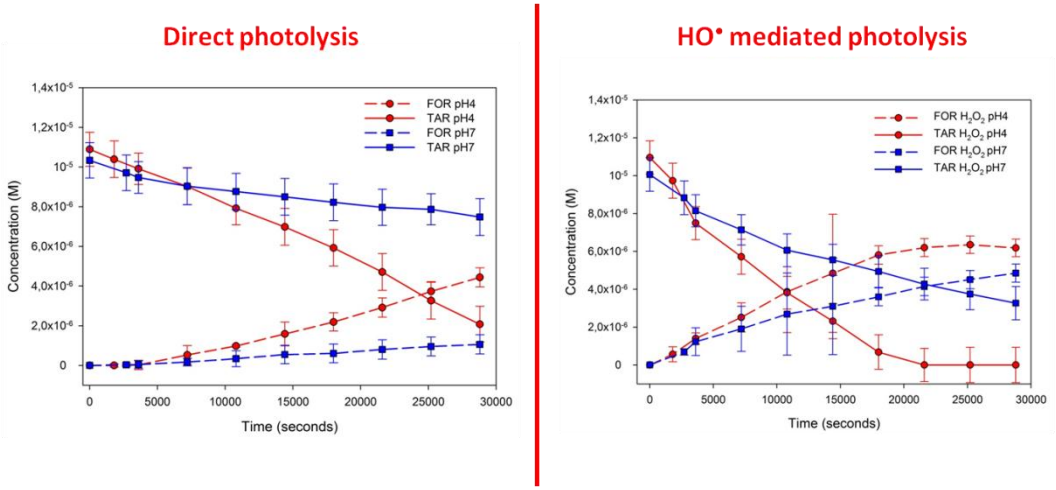

Figure 7: Photolyse indirecte (à gauche) et directe (à droite) du tartronique à valeurs de pH 4 et 7.

La forme mono-anionique, prévalent à pH 4 se dégrade plus rapidement que la forme di-anionique, présente à pH 7 (en rouge), mais les deux procédées mènent à la formation de formiate (en noir). On n'a pas observé la production d'oxalate. On a répété les mêmes manipulations en présence de peroxyde d'hydrogène à 100 µM pour étudier la réactivité avec $HO^{\bullet}$ (Figure 7 à droite). Ce graphique est le résultat de la combinaison entre photolyse directe et indirecte et on peut en déduire que le tartronique réagit avec $HO^{\bullet}$. Encore une fois la forme HT^{-} semble être la plus réactive. Les constantes de réactivité entre le tartronique et $HO^{\bullet}$ (à pH différents) ont été déterminées expérimentalement par Laser Flash Photolysis avec la méthode du thiocyanate. On a calculé une constante pour les trois valeurs de pH et estimé, en fonction de la spéciation, les constantes de second ordre pour chaque forme. La forme mono-anionique est effectivement la plus réactive avec une constante de $5.9\ 10^{8}\ M^{-1}s^{-1}$.

La conclusion présentée ici n'est que partielle : le coefficient d'extinction molaire a été déterminé ainsi que l'effet du pH, le rendement quantique de photolyse et la réactivité par irradiation continue et pulsé mais il nous reste à identifier les produits de réaction par spectroscopie RMN et chromatographie ionique, à déterminer le rapport de branchement et à comparer toutes ces données avec les sorties du modèle M2C2.

Je vous ai montré que le radical hydroxyle est produit dans l'eau de nuage et qu'il réagit avec la matière organique, comme l'acide tartronique. Le principal problème est que la composition de la matière organique est méconnue pour la quasi-totalité : le 10 % est

constitué d'acides carboxyliques et le 1 % d'aldéhydes mais on à peu d'idée, et encore moins de mesures expérimentales, sur la composition du restant 89 %.

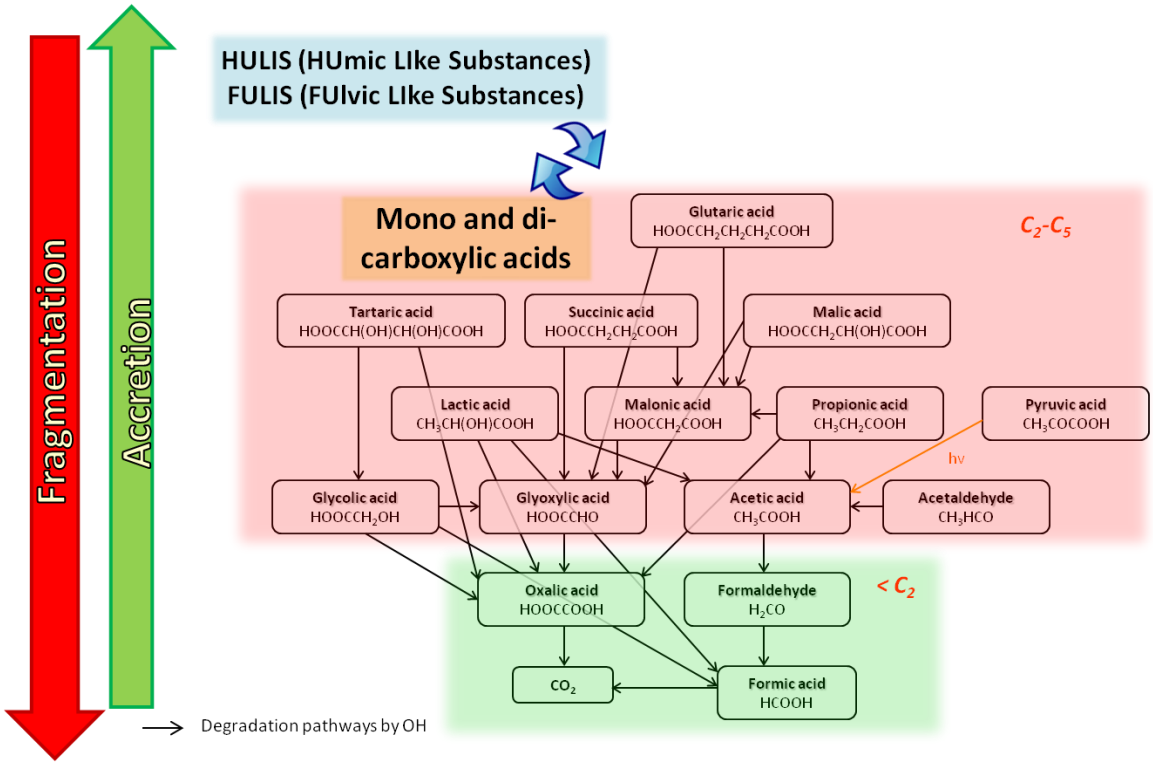

Figure 8: Mécanismes de dégradation des acides carboxyliques dans l'eau de nuage.

La Figure 8 regroupe tous les acides détectés dans l'eau des nuages et leurs chemins réactionnels d'oxydation induit par le radical hydroxyle. On peut voir que l'oxydation est généralement accompagnée par une diminution du poids moléculaire et que tous les composés mènent à la formation des acides formique, oxalique et de CO_2. Dans l'eau de nuage, on n'a pas que des acides : récemment des composés à poids moléculaire élevé (nommés HULIS et FULIS) ont été identifiés. Ils sont similaires aux acides humiques et fulviques présents dans les eaux de surface mais sont très difficiles à caractériser. On ne sait pas, mais on peut supposer, que des produits de leur dégradation soient des acides carboxyliques. La question qui se pose est : qui a-t-il entre les composés à poids moléculaire élevé et les composés très oxydés à faible poids moléculaire ?

Chaque échantillon a été analysé par matrice de fluorescence, dite matrice EEM, d'excitation-émission. Si on agrandi le signal de la matrice en Figure 9, on voit la présence de deux taches : une première A, plus intense attribuable aux HULIS et une deuxième T attribuable au tryptophane et à ses dérivés, dit TRYLIS (tryptophan like substances).

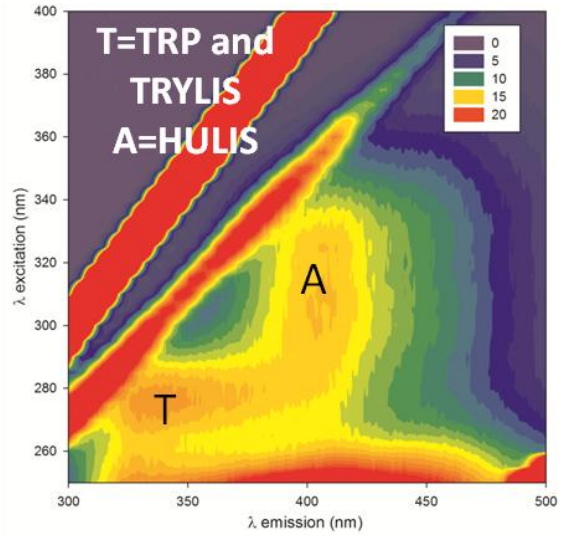

Figure 9: Matrice de fluorescence EEM d'un échantillon d'eau de nuage.

Le TRP est un acide aminé qui a déjà été quantifié comme molécule libre ou combiné dans l'aérosol continental et dans le brouillard. Le tryptophane présent deux signaux de fluorescence : un, moins intense, à la longueur d'onde d'excitation de 275 nm et un deuxième, plus intense, à la longueur d'onde d'excitation de 220 nm.

Le TRP a été quantifié dans 23 échantillons d'eau de nuage : par matrice de fluorescence on a considéré seulement le signal à excitation 275 nm et on a fait l'approximation que la fluorescence soit due uniquement au tryptophane et pas aux TRYLIS. On obtient ainsi une valeur surestimée qui ne tient ni compte de la forme libre ou combiné de la molécule, ni de la contribution au signal des dérivés du tryptophane (1.7×10^{-7} M). Les mêmes échantillons ont été analysés par chromatographie liquide avec détection en fluorescence et la concentration moyenne trouvée est de l'ordre de 60 nM, plus faible que celle déterminé par EEM. On a fait l'hypothèse que la forme combinée du tryptophane soit des résidus de protéines et on a acidifié nos échantillons pour les hydrolyser partiellement. Le TRP a alors été trouvé dans 8 échantillons.

Malgré que sa détection soit assez difficile avec cette méthode sans pré-concentration ou dérivation, le TRP dans les nuages est donc présent. On a donc étudié son devenir sous irradiation UVA. En premier lieu on a estimé le rendement quantique de photolyse du TRP de l'ordre de $8{,}4\times10^{-4}$. La photolyse directe est donc peu efficace, dans nos conditions et pour les temps considérés, pour la transformation du TRP. On est donc passé à la photolyse indirecte: la constante de réactivité de second ordre avec $HO^{\bullet}$ est de l'ordre de 10^{10} M^{-1} s^{-1}, proche de la limite de diffusion. On a suivi la dégradation du TRP à 10 µM dans l'eau ultrapure avec et sans peroxyde d'hydrogène mais également en eau synthétique de nuage d'origine

continentale ou océanique. L'eau synthétique à été préparé en multipliant par 10 la concentration moyenne de l'eau de nuage en sulfate, chlorure, nitrate et nitrite. La dégradation est accélérée en eau synthétique par la présence des ions nitrites et nitrates en concentration non négligeable et irradié dans leur domaine d'absorption.

Les solutions irradiées ont été analysée par spectrométrie de masse. On a pu voir la formation de TRP mono et di hydroxyle, de n-formylkinurenine, d'indole, de produits de déamination, des isomères de la sérotonine et de composés à poids moléculaire élevé qui n'ont pas pu être identifiés. En plus, l'analyse par chromatographie ionique a mis en évidence la formation d'acétate et de formiate.

Les solutions irradiées on été analysées aussi par spectroscopie de fluorescence et on remarque, dans la matrice B, la présence d'un nouveau signal. Si on soustrait, la matrice A de la matrice B, on voit que le signal est centré à longueur d'onde d'excitation et d'émission telles qu'il est identifiable avec l'empreinte de fluorescence des acides humiques selon la classification de Coble (Figure 10).

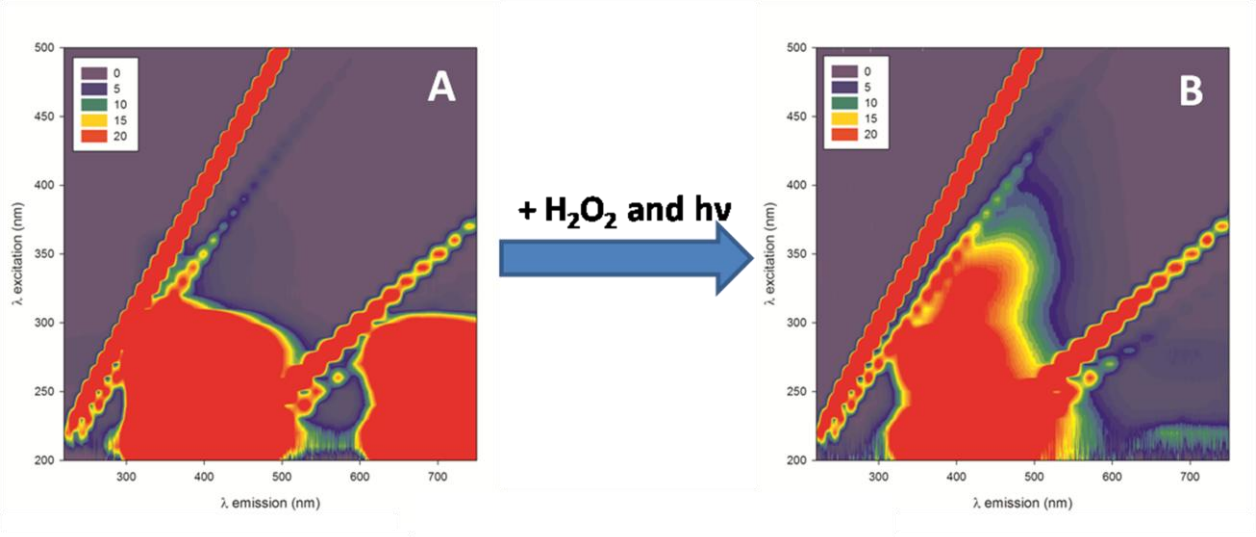

Figure 10: EEM d'une solution de TRP avant et apres irradiation.

Peut-on en déduire que l'irradiation du TRP, à faible concentration, en présence de radicaux hydroxyles, puisse mener à la formation de composés à poids moléculaire élevé avec une empreinte de fluorescence typique des acides humiques ? Ce phénomène peut-il être également observé dans l'eau de nuage ?

En résumé, j'ai quantifié pour la première fois le TRP par spectroscopie de fluorescence et par chromatographie avec détection en fluorescence dans les échantillons d'eau de nuage. Sa réactivité, avec les radicaux hydroxyles photo-générés, a été étudiée en eau ultrapure et en eau de nuage synthétique. L'analyse de solutions irradiées a mis en évidence la formation de

composés à poids moléculaire plus faibles et de composés à poids moléculaire plus élevé avec une empreinte de fluorescence des acides humiques. Ces résultats ont fait l'objet d'un article publié dans Atmospheric Environment en 2016.

Le tryptophane peut donc rentrer dans le chemin montré précédemment comme source d'acides acétique et formique et comme possible source d'HULIS et FULIS. Mais le TRP est seulement 1 des 20 acides aminés les plus communs. Que se passe-t-il pour les autres ?

Vu les résultats très intéressants obtenus pour le TRP, nous nous sommes intéressés à la détection des acides aminés dans l'eau de nuage, l'estimation de leur réactivité avec le radical hydroxyle ainsi que la comparaison avec la réactivité des acides carboxyliques et de la matière organique dissoute.

Les acides aminés sont les briques qui constituent les protéines. La structure fondamentale présente un groupement acide (carboxylique), un groupement basique (amine) et une chaine latérale R différent d'un acide aminé à l'autre. Leur présence dans le nuage n'est pas du au transfert de la phase gaz car ils ne sont pas volatiles mais ils peuvent venir de la dissolution du CCN. Une autre source hypothétique est l'activité microbienne. Les acides aminés essentiels sont au nombre de 20. Ceux sont des molécules amphotères très difficiles à détecter, car la plupart absorbe faiblement la lumière visible ou UV. Dans le cadre de ma thèse on a mis au point une méthode pour la détection de 16 acides aminés à faible concentration.

La méthode prévoit une dérivation chimique pré-colonne, fait d'une façon automatique par l'injecteur de l'appareil HPLC. Les acides aminés réagissent à température ambiante avec l'OPA, ortophthalaldehyde, en présence de MPA, acide mercaptopropionique. La solution est ensuite séparée sur colonne C18 avec détection des acides aminés dérivés par fluorescence. La limite de détection est de 5 nM.

Malheureusement, on travaille dans un milieu naturel comme l'eau de nuage et les chromatogrammes ne sont pas aussi propres que dans l'eau ultrapure. Par conséquence, une calibration a été faite en tenant compte de l'effet de matrice et on a calculé la concentration de chaque acide aminé. La Figure 11 (haut) montre la distribution des concentrations. On peut rapidement remarquer que tous les acides aminés sont présents et que les plus concentrés sont ILE, PHE, SER et TRP. La somme des concentrations des acides aminés oscille entre 1 et 4 µM.

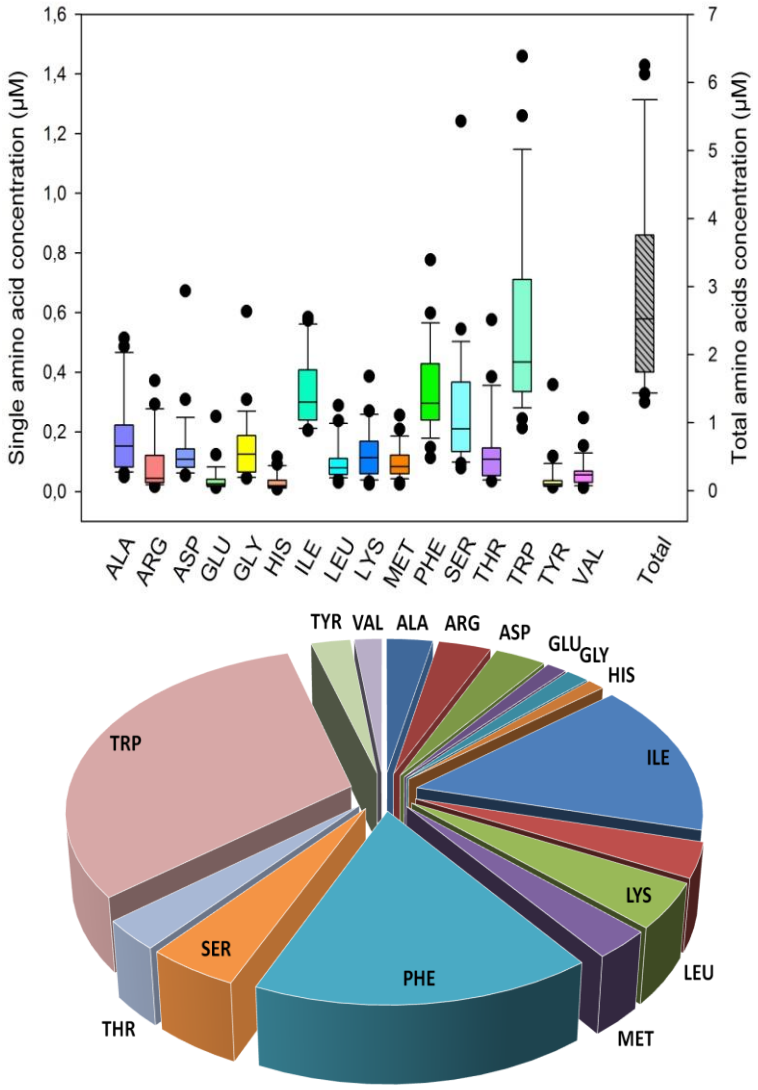

Figure 11: Concentration des acides aminés dans l'eau de nuage (haut) et distribution relative (bas).

La somme des acides aminés représente en moyenne 200 µgC/L, équivalent à 9% de la valeur moyenne de TOC dans l'eau de nuage. On peut donc mettre à jour le camembert montré en Figure 1 (droite) et diminuer le pourcentage de matière organique non caractérisée. La Figure 11 (bas) montre la distribution relative des acides aminés dans les échantillons analysés.

Vis-à-vis des concentrations trouvées dans l'eau de nuage, on est donc passé à une estimation de la réactivité des acides aminés dans l'eau de nuage, en tenant en compte leur constante de réaction avec $HO^{\bullet}$. Les valeurs sont bien différentes : on passe de 10^7 $M^{-1}s^{-1}$ pour l'ASP à 10^{10} $M^{-1}s^{-1}$ pour la TYR et le TRP. On a décidé de comparer les acides aminés avec les acides carboxyliques mesurés, dont la concentration moyenne dans l'eau de nuage et la réactivité sont connues. Les constantes de réactivité sont plus faibles et varient en fonction de la

protonation/ déprotonation de la molécule. On a calculé le ratio $C_{AA/AC}$ avec l'Equation 22 qui nous permets d'estimer qui, entre AA et CA piège plus d' $HO^{\bullet}$.

$$C_{AA/CA} = \frac{k^{II}_{HO^{\bullet},AA_i} \times [AA_i]}{k^{II}_{HO^{\bullet},CA_i} \times [CA_i]}$$

Equation 22

Si on considère la réactivité du formiate, qui est l'acide le plus concentré et le plus réactif avec $HO^{\bullet}$, les acides carboxyliques sont les plus importants piégeurs d' $HO^{\bullet}$. Si on ne tient pas compte du formiate, les acides aminés peuvent piéger de 6 à 30 fois plus de radicaux hydroxyles que les acides carboxyliques. La même comparaison est faite avec la matière organique dissoute en utilisant les constantes de second ordre de réactivité pour les acides aminés. Pour la DOC on a considéré la constante DOC- $HO^{\bullet}$ reporté en littérature par Arakaki dont la valeur est de 3.8×10^8 L/(molC s). On a pu estimer que les acides aminés peuvent piéger jusqu'à 36% de radicaux hydroxyles. La moitié de ces radicaux sont consommé par le tryptophane.

Pour conclure cette partie, j'ai détecté et quantifié les acides aminés pour la première fois dans l'eau de nuage et leur contribution à la DOC a été estimée d'environ 9%, avec des valeurs qui vont de 4 à 21 % en fonction de la composition de l'echantillon. Le TRP est le plus concentré. La réactivité des AA avec l' $HO^{\bullet}$ a été comparé avec celle des acides carboxyliques et avec la DOC. Il a été démontré que de 8 à 36 % des radicaux hydroxyles sont piégé par les AA.

En conclusion j'ai travaillé sur trois aspects de la chimie des nuages : en premier lieu sur l'estimation de la capacité oxydante : pendant ma thèse j'ai pu évaluer la vitesse de formation du radical hydroxyle et sa corrélation avec les sources inorganiques. La deuxième partie a eu comme thème générale la caractérisation de la matière organique dissoute et l'étude de sa réactivité : J'ai pu améliorer notre connaissance de la composition de la matière organique dans l'eau de nuage en ajoutant le contribue des acides aminés. J'ai ainsi étudié la réactivité des composés considérés et j'ai pu déterminer que les acides aminés sont des pièges de radicaux hydroxyles et que l'acide tartronique et le tryptophane se transforment dans l'eau de nuage et forment des acides carboxyliques tels que le formate et l'acétate.

On a donc vu l'interaction du radical hydroxyle avec la matière organique dissoute mais l'ensemble de ce que je vous ai décrit est beaucoup plus complexe : dans l'eau de nuage, sont présents des microorganismes comme les bactéries, les champignons, les algues, qui peuvent agir comme consommateurs de radicaux hydroxyles mais aussi comme inhibiteurs de leur

formation. Ces microorganismes peuvent également avoir un impact sur la concentration des AA et des AC. Plusieurs questions se posent : les microorganismes influencent-ils la vitesse de formation du radical hydroxyle d'une manière significative? De quelle façon ?

Abstract

Clouds represent a multiphase complex and reactive medium in which gases, liquid particles and aerosols are in continuous interaction. A large fraction of atmospheric chemical compounds present in the particulate and gaseous phases can be transferred to the cloud droplets where can undergo chemical, photochemical and microbiological transformations. Cloud waters were sampled at the puy de Dôme station. The first part of my PhD work is focused on the photoreactivity of cloud water. Formation of a reactive species such as hydroxyl radical, by direct photolysis of inorganic sources was investigated, as well as the correlation between the concentration of sources and the hydroxyl radical formation rate. The spectroscopic proprieties and fate of tartronic acid, were investigated under cloud water conditions. Moreover, photochemical experiments were performed using continuous irradiation (direct and hydroxyl radical mediated photolysis) and nanosecond flash photolysis in order to assess the reactivity of this compound in cloud aqueous phase. The second part of my work is centered on the characterization of organic matter in clouds. Two studies are presented: i) Detection and quantification of tryptophan by fluorescence spectroscopy and the assessment of its reactivity; ii) detection and quantification of amino acids. Amino acids are detected for the first time in cloud water using a derivatization method and this work show that they represent the 9% of the dissolved organic matter in cloud. Their reactivity with hydroxyl radical was compared to the reactivity of carboxylic acids and dissolved organic matter. These results clearly demonstrate that amino acids represent a major sink of hydroxyl radicals in cloud water.

Résumé

Les nuages représentent un milieu multiphasique complexe et réactif. Une grande partie de composés chimiques atmosphériques de la phase particulaire ou gazeuse se dissout dans les gouttelettes de nuage où peuvent subir des transformations chimiques, photochimiques et microbiologiques. L'eau de nuage a été échantillonnée à la station du puy de Dôme et caractérisée par des mesures physico-chimiques. La première partie de mon travail de thèse est focalisée sur la réactivité de l'eau du nuage. La formation d'espèces réactives, le radical hydroxyle, est étudiée par photolyse directe de sources inorganiques et photolyses nano-pulsée et sa vitesse de formation a été corrélée à la concentration de sources. Les propriétés spectroscopiques et la dégradation d'un composé modèle, l'acide tartronique, ont été étudiés. Les expériences faite par irradiation continue (photolyse directe et induite par le radical

hydroxyle) et par photolyse pulsée ont permis de comprendre la réactivité de ce composé dans le milieu nuageux. La deuxième partie de mon travail est focalisée sur la caractérisation et la réactivité de la matière organique dans la phase aqueuse des nuages. La détection et la quantification de tryptophane par spectroscopie de fluorescence et l'étude de sa réactivité ainsi que la détection et quantification d‘acides aminés représente une partie importante de ce travail. Les acides aminés ont été détectés pour la première fois dans l'eau de nuage grâce à l'utilisation d'une méthode chromatographique de dérivation et détection par fluorescence. Ce travail à démontré que les acides aminés peuvent représenter entre 4 et 21 % de la concentration en carbone de la matière organique dissoute dans le nuage. La réactivité des acides aminés avec le radical hydroxyle a été comparée avec celle des acides carboxyliques et de la matière organique dissoute. Ce résultat montre clairement que le rôle des acides aminés comme piège de radicaux hydroxyles ne peut plus être négligé.